NAZARBAYEV UNIVERSITY

DESIGN OF A 12-STORY "VERDIGRIS VIEW" HIGH-RISE RESIDENTIAL BUILDING IN LOS ANGELES, CALIFORNIA, USA

Capstone Project II

Bachelor of Engineering

(Civil and Environmental Engineering)

Group 9 members:

Temirova Tynyshtyk	202018266
Ibrayeva Darina	202087566
Baimagambetov Ayan	202079953
Revshanov Sanzhar	201962175
Bazarbek Meiirbek	201942994
Aigerim Zhubandykova	202048845

2025

This page was intentionally left blank.

DECLARATION

We formally state that this report, titled "Design of a 12-story 'Verdigris View' High-Rise Residential Building in Los Angeles, California, USA," is solely the outcome of our own efforts, except for any quotes and citations that have been properly credited. Additionally, we confirm that it has not been submitted previously or simultaneously for any other degree at Nazarbayev University.

Temirova Tynyshtyk 

Ibrayeva Darina 

Baimagambetov Ayan 

Revshanov Sanzhar 

Bazarbek Meiirbek 

Aigerim Zhubandykova 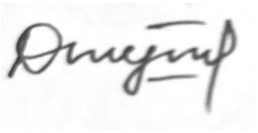

Date of Submission: Apr 25, 2025

Spring 2025

ACKNOWLEDGEMENTS

This acknowledgment is devoted to all the professors who supported us throughout our academic journey, specifically Mert Guney, Dichuan Zhang, Chang-Seon Shon, Alfrendo Satyanaga, Ferhat Karaca, Abid Nadeem, Shazim Ali Memon, Sung-Woo Moon and Jong Kim. We also wish to convey our heartfelt thanks to all the faculty members of the Civil Engineering and Environmental Department for their unwavering assistance during our coursework and throughout the capstone project.

Abstract

This report summarizes the efforts and progress of our team throughout the Capstone I project. After brainstorming potential ideas, we decided to focus on the development of a high-rise hotel. The project was divided into four major areas of civil engineering with the following weight distribution: Structural, Architectural & Materials - 40%, Geotechnical Engineering - 35%, Construction Management - 10%, and Environmental Engineering - 15%.

Based on this division, a 12-storey residential building with a basement was designed, located in a high seismic zone—Los Angeles, California. Once we obtained a soil investigation report, our final project scope was defined as: "Design of a High-Rise Residential Building in Los Angeles, California, USA."

The main challenge of the project was identifying the necessary design parameters and following the correct procedures to achieve a professional result. Our approach combined self-study, literature review, and guidance from faculty mentors. Each team member focused on specific project areas and worked towards clear objectives through independent research. Following this, we moved into the design planning phase. By applying knowledge from our academic courses, consulting secondary sources, and using our own engineering judgment, we created a working outline for the design process. With additional mentor support, we developed our own optimized approach rather than following a fixed template.

We encountered various challenges during the project, including limited expertise in some technical areas and difficulties in finding specific information. However, these challenges did not hinder the overall outcome. We managed to meet most of our objectives, and the current Capstone design is considered well-developed.

TABLE OF CONTENTS

1. Introduction

The construction project involves the design of a 12-story residential complex named “Verdigris View,” located in Los Angeles, California. The planned site will feature a residential building, a park area, and outdoor parking. “Verdigris View” represents a blend of natural elements with contemporary architectural design. The site is situated at 2217 Sunset Boulevard, bordered by Elsinore Street to the north and Mohawk Street to the east.

To ensure compliance with site-specific regulations, the design process adhered to the International Building Code (IBC), ASCE 7-10 standards, and ACI 318-19 guidelines for both architectural and structural elements. The table below outlines the division of responsibilities among team members throughout the project's development.

Table 1.1. Job Distribution.

Part	**Weight percentage**	**Responsible members**
Structural/Architectural	40%	Tynyshtyk Temirova, Meiirbek Bazarbek
Geotechnical	35%	Darina Ibrayeva, Aigerim Zhubandykova
Environmental	15%	Ayan Baimagambetov
Construction Management	10%	Sanzhar Revshanov

1.1. Project description and objectives

Sunset Boulevard is primarily characterized by aging, low-rise structures that reflect older urban planning and infrastructure standards. These conditions present an opportunity for revitalization through modern development. Introducing high-rise buildings in the area could act as a catalyst for economic development of the region by attracting commercial investments such as retail outlets, dining establishments, and service-based businesses. Moreover, given the high demand and limited availability of land in this sought-after neighborhood, vertical construction offers a practical solution. High-rises make efficient use of space, allowing for increased occupancy and functionality without the need for extensive land expansion. The objectives of the Capstone group project were initially set us the following:

- Site selection and evaluation: carefully identifying the construction site and conducting a comprehensive assessment of the location to identify geotechnical and structural design constraints, potential opportunities, zoning considerations, and environmental conditions;
- Architectural design presentation: showcasing the overall design concept, architectural layout, and aesthetic approach of the building, with a focus on harmonizing with the surrounding urban and natural environment;
- Geotechnical and structural investigation: analyzing the soil composition, climatic conditions, and seismic activity of the area to inform safe and effective structural and geotechnical engineering strategies;
- Building design in compliance with the local code and technical review: reviewing and applying all relevant building codes and design standards (International Building Code, ASCE 7-10, ACI 318-19) to ensure the safety of the building and that all the regulatory criteria are met;
- Drainage system design: designing an efficient stormwater and drainage system tailored to the site's topography and environmental characteristics to ensure sustainability and resilience against local weather conditions;
- Cost estimation and project planning: developing a preliminary budget estimate and establishing the foundational framework for project planning through the creation of a project charter.

1.2. Ethics and Professional Considerations

This capstone report, titled *"Design of a 12-story 'Verdigris View' High-Rise Residential Building in Los Angeles, California"*, was prepared in adherence to the highest ethical and professional standards. The following principles and guidelines were strictly followed throughout the preparation of this document to ensure its integrity, reliability, and proper application.

How This Report Was Prepared

The report represents the collective efforts of the team, divided among members based on expertise and project requirements, as outlined in the job distribution table. Each member contributed to their respective sections while maintaining consistent collaboration and peer review to ensure accuracy, coherence, and compliance with the objectives of the project. The preparation process included:

1. Adherence to Standards: The report follows the regulations and requirements set forth by governing bodies, including the International Building Code (IBC), ASCE-7,

and ACI standards. Ethical responsibility was a guiding principle in interpreting and applying these codes.

2. Transparency and Accuracy: All calculations, analyses, and design choices were meticulously documented and reviewed to minimize errors. Where assumptions or limitations exist, they are explicitly stated to ensure transparency.
3. Citations and Intellectual Honesty: All external sources, including design codes, tools, and references, have been properly cited to respect intellectual property and ensure the traceability of information.
4. Collaborative Review Process: The document underwent multiple iterations of reviews, both within the team and under the guidance of faculty mentors, to enhance its quality and reliability.

How This Report Should Be Used

The primary purpose of this report is to serve as a detailed record of the design process, methodologies, and decisions made during the conceptualization of the Verdigris View high-rise project. It is intended for:

- Educational Purposes: This document demonstrates the application of engineering principles and design standards in a real-world project setting. It should inspire and educate future students on the interdisciplinary nature of civil and environmental engineering.
- Reference for Stakeholders: Engineers, architects, and project managers involved in similar projects may find this report useful as a reference for site analysis, structural design considerations, and environmental planning.
- Compliance and Approval: The report includes necessary documentation, such as grading and drainage plans, that align with municipal requirements and can be used to support permit applications.

Ethical Considerations in Preparation and Usage

1. Professional Responsibility: The content was prepared with diligence to ensure public safety, environmental sustainability, and societal benefit. Decisions made during the design process prioritize the welfare of the community and compliance with ethical engineering practices.
2. Limitations and Future Work: This report reflects work completed during the first phase of the project. Certain aspects, such as detailed calculations for water volumes

and specific design dimensions, will be addressed in subsequent phases. Users must acknowledge these limitations when referencing the report.

3. Avoidance of Misuse: This report is not intended to replace professional judgment or serve as a definitive guide for construction. It should be used in conjunction with expert consultation and updated standards to ensure its relevance and applicability.

By maintaining these principles, this document embodies the ethical and professional responsibilities inherent in the field of engineering.

2. Architectural Design

2.1. Literature review on design codes

The architectural design process primarily adheres to the 2024 International Building Code (IBC). Key elements considered from the IBC include specifications for typical floor plans, entrance lobby dimensions, minimum stair and door sizes, and standard requirements for emergency exit ways, parking space layout and accessibility.

To evaluate the zoning parameters of the proposed site, the City of Los Angeles Municipal Code – Planning and Zoning Division was consulted. The analysis revealed that the project site lies within a C2 Commercial Zone, which permits mixed-use development and imposes no maximum building height restrictions. This zoning designation aligns well with the proposed high-rise structure and allows for greater architectural flexibility.

In terms of building classification, the planned residential complex is categorized as Group R-2, as defined by the IBC. This classification pertains to apartment-style housing and governs aspects such as occupancy load, egress requirements, and fire protection standards.

For parking requirements, the design follows the guidelines outlined in the Los Angeles Municipal Code (LAMC) to determine the precise number of required parking spaces based on the number and type of residential units. Additionally, the City of Los Angeles Building Code was referenced for the design of the underground parking structure, ensuring compliance with structural integrity, ventilation, and safety standards.

The structural design phase incorporated multiple design standards, including ASCE 7-10 for minimum design loads, ACI 318-19 for reinforced concrete structures, and supplementary guidelines from the Los Angeles Department of Building and Safety (LADBS). These codes collectively ensured that the building would meet all necessary performance criteria for safety, durability, and seismic resilience.

2.2. Site selection and analysis

2.2.1. Site selection

The chosen location is in Los Angeles, California, at 2217 Sunset Boulevard, close to the intersection with Mohawk Street. This area, which is part of Southeast Hollywood, is densely populated and is set to construct the development of a 12-story building named “Verdigris View”.

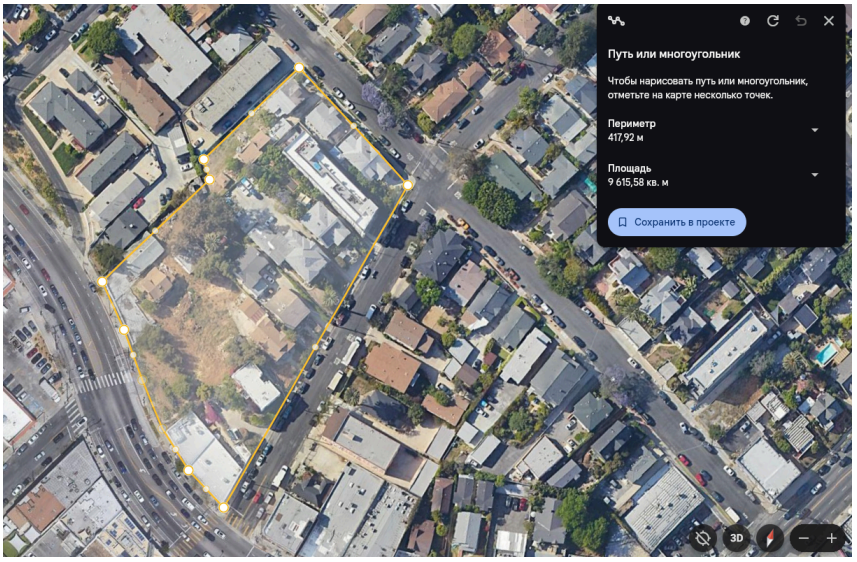

Figure 2.1. Satellite view of the selected site.

Figure 2.2. 3D view of the designed “Verdigris View” building.

A recent site investigation by Langan Engineering & Environmental Services (2019) indicates that the ground is predominantly flat and surrounded by both residential and commercial properties. Additionally, the area is well-connected to public transportation and

amenities, making it a strategic choice for development. Its proximity to various cultural attractions and entertainment venues in Hollywood adds to its appeal for both residential and commercial purposes.

2.2.2. Characteristics of the site

According to the USA Seismic zones map based on Uniform Building Code, Los Angeles lies in red zone 4, indicating high seismic risk.

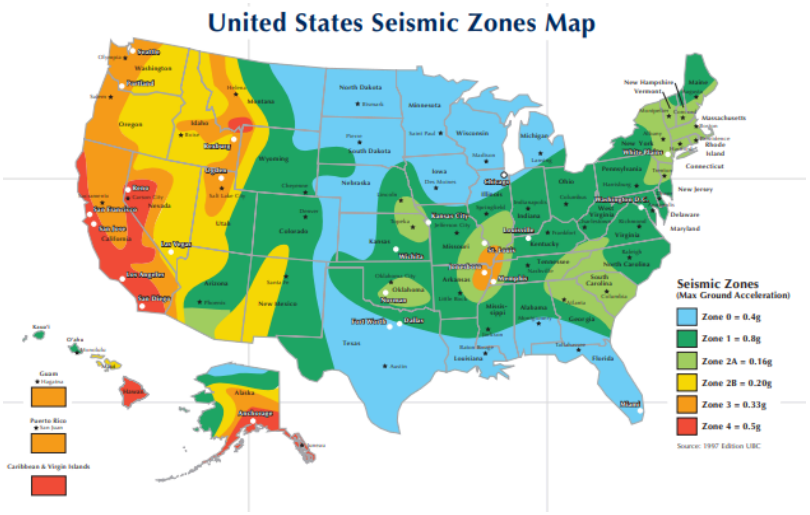

Figure 2.3. USA Seismic zones map.

Given that the structural design was conducted for the risk category II and the site soil class is D, according to the ASCE Hazard Tool, the chosen site belongs to the seismic design category E. The selected site is located in a seismic zone having a Peak Ground Acceleration of 2.619 g for a return period of T = 2475 years. The following figure represents the seismic parameters for the selected site.

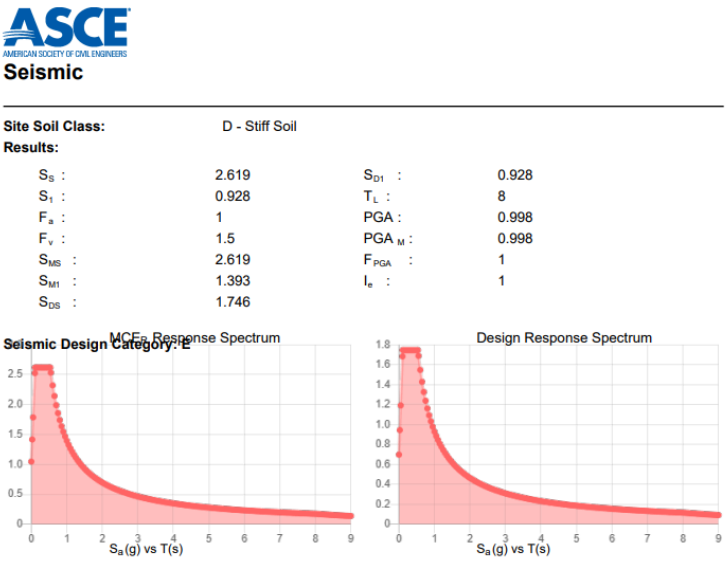

Figure 2.4. ASCE 7-10 Seismic Hazard Tool Report.

Additionally, the site was analysed for the susception to the wind load. The following figure represents the data provided by the ASCE 7-10. The report states that the selected site is not a hurricane-prone region. The provided values were later used for the wind load calculations.

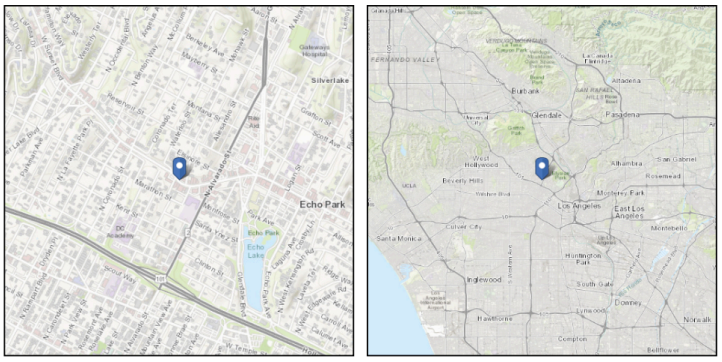

Wind

Results:

Wind Speed	110 Vmph
10-year MRI	72 Vmph
25-year MRI	79 Vmph
50-year MRI	85 Vmph
100-year MRI	91 Vmph
Special	Special Wind Region -- Mountainous terrain, gorges, and special wind regions shown in Fig. 26.5-1 shall be examined for unusual wind conditions. The Authority Having Jurisdiction shall, if necessary, adjust the values given in Fig. 26.5-1 to account for higher local wind speeds. Such adjustment shall be based on meteorological information and an estimate of the basic wind speed obtained in accordance with the provisions in Section 26.5.3.

Figure 2.5. ASCE 7-10 Wind Hazard Tool Report.

It was also found that the sites located close to the marine environments are exposed to salt-laden air, which is highly corrosive. Therefore, the selected site is highly susceptible to corrosion since Los Angeles city is located near the Pacific Ocean.

It can be concluded that the site chosen for residential building construction is located in a highly corrosive and seismically active zone having a PGA of 2.619g for T=2475 years.

2.2.2.1. Location and historical background

The plan view of the construction site is shown on Figures 2.4 and 2.5, below. The approximate area of the site is 9600 m^2 and has a perimeter of almost 420 m (the dimensions of the site can not be precisely identified because of the irregular shape). The site is bound by 2 streets and a boulevard: Elsinore St, Mohawk St, and Sunset Blvd.

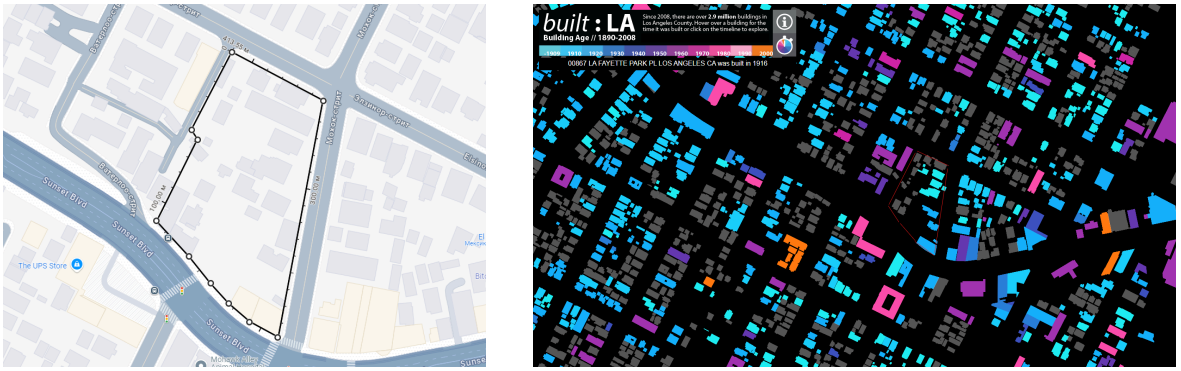

Figure 2.6 -2.7. Satellite view of the site.

The buildings located on the site are relatively old. According to the highlighted site in Figure 2.6, most of these apartments were built in 1903-1921 years. Therefore, it is concluded that these buildings can be demolished.

2.2.2.2. Climate responsive design and site-specific variables.

California is considered to be one of the hottest states in the US, however the climate in Los Angeles is Mediterranean and the average temperature is 11.6-24.5 °C (Figure 5)**.** During summer days Los Angeles sees up to 12 hours of sunshine (the longest is in July).

The Mediterranean climate means dry summers and wet winters. The highest temperature observed is 31.9 °C, so the climate can be considered almost hot. “Hot” territory is considered to be the region with the maximum temperature of 90 °F (or 32.22 °C).

Considering all this information, the building design should take into account the thermal insulation and ventilation.

	January	February	March	April	May	June	July	August	September	October	November	December
Avg. Temperature °C (°F)	11.9 °C (53.5) °F	12.2 °C (53.9) °F	14.1 °C (57.3) °F	15.8 °C (60.5) °F	18.2 °C (64.7) °F	21 °C (69.9) °F	24.1 °C (75.4) °F	24.5 °C (76.1) °F	23.2 °C (73.8) °F	19.5 °C (67.2) °F	15.4 °C (59.7) °F	11.6 °C (52.8) °F
Min. Temperature °C (°F)	6.7 °C (44.1) °F	6.8 °C (44.2) °F	8.3 °C (47) °F	9.7 °C (49.5) °F	12.3 °C (54.1) °F	15 °C (58.9) °F	17.9 °C (64.3) °F	18.2 °C (64.8) °F	17 °C (62.6) °F	13.6 °C (56.5) °F	9.8 °C (49.7) °F	6.5 °C (43.8) °F
Max. Temperature °C (°F)	19.5 °C (67.2) °F	19.4 °C (66.9) °F	21.4 °C (70.5) °F	23.3 °C (73.9) °F	25.2 °C (77.4) °F	28.1 °C (82.6) °F	31.3 °C (88.3) °F	31.9 °C (89.5) °F	31 °C (87.7) °F	27.2 °C (81) °F	23.1 °C (73.5) °F	18.8 °C (65.9) °F
Precipitation / Rainfall mm (in)	84 (3)	89 (3)	54 (2)	19 (0)	11 (0)	3 (0)	2 (0)	0 (0)	4 (0)	17 (0)	21 (0)	53 (2)
Humidity(%)	52%	57%	59%	55%	56%	55%	52%	49%	49%	49%	46%	53%
Rainy days (d)	4	5	4	2	1	0	0	0	1	2	2	4
avg. Sun hours (hours)	7.6	7.6	8.3	9.0	9.1	10.2	11.3	10.8	9.5	8.3	7.9	7.4

Figure 2.8. Climate data for Los Angeles from 1991 to 2021.

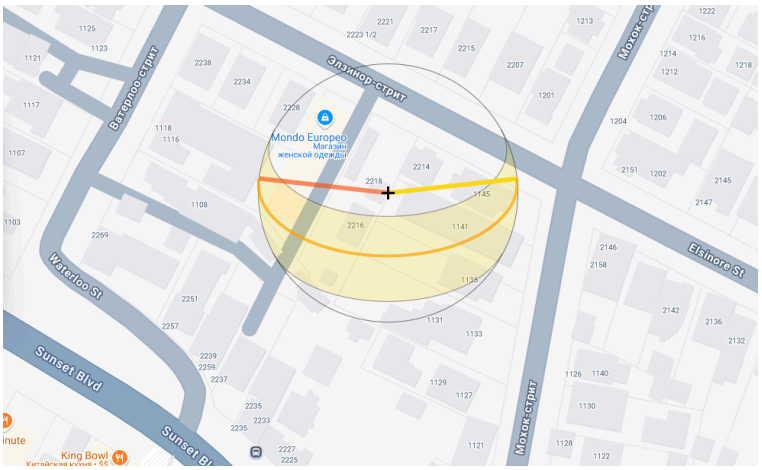

Figure 2.9. Sun direction in Los Angeles.

Wind is one of the important factors to access required ventilation, so it is necessary to take it into account. As it can be seen from Figure 6, mostly wind blows from west-southwest (or WSW) and has the velocity of 10-20 km/h. The wind direction will be considered further in the “Orientation” part.

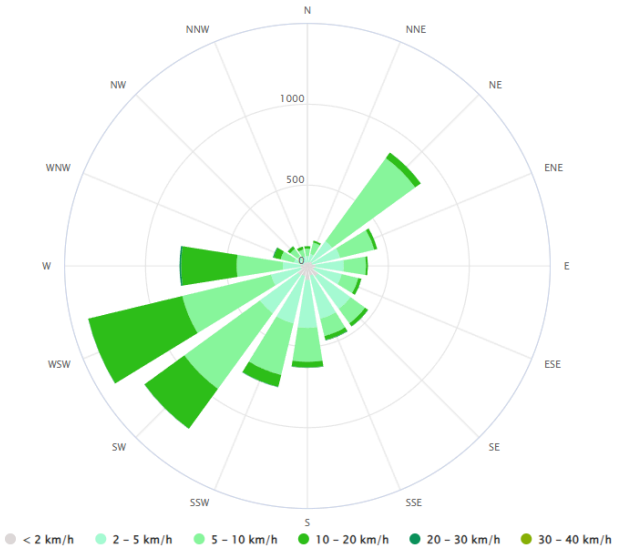

Figure 2.10. Annual wind rose in Los Angeles.

The solar day in Los Angeles is up to 12 hours, so it is important to consider the overshadowing problem. The requirement is to construct the building that will cause overshadowing of the nearby buildings and vice versa. It can be concluded that the apartment will not be covered by the shadows from nearby highrise buildings or skyscrapers because the nearest highrise building is located almost 445 metres away. Another aspect is to prevent the overshadowing of the nearby buildings. The construction site has quite large territory and if the building is placed almost in the middle of the site then the shadow will cover only the construction site.

Figure 2.11. The nearest high rise building to the construction site.

There are three key factors affecting the orientation of the building: 1) climate, 2) wind direction, and 3) solar access. First of all, it was mentioned that Los Angeles has dry summers and wet winters that make the city almost “hot”. This fact should be considered, so the shorter side of the building should face the sunshine to reduce the inner temperature of the building. Secondly, the wind is mostly directed to WSW. In order to make good ventilation, one of the sides has to be placed in the direction of the wind. This will definitely

provide cold breeze access and will lower the inner temperature. Thirdly, as it was mentioned in the previous part, the building should be placed at the middle of the site to prevent overshadowing. Finally, the orientation of Figure 8 was chosen.

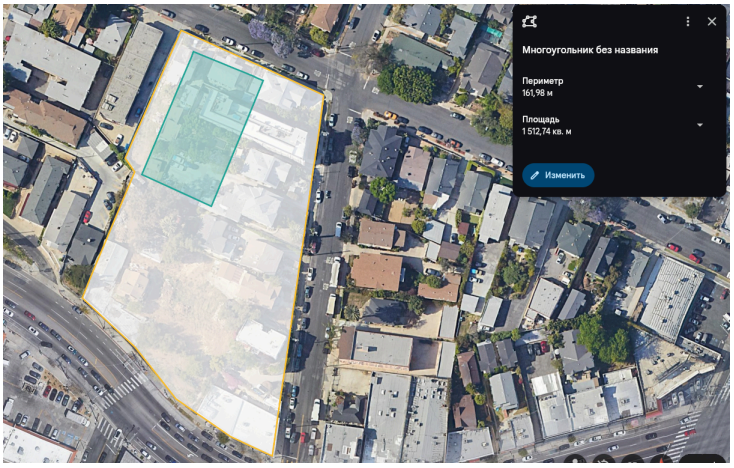

Figure 2.12. Site orientation [1]

It was already mentioned that the construction site is bound by two streets and the boulevard. Both Mohawk street and Elsinore street are considered as relatively small streets, so it can be assumed that these streets are not crowded with transport. In contrast, Sunset boulevard is one of the main streets in LA and at certain times (daily from 16:00 up to 19:00) there are long traffic jams here (Figure 11). Mostly, traffic jams occur in two regions surrounded by orange circles.

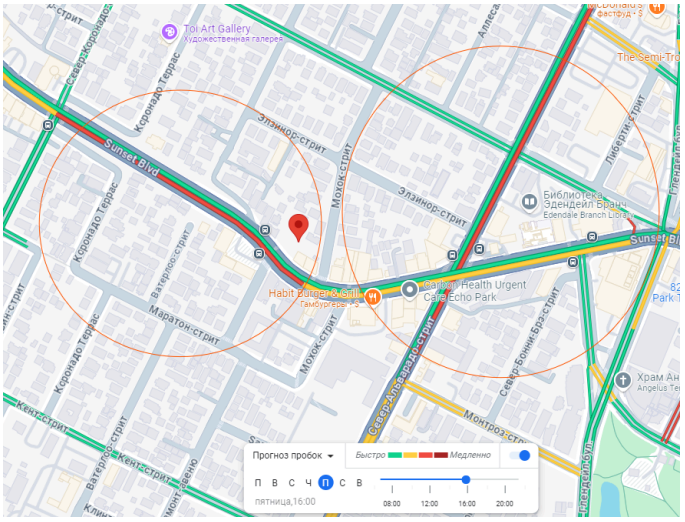

Figure 2.13. Traffic jams near the construction site.

There is a variety of public transport (buses) in LA according to their functions, these are red, orange, and silver buses. According to Figure 12, most of the buses near the

construction site are “orange”. The advantage of the orange buses is that they service more bus stops and it allows people to get closer to the destination.

Figure 2.14. Public transport near the construction site.

Although downtown Los Angeles, including the area near 2217 Sunset Blvd, is not classified as being in the highest fire-risk zones, areas just to the north, like Griffith Park and the surrounding hills, are known to face Very High Fire Hazard Severity. The Santa Ana winds that frequent the region during dry seasons can spread wildfires into urban zones, making it important to account for bushfire risk in any construction plan.

Stormwater management is critical due to the intensity of seasonal rains during winter. Los Angeles experiences heavy rainfall during short periods, causing significant runoff. Without proper drainage, urban flooding could occur, especially on a site with varying elevations like ours, sloping from 142 m to 133 m above sea level.

Although downtown Los Angeles, including the area near 2217 Sunset Blvd, is not classified as being in the highest fire-risk zones, areas just to the north, like Griffith Park and the surrounding hills, are known to face Very High Fire Hazard Severity. The Santa Ana winds that frequent the region during dry seasons can spread wildfires into urban zones, making it important to account for bushfire risk in any construction plan

To mitigate the risks for the proposed high-rise, consider:

- Fire-Resistant Building Materials: Use non-combustible materials such as steel or concrete, particularly for exteriors.
- Fire-Resistant Landscaping: Use fire-resistant plants and maintain defensible space around the building by removing dead vegetation.
- Compliance with Local Codes: Adhere to fire safety codes specific to Los Angeles, which include ensuring sufficient road access for firefighting vehicles and creating a robust emergency water supply system.

2.3.9. Stormwater Drainage

Stormwater management is critical due to the intensity of seasonal rains during winter. Los Angeles experiences heavy rainfall during short periods, causing significant runoff. Without proper drainage, urban flooding could occur, especially on a site with varying elevations like ours, sloping from 142 m to 133 m above sea level. Key strategies include:

- Permeable Pavement: To reduce runoff, implement permeable materials for pavements and sidewalks. These materials allow water to seep into the ground, reducing surface water and the burden on stormwater systems.
- Rainwater Harvesting: Install systems that collect and store rainwater for reuse in irrigation and other non-potable applications.
- Green Infrastructure: Introduce green roofs, rain gardens, and bioswales to absorb stormwater naturally and reduce the risk of flash floods(Site analysis)

2.3. Design concept

2.3.1. Site layout and dimensions

The site layout was designed in accordance with the regulatory requirements. The IBC 2024 states that at least one accessible route connecting building entrances with accessible parking spaces, public streets, and public transportation stops should be provided for a residential area. Given the site orientation and analysis from the previous part, it was decided to provide an accessible route from Mohawk street, since it is less overcrowded during the peak hours compared to the Sunset Boulevard and has available bus stops.

In order to effectively construct the chosen area, it was decided to construct a park and an outside parking lot. The park is located so that it is not overshadowed by the building. Selected dimensions of the building are 50*30 meters. An outside parking area is accessible for the entering cars. The entrance to the building is facing Mohawk street. Therefore, the parking space was located on the shortest available route to the building entrance.The final site layout is illustrated on Figure 2.16.

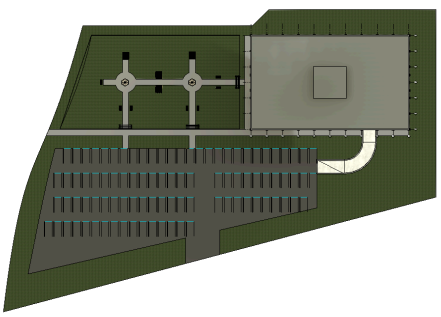

Figure 2.15. Site layout.

2.3.2. Floor plan design

For the sufficient insolation of the apartments, it was decided to separate the building into blocks with the apartments placed along the sides of the building's perimeter. Multiple apartments having the maximum of three bedrooms were designed according to the IBC requirements. It was ensured that each unit includes a separate kitchen with a clear working space of not less than 762 mm, and bathrooms. Designed apartment habitable rooms, such as bedrooms and living rooms, have a minimum area of 7 square metres and are not less than 2.5 metres in any horizontal dimension.

The door and windows dimensions were followed by the International Building Code requirements. It is stated that entrance doors should have a minimum width of 915 mm and a minimum height of 2032 mm, and a minimum width of 762 mm for interior doors. A minimum height for windows is 610 mm, and a minimum width of 508 mm. The code provides the minimum height for the residential apartments, which is 2.14 m. The typical floor height is 3 metres, and the first floor height is 3.5 metres.

First floor is for the commercial zone and the remaining 11 floors are the residential areas having 16 apartments per one floor. There are two apartments having 3 rooms, twelve 2 rooms apartments, and two 1 room apartments per each floor. The overall number of apartments is 176.

$$\#\ of\ apartments\ =\ 11\ \times\ (2\ +\ 12\ +\ 2)\ =\ 176$$

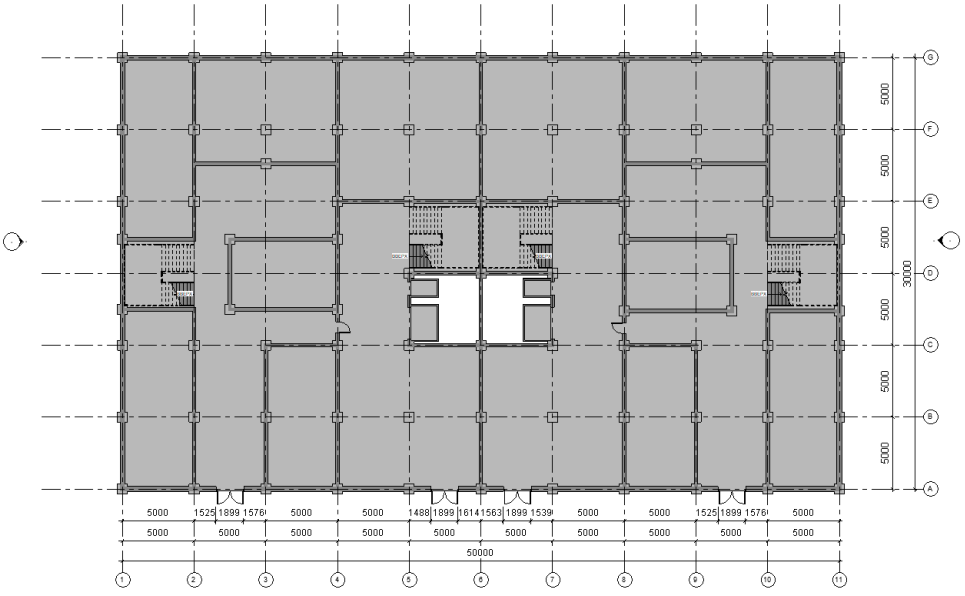

Figure 2.16. First floor plan.

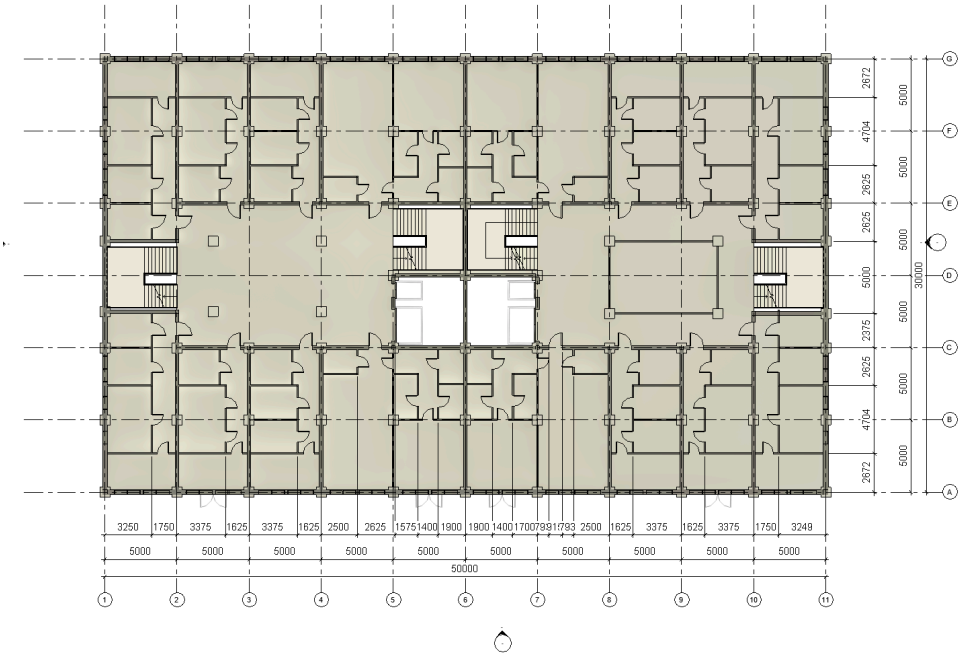

Figure 2.17. Residential floors plan.

2.3.3. Design of parking

For the design of the parking, the required number of parking spaces was calculated first. The equation followed the International Building code requirements that state that the number of parking spaces for units having 3 habitable rooms is 1.5 per unit, and 1 for units having less than 3 habitable rooms. Therefore, the required number of parking lots was calculated as:

$$N = (2 * 11) * 1.5 + (12 * 11) * 1 + (2 * 11) * 1 = 33 + 132 + 22 = 187$$

7 by 3 m dimensions were chosen for the parking lot design. An outside parking space has 77 parking lots. The remaining parking spaces are located at the underground parking.

The design of the underground parking was calculated using the dimensions presented in Table 2.1.

Table 2.1. Requirements for the underground parking lots and dimensions used in the project

Parameters	Required minimum		Dimensions used
	Feet	Meters	
Stall width	6	1.83	2.5 m

Stall length	13	3.96	3.96 m
Angle of inclination	-	-	90°

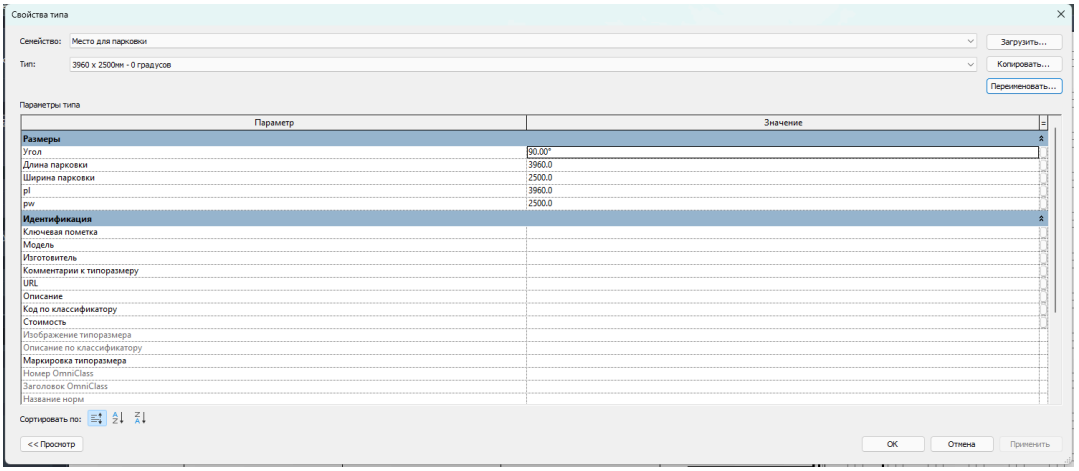

Figure 2.18. Dimensions of the underground parking lots

For the design of car ramps, the following dimensions in accordance with International Building Code were used:

Table 2. Requirements for the car ramp and dimensions used in the project

Parameters	Requirements	Values used
Ramp slope	16-20%	12%
Ramp width (for two-way)	4.5 m	4.685 m
Radius of the curvature (for two-way)	8.25 m	10.625 m

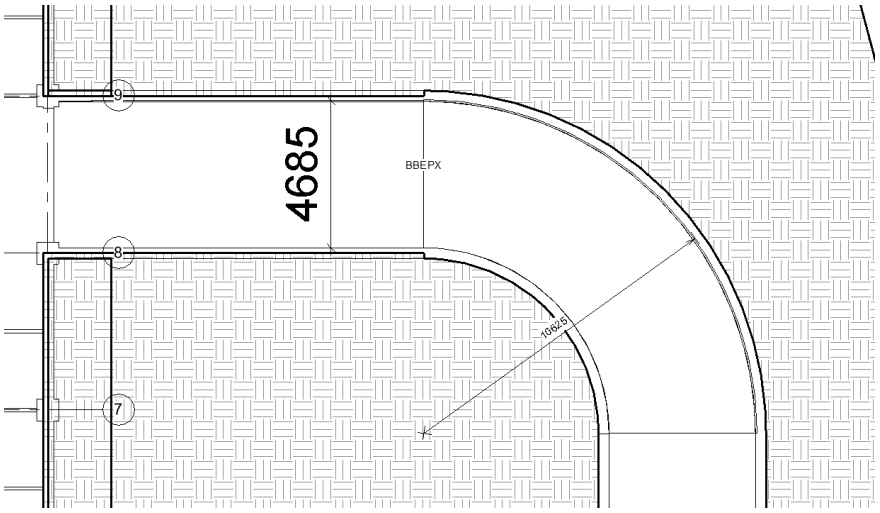

Figure 2.19. Dimensions of the car ramp.

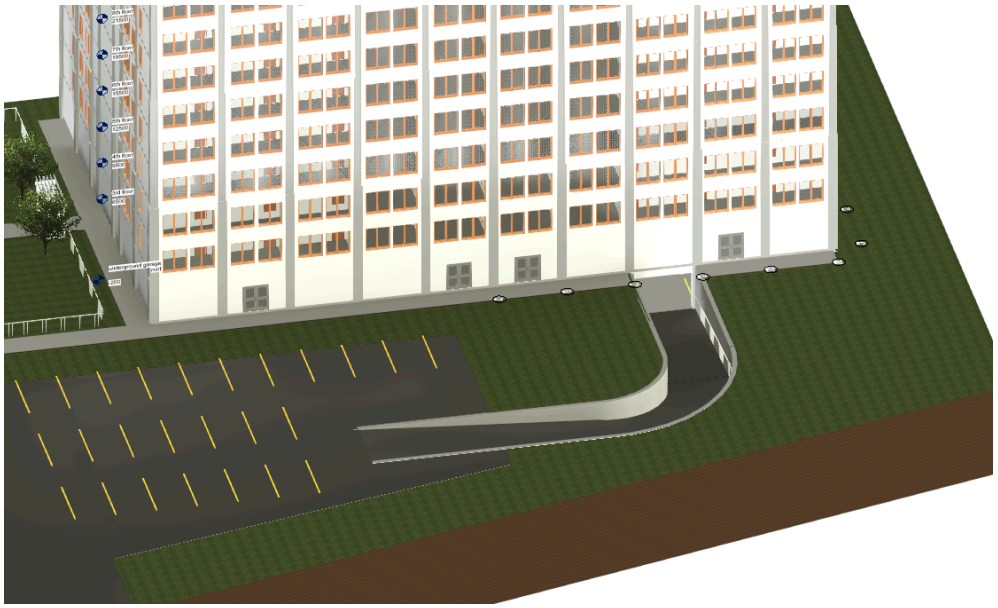

Figure 2.20. Revit 2025 3D view of the car ramp and underground parking entrance

2.4. Fire safety design

Automatic fire sprinkler systems will be installed in the building in compliance with the International Fire Code. Additionally, Class A, E, and F fire extinguishers will be provided to meet the requirements for residential buildings as specified in the 2020 International Building Code. The emergency evacuation plans are presented in figures 2.23 and 2.24.

Figure 2.21. Emergency evacuation plan of residential floors.

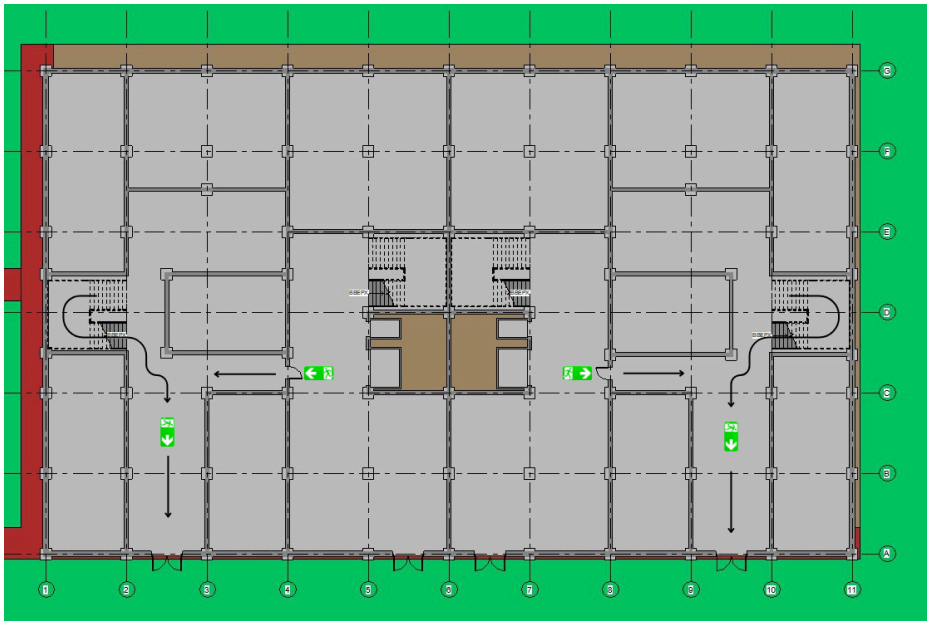

Figure 2.22. First floor emergency evacuation plan.

2.5. Non structural members design

2.5.1. Parapets design

According to the 2020 International Building Code, the minimum required height for roof parapets is 762 mm. For design purposes, a height of 1 meter was selected. The parapets will be constructed using autoclaved aerated concrete with a thickness of 250 mm. A 5 mm cement screed will be applied to the interior surface, while the exterior will be finished with

the same fiber cement cladding used elsewhere. As a result, the total thickness of the parapets will be 270 mm.

2.5.2. Floor finishing

The floor finishing materials were selected based on their aesthetic appeal, market availability, and suitability for residential buildings. For the first floor, the ceramic tile was chosen as the upper layer, while for the apartments the hardwood was chosen. The floor assembly consists of the following layers from top to bottom, in accordance with the 2020 International Building Code requirements:

- Surface layer: ceramic tiles laid on a 13 mm mortar bed
- Leveling layer: cinder concrete screed
- Waterproofing: single-ply sheet membrane
- Insulation: rigid thermal insulation
- Structural base: reinforced concrete slab with gravel aggregate

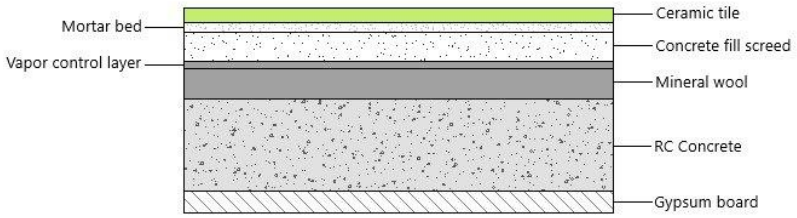

Figure 2.23. First floor and corridors floor finishing and ceiling cut view

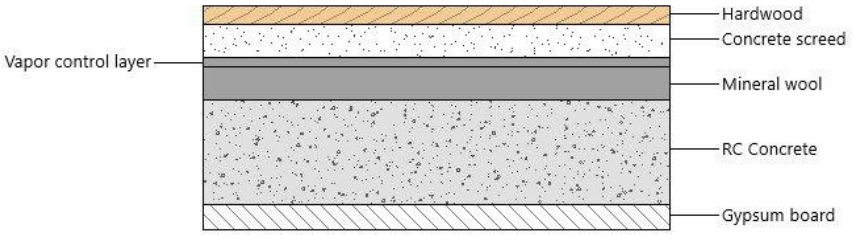

Figure 2.24. Typical floor finishing and ceiling cut view.

2.5.3. Walls section design

Autoclaved aerated concrete (AAC) was selected for the design of the partition walls due to its numerous benefits, including excellent thermal insulation, structural strength, lightweight nature, flexibility, and high fire resistance (PCA, n.d.). In addition to the AAC blocks, the partition walls incorporate proper insulation and a layer of cement plaster.

The same material—autoclaved aerated concrete—was also chosen for the exterior walls, primarily for its lightweight characteristics. The external surface will be finished with fiber

cement cladding, as previously described. Detailed illustrations of the partition and exterior walls are provided in Figures 2.7 and 2.8, respectively.

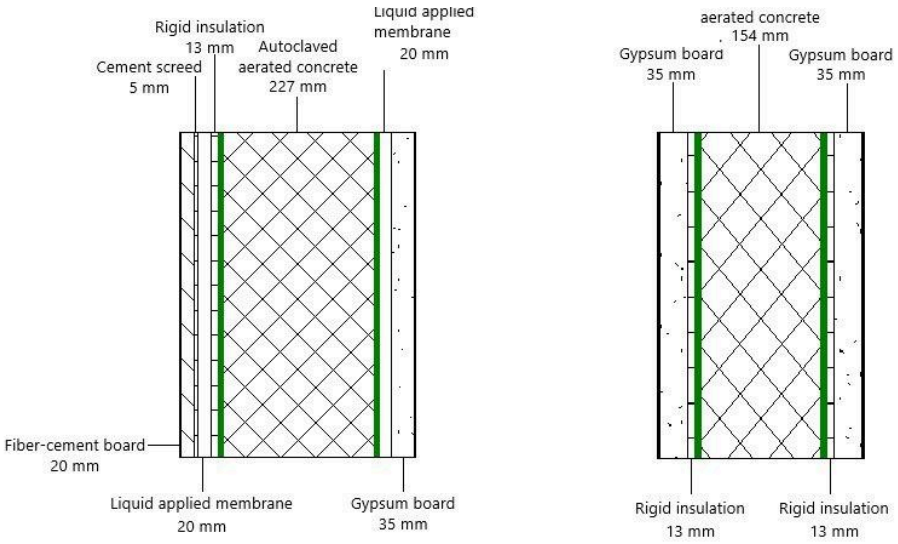

Figure 2.25. Exterior and interior walls section design.

2.5.4. Roof drainage system

For the roof drainage system, a scupper drainage system was selected due to its simplicity, cost-effectiveness, and suitability for flat roof structures with parapet walls. This system functions by allowing rainwater to exit the roof through scupper openings integrated into the parapet walls. From there, water is either directed into external downspouts or discharged through spouts to the building's exterior.

Scuppers are strategically positioned at low points on the roof to ensure efficient water removal and to prevent water accumulation. Additionally, overflow scuppers may be installed slightly above the primary drainage level to serve as a secondary drainage route in the event of blockage or excessive rainfall, thereby reducing the risk of water damage or structural stress.

A typical scupper drainage setup proposed for this building is illustrated in Figure 2.9.

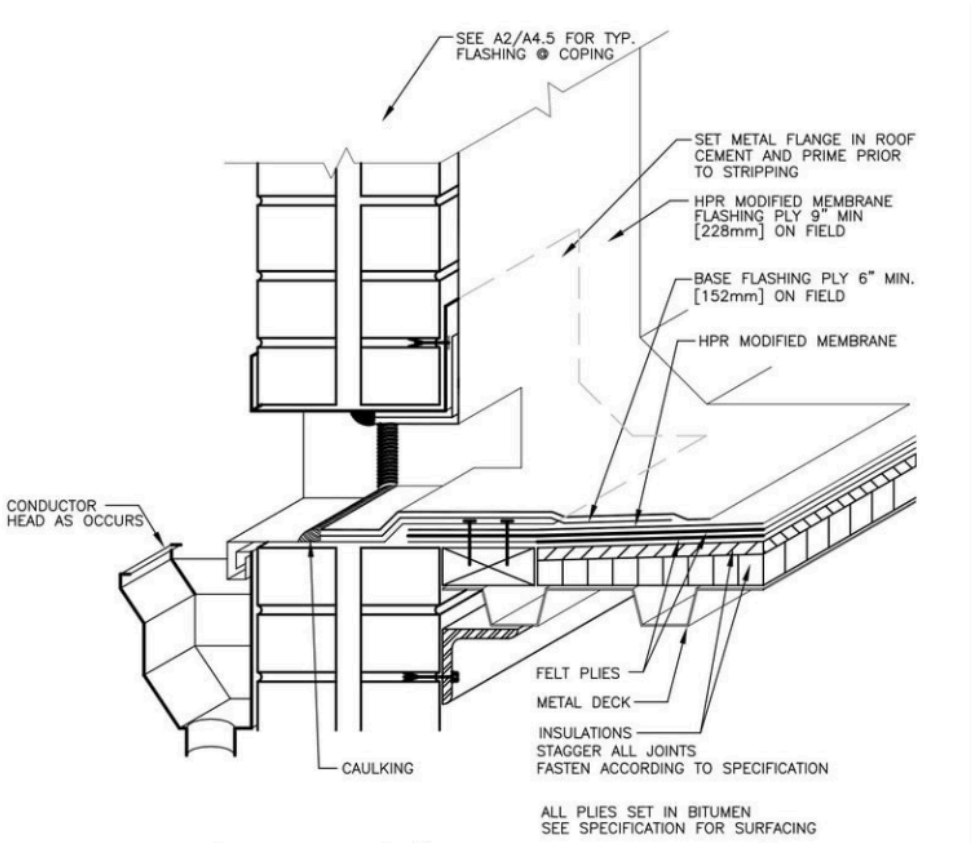

Figure 2.26. Exterior and interior walls section design.

2.6. Leadership in Energy and Environmental Design (LEED) - LEED v4.1

LEED (Leadership in Energy and Environmental Design) - green building rating system that evaluates healthiness, efficiency, and to what extent the costs are saved on the framework. The criterias may vary according to the building types, for example, mostly used three types of LEED rating systems are Building Design and Construction (BD+C), Operations and Maintenance (O+M), Interior Design and Construction (ID+C). In our case, BD+C is the rating system that is required because it mainly focuses on new constructions. According to the U.S. Green Building Council. (2023), there are eight main criterias that are assessed:

- Integrative Process (IP)
- Location and Transportation (LT)
- Sustainable Sites (SS)
- Water Efficiency (WE)

- Energy and Atmosphere
- Materials and Resources (MR)
- Indoor Environmental Quality (EQ)
- Regional Priority (RP)

The chosen location is densely populated and the high rise building provides an efficient area usage for the residents, providing easy access to various commercial areas that are developed in the selected zone. The area is well connected to multiple bus lines facilitating easy access to public transportation.

Up to this point of the project completion, some efforts have been made to ensure the sustainability of the site and efficiency of water and materials resources. The open green area provides connectivity to the environment.

LEED (Leadership in Energy and Environmental Design) is a widely recognized system for certifying buildings that are designed and built with sustainability in mind. It helps guide projects toward making smarter choices about energy, water, materials, and overall environmental impact. Buildings are awarded points in areas like energy efficiency, air quality, and waste reduction, and based on how many points they score, they can achieve different levels of certification:

- Certified - 40 to 49 points
- Silver - 50 to 59 points
- Gold - 60 to 79 points
- Platinum - 80 to 110 points

Essentially, LEED helps create buildings that are better for the planet and the people who use them, promoting a healthier, more sustainable future.

In this section most of the categories from LEED v 4.1 BD+C were analyzed:

- Location and Transportation (LT) - 15/16 points
- Sustainable Site (SS) - 8/10 points
- Water Efficiency (WE) - 6/11 points
- Energy and Atmosphere (EA) - 27/33 points
- Materials and Resources (MR) - 13/13 points

- Indoor Environmental Quality (EQ) - 14/16 points

Overall, 83 points out of 110 and the building can be classified as Platinum.

2.6.1. Location and Transportation

Y	P	N			
Y	1	N	Credit	Integrative Process	1

0	15	0	Location and Transportation		16
Y			Credit	LEED for Neighborhood Development Location	16
Y	1		Credit	Sensitive Land Protection	1
Y	2		Credit	High Priority Site and Equitable Development	2
Y	5		Credit	Surrounding Density and Diverse Uses	5
Y	5		Credit	Access to Quality Transit	5
Y	1		Credit	Bicycle Facilities	1
Y	1		Credit	Reduced Parking Footprint	1
		N	Credit	Electric Vehicles	1

Figure 2.27. LEED v 4.1 BD+C LT criterias

The project site was intentionally chosen within a certified LEED Neighborhood Development area, making it a great example of smart, sustainable urban planning. It's located in a vibrant, walkable neighborhood with easy access to public transportation, bike paths, and everyday amenities. Because the community is already designed to support reduced car use, it helps future residents rely more on greener ways of getting around—like walking, biking, or using transit. This not only cuts down on emissions but also encourages healthier lifestyles. Thanks to this thoughtful site selection, the project secured the 15 points out of 16 available in the Location and Transportation category.

2.6.2. Sustainable Site

0	8	0	Sustainable Sites		10
Y			Prereq	Construction Activity Pollution Prevention	Required
Y	1		Credit	Site Assessment	1
Y	2		Credit	Protect or Restore Habitat	2
Y	1		Credit	Open Space	1
Y	3		Credit	Rainwater Management	3
		N	Credit	Heat Island Reduction	2
Y	1		Credit	Light Pollution Reduction	1

Figure 2.28. LEED v 4.1 BD+C SS criterias

Before the design phase, the project team carefully studied the site's conditions to understand how the natural surroundings could be preserved and enhanced through design.

The ecological value of the land was assessed, and strategies were developed to protect existing habitat and encourage biodiversity. Open green spaces were incorporated into the site plan, offering residents opportunities to connect with nature while supporting environmental restoration.

Rainwater is effectively managed on-site through a well-planned drainage system that mimics natural water flow, helping to reduce runoff and replenish groundwater. Light pollution was also addressed by minimizing exterior lighting and selecting fixtures that preserve night sky visibility, allowing residents to enjoy a clear view even in an urban setting. Although the project did not meet the full requirements for Heat Island Reduction, the site design still prioritizes environmental harmony and resident well-being.

2.6.3. Water Efficiency

0	6	0	**Water Efficiency**		11
Y			Prereq	Outdoor Water Use Reduction	Required
Y			Prereq	Indoor Water Use Reduction	Required
Y			Prereq	Building-Level Water Metering	Required
		N	Credit	Outdoor Water Use Reduction	2
Y	6		Credit	Indoor Water Use Reduction	6
		N	Credit	Optimize Process Water Use	2
		N	Credit	Water Metering	1

Figure 2.29. LEED v 4.1 BD+C WE criterias

The efficient use of water is a core principle of sustainable design, and this project prioritized indoor water reduction as part of its LEED strategy. High-efficiency fixtures were installed throughout the building to significantly reduce potable water consumption. These include low-flow toilets, sensor-based faucets, and water-saving shower heads that help reduce water usage by more than 50% compared to standard baselines.

Although outdoor water use reduction and other water-related strategies were not pursued, the project's strong performance indoors demonstrates a focused effort to address water conservation. Residents will benefit from long-term reductions in water bills, while the lower demand on municipal water supply supports regional sustainability. Additional strategies such as greywater reuse were not implemented, but could further enhance the building’s water performance in future upgrades.

2.6.4. Energy and Atmosphere

0	27	0	Energy and Atmosphere		33
Y			Prereq	Fundamental Commissioning and Verification	Required
Y			Prereq	Minimum Energy Performance	Required
Y			Prereq	Building-Level Energy Metering	Required
Y			Prereq	Fundamental Refrigerant Management	Required
Y	6		Credit	Enhanced Commissioning	6
Y	18		Credit	Optimize Energy Performance	18
Y	1		Credit	Advanced Energy Metering	1
Y	2		Credit	Grid Harmonization	2
		N	Credit	Renewable Energy	5
		N	Credit	Enhanced Refrigerant Management	1

Figure 2.30. LEED v 4.1 BD+C EA criterias

The project earned 27 out of 33 points in the Energy and Atmosphere category, reflecting strong performance in energy efficiency through advanced systems, optimized design, and effective commissioning. However, no points were awarded for Renewable Energy, as no on-site systems like solar or wind were installed, and the Enhanced Refrigerant Management credit was not achieved due to the use of high-GWP refrigerants or lack of mitigation strategies. Despite these gaps, the project demonstrates a solid commitment to reducing energy consumption and operational costs.

2.6.5. Materials and Resources

0	13	0	Materials and Resources		13
Y			Prereq	Storage and Collection of Recyclables	Required
Y	5		Credit	Building Life-Cycle Impact Reduction	5
Y	2		Credit	Environmental Product Declarations	2
Y	2		Credit	Sourcing of Raw Materials	2
Y	2		Credit	Material Ingredients	2
Y	2		Credit	Construction and Demolition Waste Management	2

Figure 2.31. LEED v 4.1 BD+C MR criterias

Getting all 13 points in the Materials and Resources category means the project has really prioritized sustainability in how materials are sourced and used. This includes choosing products that are made from recycled or renewable resources, like FSC-certified wood, and using materials that are locally sourced to cut down on transportation impact. It also focuses on minimizing waste by reusing materials from the site and recycling wherever possible. By making these thoughtful choices, the project not only reduces its environmental

footprint but also contributes to a more sustainable, efficient building that lasts longer and does less harm to the planet.

2.6.6. Indoor Environmental Quality

0	14	0	Indoor Environmental Quality		16
Y			Prereq	Minimum Indoor Air Quality Performance	Required
Y			Prereq	Environmental Tobacco Smoke Control	Required
Y	2		Credit	Enhanced Indoor Air Quality Strategies	2
Y	3		Credit	Low-Emitting Materials	3
Y	1		Credit	Construction Indoor Air Quality Management Plan	1
Y	2		Credit	Indoor Air Quality Assessment	2
Y	1		Credit	Thermal Comfort	1
Y	2		Credit	Interior Lighting	2
Y	3		Credit	Daylight	3
		N	Credit	Quality Views	1
		N	Credit	Acoustic Performance	1

Figure 2.32. LEED v 4.1 BD+C EQ criterias

Scoring 14 out of 16 in the Indoor Environmental Quality category shows that the project has done a great job creating a healthy and comfortable indoor space. It's made improvements in air quality, ventilation, and using materials that are safer for people inside the building. However, we lost points in Quality Views and Acoustic Performance, meaning the project didn't fully meet the standards for giving people good views of the outdoors or making sure the sound inside is ideal. Even though these areas weren't perfect, the overall indoor environment still provides a positive and healthy place for people to work or live.

2.7. Life Cycle Cost Analysis Using Life-365 Software

Life-365 is a software tool used by engineers and construction professionals to help make buildings more sustainable and cost-effective. Its main goal is to evaluate the long-term costs and environmental impact of building materials and systems throughout their entire life cycle—from how they're made, used, and maintained, to how they're disposed of or recycled.

Default units of measurement:

- Base Units: US Units
- Concentration Units: % wt. conc.

Step 1. Default Settings

Figure 2.33. Life-365 software, “Default Settings” part

Step 2. Project Details

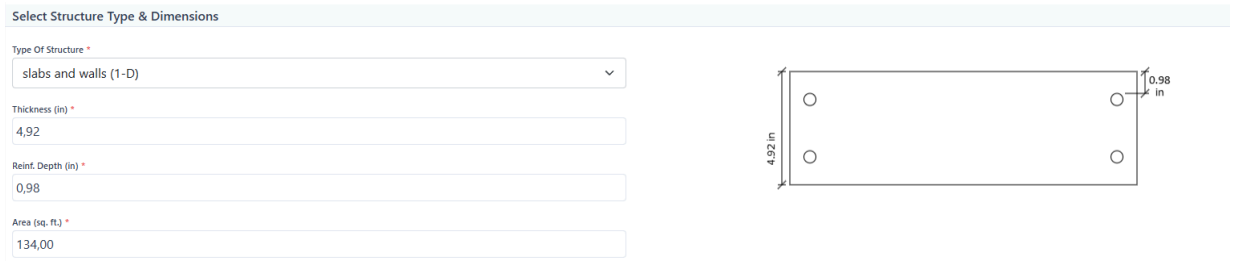

Figure 2.34. Life-365 software, “Project Details” part

Step 3. Exposure

Figure 2.35. Chloride Exposure of the site

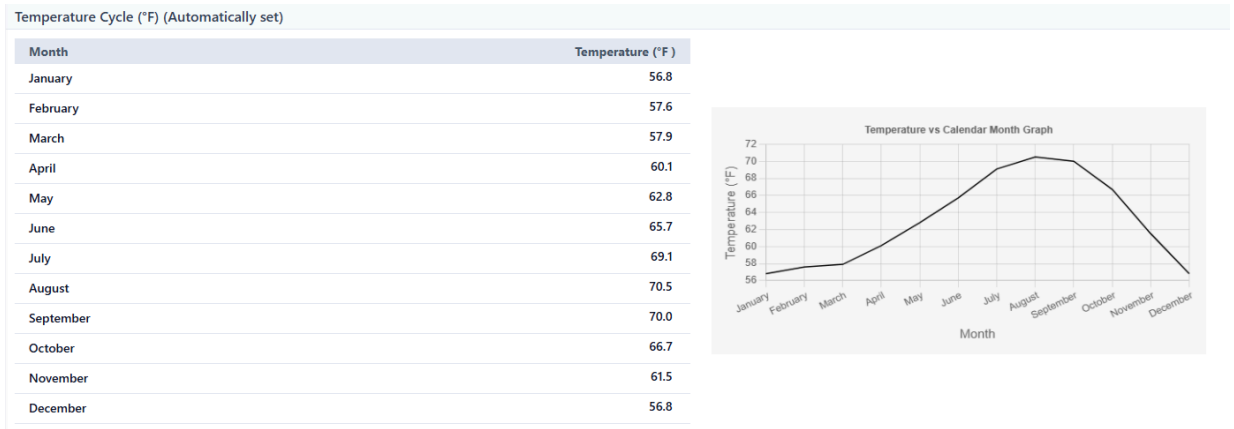

Figure 2.36. Temperature Cycle in Farenheits

Step 4. Concrete Mixtures

Figure 2.37. Concrete Mixture used in Life-365 software

C25/30 concrete was used for the columns and beams. The Optimum value of water to cement ratio for this type of concrete is around 0.45-0.55, however it is very high for our case because the aim is to make the concrete able to withstand 40 MPa force. As a result, w/cm was taken as 0.35.

We chose C25/30 concrete with a 0.35 water-cement ratio and black steel rebars because it strikes the right balance between strength, durability, and what's actually realistic on a construction site. The concrete grade gives us solid structural performance, and by keeping the water-cement ratio low, we make the concrete denser and more durable—better protected against things like moisture and long-term wear.

While materials like fly ash, slag, and silica fume can improve concrete in theory, they’re not commonly used in real-world projects around here. Most construction companies don't add them regularly because they're either hard to source, more expensive, or require special handling that can slow down the work. So instead of aiming for a “perfect” mix on paper, we focused on what’s practical and reliable in real conditions.

We also went with standard black steel rebars because they’re cost-effective, easy to work with, and familiar to local crews. Options like epoxy-coated or stainless steel could improve corrosion resistance, but they’d add unnecessary cost for this type of project and aren't really needed given the exposure conditions.

In short, our mix is strong, durable, and realistic—something that delivers good performance without complicating construction or inflating the budget.

2.8. Corrosion Prevention

Even though we’re using regular black steel rebars—which aren’t coated or stainless—we’ve still taken solid steps to protect them from corrosion. The low

water-cement ratio of 0.35 makes the concrete much denser, which means it's harder for water, air, and harmful chemicals to get in and reach the steel. That alone goes a long way in preventing rust.

The C25/30 concrete also gives us good strength and durability, and as long as we stick to proper construction practices—like making sure the rebars have the right concrete cover, and the concrete is well compacted and cured—we're creating a solid barrier that keeps the steel safe over time.

We didn't go with special corrosion-resistant rebars or extra additives, mainly because in real-world conditions like this, they're not really needed and would just add extra cost. Our approach keeps things practical: durable concrete, good workmanship, and proven protection that works well for the expected environment. It's about doing the basics right—which is often the most reliable form of prevention.

Structural Design

3.1. Preliminary design parameters

To properly select the main material of the project building, it is mandatory to identify the most important characteristics that would satisfy the safety, efficiency, and cost requirements. The chosen criterions that are considered in the selection process are:

- Fire and corrosion resistance;
- Cost;
- Structural properties, such as compressive/tensile strength, weight, earthquake resistance;
- Durability;
- Required labour force.

There are four possible material types that can be used in construction: steel, reinforced concrete, masonry, and wood. Masonry units are relatively heavy and have lower strength compared to steel and concrete. Wood is susceptible to fire and is not suitable for high rise buildings. Steel and reinforced concrete meet most of the criterions, so the further selection was considered between them.

Table 3.1. Reinforced concrete and steel comparison.

	Reinforced Concrete	**Steel**
Maintenance	Properties of RC may change over	Susceptible to corrosion, so

and durability	time, so constant checking is required	needs to be painted periodically
Availability and cost	Materials for RC are easily available	Has higher cost
Material quality control	Material quality control can be conducted on site	Fabricated out of the site
Labour skills	Does not require high labour skills	Requires higher labour skills
Fire resistance	High fire resistance; does not loose structural properties during the fire	Lower fire resistance, strength reduces considerably during the fire
Corrosion resistance	Not susceptible to corrosion	Susceptible to corrosion
Strength	Has higher compressive strength	Resists tensile forces produced by earthquakes due to higher tensile strength
Lateral force resistance	Less ductile, has lower resistance to vertical loads	High resistance under earthquake and wind loads

The selected site is located in a high seismic zone. Even though the steel structures demonstrate better performance under seismic loads, the reinforced concrete was chosen as the main construction material for the building. It has higher corrosion resistance, which is also an important factor for the site, less costly, requires less maintenance and lower labour skills.

The design and analysis of the residential building were carried out in accordance with U.S. standards, specifically following the American Concrete Institute's *Building Code Requirements for Structural Concrete* (ACI 318-22) and the American Society of Civil Engineers' *Minimum Design Loads and Associated Criteria for Buildings and Other Structures* (ASCE 7-16) (ACI, 2022; ASCE, 2016).

For the lateral force resisting system, different options were taken into consideration, such as a moment-resisting frame with rigid joints, shear walls, and dual systems, including

shear wall with moment-frame; shear wall with braced system, and moment frame with braced system. The comparison between each system was conducted based on such characteristics as seismic performance, cost, architectural flexibility, ease of construction, and the best application (LADBS, 2024).

Table 3.2. Comparison of lateral force resisting systems.

	Moment-Resisting Frame	**Shear Walls**	**Shear Walls + Moment Frames**
Seismic Performance	Good ductility, higher drift	High stiffness, lower drift	Combines both stiffness and ductility
Cost	High due to member sizes and detailing	Low to moderate for mid-rise buildings	Highest due to dual-system complexity
Architectural flexibility	High (open spaces)	Low to moderate (walls limit design)	Moderate to high
Ease of construction	Complex	Relatively simple	Complex
Best application	Low-rise or where flexibility needed	Mid-rise or buildings with regular layouts	High-rise or irregular buildings in seismic zones

Based on the properties listed in the table, the shear walls were chosen to be the main lateral force resisting system due to the regularity of the building design and an economical feasibility. Also, compared to the moment-frame resisting system, lower drift and higher stiffness is preferred for the given seismic design category. However, the dual system has the most advantages and might be also considered in the later design, based on the the performance of a building under lateral forces.

Given the building dimensions as 50 by 30 metres, the spacing between columns was decided to be 5 metres in both directions.

The next step is to choose the type of slab between two options, one way slab with minor beams, and two way slabs with minor beams.

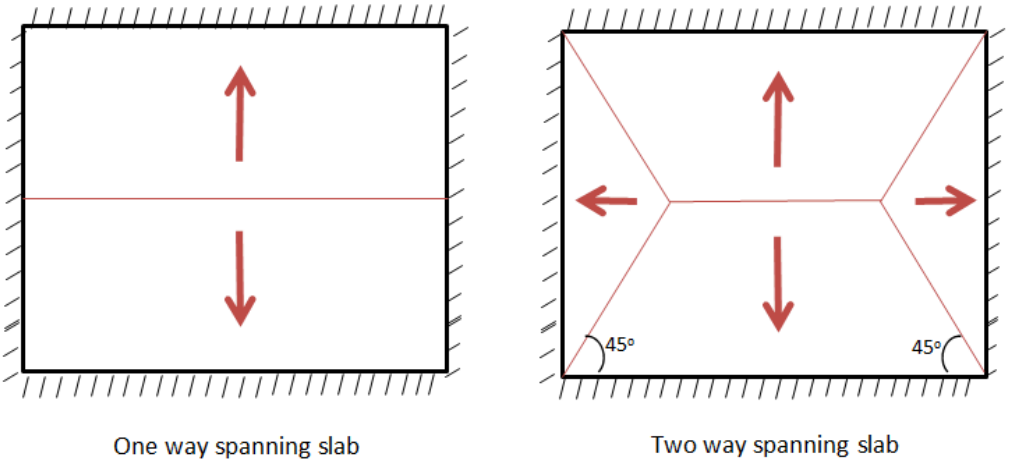

Figure 3.1. One way slab and two way slab concepts.

The comparison was made by evaluating both options on the material use, formwork cost, span suitability, and cost efficiency.

Table 3.3. One way and two way slab comparison.

	One way slab	**Two way slab**
Material use	Smaller amount of reinforcement for one direction	Greater amount of reinforcement for both directions
Formwork cost	Simple and economical	More complex, higher cost
Span suitability	Best for short spans (<6 meters)	Best for larger spans (>6 meters)
Cost Efficiency	More economical for smaller spans	Economical for larger spans or square areas

Since the thickness of two way slabs is generally smaller, more steel reinforcement is required. Given that the span length is 5 metres, one way slabs are considered to be the most economical option, and, therefore, will be used for the structural layout.

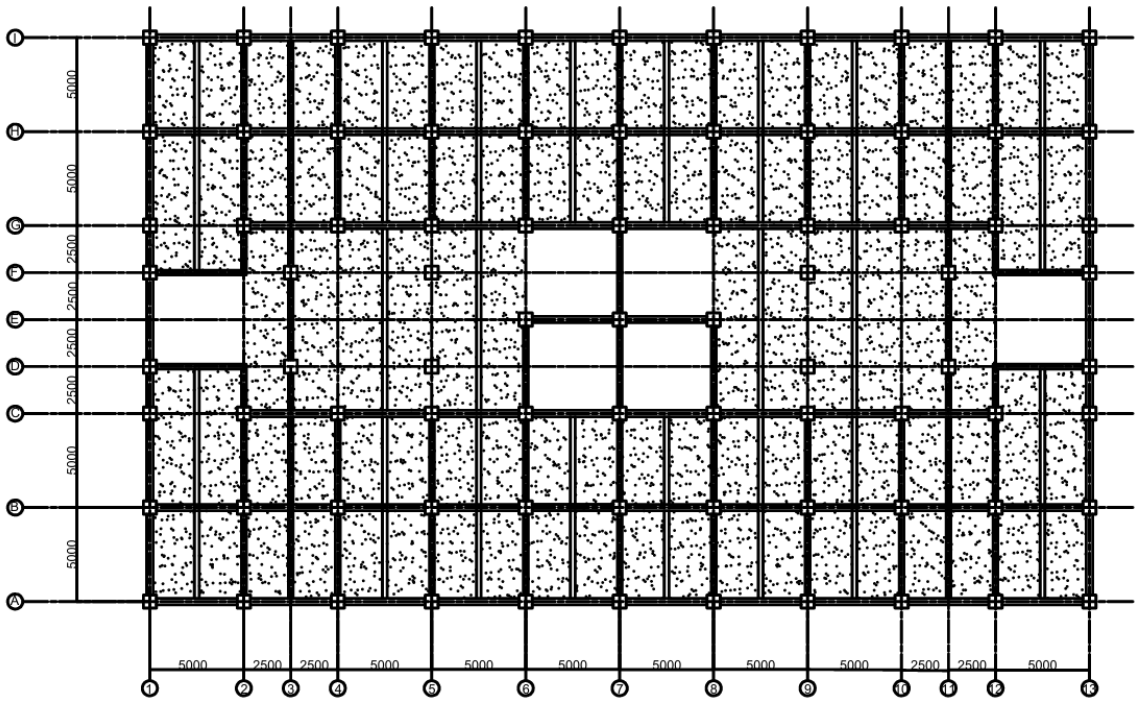

Figure 3.2. Structural layout.

According to the structural layout, a one way slab is given since a = 5 m; b = a/2 = 2.5 m, due to the presence of minor beams. Based on the design procedure, the following calculations were done:

- Slab thickness = span/20 = 2500/20 = **125 mm.**
- Minor beam height h = L/15 = 5000/15 =333.3 mm, b = h/2 = 333.33/2 =166.7 mm.

333.3*166.7 mm

- Major beams height h = L/10 = 5000/10 = 500 mm, b = h/2 = 500/2 = 250 mm.

500*250 mm

Finally, considering the increment of 50 mm and 20 mm for slab dimensions, the final dimensions are shown in the following table.

Table 3.4. One way slab dimensions.

	L (m)	h (m)	b (m)	V (m^3)
Slab	5.000	0.120	2.400	2.880
Major Beam	5.000	0.400	0.200	1.600
Minor Beam	5.000	0.300	0.150	0.225
				4.705

For the columns sizing, the design equation provided by the ACI 318-19 will be used:

$$\varphi P_{max} = 0.85\varphi(\beta f_c'(A_g - A_{st}) + f_y A_{st}$$

φP_{max}- total axial force of the first floor's column;

A_g- gross area of the column's cross-section;

A_{st}-area of steel rebars in the column's cross-section.

Assume Ast = 0.01Ag

Design load combination according to the ACI 2.3.2:

$$\varphi P_{max} = 1.2D + 1.6L + 0.5L_r$$

Calculated values of dead, live, and live roof loads were considered. Iterations were done with the given equations until the alignment of cross-sectional values. The columns were divided into 4 categories according to their sizes. Therefore, the cross-sectional areas of the columns will vary every 3 floors. The total load on interior columns under each slab including self weights of the major, minor beams and slabs is calculated:

Table 3.5. Total loads on columns under slabs.

Location (under)	Dead	Live	Roof	Snow	Factored load	At	R	R (with beams and slab)
Slab 12	12.81		0.96	0	15.85	6.25	99.07	153.83
Slab 2-12	7.98	4.79	0	0	17.24	25	430.91	485.67
Slab 1	8.27	4.79	0	0	17.58	25	439.56	494.32
Slab 0	6.38	4.79	0	0	15.32	25	383.11	437.87

With the calculated reaction force values, the iterations using the equation x were completed for each assumed column size. After performing the iterations, the final column sizes were chosen as follows:

Table 3.6. Column sizes.

Column sizes	
Floors	a (m)
0-3	0.65

4-6	0.55
7-9	0.45
10-12	0.3

Finally, total load on each column was calculated considering the self weight.

Table 3.7. Load on each column including the self weight.

Location	Axial load	Type	Self-weight (column)	Total load (column)
12	153.83	1	6.75	160.58
11	485.67	1	6.75	492.42
10	971.34	1	6.75	978.09
9	1457.01	2	15.19	1472.20
8	1942.68	2	15.19	1957.87
7	2428.35	2	15.19	2443.54
6	2914.03	3	22.69	2936.71
5	3399.70	3	22.69	3422.38
4	3885.37	3	22.69	3908.05
3	4371.04	4	31.69	4402.73
2	4856.71	4	31.69	4888.40
1	5351.03	4	36.97	5388.00
0	5788.90	4	36.97	5825.87

In order to calculate the axial load on interior, exterior, and corner columns, dead loads of walls and parapets were also considered.

Table 3.8. Dead loads on columns.

Per area	From roof parapets per area	0.220	kN/m2
Interior columns	From beams	26.104	kN
Exterior columns	From beams	21.104	kN
Corner columns	From beams	11.526	kN
Per area	From interior walls per area	2.400	kN/m2
Per area	From exterior walls per area	0.970	kN/m2

The axial load on the columns on level 0 were calculated. These values were later used for calculations in the geotechnical part.

$$P_u(interior) = 6287.446\ kN$$

$$P_u(exterior) = 3507.604\ kN$$

$$P_u(corner) = 2324.301\ kN$$

3.2. Loads summary

In order to conduct the proper structural design and analysis of members, the design check was conducted in SAP 2000. The members had to be resized in order to pass the design check. The new sizes of the members are presented in Table 3.1.

Table 3.9. Updated member sizes after the design check.

Structural member	Major beam	Minor beam	Slab
Dimensions, mm	700 x 500	500 x 300	125 x 2500

3.2.1. Dead loads

By using the design values provided by ASCE 7 for the given materials, the dead load from floor finishing and ceiling was calculated.

Table 3.10. Corridors/first floor dead load calculations.

	Corridors/First floor		
	Material type	**Thickness (mm)**	**Load (kN/m^2)**
	Ceramic tile	20	
	Mortar bed	13	0.77
	Concrete fill screed(per mm thickness)	40	0.023
	Vapour control layer	10	0.03
	Mineral wool	40	2.2
	RC concrete	125	25
Floor finishing	Overall		**4.933**
Ceiling	Mechanical duct		0.19

	allowance		
	Gypsum board (per mm)	30	0.008
	Acoustic fiber	0	0.05
	Overall		**0.48**
	D	278	**5.41**

Table 3.11. Typical floor dead load calculations.

	Apartments		
	Material type	**Thickness (mm)**	**Load (kN/m^2)**
	Hardwood	22	0.19
	Concrete screed (per mm)	40	0.023
	Vapour control layer	10	0.03
	Mineral wool	40	2.2
	RC concrete	125	25
Floor finishing	Overall		**4.265**
	Mechanical duct allowance		0.19
	Gypsum board (per mm)	30	0.008
	Acoustic fiber	0	0.05
Ceiling	Overall		**0.48**
	D	267	**4.75**

Table 3.12. Roof dead load calculations.

	Roof		
	Material type	**Thickness (mm)**	**Load (kN/m^2)**
	Three-ply ready roofing		0.05
	Polystyrene foam (per mm)	100	0.0004

Floor finishing

	Bituminous, smooth surface	5	0.07
	Concrete screed (per mm)	40	0.023
	RC concrete	125	25
			4.13535
	Mechanical duct allowance		0.19
	Gypsum board	30	0.008
	Acoustic fiber	0	0.05
Ceiling	Overall		0.48
	D	300	**4.62**

Table 3.13. Interior walls dead loads calculation.

Interior walls		
Material type	**Thickness (mm)**	**Load (kN/m^2)**
Gypsum board	35	0.008
Rigid insulation	13	0.04
Autoclaved aerated concrete	154	7.85
Rigid insulation	13	0.04
Gypsum board	35	0.008
Overall		**1.85**

The interior walls dead load equivalent per area was calculated by multiplying the calculated dead load value by the overall perimeter of the interior walls and dividing by the height.

Table 3.14. Total equivalent dead load per area of the interior walls.

Equivalent load per area			
Floor	Total length	Height	Load (kN/ m^2)

0	0	3.5	0
1	420	3.5	1.88
2-12	625	3	**2.40**

The same procedure was completed for the exterior walls.

Table 3.15. Exterior walls dead loads calculation.

Exterior walls		
Material type	**Thickness (mm)**	**Load (kN/m^2)**
Fiber-cement board	20	0.015
Cement screed	5	0.02
Liquid applied membrane	20	0.05
Rigid insulation	13	0.04
Autoclaved aerated concrete	227	7.85
Liquid applied membrane	20	0.05
Gypsum board	35	0.008
Overall		**2.50**

Table 3.16. Total equivalent dead load per area of the exterior walls.

Equivalent load per area			
Floor	Total length	Height	Load (kN/ m^2)
0-1	160	3.5	**0.97**
2-12	160	3	0.83

The autoclaved aerated concrete as for the exterior walls was used for the parapets design. The height of the parapets is one metre.

Table 3.17. Dead loads from parapets.

Parapetes					
Material type	**Load**	**Thickness**	**Height**	**Length**	**Eq. Load**

		(mm)	(m)		(kN/ m^2)
Autoclaved aerated concrete block	1.9625	250	1	160	**0.22**

3.2.2. Live loads

According to the ASCE 7-10, minimum design value for floors 2-11: L_0= **1.92 kPa** for private rooms and corridors serving them. The following formula will be used for live load reduction:

$$L = L_0(0.25 + \frac{4.57}{\sqrt{K_{LL}A_T}})$$

$L \geq 0.4L_0$ for columns; $L \geq 0.5L_0$ for other members.

No reduction when: $K_{LL}A_T < 37.16\ m^2$

Table 3.18. Live loads calculations for private rooms and corridors serving them.

Member	$A_T,\ m^2$	K_{LL}	$K_{LL}A_T$	$L,\ kPa$
Column (interior)	25	4	100	1.92*0.7=1.35
Column (edge)	12.5	4	50	1.92*0.9=1.72
Column (corner)	6.25	1	6.25<37.16	1.92
Beam (major interior)	12.5	2	25<37.16	1.92
Beam (major, exterior)	6.25	2	12.5<37.16	1.92

However, for the first floor having public rooms and corridors serving them, L_0= **4.79 kPa**. This design value will be used as the critical value to be conservative.

Design value for the ordinary flat roof: L_0= **0.96 kPa**

$$L_r = L_0R_1R_2,\ 0.58 \leq L_r \leq 0.96$$

$$R_1 = 1,\ A_T \leq 18.58\ m^2$$

$$R_1 = 1.2 - 0.011\ A_T,\ 18.58\ m^2 < A_T < 55.74\ m^2$$

$$R_2 = 1$$

Table 3.19. Roof live loads calculations.

Member	$A_T,\ m^2$	R_1	L_r, kPa
Column (interior)	25	1.2 - 0.011*25 = 0.925	0.925*1*0.96 = 0.89
Column (edge)	12.5	1	0.96
Column (corner)	6.25	1	0.96
Beam (major interior)	12.5	1	0.96
Beam (major, exterior)	6.25	1	0.96

3.2.3. Snow loads calculation

As stated in ASCE 7-10 and the site analysis, there is no need to calculate snow loads for the buildings in the selected area

3.2.4. Wind loads

Wind loads were calculated according to the ASCE 7-10. Basic information used for the calculations:

- Basic wind speed = 110 Vmph = 49.17 m/s
- Exposure category = B
- Directional factor (K_d) = 0.85

The construction site is located in Los Angeles city, so the exposure category is B. According to the table below values of α (7.0) and z_g (365.76) were identified.

Table 3.20. Exposure categories and corresponding values from ASCE 7-10

In metric

Exposure	α	z_g (m)	$\hat{\alpha}$	$\hat{b}$	$\bar{\alpha}$	$\bar{b}$	c	ℓ (m)	$\bar{\epsilon}$	z_{min} (m)*
B	7.0	365.76	1/7	0.84	1/4.0	0.45	0.30	97.54	1/3.0	9.14
C	9.5	274.32	1/9.5	1.00	1/6.5	0.65	0.20	152.4	1/5.0	4.57
D	11.5	213.36	1/11.5	1.07	1/9.0	0.80	0.15	198.12	1/8.0	2.13

Table 3.21. Height effect.

Story	h (m)	z (m)	K_z
13	3	39.5	1.064
12	3	36.5	1.040
11	3	33.5	1.015
10	3	30.5	0.988
9	3	27.5	0.960
8	3	24.5	0.928
7	3	21.5	0.894
6	3	18.5	0.857
5	3	15.5	0.815
4	3	12.5	0.766
3	3	9.5	0.708
2	3	6.5	0.635
1	3.5	3.5	0.807

The following tables presents the values that will be used for further calculations:

h(m) - the height of each floor

z(m) - total elevation of the floors

K_z - velocity pressure exposure coefficient

To determine the values of K_z for each floor the following formulas were used:

$$K_z = 2.01(z/z_g)^{2/\alpha} \; for \; 15\,ft. \leq z \leq z_g$$

$$K_z = 2.01(15/z_g)^{2/\alpha} \; for \; z < 15ft.$$

Gustt effect

Values required for the calculation of Gust effect:

- The total height of the building (h) = 39.5 m;
- Damping ratio, percent critical for buildings or other structures (β) = 0.02.
- Turbulence intensity factor (c) = 0.3;
- Integral length scale factor (l) = 97.54 m;
- Integral length scale power law exponent ($\bar{\epsilon}$) = ⅓;
- Mean hourly wind-speed power law exponent ($\bar{\alpha}$) = ¼;
- Mean hourly wind speed factor ($\bar{b}$) = 0.45

There are 2 cases because the values of B and L change, so that in Case 1: B = 30.7 m and L = 50.7 m; in Case 2: B = 50.7 m and L = 30.7 m.

Formulas used for the calculation of Gust effect:

Approximate lower bound natural frequency (Hz)

$$n_a = \frac{43.5}{h^{0.9}}$$

Equivalent height of structure

$$\bar{z} = 0.6h$$

Intensity of turbulence

$$I_{\bar{z}} = c\left(\frac{10}{\bar{z}}\right)^{1/6}$$

Integral length scale of turbulence

$$L_{\bar{z}} = l\left(\frac{\bar{z}}{10}\right)^{\bar{\epsilon}}$$

Mean hourly wind speed at height $\bar{z}$

$$V_{\bar{z}} = \bar{b}\left(\frac{\bar{z}}{10}\right)^{\bar{\alpha}} V$$

Reduced frequency

$$N_1 = \frac{n_1 * L_{\bar{z}}}{V_{\bar{z}}}$$

The R factor is calculated by the following formula:

$$R_n = \frac{7.47 * N_1}{(1+10.3 * N_1)^{5/3}}$$

Different R values are found by:

$$R_l = R_h \; setting \; \eta = 4.6 n_1 h / \bar{V}_{\bar{z}}$$

$$R_l = R_B \; setting \; \eta = 4.6 n_1 B / \bar{V}_{\bar{z}}$$

$$R_l = R_L \; setting \; \eta = 15.4 n_1 L / \bar{V}_{\bar{z}}$$

and

$$R_l = \frac{1}{\eta} - \frac{1}{2\eta^2}(1 - e^{-2\eta}) \; for \; \eta > 0$$

$$R_l = 1 \; for \; \eta = 0$$

Resonant response factor

$$R = \sqrt{\frac{1}{\beta} R_n R_h R_B (0.53 + 0.47 R_L)}$$

Peak factor for resonant response

$$g_R = \sqrt{2ln(3600 n_1)} + \frac{0.577}{\sqrt{2ln(3600 n_1)}}$$

Background response factor

$$Q = \sqrt{\frac{1}{1+0.63(\frac{B+h}{L_{\bar{z}}})^{0.63}}}$$

Gust-effect factor for MWFRS of flexible buildings and other structures

$$G_f = 0.925(\frac{1+1.7 I_{\bar{z}} \sqrt{g_Q^2 Q^2 + g_R^2 R^2}}{1+1.7 g_V I_{\bar{z}}})$$

Here g_Q and g_V equal to 3.4.

Calculations:

$$n_a = n_1 = \frac{43.5}{129.59^{0.9}} = 0.546\ (h = 39.5\,m = 129.59\,ft)$$

$$\bar{z} = 0.6 * 39.5 = 23.7\,m$$

$$I_{\bar{z}} = 0.3 * \left(\frac{10}{23.7}\right)^{1/6} = 0.260$$

$$L_{\bar{z}} = 97.54 * \left(\frac{23.7}{10}\right)^{1/3} = 130.047$$

$$V_{\bar{z}} = 0.45 * \left(\frac{23.7}{10}\right)^{1/4} * 49.17 = 27.454$$

$$N_1 = \frac{0.546*130.047}{27.454} = 2.586$$

$$R_n = \frac{7.47*2.586}{(1+10.3*2.586)^{5/3}} = 0.076$$

Table 3.22. R_h, R_B, and R_L and corresponding η values for both cases.

	Case 1		Case 2	
	η		η	
R_h	3.613	0.238	3.613	0.238
R_B	2.808	0.293	4.638	0.192
R_L	15.527	0.062	9.402	0.101

Case 1:

$$R = \sqrt{\frac{1}{0.02} * 0.076 * 0.238 * 0.293 * (0.53 + 0.47 * 0.062)} = 0.422$$

Case 2:

$$R = \sqrt{\frac{1}{0.02} * 0.076 * 0.238 * 0.192 * (0.53 + 0.47 * 0.101)} = 0.318$$

Now, it is required to calculate peak factor for resonant response (g_R):

$$g_R = \sqrt{2ln(3600 * 0.546)} + \frac{0.577}{\sqrt{2ln(3600*0.546)}} = 4.043$$

Case 1:

$$Q = \sqrt{\frac{1}{1+0.63(\frac{30.7+39.5}{130.047})^{0.63}}} = 0.837$$

$$G_f = 0.925(\frac{1+1.7*0.260*\sqrt{3.4^2*0.837^2+4.043^2*0.422^2}}{1+1.7*3.4*0.260}) = 0.912$$

Case 2:

$$Q = \sqrt{\frac{1}{1+0.63(\frac{50.7+39.5}{130.047})^{0.63}}} = 0.816$$

$$G_f = 0.925(\frac{1+1.7*0.260*\sqrt{3.4^2*0.816^2+4.043^2*0.318^2}}{1+1.7*3.4*0.260}) = 0.869$$

There are 4 cases while calculating wind loads:

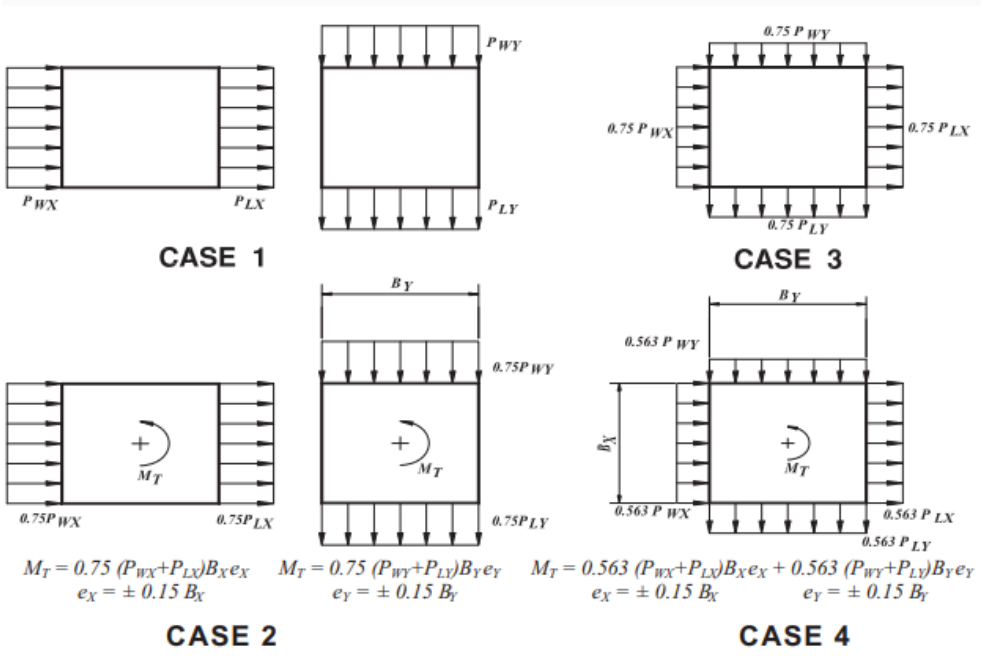

Figure 3.3. Wind load cases

Case 1:

Long side with number of frames (m) = 10, B = 50.7 m, and L = 30.7 m.

Wall Pressure Coefficients, C_p			
Surface	**L/B**	**C_p**	**Use With**
Windward Wall	All values	0.8	q_z
Leeward Wall	0-1	-0.5	q_h
	2	-0.3	
	≥4	-0.2	
Side Wall	All values	-0.7	q_h

Figure 3.4. Wall Pressure Coefficient values from ASCE 7-10

For Windward $C_p = 0.8$ and for Leeward $C_p = -0.5$ because L/B=30.7/50.7 = 0.606 which is in the range 0-1. Z and K_z values are taken from the design table.

$$K_{zt} = 1$$

Velocity pressure evaluated at height z above ground

$$q_z = 0.613 K_z K_{zt} K_d V^2$$

Design pressure to be used in determination of wind loads for buildings

$$P = q_z G_f C_{p,Windward} - q_h G_f C_{p,Leeward}$$

Design wind force:

$$F_i = B\left(\frac{h*P}{2}\right)$$

$$F\ per\ frame = \frac{F_i}{m}$$

Table 3.23. Wind loads for Case 1 and long side

Story	z, m	K_z	q_z	P_w, P_l	P	F_i	F per frame
13	39.5	1.064	1340.617	977.819	1575.318	119.803	59.901
12	36.5	1.040	1310.701	955.999	1553.498	237.946	23.795
11	33.5	1.015	1278.972	932.857	1530.356	234.527	23.453
10	30.5	0.988	1245.145	908.183	1505.682	230.891	23.089
9	27.5	0.960	1208.849	881.710	1479.209	227.001	22.700

8	24.5	0.928	1169.604	853.085	1450.584	222.811	22.281
7	21.5	0.894	1126.758	821.835	1419.334	218.257	21.826
6	18.5	0.857	1079.402	787.294	1384.793	213.254	21.325
5	15.5	0.815	1026.193	748.484	1345.983	207.676	20.768
4	12.5	0.766	965.021	703.867	1301.366	201.331	20.133
3	9.5	0.708	892.244	650.785	1248.284	193.901	19.390
2	6.5	0.635	800.562	583.914	1181.413	184.778	18.478
1	3.5	0.807	1016.624	741.505	1339.004	208.650	20.865

Short side with number of frames (m) = 6, B = 30.7 m, and L = 50.7 m.

Windward: $C_p = 0.8$ and Leeward: $C_p = -0.37$ (by linear interpolation)

Table 3.24. Wind loads for Case 1 and short side

Story	z, m	K_z	q_z	P_w, P_l	P	F_i	F per frame
13	39.5	1.064	1340.617	932.403	1354.016	62.352	31.176
12	36.5	1.040	1310.701	911.596	1333.210	123.747	20.624
11	33.5	1.015	1278.972	889.529	1311.143	121.772	20.295
10	30.5	0.988	1245.145	866.002	1287.615	119.673	19.945
9	27.5	0.960	1208.849	840.758	1262.371	117.427	19.571
8	24.5	0.928	1169.604	813.463	1235.076	115.007	19.168
7	21.5	0.894	1126.758	783.664	1205.277	112.378	18.730
6	18.5	0.857	1079.402	750.727	1172.341	109.489	18.248
5	15.5	0.815	1026.193	713.720	1135.333	106.268	17.711

4	12.5	0.766	965.021	671.175	1092.789	102.605	17.101
3	9.5	0.708	892.244	620.559	1042.172	98.315	16.386
2	6.5	0.635	800.562	556.793	978.407	93.048	15.508
1	3.5	0.807	1016.624	707.065	1128.678	105.694	17.616

Case 2:

$$e_x = 0.15B_x$$

$$e_y = 0.15B_y$$

Long side: $e_x = 7.605$

Table 3.25. Wind loads for Case 2 and long side

Story	P_w, P_l	M_T	$0.75F_i$	F direct
13	977.819	59.676	89.852	44.926
12	955.999	276.456	178.460	17.846
11	932.857	269.764	175.895	17.590
10	908.183	262.629	173.168	17.317
9	881.710	254.973	170.251	17.025
8	853.085	246.695	167.108	16.711
7	821.835	237.658	163.693	16.369
6	787.294	227.670	159.940	15.994
5	748.484	216.447	155.757	15.576
4	703.867	203.544	150.998	15.100
3	650.785	188.194	145.426	14.543
2	583.914	168.856	138.584	13.858
1	741.505	214.428	156.487	15.649

Short side: $e_y = 4.605$

Table 3.26. Wind loads for Case 2 and short side

Story	P_w, P_l	M_T	$0.75F_i$	F direct
13	932.403	26.656	46.764	23.382
12	911.596	141.360	92.810	15.468
11	889.529	139.021	91.329	15.222
10	866.002	136.526	89.755	14.959
9	840.758	133.849	88.070	14.678
8	813.463	130.955	86.256	14.376
7	783.664	127.796	84.284	14.047
6	750.727	124.303	82.117	13.686
5	713.720	120.380	79.701	13.284
4	671.175	115.869	76.954	12.826
3	620.559	110.502	73.736	12.289
2	556.793	103.741	69.786	11.631
1	707.065	119.674	79.270	13.212

Table 3.27. Wind loads for each frame on the first floor (Case 2)

Story	Short side				Long side			
	Frame	$F_{torsion}$	F_{direct}	F_{total}	Frame	$F_{torsion}$	F_{direct}	F_{total}
1	1	-2.380	13.212	10.831	1	-0.711	15.649	14.938
	2	-1.428		11.784	2	-0.553		15.096
	3	-0.476		12.736	3	-0.395		15.254
	4	0.476		13.688	4	-0.237		15.412

	5	1.428		14.640	5	-0.079		15.570
	6	2.380		15.592	6	0.079		15.728
					7	0.237		15.886
					8	0.395		16.044
					9	0.553		16.202
					10	0.711		16.360

Case 3:

Table 3.28. Wind loads for Case 3

Story	$0.75F_1$	$F_1\ direct$	$0.75F_2$	$F_2\ direct$
13	89.852	44.926	46.764	23.382
12	178.460	17.846	92.810	15.468
11	175.895	17.590	91.329	15.222
10	173.168	17.317	89.755	14.959
9	170.251	17.025	88.070	14.678
8	167.108	16.711	86.256	14.376
7	163.693	16.369	84.284	14.047
6	159.940	15.994	82.117	13.686
5	155.757	15.576	79.701	13.284
4	150.998	15.100	76.954	12.826
3	145.426	14.543	73.736	12.289
2	138.584	13.858	69.786	11.631
1	156.487	15.649	79.270	13.212

Case 4:

Table 3.29. Wind loads for Case 4

Story	P_w, P_l - x axis	P_w, P_l - y axis	M_T	$0.563F_1$	$0.563F_2$	F_1 direct	F_2 direct
13	977.819	932.403	250.150	67.449	35.104	33.725	17.552
12	955.999	911.596	379.445	133.964	69.669	13.396	11.612
11	932.857	889.529	373.502	132.039	68.558	13.204	11.426
10	908.183	866.002	367.167	129.991	67.376	12.999	11.229
9	881.710	840.758	360.369	127.802	66.111	12.780	11.019
8	853.085	813.463	353.018	125.442	64.749	12.544	10.792
7	821.835	783.664	344.994	122.879	63.269	12.288	10.545
6	787.294	750.727	336.124	120.062	61.642	12.006	10.274
5	748.484	713.720	326.158	116.921	59.829	11.692	9.972
4	703.867	671.175	314.701	113.349	57.767	11.335	9.628
3	650.785	620.559	301.070	109.166	55.351	10.917	9.225
2	583.914	556.793	283.899	104.030	52.386	10.403	8.731
1	741.505	707.065	324.366	117.470	59.506	11.747	9.918

Table 3.30. Wind loads for each frame on the first floor (Case 4)

Story	Short side				Long side			
	Frame	$F_{torsion}$	F_{direct}	F_{total}	Frame	$F_{torsion}$	F_{direct}	F_{total}
1	1	-1.622	11.747	10.125	1	-2.919	9.918	6.998
	2	-0.973		10.774	2	-2.271		7.647
	3	-0.324		11.423	3	-1.622		8.296
	4	0.324		12.071	4	-0.973		8.945

	5	0.973		12.720	5	-0.324		9.593
	6	1.622		13.369	6	0.324		10.242
					7	0.973		10.891
					8	1.622		11.539
					9	2.271		12.188
					10	2.919		12.837

3.2.5. Seismic loads

For the seismic loads calculations, design values provided by the ASCE 7-10 hazard tool were used for the equivalent lateral force procedure. According to the geotechnical investigation report, the site soil class is D (stiff soil), and the risk category is conventionally taken as II. By inserting these characteristics into the hazard tool, the following design values are obtained:

Table 3.31. Seismic design values.

S_S	S_1	F_a	F_v	S_{MS}	S_{M1}	S_{DS}	S_{D1}	T_L	I_e
2.619	0.928	1	1.5	2.619	1.393	1.746	0.92	8	1

The values provided in the table were calculated according to the equations:

$$S_{MS} = S_S * F_a$$

$$S_{M1} = S_1 * F_v$$

$$S_{DS} = \frac{2}{3} S_{MS}$$

$$S_{D1} = \frac{2}{3} S_{M1}$$

According to the ASCE 7, the site belongs to seismic design E category, since S_1=0.928 > 0.75.

For the reinforced concrete building located in seismic design category E, special reinforced concrete frames are the most suitable option for the seismic force resisting system, since they permit unlimited height for the building. This seismic force resisting system will be used in both transverse and longitudinal directions.

Seismic Force-Resisting System	ASCE 7 Section Where Detailing Requirements Are Specified	Response Modification Coefficient, R[a]	Overstrength Factor, Ω_0[g]	Deflection Amplification Factor, C_d[b]	Structural System Limitations Including Structural Height, h_n (ft) Limits[c]				
					Seismic Design Category				
					B	C	D[d]	E[d]	F[e]
C. MOMENT-RESISTING FRAME SYSTEMS									
1. Steel special moment frames	14.1 and 12.2.5.5	8	3	5½	NL	NL	NL	NL	NL
2. Steel special truss moment frames	14.1	7	3	5½	NL	NL	160	100	NP
3. Steel intermediate moment frames	12.2.5.7 and 14.1	4½	3	4	NL	NL	35[h]	NP[h]	NP[h]
4. Steel ordinary moment frames	12.2.5.6 and 14.1	3½	3	3	NL	NL	NP[i]	NP[i]	NP[i]
5. Special reinforced concrete moment frames[a]	12.2.5.5 and 14.2	8	3	5½	NL	NL	NL	NL	NL
6. Intermediate reinforced concrete moment frames	14.2	5	3	4½	NL	NL	NP	NP	NP
7. Ordinary reinforced concrete moment frames	14.2	3	3	2½	NL	NP	NP	NP	NP

Figure 3.3. Seismic force resisting systems with limitations.

Table 3.24. Design coefficients for the special reinforced concrete moment frame.

R^a	$\Omega_0^{\ g}$	$C_d^{\ b}$
8	3	5.5

3.2.5.1. Fundamental period calculations

First, modal analysis for the fundamental period was run in SAP 2000 software. The results of the modal analysis are presented in Figure 3.5. Fundamental period is taken as 1.118 s.

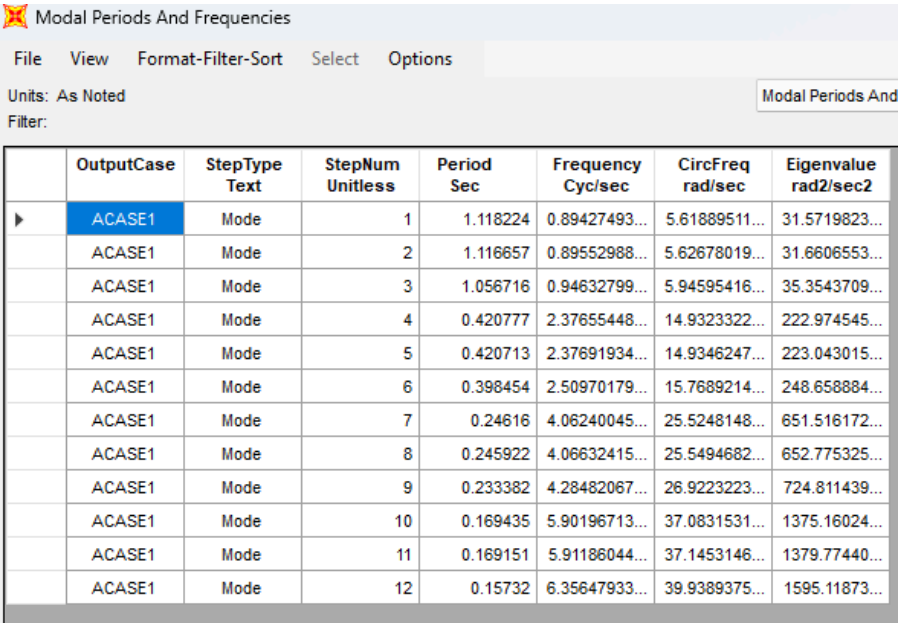

Modal Periods And Frequencies

File View Format-Filter-Sort Select Options

Units: As Noted

Filter:

	OutputCase	StepType Text	StepNum Unitless	Period Sec	Frequency Cyc/sec	CircFreq rad/sec	Eigenvalue rad2/sec2
▶	ACASE1	Mode	1	1.118224	0.89427493...	5.61889511...	31.5719823...
	ACASE1	Mode	2	1.116657	0.89552988...	5.62678019...	31.6606553...
	ACASE1	Mode	3	1.056716	0.94632799...	5.94595416...	35.3543709...
	ACASE1	Mode	4	0.420777	2.37655448...	14.9323322...	222.974545...
	ACASE1	Mode	5	0.420713	2.37691934...	14.9346247...	223.043015...
	ACASE1	Mode	6	0.398454	2.50970179...	15.7689214...	248.658884...
	ACASE1	Mode	7	0.24616	4.06240045...	25.5248148...	651.516172...
	ACASE1	Mode	8	0.245922	4.06632415...	25.5494682...	652.775325...
	ACASE1	Mode	9	0.233382	4.28482067...	26.9223223...	724.811439...
	ACASE1	Mode	10	0.169435	5.90196713...	37.0831531...	1375.16024...
	ACASE1	Mode	11	0.169151	5.91186044...	37.1453146...	1379.77440...
	ACASE1	Mode	12	0.15732	6.35647933...	39.9389375...	1595.11873...

Figure 3.4. Modal analysis for the fundamental period in SAP 2000.

For the fundamental period, both actual and approximate fundamental periods were calculated and the smaller value was chosen for a conservative design.

$$T \leq C_u T_a$$

Given that the S_{D1} value is bigger than 0.4, the C_u was taken as 1.4.

An approximate period was calculated as:

$$T_a = C_t h_n^{\,x}$$

Structure Type	C_t	x
Moment-resisting frame systems in which the frames resist 100% of the required seismic force and are not enclosed or adjoined by components that are more rigid and will prevent the frames from deflecting where subjected to seismic forces:		
Steel moment-resisting frames	0.028 (0.0724)[a]	0.8
Concrete moment-resisting frames	0.016 (0.0466)[a]	0.9
Steel eccentrically braced frames in accordance with Table 12.2-1 lines B1 or D1	0.03 (0.0731)[a]	0.75
Steel buckling-restrained braced frames	0.03 (0.0731)[a]	0.75
All other structural systems	0.02 (0.0488)[a]	0.75

[a]Metric equivalents are shown in parentheses.

Figure 3.5. Corresponding values for special RC moment frames.

It can be seen from the figure, that C_t=0.0466, amd x=0.9. The height of the building is 39.5 m. With the given data, fundamental periods were calculated.

Table 3.32. Calculated design properties.

x	0.9
Ct	0.0466
Cu	1.4
Ta	1.274
T	**1.784**

3.2.5.2. Base Shear Calculations

The base shear was calculated by using the following formula:

$$V = C_s W$$

Seismic response coefficients were calculated by the following formulas:

$$C_s = min[\frac{S_{DS}}{R/I_e}, \frac{S_{D1}}{(T(R/I_e))}], \text{ since T=1.784<} T_L$$

$$C_{s,\,min} = \frac{0.5S_1}{R/I_e}. \text{ sinse S1=0.928g > 0.6g}$$

The weight of each floor was calculated by taking into account the structural weight of the components along with the dead loads calculated in the previous sections.

The total building weight was calculated as the summation of all floor weights. The total weight of the building was calculated as 284669 kN.

The following table presents the completed calculations for the base shear.

Table 3.33. Base shear calculations.

Cs	0.070
Cs,max	0.070
Cs,min	0.058
Vu = CsW	**19926 kN**

3.2.5.3. Equivalent lateral force procedure

The story seismic force was found by the following formulas:

$$F_x = C_{vx} V$$

$$C_{vx} = \frac{w_x h_x^{\,k}}{\sum_{i=1}^{n} w_i h_i^{\,k}}$$

Given that k value for T≤0.5 s is 1, and for T≥2.5 s is 2, interpolation method was used to calculate the value for the fundamental period T=1.784:

$$k = \frac{2-1}{2.5-0.5} * 1.784 + 1 = 1.892$$

Table 3.34. Equivalent seismic force on each floor.

Floors	hi (m)	Wx (kN)	Wx*hxk	Cvx	Fx (kN)
12	36.5	29759.2	3737307	0.24	4269.94
11	33.5	19182.5	2146841	0.14	2452.80
10	30.5	19182.5	1892601	0.12	2162.33
9	27.5	19865.9	1705492	0.11	1948.55
8	24.5	19865.9	1460330	0.09	1668.45
7	21.5	19865.9	1225286	0.08	1399.91
6	18.5	20473.4	1031890	0.07	1178.95
5	15.5	20473.4	813578	0.05	929.53
4	12.5	20473.4	609378	0.04	696.23
3	9.5	21202.4	436471	0.03	498.68
2	6.5	21202.4	262140	0.02	299.50
1	3.5	21081.7	113465	0.01	129.64

3.2.5.4. Torsional Effect

In-plane torsion effect was checked by calculating the location of the mass center and the stiffness center. Even though the shear walls were not placed yet, as their design will be considered in the next part of the report, the mass and stiffness centres do not align due to the presence of elevator and stairs shafts. In order to calculate the coordinates of the mass center, the following formula was used:

$$y = \frac{y_{floor}A_{floor} - y_{elevator\ shaft}A_{elevator\ shaft} - y_{stairs\ shaft}A_{stairs\ shaft}}{A_{floors} - A_{shafts}}$$

The coordinates and areas of the shafts are given in the table:

Table 3.35. Shafts' coordinates and areas.

	Area	x dist, m	y dist, m
Elevator shaft	40.88	25	7.5
Stair #1 shaft	40.88	25	12.5
Stair #2 shaft	40.88	25	15

Area of the floor represents the total area of the slabs, which is 1050 m2. The center of the slabs is at y=15 m, which is exactly at the center of the building due to its symmetric design. By using the above formula, it was found that the coordinates of the mass centre are x=30 m and y=15.44 m. The stiffness centre has coordinates of y=15 m and x=30 m. The eccentricity is the difference between these centres.

$$e_y' = 15.44 - 15 = 0.44\,m$$

An accidental torsion was also considered as 5% of the building dimensions perpendicular to the horizontal load.

$$e_{ax} = 0.05 * 50\,m = 2.5\,m$$

$$e_{ay} = 0.05 * 30\,m = 1.5\,m$$

The eccentricity values used for the torsional effect are the summation of both eccentricities. The final results are shown in the following table:

Table 3.36. Eccentricity values.

e_x'	0
e_y'	0.44
e_{ax}	2.5
e_{ay}	1.5
e_x	**2.5**
e_y	**1.94**

Force considering the torsional effect was calculated as:

$$T = eF$$

Direct force per frame was also calculated:

$$F_{direct} = \frac{F}{\#of\ frames}$$

Table 3.37. Direct and torsional forces per each floor.

	Longitudinal (y)			*Transverse (x)*		
Floor	Fx (kN)	F direct (kN)	T (kN- m)	Fx (kN)	F direct (kN)	T (kN-m)
12	4012.88	668.81	7788.28	4012.88	364.81	10032.19
11	2326.23	387.70	4514.79	2326.23	211.48	5815.57
10	2073.05	345.51	4023.41	2073.05	188.46	5182.62
9	1827.55	304.59	3546.94	1827.55	166.14	4568.87
8	1646.87	274.48	3196.28	1646.87	149.72	4117.17
7	1410.13	235.02	2736.82	1410.13	128.19	3525.33
6	1183.17	197.19	2296.32	1183.17	107.56	2957.92
5	996.42	166.07	1933.87	996.42	90.58	2491.05
4	785.61	130.94	1524.73	785.61	71.42	1964.03
3	588.43	98.07	1142.04	588.43	53.49	1471.08
2	421.47	70.24	817.99	421.47	38.32	1053.67
1	253.13	42.19	491.28	253.13	23.01	632.82

3.2.5.5. Frame stiffness

Frame stiffness was calculated by using the following formula:

$$D = \frac{12E}{h^2} * \frac{I_b I_c}{(LI_c + hI_b)}$$

$$I_{b,cr} = 0.35 * \frac{bh^3}{12}$$

$$I_{b,cr} = 0.7 * \frac{bh^3}{12}$$

Forces needed to generate a unit inter-story rotation are calculated as:

$$C_F = h\Sigma D_j$$

Table 3.38. Frame stiffness calculations.

							x	y
Floor	**Column size**	**Ic,cr, m4**	**Ib,cr, m4**	**Minor b, Ib,cr**	**D, kN/m**	**h, m**	**Cf, kN/rad**	**Cf, kN/rad**
1	0.850	3.05E-02	3.73E-04	1.23E-04	2156	3.5	407427	37725
2	0.850	3.05E-02	3.73E-04	1.23E-04	2938	3	475911	44066
3	0.850	3.05E-02	3.73E-04	1.23E-04	2938	3	475911	44066
4	0.750	1.85E-02	3.73E-04	1.23E-04	2924	3	473663	43858
5	0.750	1.85E-02	3.73E-04	1.23E-04	2924	3	473663	43858
6	0.750	1.85E-02	3.73E-04	1.23E-04	2924	3	473663	43858
7	0.600	1.85E-02	3.73E-04	1.23E-04	2924	3	473663	43858
8	0.600	7.56E-03	3.73E-04	1.23E-04	2874	3	465615	43113
9	0.600	7.56E-03	3.73E-04	1.23E-04	2874	3	465615	43113
10	0.450	7.56E-03	3.73E-04	1.23E-04	2874	3	465615	43113
11	0.450	2.39E-03	3.73E-04	1.23E-04	2706	3	438361	40589
12	0.450	2.39E-03	3.73E-04	1.23E-04	2706	3	438361	40589

3.3. SAP 2000 model

3.3.1. Model geometry

The 3D frame was built in the SAP 200 software.

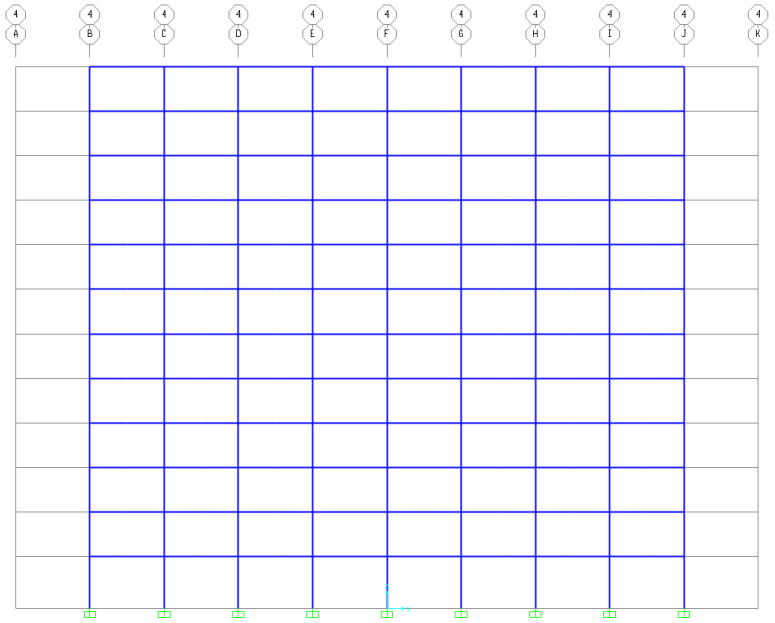

Figure 3.6. 2D frame, x-z view.

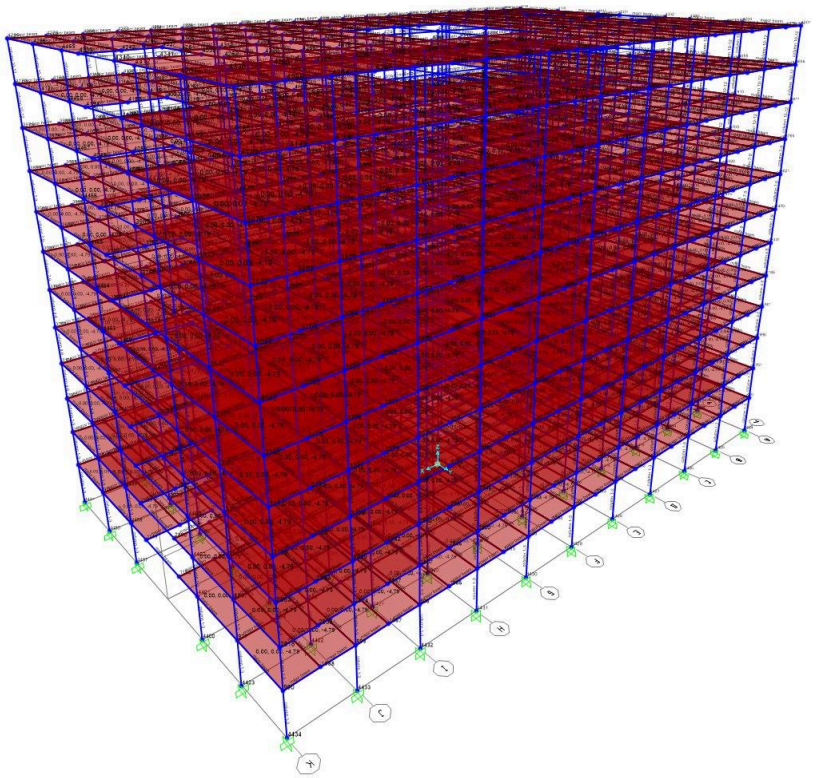

Figure 3.7. SAP 2000 3D Model.

The materials assigned for the frame are C25/30 concrete and grade 60 steel, which is suggested by the EuroCode design.

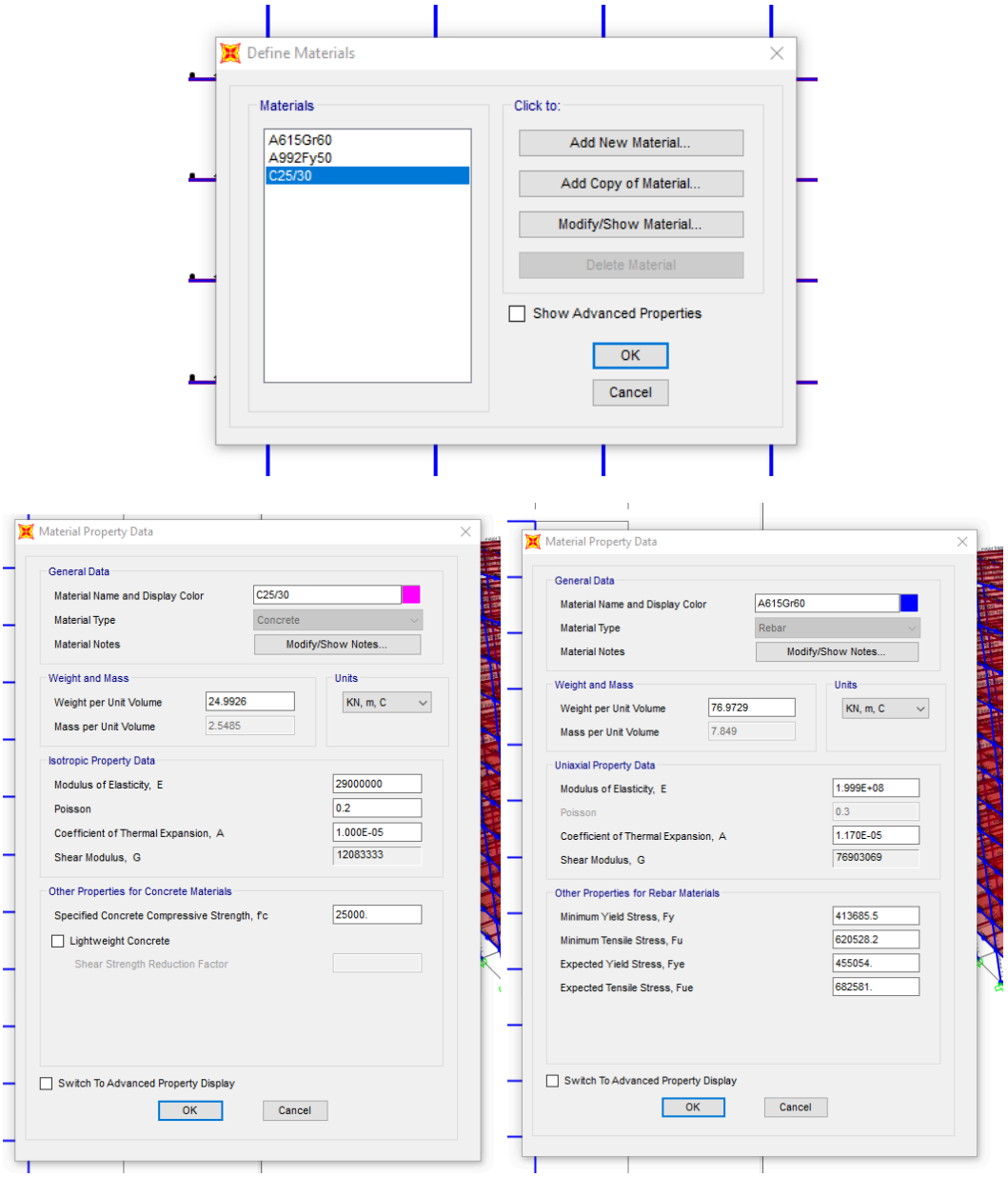

Figures 3.8-3.10. Assigned materials and their properties.

Cross sectional dimensions were also assigned considering the cracking effect in the ‘set modifiers’ section. The modification factor is 0.7 for columns and 0.35 for beams.

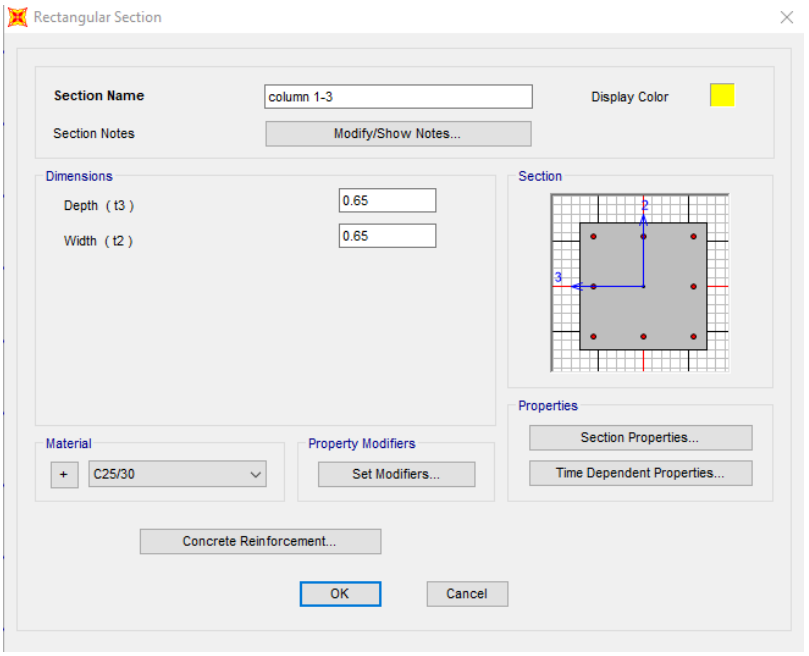

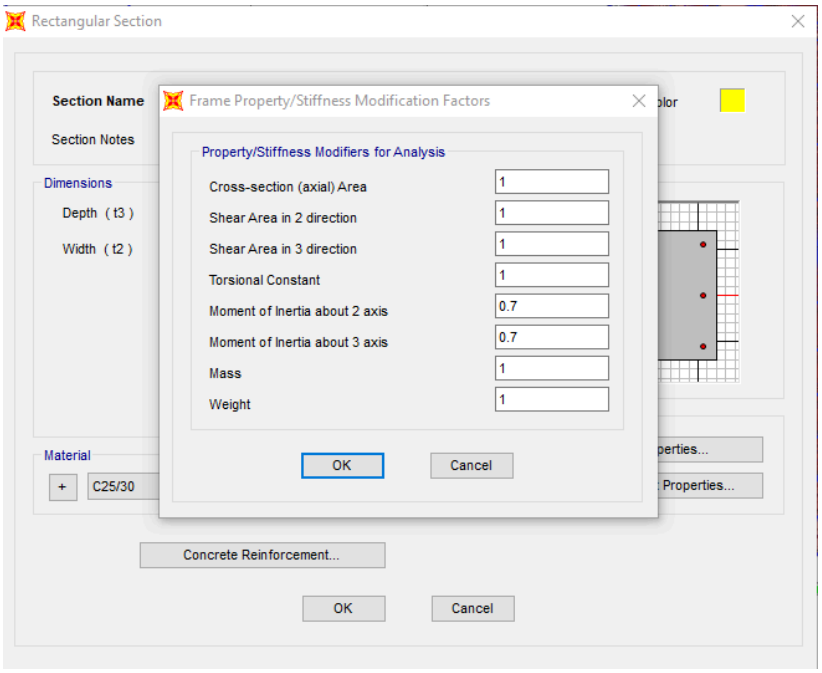

Figures 3.11-3.12. Assigning column frame sections considering the cracking effect.

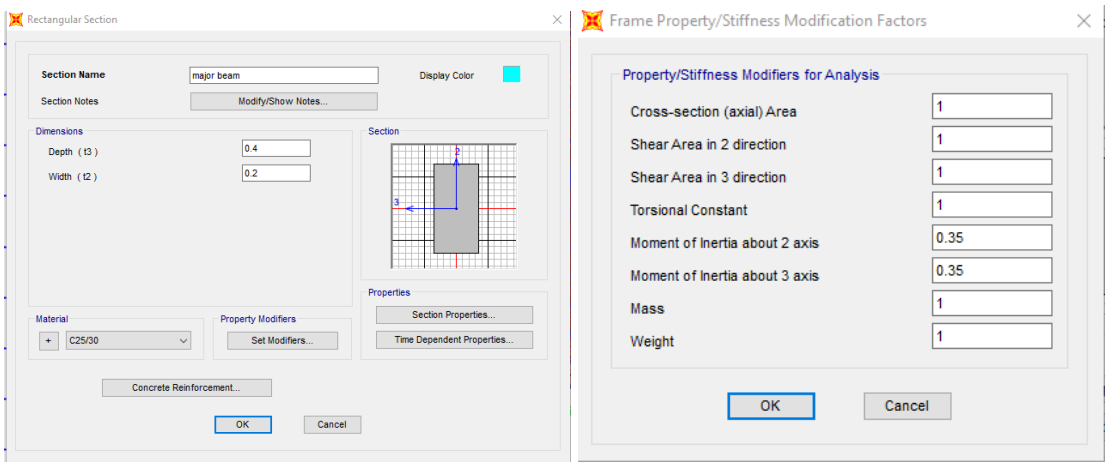

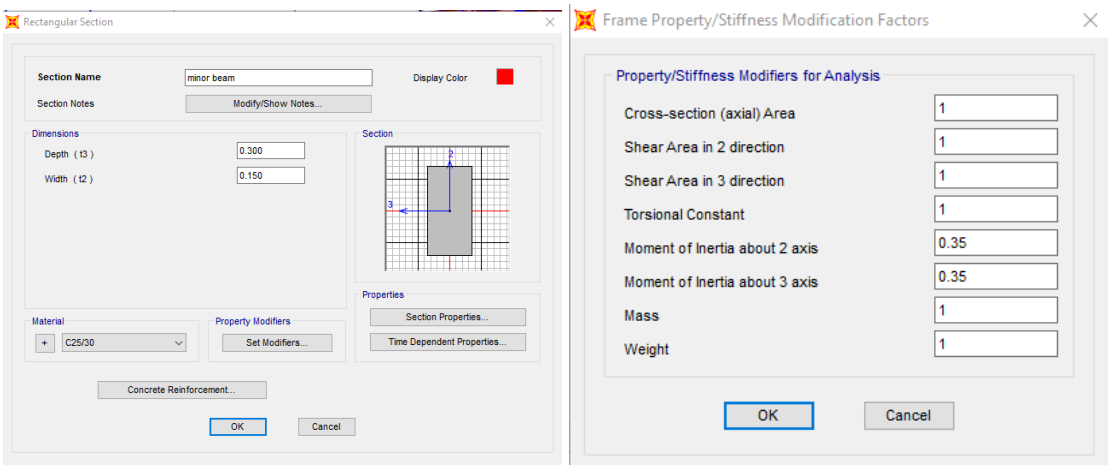

Figures 3.13-3.16. Major and minor beams cross sectional properties.

Structural slab was assigned as an area section:

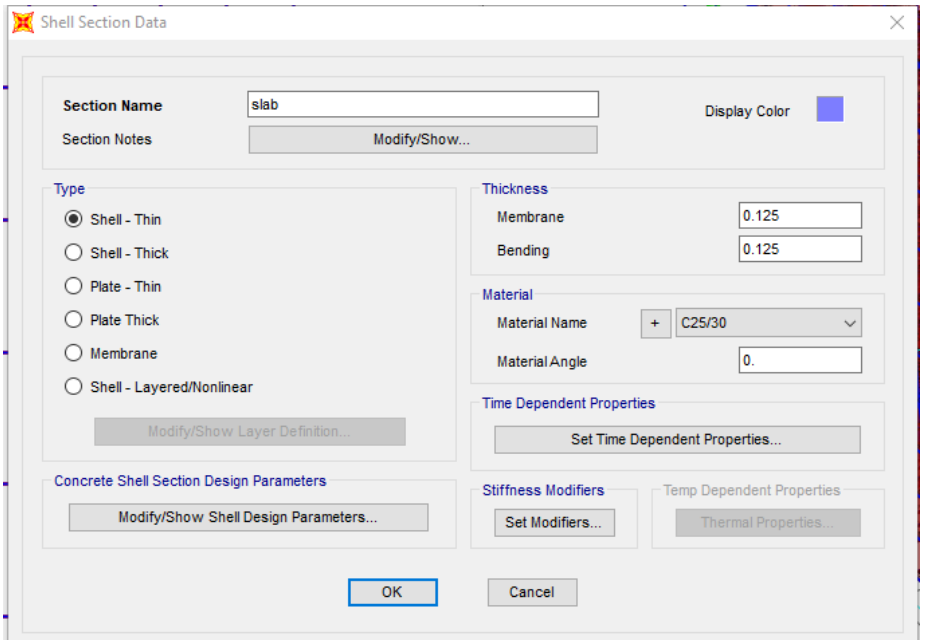

Figure 3.17. Assigning slab properties to the area sections.

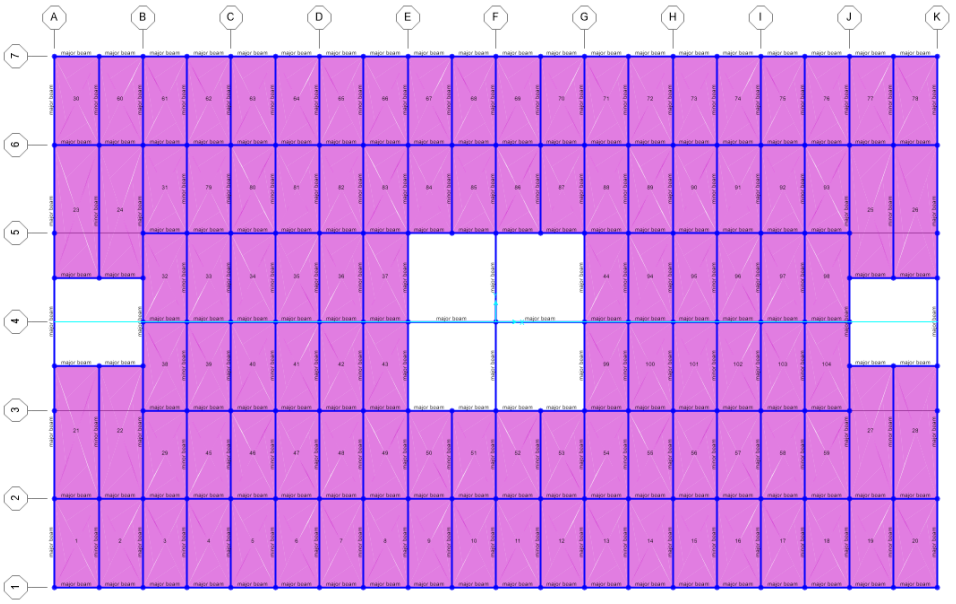

Figure 3.18. Structural layout assigned to the SAP 2000 model.

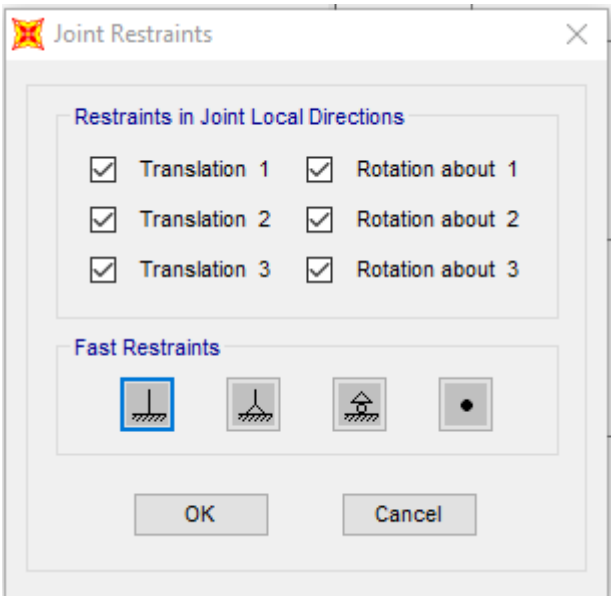

Figure 3.19. Assigned joint restraints.

Fixed joint restraints were assigned. Dead, live, and roof loads were assigned to the slab area sections as shown in the following figures:

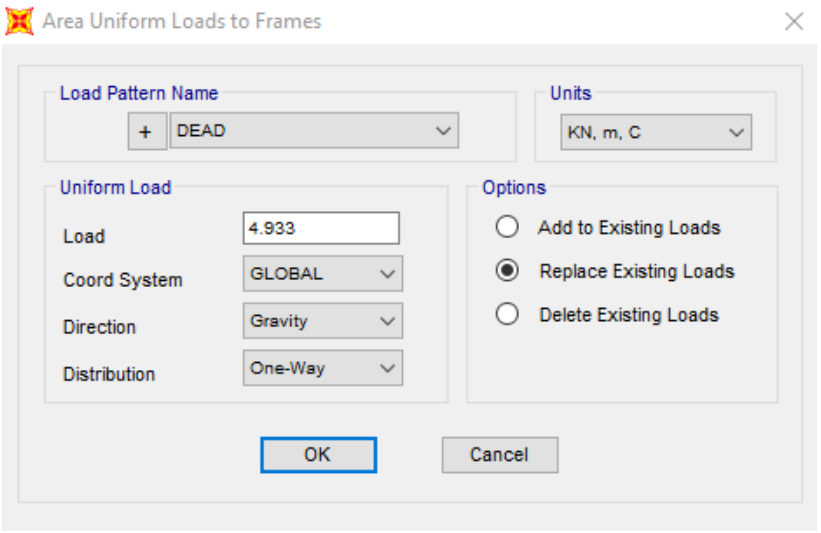

Figure 3.20. Dead loads assigned to the second floor slab.

Wind loads calculated for each floor were assigned to joints separately, as shown in the following figure.

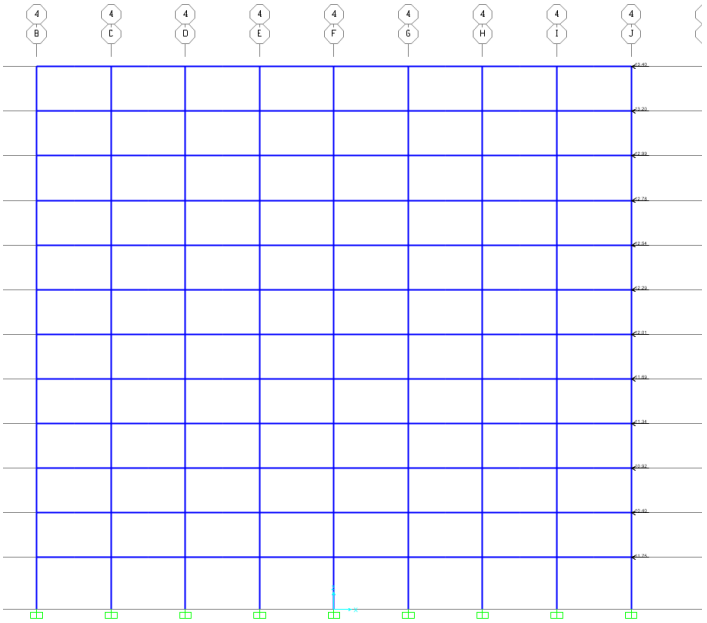

Figure 3.21. Assigned wind loads to the x-z frame

3.6.2. Analysis of the 3D frame under lateral loads.

The design load combination was defined according to the following ASCE equation:

$$\varphi P_{max} = 1.2D + 1.6L + 0.5L_r$$

By running an analysis, the following deformed shape was generated by the software:

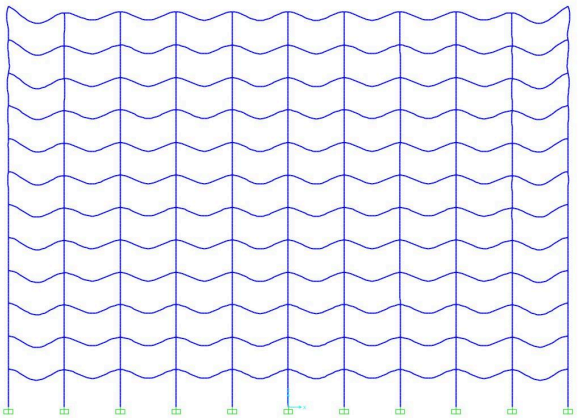

Figure 3.22. Deformed shape of 2D frame, x-z plane.

Axial, shear, and moment diagrams were also provided:

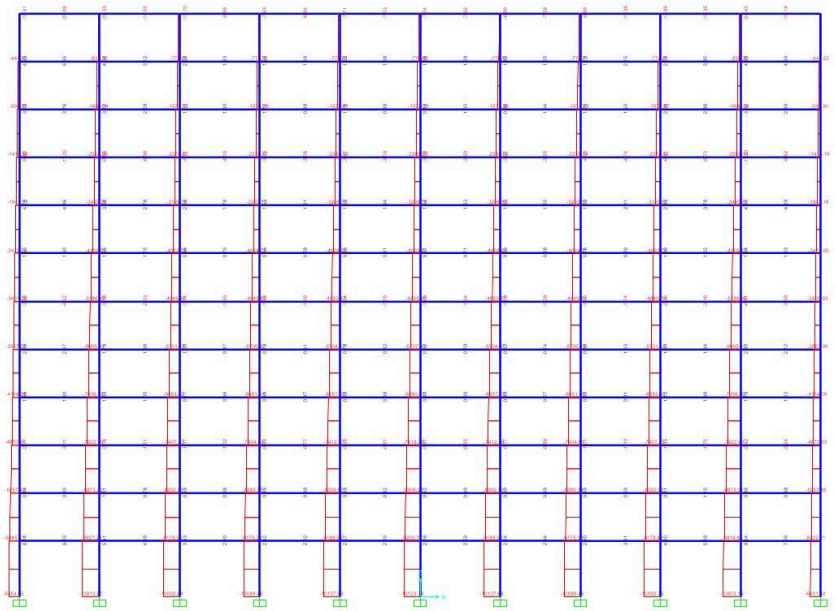

Figure 3.23. Axial force diagram under combination gravity loads.

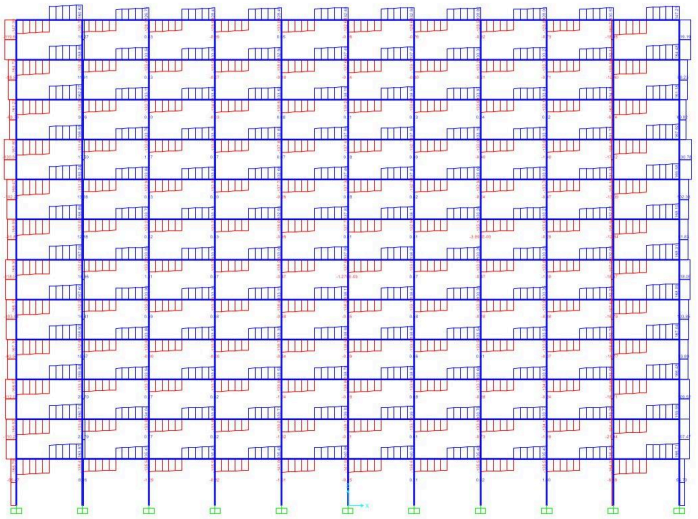

Figure 3.24. Shear force diagram under combination gravity loads.

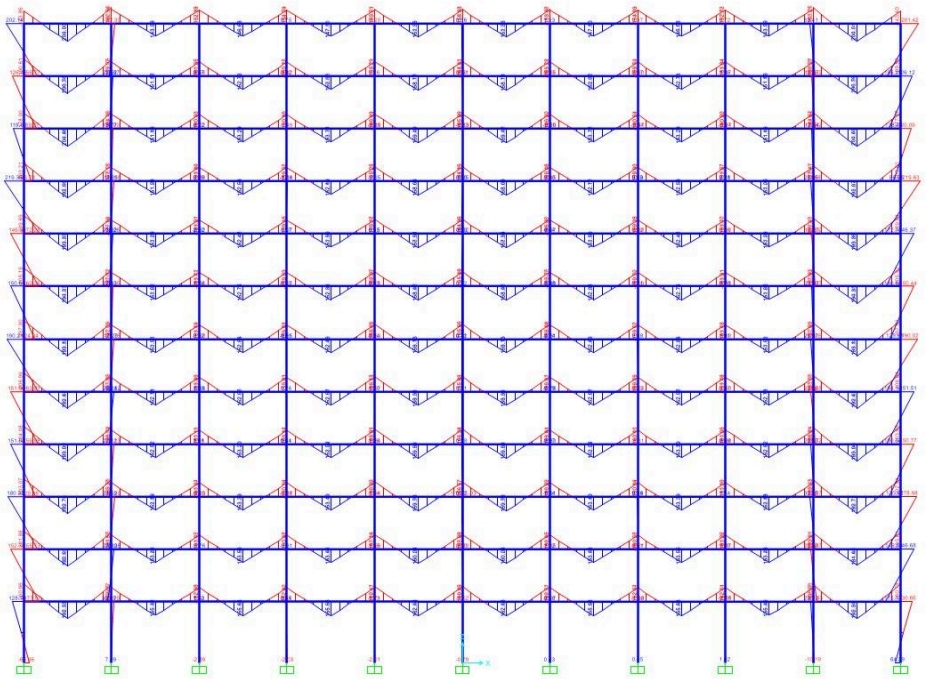

Figure 3.25. Moment diagram under combination gravity loads.

At the base of the basement floor columns, fixed supports were assigned, fully restraining all translations and rotations. At the interface between the basement and the first floor, where the structure interacts with the ground, vertical and horizontal displacements were restrained, while rotational degrees of freedom were released. This allows the building to rotate under lateral loads, such as those from seismic action, while preventing any translational movement at these joints.

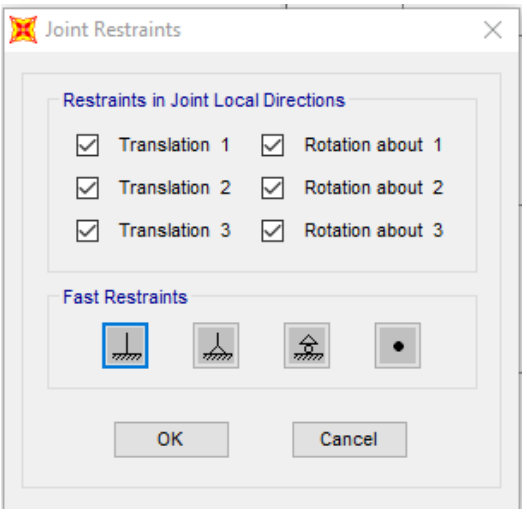

Figure 3.26. Assigning joint restraints to the structure.

Final 3D model based on the geometry assigned can be seen in Figure 3.27.

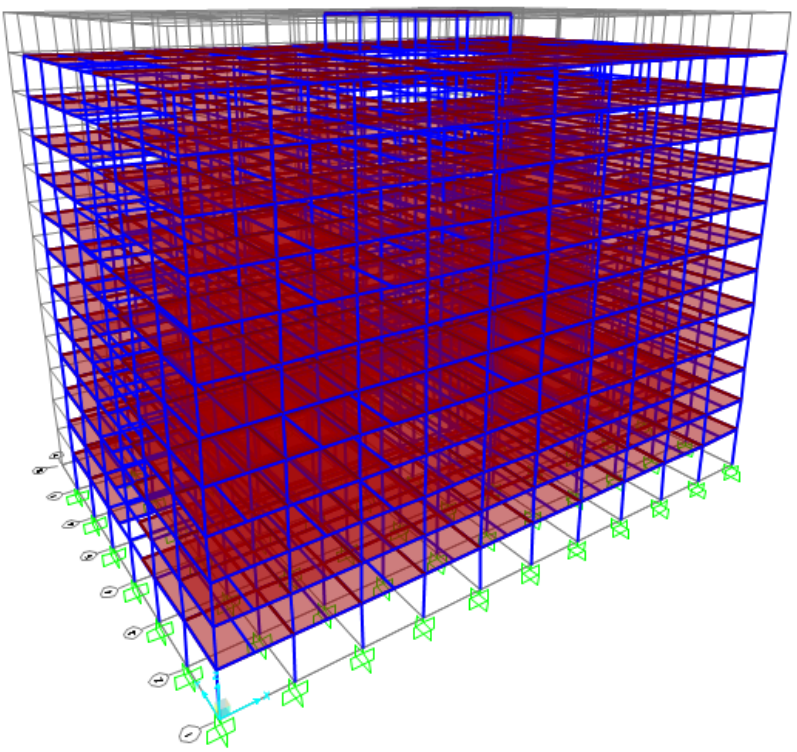

Figure 3.27. SAP 2000 3D Model.

3.3.2. Materials selected

The material properties of the concrete used for the building can be seen in Table 3.6.

Table 3.39. Concrete properties.

Component	**f'_c, MPa**	**ρ, kN/m^3**	**E_c, MPa**	**v**	**G_c, MPa**
Beams, columns slabs	40	23.6	30442	0.2	12684

The C40 grade concrete was chosen for all the structural members due to the common usage of this type of concrete for heavy buildings (Base Concrete, 2023). The Young's modulus of elasticity E_c was calculated using the following formula:

The properties of the reinforcement can be seen in Table 3.7.

Table 3.40. Reinforcing steel properties.

E, MPa	ρ, kN/m^3	v	f_y, MPa
200000	76.97	0.3	413.69

3.4. Structural analysis

3.4.1. Analyzing LFRS to determine the drift.

3.4.1.1. Approximate hand calculations for the frame under wind load.

Since the hand calculations will be compared to SAP2000 results, only Case I in both directions is considered for the drift analysis. The drift check is done using service level (50 years-basic wind speed), without 1.6 load factor from ASCE 7-10.

$$Basic\ wind\ speed\ =\ 110\ Vmph\ =\ 49.2\ m/s$$

Taking the corresponding basic wind speed, new wind loads were calculated and used for drift calculations.

Drift calculations have been performed for frame C in y direction and frame 3 in x direction.

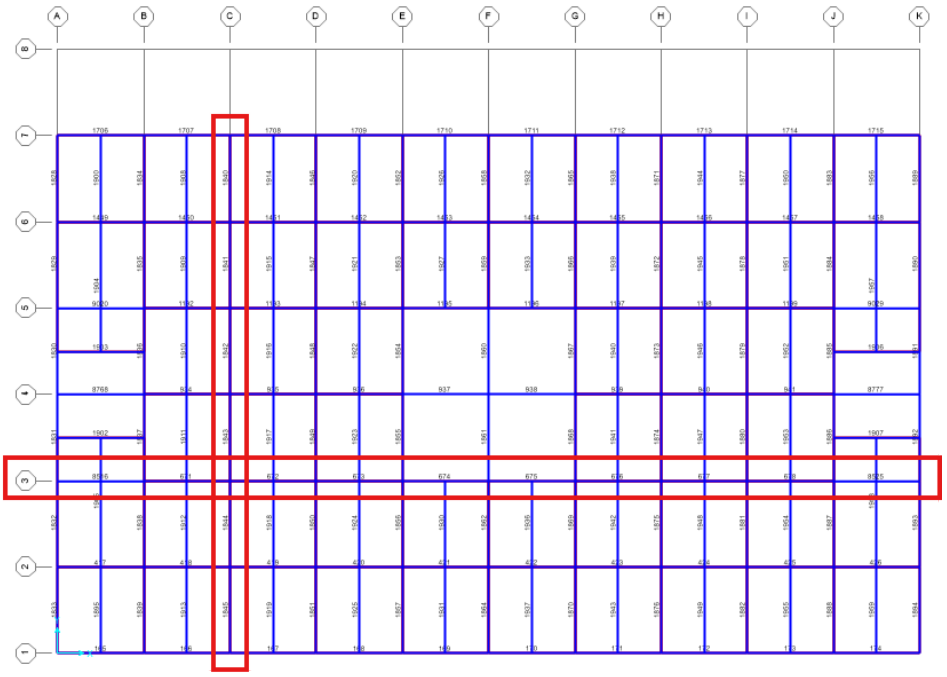

Figure 3.28. Frames chosen for the drift calculations

Cracking moment of inertia coefficient was taken as 0.35 for beams and 0.7 for columns.

Table 3.41. Shear drift under wind load calculations (parallel).

Floor	Fi (kN)	Vi (kN)	Vi col (kN)	Vi avg (kN)	Ic (mm4)	Ib (mm4)	□b (mm)	□c (mm)	□t (mm)	□i (mm)	Δ (mm)
13	31.176	31.2	7.8	7.8	2.36E+08	3.73E+08	0.093	0.177	0.270	0.753	24.806
12	20.624	51.8	13.0	10.4	2.36E+08	3.73E+08	0.496	0.470	0.967	1.205	24.053
11	20.295	72.1	18.0	15.5	2.36E+08	3.73E+08	0.741	0.702	1.443	1.677	22.848
10	19.945	92.0	23.0	20.5	2.36E+08	3.73E+08	0.981	0.930	1.912	1.669	21.171
9	19.571	111.6	27.9	25.5	1.31E+09	3.73E+08	1.218	0.208	1.425	1.505	19.502
8	19.168	130.8	32.7	30.3	2.39E+09	3.73E+08	1.449	0.136	1.585	1.709	17.997
7	18.730	149.5	37.4	35.0	2.39E+09	3.73E+08	1.676	0.157	1.833	1.920	16.288
6	18.248	167.8	41.9	39.7	3.86E+09	3.73E+08	1.897	0.110	2.007	2.104	14.368
5	17.711	185.5	46.4	44.2	5.34E+09	3.73E+08	2.112	0.089	2.201	2.309	12.265
4	17.101	202.6	50.6	48.5	5.34E+09	3.73E+08	2.320	0.097	2.417	2.505	9.956
3	16.386	219.0	54.7	52.7	7.88E+09	3.73E+08	2.520	0.072	2.592	2.681	7.451
2	15.508	234.5	58.6	56.7	1.04E+10	3.73E+08	2.711	0.058	2.769	3.078	4.770
1	17.616	252.1	63.0	60.8	1.04E+10	3.73E+08	3.310	0.076	3.386	1.693	1.693

Table 3.42. Shear drift under wind load calculations (perpendicular).

Floor	Fi (kN)	Vi (kN)	Vi col (kN)	Vi avg (kN)	Ic avg (mm4)	Ib (mm4)	□b (mm)	□c (mm)	□t (mm)	□i (mm)	Δ (mm)
13	59.901	59.9	15.0	15.0	2.36E+08	3.73E+08	0.179	0.340	0.519	1.355	33.429
12	23.795	83.7	20.9	17.9	2.36E+08	3.73E+08	0.859	0.814	1.673	1.948	32.074
11	23.453	107.1	26.8	23.9	2.36E+08	3.73E+08	1.141	1.082	2.223	2.494	30.126
10	23.089	130.2	32.6	29.7	2.36E+08	3.73E+08	1.419	1.346	2.765	2.373	27.632

9	22.700	152.9	38.2	35.4	1.31E+09	3.73E+08	1.693	0.289	1.982	2.064	25.259
8	22.281	175.2	43.8	41.0	2.39E+09	3.73E+08	1.962	0.184	2.146	2.290	23.195
7	21.826	197.0	49.3	46.5	2.39E+09	3.73E+08	2.226	0.208	2.434	2.531	20.905
6	21.325	218.4	54.6	51.9	3.86E+09	3.73E+08	2.484	0.144	2.628	2.739	18.374
5	20.768	239.1	59.8	57.2	5.34E+09	3.73E+08	2.735	0.115	2.850	2.978	15.635
4	20.133	259.3	64.8	62.3	5.34E+09	3.73E+08	2.980	0.125	3.105	3.206	12.658
3	19.390	278.7	69.7	67.2	7.88E+09	3.73E+08	3.216	0.091	3.308	3.412	9.451
2	18.478	297.1	74.3	72.0	1.04E+10	3.73E+08	3.443	0.074	3.517	3.899	6.039
1	20.865	318.0	79.5	76.9	1.04E+10	3.73E+08	4.185	0.096	4.281	2.140	2.140

Table 3.43. Flexural drift under wind load calculations (parallel).

Floor	Fi (kN)	Vi (kN)	Mi (kN-mm)	Ac (mm2)	φ(1/mm)	Δθ (rad)	θi (rad)	□i (mm)	Δ (mm)
13	31.176	31.2	93528.69	90000	4.0E-12	1.2E-08	1.2E-06	0.004	0.032
12	20.624	51.8	248930.75	90000	1.1E-11	3.2E-08	1.2E-06	0.004	0.028
11	20.295	72.1	465219.02	90000	2.0E-11	5.9E-08	1.2E-06	0.004	0.024
10	19.945	92.0	741343.69	90000	3.1E-11	9.4E-08	1.1E-06	0.003	0.021
9	19.571	111.6	1076181.79	202500	2.0E-11	6.1E-08	1.0E-06	0.003	0.018
8	19.168	130.8	1468523.62	202500	2.8E-11	8.3E-08	9.6E-07	0.003	0.014
7	18.730	149.5	1917054.59	202500	3.6E-11	1.1E-07	8.8E-07	0.003	0.012

6	18.248	167.8	2420330.21	302500	3.0E-11	9.1E-08	7.7E-07	0.002	0.009
5	17.711	185.5	2976740.01	302500	3.7E-11	1.1E-07	6.8E-07	0.002	0.007
4	17.101	202.6	3584452.33	302500	4.5E-11	1.4E-07	5.7E-07	0.002	0.005
3	16.386	219.0	4241322.11	422500	3.8E-11	1.1E-07	4.3E-07	0.001	0.003
2	15.508	234.5	4944715.71	422500	4.5E-11	1.3E-07	3.2E-07	0.001	0.002
1	17.616	252.1	5826996.33	422500	5.3E-11	1.8E-07	1.8E-07	0.001	0.001

Table 3.44. Flexural drift under wind load calculations (perpendicular).

Floor	Fi (kN)	Vi (kN)	Mi (kN-mm)	Ac (mm2)	φ(1/mm)	Δθ (rad)	θi (rad)	□i (mm)	Δ (mm)
13	59.901	59.9	179704.41	90000	7.6E-12	2.3E-08	1.7E-06	0.005	0.044
12	23.795	83.7	430792.76	90000	1.8E-11	5.5E-08	1.7E-06	0.005	0.038
11	23.453	107.1	752239.23	90000	3.2E-11	9.6E-08	1.6E-06	0.005	0.033
10	23.089	130.2	1142952.92	90000	4.8E-11	1.5E-07	1.6E-06	0.005	0.028
9	22.700	152.9	1601766.90	202500	3.0E-11	9.0E-08	1.4E-06	0.004	0.024
8	22.281	175.2	2127424.13	202500	4.0E-11	1.2E-07	1.3E-06	0.004	0.020
7	21.826	197.0	2718558.55	202500	5.1E-11	1.5E-07	1.2E-06	0.004	0.016
6	21.325	218.4	3373669.13	302500	4.2E-11	1.3E-07	1.0E-06	0.003	0.012
5	20.768	239.1	4091082.37	302500	5.2E-11	1.5E-07	9.1E-07	0.003	0.009
4	20.133	259.3	4868894.90	302500	6.1E-11	1.8E-07	7.6E-07	0.002	0.006

3	19.390	278.7	5704877.70	422500	5.1E-11	1.5E-07	5.8E-07	0.002	0.004
2	18.478	297.1	6596294.04	422500	5.9E-11	1.8E-07	4.2E-07	0.001	0.002
1	20.865	318.0	7709307.12	422500	7.0E-11	2.4E-07	2.4E-07	0.001	0.001

3.4.1.2. Approximate hand calculations for the frame under seismic load.

Table 3.45. Shear drift under seismic load calculations (parallel).

Floor	Fi (kN)	Vi (kN)	Vi col (kN)	Vi avg (kN)	Ic avg (mm4)	Ib (mm4)	□b (mm)	□c (mm)	□t (mm)	□i (mm)	Δ (mm)
13	364.81	364.8	91.2	91.2	2.39E+09	3.73E+08	1.091	0.204	1.295	4.372	189.423
12	211.48	576.3	144.1	117.6	2.36E+08	3.73E+08	4.642	4.401	9.043	10.341	188.064
11	188.46	764.7	191.2	167.6	2.36E+08	3.73E+08	5.975	5.665	11.640	14.084	177.723
10	166.14	930.9	232.7	212.0	2.36E+08	3.73E+08	8.483	8.044	16.527	14.536	163.639
9	149.72	1080.6	270.1	251.4	1.31E+09	3.73E+08	10.718	1.827	12.545	13.208	149.103
8	128.19	1208.8	302.2	286.2	2.39E+09	3.73E+08	12.684	1.188	13.872	14.784	135.895
7	107.56	1316.4	329.1	315.6	2.39E+09	3.73E+08	14.352	1.344	15.696	16.181	121.111
6	90.58	1406.9	351.7	340.4	3.86E+09	3.73E+08	15.753	0.913	16.666	17.138	104.930
5	71.42	1478.4	369.6	360.7	5.34E+09	3.73E+08	16.899	0.709	17.609	18.069	87.793
4	53.49	1531.8	383.0	376.3	5.34E+09	3.73E+08	17.783	0.746	18.529	18.743	69.724
3	38.32	1570.2	392.5	387.8	7.88E+09	3.73E+08	18.433	0.524	18.957	19.115	50.981
2	23.01	1593.2	398.3	395.4	1.04E+10	3.73E+08	18.866	0.406	19.272	20.751	31.866
1	9.96	1603.1	400.8	399.5	1.04E+10	3.73E+08	21.731	0.499	22.230	11.115	11.115

Table 3.46. Shear drift under seismic load calculations (perpendicular).

Floor	Fi (kN)	Vi (kN)	Vi col (kN)	Vi avg (kN)	Ic avg (mm4)	Ib (mm4)	□b (mm)	□c (mm)	□t (mm)	□i (mm)	Δ (mm)
13	668.81	668.8	167.2	167.2	2.39E+09	3.73E+08	1.999	0.374	2.374	8.015	347.276
12	387.70	1056.5	264.1	215.7	2.39E+09	3.73E+08	10.316	0.966	11.282	13.679	339.261
11	345.51	1402.0	350.5	307.3	2.39E+09	3.73E+08	14.700	1.377	16.076	18.201	325.582
10	304.59	1706.6	426.7	388.6	2.39E+09	3.73E+08	18.586	1.741	20.327	22.220	307.381
9	274.48	1981.1	495.3	461.0	2.39E+09	3.73E+08	22.049	2.065	24.113	25.331	285.160
8	235.02	2216.1	554.0	524.7	3.86E+09	3.73E+08	25.095	1.454	26.549	27.695	259.829
7	197.19	2413.3	603.3	578.7	5.34E+09	3.73E+08	27.679	1.162	28.841	29.972	232.134
6	166.07	2579.4	644.8	624.1	5.34E+09	3.73E+08	29.851	1.253	31.104	32.029	202.162
5	130.94	2710.3	677.6	661.2	5.34E+09	3.73E+08	31.627	1.327	32.954	33.667	170.133
4	98.07	2808.4	702.1	689.8	5.34E+09	3.73E+08	32.996	1.385	34.381	34.675	136.465
3	70.24	2878.6	719.7	710.9	7.88E+09	3.73E+08	34.002	0.967	34.970	35.195	101.790
2	42.19	2920.8	730.2	724.9	1.04E+10	3.73E+08	34.675	0.746	35.421	42.153	66.595
1	18.26	2939.1	734.8	732.5	1.04E+10	3.73E+08	47.688	1.197	48.885	24.442	24.442

Table 3.47. Flexural drift under seismic load calculations (perpendicular).

Floor	Fi (kN)	Vi (kN)	Mi (kN-mm)	Ac (mm2)	φ(1/mm)	Δθ (rad)	θi (rad)	□i (mm)	Δ (mm)
13	668.81	668.8	2006438.65	202500	3.8E-11	1.1E-07	1.6E-05	0.047	0.435
12	387.70	1056.5	5175990.46	202500	9.7E-11	2.9E-07	1.6E-05	0.047	0.388

11	345.51	1402.0	9382066.03	202500	1.8E-10	5.3E-07	1.5E-05	0.046	0.341
10	304.59	1706.6	14501914.91	302500	1.8E-10	5.5E-07	1.5E-05	0.044	0.295
9	274.48	1981.1	20445198.29	302500	2.6E-10	7.7E-07	1.4E-05	0.043	0.251
8	235.02	2216.1	27093548.54	302500	3.4E-10	1.0E-06	1.3E-05	0.040	0.208
7	197.19	2413.3	34333483.35	302500	4.3E-10	1.3E-06	1.2E-05	0.037	0.168
6	166.07	2579.4	42071628.58	302500	5.3E-10	1.6E-06	1.1E-05	0.033	0.130
5	130.94	2710.3	50202580.03	422500	4.5E-10	1.4E-06	9.5E-06	0.029	0.097
4	98.07	2808.4	58627747.61	422500	5.3E-10	1.6E-06	8.2E-06	0.025	0.068
3	70.24	2878.6	67263649.27	422500	6.1E-10	1.8E-06	6.6E-06	0.020	0.044
2	42.19	2920.8	76026115.60	422500	6.9E-10	2.1E-06	4.8E-06	0.014	0.024
1	18.26	2939.1	86312905.58	422500	7.8E-10	2.7E-06	2.7E-06	0.010	0.010

Table 3.48. Flexural drift under seismic load calculations (parallel).

Floor	Fi (kN)	Vi (kN)	Mi (kN-mm)	Ac (mm2)	φ(1/mm)	Δθ (rad)	θi (rad)	□i (mm)	Δ (mm)
13	364.81	364.8	1094421.08	90000	4.6E-11	1.4E-07	1.1E-05	0.034	0.284
12	211.48	576.3	2823267.52	90000	1.2E-10	3.6E-07	1.1E-05	0.034	0.250
11	188.46	764.7	5117490.56	90000	2.2E-10	6.5E-07	1.1E-05	0.033	0.216
10	166.14	930.9	7910135.41	90000	3.3E-10	1.0E-06	1.0E-05	0.031	0.183
9	149.72	1080.6	11151926.34	202500	2.1E-10	6.3E-07	9.2E-06	0.028	0.153
8	128.19	1208.8	14778299.20	202500	2.8E-10	8.3E-07	8.6E-06	0.026	0.125
7	107.56	1316.4	18727354.55	202500	3.5E-10	1.1E-06	7.8E-06	0.023	0.099
6	90.58	1406.9	22948161.04	302500	2.9E-10	8.7E-07	6.7E-06	0.020	0.076
5	71.42	1478.4	27383225.47	302500	3.4E-10	1.0E-06	5.8E-06	0.018	0.056

4	53.49	1531.8	31978771.42	302500	4.0E-10	1.2E-06	4.8E-06	0.014	0.038
3	38.32	1570.2	36689263.24	422500	3.3E-10	9.9E-07	3.6E-06	0.011	0.024
2	23.01	1593.2	41468790.33	422500	3.7E-10	1.1E-06	2.6E-06	0.008	0.013
1	9.96	1603.1	47079766.68	422500	4.2E-10	1.5E-06	1.5E-06	0.005	0.005

3.4.1.3. Comparison of hand calculations with 2D and 3D SAP 2000 model results.

The obtained results for the 2D and 3D models are summarized in the following tables:

Table 3.49. Drift under wind load results for the 2D model.

	Wind total drift parallel			Wind total drift perpendicular		
Floor	□i (mm)	Δ (mm)	% drift	□i (mm)	Δ (mm)	% drift
13	0.757	24.832	0.019	1.36	33.473	0.039
12	1.100	28.700	0.037	0.600	18.500	0.065
11	1.900	27.600	0.063	1.000	17.900	0.083
10	2.600	25.700	0.087	1.700	16.900	0.079
9	2.000	23.100	0.067	1.200	15.200	0.069
8	2.300	21.100	0.077	1.500	14.000	0.076
7	2.700	18.800	0.090	1.700	12.500	0.084
6	2.700	16.100	0.090	1.800	10.800	0.091
5	3.000	13.400	0.100	2.000	9.000	0.099
4	3.200	10.400	0.107	2.084	7.000	0.107
3	3.000	7.200	0.100	2.002	4.916	0.114
2	2.600	4.200	0.087	1.790	2.914	0.144

1	1.600	1.600	0.046	1.124	1.124	0.073

Table 3.50. Drift under seismic load results for the 2D model.

	Seismic total drift parallel			Seismic total drift perpendicular		
Floor	□i (mm)	Δ (mm)	% drift	□i (mm)	Δ (mm)	% drift
13	8.062	4.406	0.059	8.062	347.706	0.212
12	11.800	227.100	0.250	13.726	339.648	0.458
11	18.700	215.300	0.332	18.247	325.923	0.608
10	22.500	196.600	0.405	22.264	307.675	0.742
9	17.600	171.600	0.461	25.374	285.411	0.846
8	20.000	154.000	0.504	27.735	260.037	0.925
7	21.900	134.000	0.546	30.010	232.302	1.000
6	21.900	119.900	0.583	32.062	202.292	1.069
5	22.200	90.600	0.613	33.696	170.230	1.123
4	22.100	68.400	0.631	34.700	136.534	1.157
3	19.900	46.300	0.640	35.215	101.834	1.174
2	16.700	26.400	0.767	42.167	66.619	1.406
1	9.700	9.700	0.381	24.452	24.452	0.699

Table 3.51. Drift under wind load results for the 3D model.

	Wind total drift parallel			Wind total drift perpendicular		

Floor	□i (mm)	Δ (mm)	% drift	□i (mm)	Δ (mm)	% drift
13	0.423	18.920	0.012	0.210	15.400	0.010
12	0.600	18.500	0.020	0.450	14.800	0.025
11	1.000	17.900	0.033	0.800	13.700	0.038
10	1.700	16.900	0.057	1.010	12.400	0.046
9	1.200	15.200	0.040	1.200	11.250	0.054
8	1.500	14.000	0.050	1.310	10.010	0.061
7	1.700	12.500	0.057	1.400	9.900	0.065
6	1.800	10.800	0.060	1.500	8.200	0.072
5	2.000	9.000	0.067	1.700	7.800	0.080
4	2.084	7.000	0.069	1.800	6.100	0.092
3	2.002	4.916	0.067	1.870	4.200	0.098
2	1.790	2.914	0.060	1.900	1.900	0.093
1	1.124	1.124	0.037	2.000	0.700	0.080

Table 3.52. Drift under seismic load results for the 3D model.

	Seismic total drift parallel			Seismic total drift perpendicular		
Floor	□i (mm)	Δ (mm)	% drift	□i (mm)	Δ (mm)	% drift
12	5.800	141.100	0.250	13.726	339.648	0.458
11	10.700	135.300	0.332	18.247	325.923	0.608
10	15.100	124.600	0.405	22.264	307.675	0.742

9	10.900	109.500	0.461	25.374	285.411	0.846
8	12.400	98.600	0.504	27.735	260.037	0.925
7	14.000	86.200	0.546	30.010	232.302	1.000
6	13.600	72.200	0.583	32.062	202.292	1.069
5	14.100	58.600	0.613	33.696	170.230	1.123
4	14.300	44.500	0.631	34.700	136.534	1.157
3	12.900	30.200	0.640	35.215	101.834	1.174
2	11.000	17.300	0.767	42.167	66.619	1.406
1	6.300	6.300	0.381	24.452	24.452	0.699

In order to check the allowable limit, the obtained drifts were multiplied by the amplification factor. The structural system used for our building is the moment frame. ASCE 7-10 states that the amplification factor Cd is then equal to 5.5. Therefore, the inter-story deflections were amplified by using the following formula:

$$\delta = \frac{C_d \delta_{xe}}{I_e}$$

C_d=5.5, and δ_{xe} is an inter-story drift.

In order to check the allowable story drift limit under the seismic load, the following formula is used:

$$\Delta_{allowable} = 0.02 * h_{sx}$$

h_{sx} is the story height, which is 3.5 m for the first floor and 3 m for the typical floor.

The drift under wind load is taken as h /600, which is equal to 65.8 given that the h of the building is 39.5 m. The inter-story drift under wind load does not exceed this value.

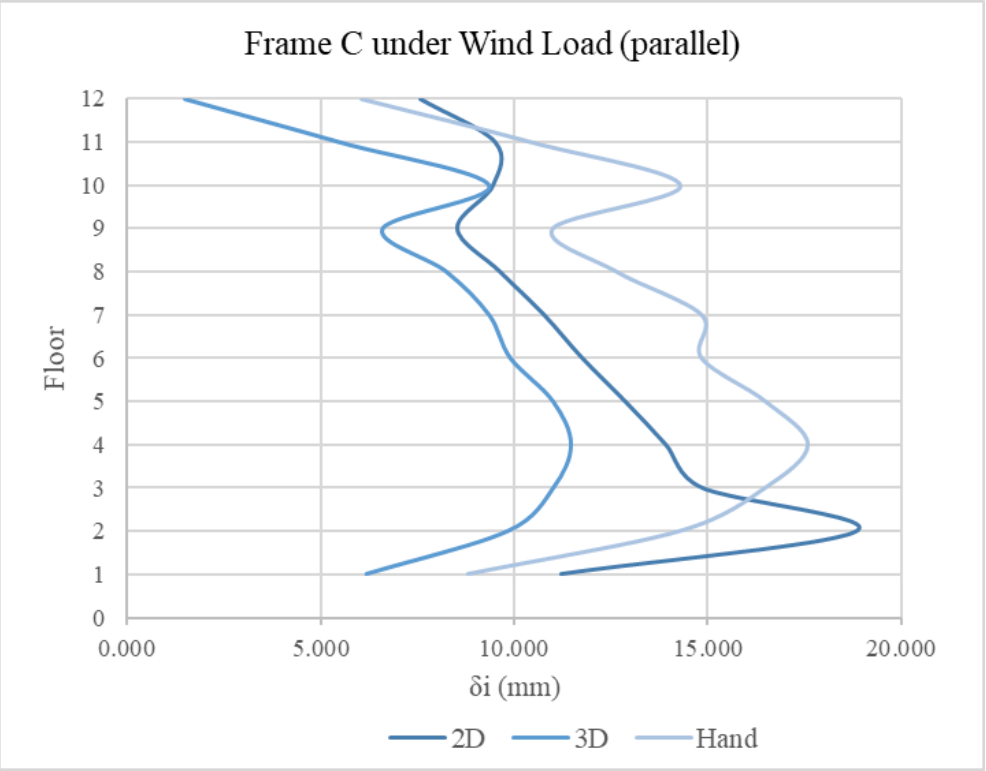

Figure 3.29. Frame C under wind load comparison of hand, 2D, and 3D calculations.

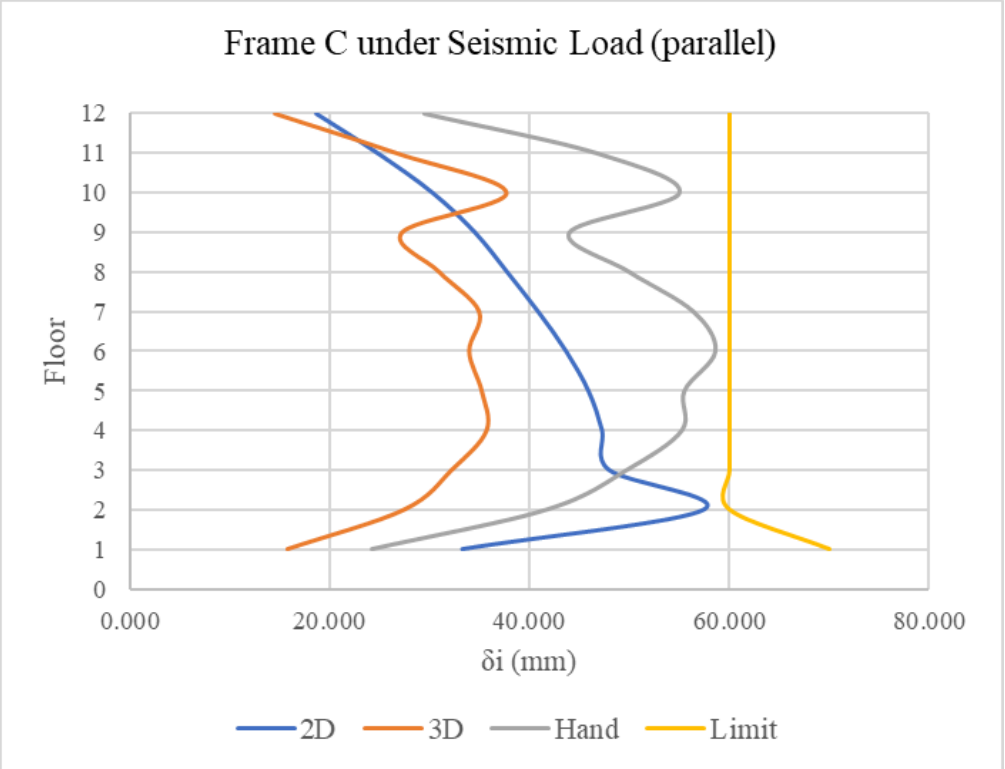

Figure 3.30. Frame C under seismic load comparison of hand, 2D, and 3D calculations.

From the figures above, it can be observed that the deflections obtained from the 2D and 3D are nearly identical, while hand calculations results show some variation. This

discrepancy may be attributed to the fact that wind loads in the 3D SAP2000 model were assigned automatically, potentially differing from the assumptions used in the hand calculations. All wind drift values remained within the allowable limits, thereby meeting structural performance requirements. Similarly, seismic deflections from all three methods were consistent and within the permissible drift limits.

3.4.2. Internal Forces calculation

3.4.2.2. Internal forces verifications under Dead load

Internal beams for floor are arranged as in the Figure below:

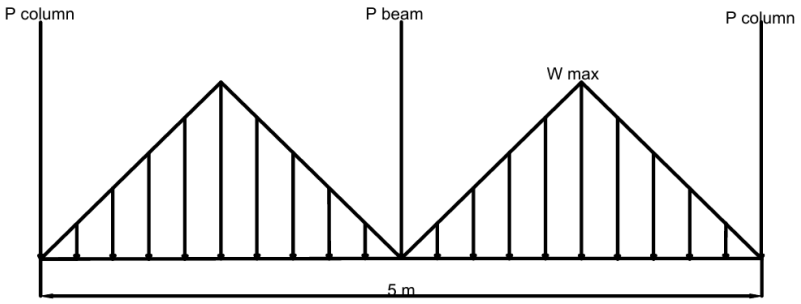

Figure 3.31. Load arrangement in internal beams

Inflection point is assumed to be 0.283L

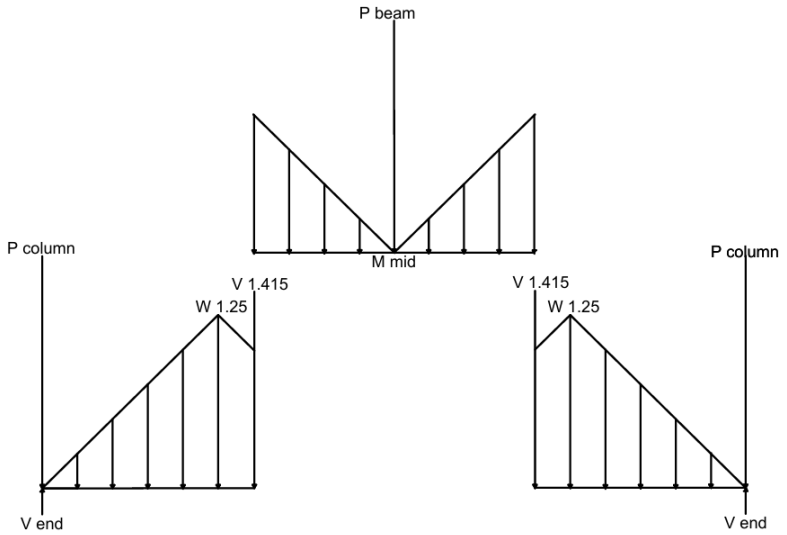

Figure 3.32. Load arrangement after approximate analysis

Here, L = 5 m, 0.283L = 1.415 m, 0.717L = 3.585 m

Floor dead load:

$w_{1.25} = 27.05\ kN/m$

$w_{1.415} = 20.74\ kN/m \rightarrow V_{1.415} = 51.60\ kN$

$V_{end} = 217.15\ kN$

$M_{mid} = 64.13\ kN - m$

$M_{end} = 92.47\ kN - m$

The first floor has different height, so its top and bottom moments need to be calculated:

$$M_{top} = \frac{\frac{1}{L_t}}{\frac{1}{L_t}+\frac{1}{L_b}} * M = 49.79\ kN - m$$

$$M_{bottom} = \frac{\frac{1}{L_b}}{\frac{1}{L_t}+\frac{1}{L_b}} * M = 42.68\ kN - m$$

Roof dead load:

$w_{1.25} = 23.10\ kN/m$

$w_{1.415} = 17.71\ kN/m \rightarrow V_{1.415} = 38.91\ kN$

$V_{end} = 169.15\ kN$

$M_{mid} = 49.17\ kN - m$

$M_{end} = 71.67\ kN - m$

Shear forces:

$$V = \frac{M_{top}+M_{bottom}}{h_i}$$

$For\ floor\ 12\colon\ V\ =\ 33.69\ kN$

$For\ floors\ 1\ -\ 11\colon\ V\ =\ 30.82\ kN$

Axial forces:

$For\ floor\ 12\colon\ V\ =\ 169.15\ kN$

$For\ floor\ 11\colon\ V\ =\ 169.15\ +\ 217.15\ +\ W_{col}\ =\ 392.67\ kN$

And so on.

3.4.2.3. Comparison of internal forces between 2D, 3D, and hand calculations

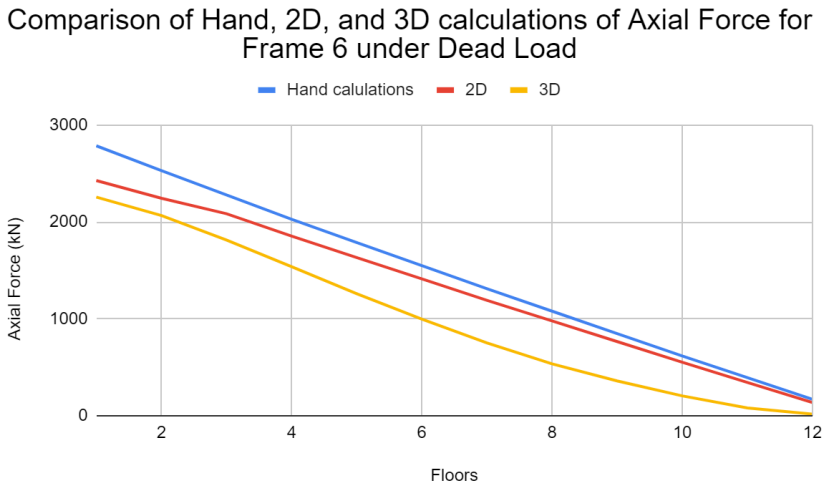

Figure 3.33. Comparison of Hand, 2D, and 3D calculations of Axial Force for Frame 6 under Dead Load

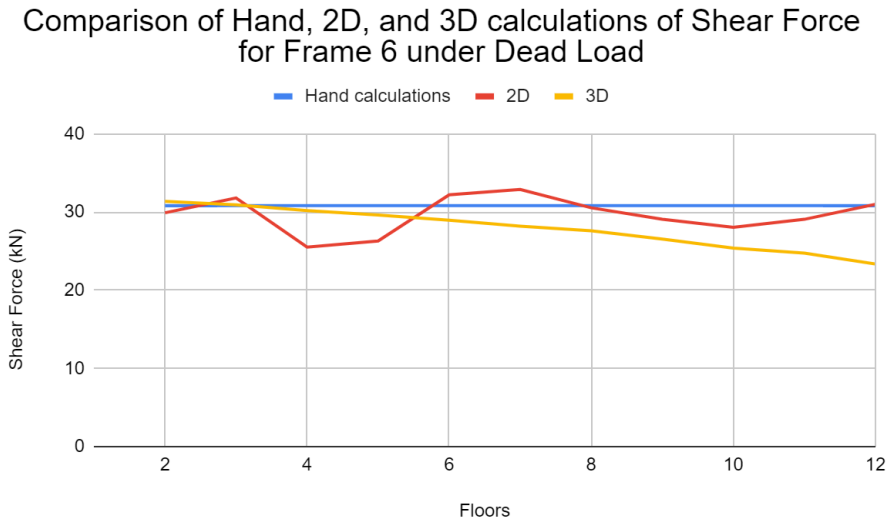

Figure 3.34. Comparison of Hand, 2D, and 3D calculations of Shear Force for Frame 6 under Dead Load

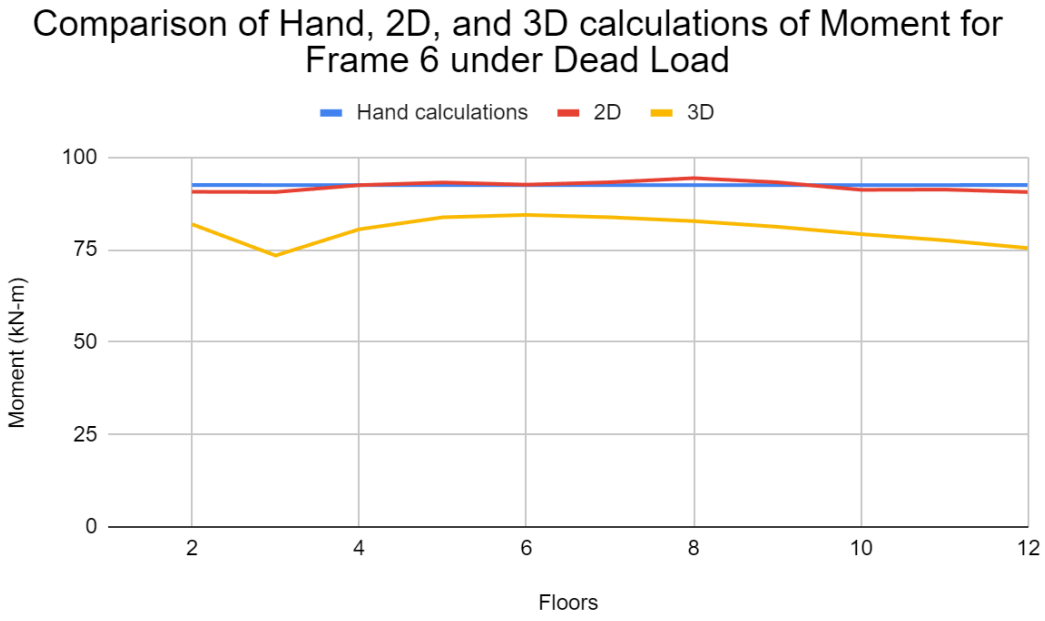

Figure 3.35. Comparison of Hand, 2D, and 3D calculations of Moment for Frame 6 under Dead Load

Table 3.53. Internal forces dealt by Dead Load (Hand Calculations, 2D, 3D)

Floors	Hand calculations	2D	3D

	Axial force	Shear force	Moment	Axial force	Shear force	Moment	Axial force	Shear force	Moment
12	169,1537005	33,6859629	71,66688603	136,846	31,86	72,61	17,1	21,737	73,0417
11	392,6650252	30,82265609	92,46796827	343,636	31	90,59	80,6	23,352	75,4251
10	616,1763498	30,82265609	92,46796827	551,874	29,07	91,26	204,9	24,747	77,5275
9	847,6276745	30,82265609	92,46796827	765,334	28,05	91,19	359,1	25,383	79,2098
8	1079,078999	30,82265609	92,46796827	977,831	29,085	93,23	535,8	26,538	81,1928
7	1310,530324	30,82265609	92,46796827	1191,049	30,54	94,35	751,5	27,597	82,7277
6	1549,051648	30,82265609	92,46796827	1411,689	32,895	93,25	997,1	28,19	83,7697
5	1787,572973	30,82265609	92,46796827	1632,44	32,2	92,58	1259,6	28,953	84,4048
4	2026,094298	30,82265609	92,46796827	1853,731	26,295	93,17	1538,2	29,623	83,7644
3	2277,855622	30,82265609	92,46796827	2084,334	25,515	92,46	1812,7	30,179	80,5238
2	2529,616947	30,82265609	92,46796827	2243,995	31,8	90,60	2065,3	30,917	73,4224
1	2784,838272	30,82265609	92,46796827	2426,111	29,9	90,66	2256,1	31,38	81,8888

3.4.3. Critical load combinations

The load combinations used in the structural analysis were selected in accordance with Chapter 2 of ASCE 7-16. These combinations account for dead, live, roof live, seismic, and wind loads. All relevant wind load cases were incorporated into the analysis and design process. The load combinations created in SAP2000 can be seen on Figure 3.17.

1.4 D
1.2 D + 1.6 L + 0.5 Lr
1.2 D + 1.6 Lr + L
1.2 D + 1.6 Lr + 0.8 W
1.2 D + 1.6 W + L + 0.5 Lr
1.2 D + 1 E + 1 L
0.9 D + 1.6 W
0.9 D + 1 E

Figure 3.36. Design load cases assigned to SAP 2000 model.

During the analysis, the critical load combinations that produced the maximum internal forces and moments were identified: 1.2D + 1.0L ± 1.0Ey. In this project, earthquake forces were found to be controlled in the structural design. This is primarily due to the relatively high seismic demands compared to wind forces, especially in regions classified with significant seismic activity. Unlike wind loads, which are more uniformly distributed and typically reversible, seismic loads are dynamic, multi-directional, and involve rapid ground accelerations that can induce large inertial forces throughout the structure. Therefore, these combinations governed the design for the majority of the structural elements.

3.5. Structural design of members

3.5.1. Structural member design using software

Structural member design was performed in SAP 2000 software for major and minor beams and columns. Since the software does not provide structural design for the slab, the one way slab design calculations were performed by hand. SAP 2000 provided with the critical negative and positive moments, and reinforcement ratio for different segments of the members based on ACI 318 design code requirements. It has also provided with maximum axial loads, shear forces, and moment values for different load combinations. As the critical load combinations were already identified, the corresponding values were taken into consideration for the design. As the goal is to design a stable structure, the critical load cases are used for conservative reinforcement design.

In order to perform accurate design of a structure, the design check was conducted in SAP 2000 software. Member sections were slightly resized in order to pass the design check. Member sizes can be found in section 3.2.

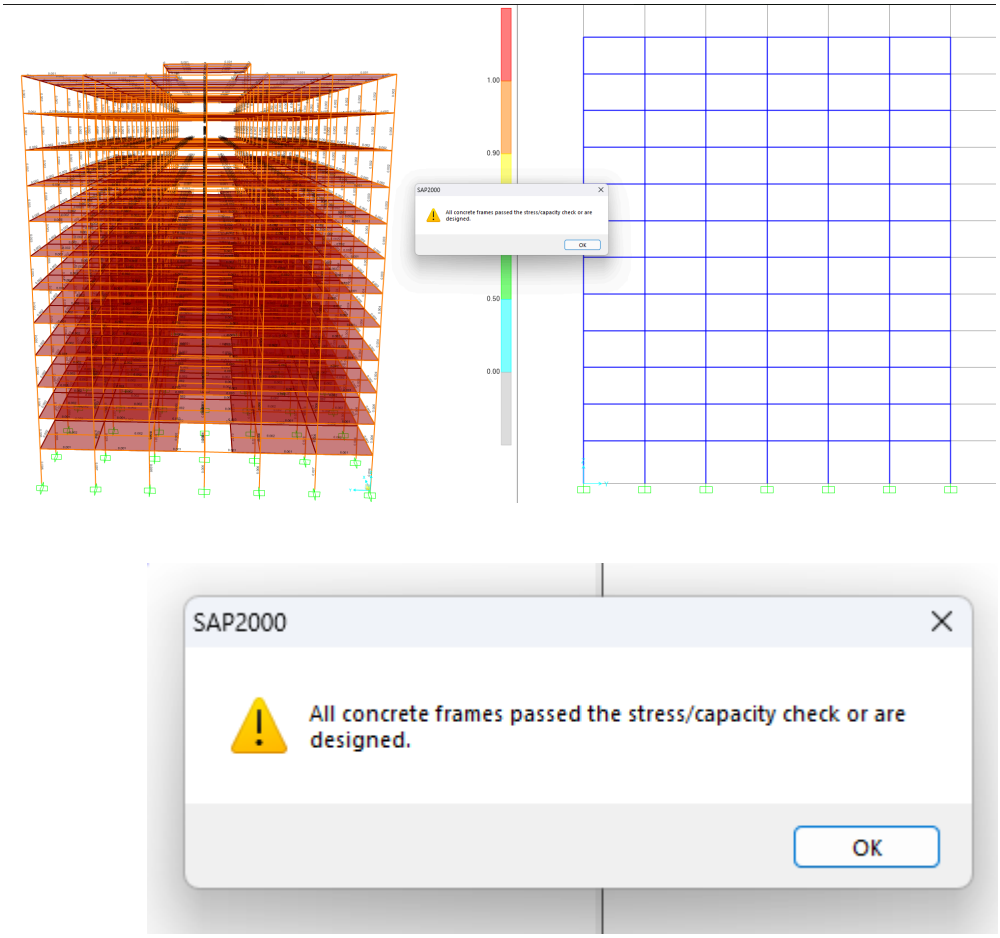

Figure 3.37-3.38. Passed design check of members.

3.5.1.1. Major beam design from SAP 2000

The beam design was performed based on the maximum positive and negative moments from the SAP 2000 analysis. As the earthquake loads are controlled, the biggest values are found for the edge beams on the first floor, given that critical load combinations include gravity loads that are critical in the lowest floor.

Phi(Bending): 0.900
Phi(Shear): 0.750
Phi(Seis Shear): 0.600
Phi(Torsion): 0.750

Design Moments, M3

Positive Moment	Negative Moment	Special +Moment	Special -Moment
189477.644	-57146.121	57146.121	-57146.121

Flexural Reinforcement for Moment, M3

	Required Rebar	+Moment Rebar	-Moment Rebar	Minimum Rebar
Top (+2 Axis)	322.134	0.000	241.600	322.134
Bottom (-2 Axis)	1066.667	815.404	0.000	1066.667

Shear Reinforcement for Shear, V2

Rebar Av/s	Shear Vu	Shear phi*Vc	Shear phi*Vs	Shear Vp
0.000	132.235	199.283	0.000	0.000

Reinforcement for Torsion, T

Rebar At/s	Rebar Al	Torsion Tu	Critical Phi*Tcr	Area Ao	Perimeter Ph
0.000	0.000	529.680	62783.730	213539.729	2044.400

Figure 3.39. Maximum positive moment for the major beam.

Element : 1449 D=0.550 B=0.350 bf=0.350
Section ID : major beam ds=0.000 dct=0.060 dcb=0.060
Combo ID : DCON1 E=29000000.0 fc=25000.000 Lt.Wt. Fac.=1.000
Station Loc : 0.000 L=5.000 fy=413685.473 fys=413685.473

Phi(Bending): 0.900
Phi(Shear): 0.750
Phi(Seis Shear): 0.600
Phi(Torsion): 0.750

Design Moments, M3

Positive Moment	Negative Moment	Special +Moment	Special -Moment
89.908	-179.817	89.908	-179.817

Flexural Reinforcement for Moment, M3

	Required Rebar	+Moment Rebar	-Moment Rebar	Minimum Rebar
Top (+2 Axis)	0.001	0.000	0.001	5.717E-04
Bottom (-2 Axis)	5.717E-04	5.074E-04	0.000	5.717E-04

Shear Reinforcement for Shear, V2

Rebar Av/s	Shear Vu	Shear phi*Vc	Shear phi*Vs	Shear Vp
3.419E-04	158.781	106.803	51.978	0.000

Reinforcement for Torsion, T

Rebar At/s	Rebar Al	Torsion Tu	Critical Phi*Tcr	Area Ao	Perimeter Ph
0.000	0.000	0.394	25.334	0.102	1.444

Figure 3.40. Maximum negative moment for the major beam.

3.5.1.2. Minor beam design from SAP 2000

Minor beam design procedure will follow the major beam design procedure. Therefore, maximum positive and negative moments are identified.

Phi(Bending):	0.900
Phi(Shear):	0.750
Phi(Seis Shear):	0.600
Phi(Torsion):	0.750

Design Moments, M3

Positive Moment	Negative Moment	Special +Moment	Special -Moment
56408.322	-25911.773	25911.773	-25911.773

Flexural Reinforcement for Moment, M3

	Required Rebar	+Moment Rebar	-Moment Rebar	Minimum Rebar
Top (+2 Axis)	213.416	0.000	160.062	213.416
Bottom (-2 Axis)	440.000	353.550	0.000	440.000

Shear Reinforcement for Shear, V2

Rebar Av/s	Shear Vu	Shear phi*Vc	Shear phi*Vs	Shear Vp
0.000	1.527	82.204	0.000	0.000

Reinforcement for Torsion, T

Rebar At/s	Rebar Al	Torsion Tu	Critical Phi*Tcr	Area Ao	Perimeter Ph
0.000	0.000	417.405	17485.426	73765.729	1244.400

Figure 3.41. Maximum positive moment for the minor beam.

Design Moments, M3

Positive Moment	Negative Moment	Special +Moment	Special -Moment
27.239	-54.479	27.239	-54.479

Flexural Reinforcement for Moment, M3

	Required Rebar	+Moment Rebar	-Moment Rebar	Minimum Rebar
Top (+2 Axis)	4.608E-04	0.000	4.608E-04	2.267E-04
Bottom (-2 Axis)	2.267E-04	2.223E-04	0.000	2.267E-04

Shear Reinforcement for Shear, V2

Rebar Av/s	Shear Vu	Shear phi*Vc	Shear phi*Vs	Shear Vp
2.514E-04	68.865	42.348	26.517	0.000

Reinforcement for Torsion, T

Rebar At/s	Rebar Al	Torsion Tu	Critical Phi*Tcr	Area Ao	Perimeter Ph
0.000	0.000	0.623	6.653	0.029	0.844

Figure 3.42. Maximum negative moment for the minor beam.

3.5.1.3. Column design from SAP 2000.

Column design was performed for the corner column.

AXIAL FORCE & BIAXIAL MOMENT DESIGN FOR PU, M2, M3

Rebar Area	Design Pu	Design M2	Design M3	Minimum M2	Minimum M3
3013.074	317.889	-138930.333	-127808.959	9136.140	9136.140

AXIAL FORCE & BIAXIAL MOMENT FACTORS

	Cm Factor	Delta_ns Factor	Delta_s Factor	K Factor	L Length
Major Bending(M3)	0.400	1.000	1.000	1.000	3000.000
Minor Bending(M2)	0.400	1.000	1.000	1.000	3000.000

SHEAR DESIGN FOR V2,V3

	Rebar Av/s	Shear Vu	Shear phi*Vc	Shear phi*Vs	Shear Vp
Major Shear(V2)	0.375	76.760	119.544	44.559	0.000
Minor Shear(V3)	0.375	83.696	119.544	44.559	0.000

JOINT SHEAR DESIGN

	Joint Shear Ratio	Shear VuTop	Shear VuTot	Shear phi*Vc	Joint Area
Major Shear(V2)	N/A	N/A	N/A	N/A	N/A
Minor Shear(V3)	N/A	N/A	N/A	N/A	N/A

(6/5) BEAM/COLUMN CAPACITY RATIOS

Major Ratio	Minor Ratio
N/A	N/A

Notes:
N/A: Not Applicable
N/C: Not Calculated
N/N: Not Needed

Figure 3.43. Design for the corner column from SAP 2000.

3.5.2. Structural design using hand calculations

3.5.2.1. Major beam design

For the main compression and tension reinforcement, rebar design will be conducted based on the critical negative and positive moments. Negative moment is used for the calculation of tension reinforcement, and positive moment for the compression reinforcement of the beam.

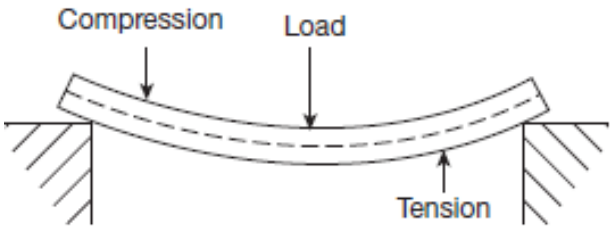

Figure 3.44. Compression and tension sides of the beam under bending.

Negative moment

$$f'_c = 40\ MPa;\ f_y = 413\ MPa$$

$$M_u = -179.817 \text{ kN-m}$$

$$d = h - 2.5\,in = 700\,mm - 2.5\,in * 25.4\,mm/in = 630\,mm$$

$$R_n = \frac{M_u}{\phi bd^2} = \frac{179.817}{0.9*500*630^2} = 634.27\,kN/m^2$$

$$\rho = \frac{0.85f'_c}{f_y}\left[1 - \sqrt{1 - \frac{2R_n}{0.85f'_c}}\right] = 0.001$$

$$A_s = \rho bd = 0.001 * 500 * 630 = 488\,mm^2$$

$$a = \frac{A_s f_y}{0.85f'_c b} = 11.8\,mm$$

$$\beta_1 = 0.85 - 0.05 * \left(\frac{5801-4000}{1000}\right) = 0.76$$

$$c = \frac{a}{\beta_1} = 15.59\,mm$$

$$\varepsilon_t = 0.003\left(\frac{d-c}{c}\right) = 0.11 > 0.005$$

The section is tension controlled and ductile. Given that As calculated by the SAP 2000 is 572 mm2, the error is:

$$Error = \left(\frac{572-488}{572}\right) * 100\% = 14.5\%$$

The large error can be explained by the calculation of both tension and compression reinforcement by SAP 2000. A_s = 488 mm^2 (1.47 in^2) will be used for bar selection. Accordingly, at the negative moment locations, 4#6 bars with A_s = 1.77 in^2 will be chosen. With the assumption that #3 stirrups will be used, b_{min} = 266.7 mm < b = 500 mm.

Positive moment

$$M_u = 189.477 \text{ kN-m}$$

$$d = h - 2.5\,in = 700\,mm - 2.5\,in * 25.4\,mm/in = 630\,mm$$

$$R_n = \frac{M_u}{\phi bd^2} = \frac{189.477}{0.9*500*630^2} = 935.39\,kN/m^2$$

$$\rho = \frac{0.85f'_c}{f_y}\left[1 - \sqrt{1 - \frac{2R_n}{0.85f'_c}}\right] = 0.0022$$

$$A_s = \rho bd = 0.001 * 500 * 630 = 718.81\,mm^2$$

$$a = \frac{A_s f_y}{0.85f'_c b} = 17.4\,mm$$

$$\beta_1 = 0.85 - 0.05 * \left(\frac{5801-4000}{1000}\right) = 0.76$$

$$c = \frac{a}{\beta_1} = 22.9\ mm$$

$$\varepsilon_t = 0.003(\frac{d-c}{c}) = 0.077 > 0.005$$

The section is tension controlled and ductile. Given that As calculated by the SAP 2000 is 1066.667 mm2, the error is:

$$Error = (\frac{1066.667-718.85}{1066.667}) * 100\% = 22\%$$

The large error can be explained by the calculation of both tension and compression reinforcement by SAP 2000. A_s = 1066.67 mm^2 (1.65 in^2) will be used for bar selection. Accordingly, at the negative moment locations, 2#9 bars with A_s = 2 in^2 will be chosen. With the assumption that #3 stirrups will be used, b_{min} = 266.7 mm < b = 500 mm.

Shear reinforcement

The maximum shear value generated in beam sections is 202.215 kN. λ = 1 for normal-weight concrete.

$\phi V_c = \phi * 2\lambda\sqrt{f'_c} b_w d = 95.475\ kN < 202.215\ kN$ - shear reinforcement should be provided.

$$V_{c1} = 4\sqrt{f'_c} b_w d = 254.6\ kN, V_{c2} = 8\sqrt{f'_c} b_w d = 509.2\ kN$$

$$V_s = \frac{V_u - \phi V_c}{\phi} = 142.32 < V_{c1}$$

$$\frac{A_v}{s} = 0.532\ mm^2/mm$$

#3 stirrups at 0.3 m distance should be used.

3.5.2.2. Major beam design

Negative moment

$$f'_c = 40\ MPa;\ f_y = 413\ MPa$$

$$M_u = -\ 103.467 \text{ kN-m}$$

$$d = h - 2.5\ in = 500\ mm - 2.5\ in * 25.4\ mm/in = 436.5\ mm$$

$$R_n = \frac{M_u}{\phi b d^2} = \frac{103.467}{0.9*300*436.5^2} = 2011.2\ kN/m^2$$

$$\rho = \frac{0.85f'_c}{f_y}[1 - \sqrt{1 - \frac{2R_n}{0.85f'_c}}] = 0.005$$

$$A_s = \rho bd = 0.0023 * 300 * 436.5 = 665.285\, mm^2$$

$$a = \frac{A_s f_y}{0.85 f'_c b} = 20.6\, mm$$

$$\beta_1 = 0.85 - 0.05 * (\frac{5801-4000}{1000}) = 0.76$$

$$c = \frac{a}{\beta_1} = 28.61\, mm$$

$$\varepsilon_t = 0.003(\frac{d-c}{c}) = 0.02 > 0.005$$

The section is tension controlled and ductile. Given that As calculated by the SAP 2000 is 785 mm2, the error is:

$$Error = (\frac{785-665.285}{785}) * 100\% = 15.2\,\%$$

The large error can be explained by the calculation of both tension and compression reinforcement by SAP 2000. A_s = 665.285 mm^2 (1.03 in^2) will be used for bar selection. Accordingly, at the negative moment locations, 4#5 bars with A_s = 1.23 in^2 will be chosen. With the assumption that #3 stirrups will be used, b_{min} = 257.32 mm < b = 500 mm.

Positive moment

$$M_u = 56.408 \text{ kN-m}$$

$$d = h - 2.5\, in = 500\, mm - 2.5\, in * 25.4\, mm/in = 436.5\, mm$$

$$R_n = \frac{M_u}{\phi bd^2} = \frac{56.408}{0.9*300*436.5^2} = 986.84\, kN/m^2$$

$$\rho = \frac{0.85 f'_c}{f_y}[1 - \sqrt{1 - \frac{2R_n}{0.85 f'_c}}] = 0.0023$$

$$A_s = \rho bd = 0.0023 * 300 * 436.5 = 312.285\, mm^2$$

$$a = \frac{A_s f_y}{0.85 f'_c b} = 12.6\, mm$$

$$\beta_1 = 0.85 - 0.05 * (\frac{5801-4000}{1000}) = 0.76$$

$$c = \frac{a}{\beta_1} = 16.63\, mm$$

$$\varepsilon_t = 0.003(\frac{d-c}{c}) = 0.028 > 0.005$$

The section is tension controlled and ductile. Given that As calculated by the SAP 2000 is 362 mm2, the error is:

$$Error = (\frac{362-312.285}{362}) * 100\% = 13.7\ \%$$

The large error can be explained by the calculation of both tension and compression reinforcement by SAP 2000. A_s = 362 mm^2 (0.68 in^2) will be used for bar selection. Accordingly, at the negative moment locations, 2#7 bars with A_s = 1.20 in^2 will be chosen. With the assumption that #3 stirrups will be used, b_{min} = 257.32 mm < b = 500 mm.

Shear reinforcement

The maximum shear value generated in beam sections is 126.518 kN. λ = 1 for normal-weight concrete.

$\phi V_c = \phi * 2\lambda\sqrt{f'_c} b_w d = 39.285\ kN < 126.518\ kN$ - shear reinforcement should be provided.

$$V_{c1} = 4\sqrt{f'_c} b_w d = 104.76\ kN, V_{c2} = 8\sqrt{f'_c} b_w d = 209.52\ kN$$

$$V_s = \frac{V_u - \phi V_c}{\phi} = 116.31 < V_{c1}$$

$$\frac{A_v}{s} = 0.63\ mm^2/mm$$

#3 stirrups at 0.2 m distance should be used.

3.5.2.3. Column design

Steel reinforcement was provided for each column type used in the structural design of the building. For the purpose of hand calculation verification, a representative corner column from Floor 19 with cross-sectional dimensions of 0.5 m × 0.5 m was selected. The first step is to assess the slenderness of the column to determine whether it behaves as a short or slender (long) column. Given that the structure lacks lateral bracing or shear walls, the columns are considered *sway* columns, which are more susceptible to second-order effects.

The slenderness ratio check for sway columns is presented below:

$$\Psi_A = \frac{\Sigma(EI/l)columns}{beams} = 0.8$$

$$\Psi_B = \frac{\Sigma(EI/l)columns}{beams} = 0.4$$

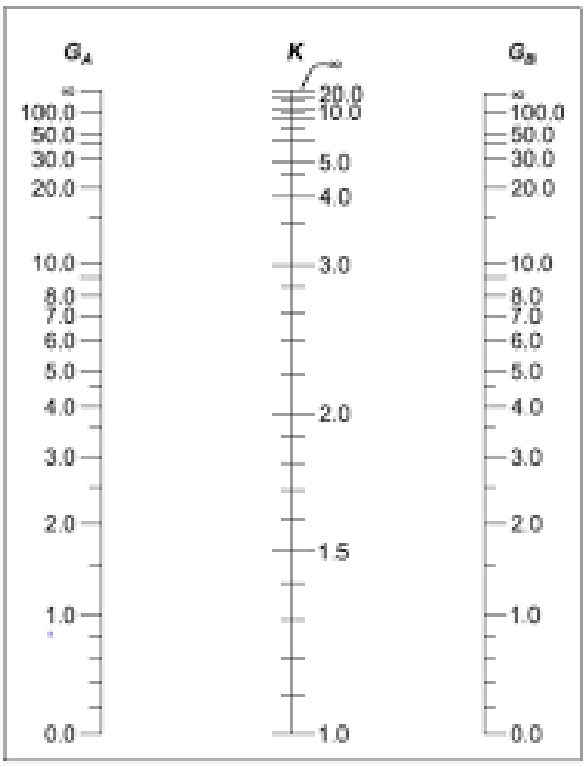

Figure 3.45. Slenderness coefficient k determination.

From the Figure 3.45, k = 1.17. Therefore, the slenderness ratio is 21.375<22. Therefore, short column design will be carried out for the column design. φ for the tied column is 0.65. The values from the SAP 2000 design of the column are the following:

$$M_u = 138.93\ kN - m; M_n = \frac{M_u}{0.65} = 196.62\ kN - m;$$

$$P_u = 317.889\ kN - m; P_n = \frac{P_u}{0.65} = 489.06\ kN - m$$

$$e = \frac{M_n}{P_n} = 0.4$$

$$\gamma = \frac{0.45-0.07*2}{0.45} = 0.69$$

$$K_n = \frac{P_n}{A_g f'_c} = 0.06$$

$$R_n = \frac{P_n e}{A_g f'_c h} = 0.058$$

The interaction diagrams from ACI 318 for different values of γ are used for the determination of reinforcement ratio.

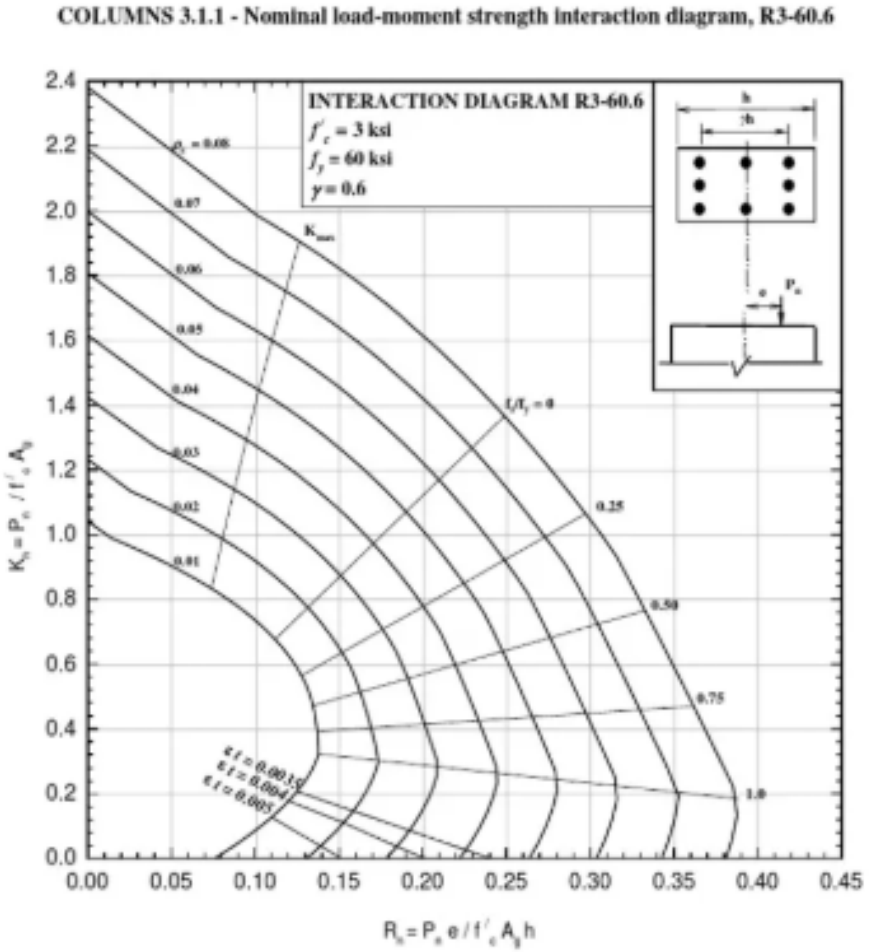

Figure 3.46. Interaction diagram.

$$\rho = 1\%$$

$A_s = 0.01 * A_g = 0.00205\ m^2$ - 6#7 bars are selected.

Shear reinforcement

$$V_c = 0.17(1 + \frac{P_u}{14A_g})\lambda\sqrt{f'_c}b_w d = 712.95\ kN$$

$$\varphi V_c = 0.65 * 712.95 = 534.715\ kN$$

$\frac{\varphi V_c}{2} = 267.357\ kN > V_u = 83.2\ kN$ - only minimum reinforcement is required.

The maximum tie spacing is then:

$$48d_t = 0.457$$

$$16d_l = 0.3556$$ - selected

0.45 m

#3 ties at 200 center to center spacing.

Biaxial bending

$$M_{ux} = 127.809\ kN - m; M_{nx} = \frac{M_{ux}}{0.65} = 196.62\ kN - m$$

$$M_{uy} = 138.93\ kN - m; M_{ny} = \frac{M_{ux}}{0.65} = 213.73\ kN - m$$

$$P_u = 317.889\ kN - m; P_n = \frac{P_u}{0.65} = 489.06\ kN - m$$

$$e_x = \frac{M_{nx}}{P_{nx}} = 0.4$$

$$e_y = \frac{M_{ny}}{P_{ny}} = 0.437$$

$$\gamma_x = \gamma_y = \frac{0.45-0.07*2}{0.45} = 0.69$$

$$\rho = 0.01$$

$$e_x/h = 0.89$$

$$e_y/h = 0.97$$

From the interaction diagram, Kn values are 0.18 for x axis and 0.23 for y axis.

$$P_{nx} = 2492.3\ kN; P_{ny} = 3738.46\ kN$$

$$P_0 = 0.85f'_c * A_g + A_{st}(f_y - 0.850.85f'_c) = 6885.88\ kN$$

$$\frac{1}{P_n} = \frac{1}{P_{nx}} + \frac{1}{P_{ny}} - \frac{1}{P_0}$$

$P_n = 1910.221\ kN$>688.5 kN - the method is valid

$\varphi P_n = 1241.64\ kN > 317.889\ kN$ - the column is safe against biaxial bending.

3.5.2.4. One way slab design

The one way slab design was followed by the ACI 318 procedure. The gravity load applied on the slab has been taken into account while calculating the moments generated in the slab.

$$w_u = 1.2DL + 1.6LL$$

$$M_u = \frac{w_u l^2}{8}$$

The top and bottom reinforcement bars selection and the spacings between the bars are based on the ACI procedure. As a result, 2#4 bars are placed at bottom reinforcement and 3#4 bars are placed on top.

3.5.3. Reinforcement Detailing

3.5.3.1. Bar selection and Spacing

Table 3.54. Reinforcement of the beams

Component	Top reinforcement	Bottom reinforcement	Stirrups
Major beam	2#9	4#6	#3 at 300 mm
Minor beam	2#7	4#5	#3 at 150 mm

Table 3.55. Reinforcement of the columns

Component	Reinforcement	Ties
Column 1-3 floors (850 x 850)	8#11	#3 at 200 mm
Column 4-6 floors (750 x 750)	8#9	#3 at 200 mm
Column 7-9 floors (600 x 600)	8#8	#3 at 200 mm
Column 10-13 floors (450 x 450)	6#7	#3 at 200 mm

3.5.3.2. Development Length

The formula used for the calculation of the development length:

$$l_d = \frac{f_y \psi_t \psi_e \psi_g}{20\lambda\sqrt{f'_c}} d_b = 44.41\ in > \frac{450}{25.4} = 17.7\ in$$

where

ψ_t - reinforcement location factor (1.0)

ψ_e - bar coating factor (since no coating, the factor is equal to 1.0)

λ - lightweight concrete modification factor (1.0)

$$l_{dh} = \frac{f_y \psi_e \psi_r \psi_o \psi_c}{55\lambda\sqrt{f'_c}} d_b^{1.5} = 16.93\ in = 430\ mm$$

3.5.3.3. Lap Splices

For the beams:

- In tension: $l_{st} = l_{dh} = 430\ mm$

$$l_{sc} = 0.0005 f_y d_b$$

- In compression: $l_{sc} = 762\ mm$

For columns:

- $l_{sc} = 667\ mm$

3.5.4. Structural serviceability design

3.5.4.1. Deflection

Before checking for the deflection, the member should be checked for the thickness requirements. It is an important part, because if the member size exceeds the minimum requirements, checking for the deflection may not be conducted.

The formula for the calculation of minimum thickness:

$$h_b = \frac{L}{21} = \frac{6000}{21} = 299.91\ mm$$

which is almost 300 mm (minor beam dimension), but still less. As a result, deflection checks can be ignored.

3.5.4.2. Crack Width

Maximum width of flexural crack will be calculated by the following formula:

$$w = 0.076\beta_h f_s \sqrt[3]{d_c A}$$

where

β_h - ratio of the distance to the neutral axis from the extreme tension fiber to the distance to the centroid of the tension steel (1.20 for beams and 1.35 for one-way slab) = 1.20

f_s - steel stress at service load ($0.6f_y$) = 36 ksi

d_c - cover to the outermost bar measured from the extreme tension fiber to the center of the closest bar = 2.25 in

A - effective tension area of concrete around the main reinforcement divided by the number of bars = 22.5 in^2

$$w = 0.076 * 1.20 * 36\sqrt[3]{2.25 * 22.5} = 0.012\,in < 0.016\,in$$

As a result, estimated crack width does not exceed allowable maximum, so the crack width can be considered as satisfactory

3.5.5. Special seismic detailing for the reinforcement

3.5.5.1. Beams

As the building is located in a high seismicity zone, special seismic detailing measures have been implemented in accordance with ACI 318-19, Section 18.6. The beam clear spans and width-to-depth ratios meet the code requirements, ensuring appropriate flexural behavior under seismic loading.

A minimum of two continuous longitudinal reinforcement bars is provided at both the top and bottom faces of the beams, as specified in Section 18.6.3.1. Additionally, the positive moment strength at the face of the joint exceeds 50% of the negative moment strength, ensuring balanced flexural capacity to promote ductile hinging behavior.

Transverse reinforcement is provided in the form of closed hoops over a length equal to twice the member depth (2h) from the face of the supporting element. The spacing of hoops does not exceed the smallest of d/4, 6db, or 150 mm, in line with the confinement requirements. The first hoop is placed 50 mm from the support face to ensure confinement in critical shear and plastic hinge zones, as per ACI 318-19, Section 18.6.4.

3.5.5.2. Columns

Seismic detailing for columns complies with ACI 318-19, Section 18.7. The provided longitudinal reinforcement area is within the prescribed range of 1% to 6% of the gross cross-sectional area (Section 18.7.4.1), ensuring sufficient axial and flexural capacity.

Transverse reinforcement is extended beyond the joint region by a length l_0, defined as one-sixth of the column's clear span. In this case, l_0 = 400 mm, which satisfies the confinement length criteria. The transverse reinforcement configuration provides adequate confinement and shear resistance within potential plastic hinge regions, as required by Section 18.7.5. All other relevant provisions, including minimum bar spacing, hoop configuration, and anchorage, were considered to ensure ductile performance under cyclic loading.

3.5.5.3. Joints

The seismic design of beam-column joints ensures proper anchorage and confinement in accordance with ACI 318-19, Section 18.8. Longitudinal reinforcement from the beams extends to the far face of the column, promoting moment continuity and effective force transfer across the joint. Where reinforcement passes through the column core, the column depth (h) is greater than 20 times the bar diameter (20db), satisfying development length criteria for full anchorage and preventing premature bond failure (Section 18.8.3).

Development lengths for all reinforcing bars were calculated using the provisions of Chapter 25, taking into account concrete strength, bar size, concrete cover, and confinement conditions. The joints are detailed with closely spaced transverse reinforcement to confine core concrete and mitigate joint shear failure during seismic events. Where lap splices are required, they are located away from potential plastic hinge zones and comply with the restrictions outlined in Sections 18.8.5 and 25.5.2.

These provisions ensure that the joints maintain structural integrity, energy dissipation capacity, and ductile behavior under seismic excitation.

4. Geotechnical Engineering

4.1 Site analysis

4.1.1 Soil Data

The chosen location is in Los Angeles, California, at 2217 Sunset Boulevard, close to the intersection with Mohawk Street. This area, which is part of Southeast Hollywood, is densely populated and is set to construct the development of a 12-story building named "Verdigris View". A recent site investigation by Langan Engineering & Environmental Services (2019) indicates that the ground is predominantly flat and surrounded by both residential and commercial properties. Additionally, the area is well-connected to public transportation and amenities, making it a strategic choice for development. Its proximity to various cultural attractions and entertainment venues in Hollywood adds to its appeal for both residential and commercial purposes.

Nearby, a geotechnical field investigation was conducted, which included drilling three boreholes to a total depth of approximately 18.89 m, 4.572 m, and 10.06 m. Soil samples collected at borehole 1 with a depth of 18.89 m were classified according to the Unified Soil Classification System (USCS) using Standard Penetration Test (SPT). This borehole was chosen because it is located right under the projected building as illustrated in Figure 4.1.

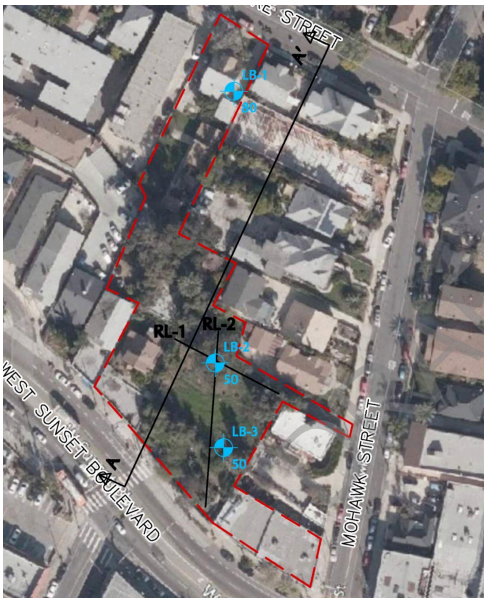

Figure 4.1. Approximate boreholes' location

The friction angles and cohesion values were taken from the report, remaining properties, namely elastic modulus, Poisson ratio, and unit weight, were calculated according to their SPT values. Firstly, the SPT N-values were corrected for field condition using Coduto (2001) equation (4.1):

$$N_{60} = \frac{E_m C_B C_s C_R N}{0.6} \quad (4.1)$$

Where,

N_{60} - N-value corrected for field condition

N - measured SPT value from the report

E_m - hammer efficiency

C_B - borehole diameter correction factor

C_s - sampler correction

C_R - rod length correction factor

Hammer efficiency was taken as 0.7, as automatic trip was used (BNBC, 2015, as cited in Rahman, 2020). C_B, C_s, C_R values were taken as 1.15 (8 inches), 1 (standard sampler), and 1 (more than 10 meters length) respectively (BNBC, 2015, as cited in Rahman, 2020).

Since the SPT values can be affected by the weight of the soils above, the overburden pressure should be considered. To calculate the SPT N-values for field conditions and overburden tests, next formula (4.2) from Coduto (2001) was used:

$$N_{1,60} = N_{60} * C_N \quad (4.2)$$

Where C_N is the overburden correction factor, taken as the average of the next two equations (4.3) and (4.4), (Liao & Whitman, 1986) and (Peck et al.,1974) respectively.

$$C_N = 9.78 * \left(\frac{1}{\sigma'}\right)^{0.5} \quad (4.3)$$

$$C_N = 0.77 * \left(\frac{2000}{\sigma'}\right) \quad (4.4)$$

For both equations it is first needed to calculate the effective stress. The unit weight was calculated according to Rahman (2020), for cohesionless (4.5) and cohesive (4.6) soils respectively:

$$\gamma = 16 + 0.1 * N_{60} \quad (4.5)$$

$$\gamma = 16.8 + 0.15 * N_{60} \quad (4.6)$$

Then, effective stress was calculated by multiplying the unit weight by the depth as stated in the following equation (4.7):

$$\sigma = \gamma z \quad (4.7)$$

For further calculations of the foundation design and future simulations in the software, the elastic modulus and Poissin ratio were calculated. For the elastic modulus of the two silty sand soils two equations (4.8) and (4.9) were used, (FHWA, 2002):

$$E = (40 + 3(N + 6)) * 98.0665 \quad (4.8)$$

$$E = 400 * N_{1(60)} \quad (4.9)$$

While the elastic modulus for the remaining soil layers was calculated as follows (4.10), (FHWA, 2002):

$$E = 1200 * N_{1(60)} \quad (4.10)$$

According to Das and Sivakugan (2019), poisson's ratio was calculated (4.11) for further work with the software simulations:

$$\mu_s = 0.1 * 0.3 \frac{\varphi - 25}{45 - 25} \quad (4.11)$$

Table 4.1 shows the soil classification that was obtained.

Table 4.1. Soil properties

Section	Depth	Soil type	N1,60	Unit wt, kN/m^3	Eff.Stress, kN/m^2	Cohesion, kPa	Friction angle, deg	Elastic Modulus, MPa
1	0.3	Clay	0	16.00	4.88	21.64	24.70	-
2	1.5	MD Clayey Sandstone	31	17.81	26.59	19.07	37.89	-
3	3.0	D Silty Sand	63	21.03	58.64	14.36	46.97	22.80
4	4.6	D F Sandstone	50	20.79	90.32	25.62	43.49	59.95
5	6.1	D F-M Sandstone	51	21.70	123.40	25.62	43.89	61.73
6	7.6	VD F Sandstone	75	25.56	162.35	45.91	50.01	89.96
7	9.1	D F-M Sandstone	45	22.37	196.44	21.57	42.09	53.93
8	10.4	D F Silty Sand	44	22.71	224.13	0	41.75	18.94
9	11.9	F-M Sandstone	51	24.72	261.80	31.03	43.90	61.75
10	13.4	D F-M Silty Sand	36	22.71	296.40	23.94	39.61	43.60
11	14.9	F-M Sandstone	45	25.12	334.69	25.31	42.15	54.18
12	16.5	F-M Sandstone	50	27.00	375.84	34.25	43.39	59.53
13	17.9	VD F-M Sandstone	36	24.72	413.51	43.99	39.57	43.44
14	18.9	F-M Sandstone	37	25.39	436.73	24.53	39.83	44.49

4.1.2 Shear Wave Velocity

Importantly, the site lies in a seismically active area, as outlined in Chapter 20 of ASCE 7-16. The shear wave velocity, a crucial parameter for assessing the dynamic properties and responses of soil, was analyzed. The seismic evaluation involved plotting the shear wave velocities to determine the average shear wave velocity (Vs) for a depth of 30 m, which is essential for understanding the site's response during seismic events. The graphs in Figures 4.2-4.3 below display the shear wave velocity results for two different locations within the selected area: one in the north and the other in the southeast.

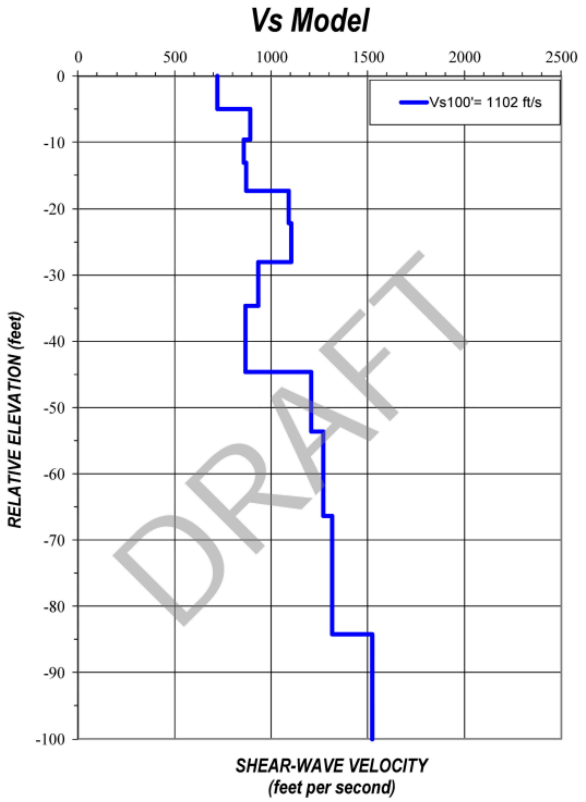

Figure 4.2. Shear wave velocity to the north side

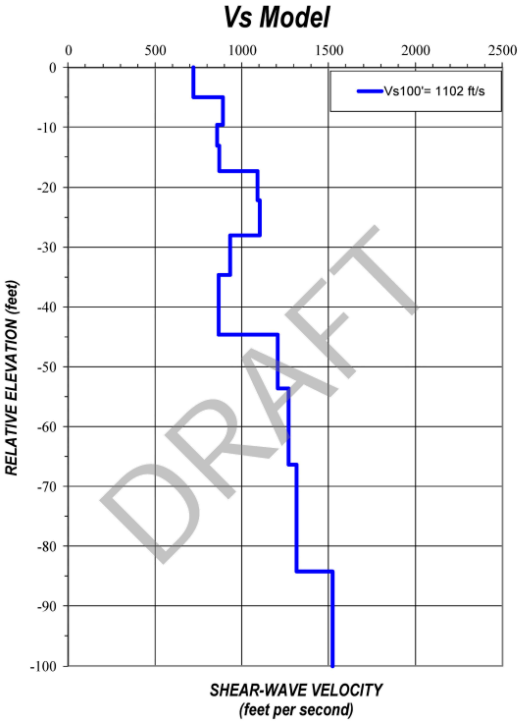

Figure 4.3. Shear wave velocity to the southeast side

The graph shows that the average shear wave velocity ranges from 354.48 to 335.89 m/s, which corresponds to Site Class D and Risk Category III, indicating a high seismic risk for the area.

4.1.3 LPI Estimation

Related to liquefaction, which occurs when the ground (typically sandy soil) weakens and behaves like liquid during an earthquake, it is not a concern here because the soil is not sandy.. Additionally, the 2019 geotechnical investigation report by Langan Engineering & Environmental Services confirms that the site is not located within an established liquefaction potential investigation zone (Langan, 2019).

4.2 Foundation Design

4.2.1 Shallow Foundation

The bearing capacity for a shallow foundation was calculated using two ways. By Meyerhof's method (4.12), the approximate dimensions of the square foundation were found. The new and allowable ultimate bering capacities were calculated nd compared with the axial loads.

$$q_u = cN_c F_{cs} F_{cd} F_{ci} + qN_q F_{qs} F_{qd} F_{qi} + 0.5\gamma B N_\gamma F_{\gamma s} F_{\gamma d} F_{\gamma i} \quad (4.12)$$

$$q_{net} = q_u - q \quad (4.13)$$

$$q_{all} = \frac{q_{net}}{FS} \quad (4.14)$$

The following values in Table 4.2 were taken as the constants:

Table 4.2. Shallow foundation calculation values

Safety factor	3
Df, m	2
Friction angle, deg	43.89
Cohesion, kPa	25.62
Unit weight, kN/m^3	21.702
Width, B, m	B

Considering the values in table above, the vertical effective stress was calculated using next formula (4.15):

$$q = D_f * \gamma \tag{4.15}$$

Then, the bearing capacity factors were calculated.

$$N_q = tan(45 + \varphi'/2)e^{\pi tan\varphi'} \tag{4.16}$$

$$N_c = cot\varphi'(N_q - 1) \tag{4.17}$$

$$N_\gamma = tan(1.4\varphi')(N_q - 1) \tag{4.18}$$

Then, as friction angle is greater than 0, the shape factors were calculated as following, according to DeBeer (1970):

$$F_{cs} = 1 + \left(\frac{B}{L}\right)\left(\frac{N_q}{N_c}\right) \tag{4.19}$$

$$F_{qs} = 1 + \left(\frac{B}{L}\right)tan\varphi' \tag{4.20}$$

$$F_{\gamma s} = 1 - 0.4\left(\frac{B}{L}\right) \tag{4.21}$$

Depth factors were calculated using formulas for $\frac{D_f}{B} > 1$, and friction angle > 0.

$$F_{cd} = F_{qd} - \frac{1-F_{qd}}{N_c tan\varphi'} \tag{4.22}$$

$$F_{qd} = 1 + 2tan\varphi'(1 - sin\varphi')^2 tan^{-1}\left(\frac{D_f}{B}\right) \tag{4.23}$$

$$F_{\gamma d} = 1 \tag{4.24}$$

For the inclination factors next equations were used Meyerhof (1963) and Hanna and Meyerhof (1981)

$$F_{ci} = F_{qi} = \left(1 - \frac{\beta}{90}\right)^2 \tag{4.25}$$

$$F_{\gamma i} = \left(1 - \frac{\beta}{\varphi'}\right)^2 \quad (4.26)$$

Next Table 4.3 shows all calculated values for Meyerhof's method.

Table 4.3. Meyerhof's and Vesic's method factors

	Meyerhof's method	Vesic's method	
Fcs	1.9576	Sc	1.85435
Fqs	1.9486	Sq	1.06105
Fys	0.6	Sy	0.64520
Fcd	1+0.268tan'(0.5B)	dc	1.33898
Fqd	1+0.2705tan'(0.5B)	dq	1.22786
Fyd	1	dr	1.00000
Fci, qi, yi	1, 1, 1.1	k	0.84746
Nc	116.91	Nc	116.91
Nq	113.48	Nq	113.48
Ny	206.75	Ny	220.29

After calculating all needed values, they were put into equation (4.12). From the Meyerhof's method, it was identified that the foundation columns should be at least 1.49 m for corner, 2.37 for inner, and 1.84 for edge columns. To make sure that such dimensions satisfy the allowable vertical load, the Vesic's method (4.27) was used:

$$q_u = cN_c s_c i_c d_c g_c b_c + qN_q s_q i_q d_q g_q b_q + 0.5\gamma B' N_\gamma s_\gamma i_\gamma d_\gamma g_\gamma b_\gamma \quad (4.27)$$

The N_q and N_c values are same as in Meyerhof's method. To find the N_γ, next formula (4.28) was used:

$$N_\gamma = 2tan\varphi'(N_q + 1) \quad (4.28)$$

The calculated shape, depth, and inclination factors are presented in Table N. Calculating the ultimate and allowable bearing capacities showed that the foundation design satisfy the load of the building. Table 4.4 shows the Vesic's method results

Table 4.4. Vesic's method

Estimated load		Df=2m		
Column	Qload, kN	Width, m	q all,	q load,
Corner	2324.3	1.49	1073.21	1046.94
Inner	6287.446	2.37	1182.87	1119.38
Edge	3507.604	1.84	1163.34	1036.036

4.2.2 Mat Foundation

The dimensions of Mat foundation was taken as 30m*50m according to building's width and length. The embedded depth of the foundation was taken as 1.5 m., considering the basement, the foundation will lay in the sixth soil layer, dense, find to medium sandstone. The same Meyerhof's method and procedure was used as well, resulting in $q_u = 6506.5 kN/m^2$.

$$q_{net} = 6506.5 - 21.7 * 1.5 = 6474\, kN/m^2$$

$$q_{all} = \frac{6474}{3} = 2157\, kN/m^2$$

Allowable ultimate bearing capacity is more the the ultimate load, meaning that Mat foundation can be used as well. However, considering the high seismic risks and high rise building type, it is better to use the deep foundations. According to Poulos (2010), the regions with high seismic activity mostly use the pile foundations due to their stability, piles transfer the load to deeper soil layers. While shallow and mat foundations lay in the topper soil layers which are intensely affected by seismic loads during the earthquakes.

4.3 Pile Foundations

4.3.1 Bearing Capacity

4.3.1.1 Single Pile

A pile foundation, a type of deep foundation, is essentially a slender column or long cylinder, often made of concrete or steel, that supports structures by transferring loads to a

specified depth through either end bearing or skin friction. In this process, two key factors contribute to the pile's bearing capacity: the skin friction along its surface and the bearing capacity at its tip. Together, these factors enable the pile to bear the structural load applied by the building. However, the allowable bearing capacity of a deep foundation is calculated in a similar way to that of a shallow foundation, by dividing the ultimate bearing capacity by a factor of safety. The equation determining the ultimate bearing capacity of the pile (Q_u, kN) by summing the pile's point-bearing capacity (Q_p, kN) and its shaft or skin resistance (Q_s, kN) will be used:

$$Q_u = Q_p + Q_s \tag{4.29}$$

For subsequent calculations, we assumed the diameter of the circular pile to be 0.4 m for interior column, taking into account that usually minimum diameter length for single pile ranges from 0.3 m to 0.9 m ("Pile Foundation," 2021).

$$P = \pi D = \pi * 0.4 = 1.26\,m \tag{4.30}$$

$$A = \pi\frac{D^2}{4} = \pi\frac{0.4^2}{4} = 0.25\,m^2 \tag{4.31}$$

Additionally, the height of the basement (3.81m) should be taken into account when determining the point-bearing capacity of the pile. This calculation considers both sand and sandstone layers, as the pile's length may position it within either soil type.

Point-Bearing Capacity in Sand and Sandstone

First, a pile that is 6 meters long was chosen to test how well it can support weight in sand. Instead of being set at the planned depth of 6 meters, the bottom of the pile will reach down to 8.81 meters, where there is dense silty sand that is fine to medium in size. Even though sandstone can be considered a weak rock, it can still act like a sandy material due to the factors such as weathering. Therefore, the same formulas used for sand were applied to sandstone to calculate point bearing capacity and frictional resistance. The following calculation procedure for each method will be only for L=6 m, after which table with other length piles will be shown.

Method 1: Meyerhof's method for homogeneous granular soil

$$Q_p = A_p * q_p = A_p * q' N_q^* \leq A_p * q_l \quad (4.32)$$

$$q_l = 0.5 * p_a * N_q^* * tan\phi' \quad (4.33)$$

where,

A_p - area of the pile tip, $0.32\ m^2$;

q' - effective vertical stress at the level of the pile tip;

ϕ' - friction angle, $42.09°$ for $L = 6m$;

N_q^* - the bearing capacity factor for piles, from Figure 12.18 (Das & Sivakugan, 2019), 538 for $\phi' = 42.09°$;

q_l - the limiting point resistance;

p_a - atmospheric pressure, $100kN/m^2$;

$$q' = \sum(\gamma * \Delta L) = 16 * 0.3 + 17.81 * 1.22 + 21.03 * 1.52 + 20.79 * 1.53 + 21.7 *$$

$$* 1.52 + 25.56 * 1.53 + 22.37 * (8.81 - 7.62) = 189.01\ kN/m^2$$

$$Q_p = 0.32\ m^2 * 189.00\ kN/m^2 * 538 = 32712.1\ kN$$

$$Q_l = 0.32\ m^2 * 0.5 * 100kN/m^2 * 538 * tan(42.09^\circ) = 7816.48\ kN$$

$Q_p = 32712.1 > Q_l = 7816.48\ kN$, therefore, $Q_p = 7816.48\ kN$

Method 2: Vesic's method

$$Q_p = A_p * q_p = A_p \overline{\sigma'_0} N_\sigma^* \quad (4.34)$$

To determine the bearing capacity factor, which relies on the soil's reduced rigidity index, the following series of equations can be applied step by step:

$$E_s = 53930\ MPa \text{ for } L = 6m$$

where, $E_s - \ modulus\ of\ elasticity$;

$$\mu_s = 0.1 + 0.3(\frac{\phi^{'}-25}{20}) = 0.1 + 0.3(\frac{42.09-25}{20}) = 0.356$$

where, $\mu_s = 0.1 + 0.3(\frac{\phi^{'}-25}{20})$ for $25^{\circ} \leq \phi^{'} \leq 45^{\circ}$, which is Poisson's ratio;

$$\Delta = 0.005(1 - \frac{\phi^{'}-25}{20}) * \frac{q^{'}}{p_a} = 0.005(1 - \frac{42.09-25}{20}) * \frac{189.01}{100} = 0.00138$$

where, Δ - is average volumetric strain below the pile point;

$$I_r = \frac{E_s}{2(1+\Delta)*q^{'}tan\phi^{'}} = \frac{53930}{2*(1+0.00138)*189.01*tan(42.09^{\circ})} = 116.45 \quad (4.35)$$

where, I_r - rigidity index;

$$I_{rr} = \frac{I_r}{1+I_r\Delta} = \frac{116.45}{1+0.00138*116.45} = 100.378 \quad (4.36)$$

where, I_{rr} - reduced rigidity index;

$$K_\sigma = 1 - sin\phi^{'} = 1 - sin(42.09^{\circ}) = 0.3297 \quad (4.37)$$

$$\overline{\sigma_0^{'}} = (\frac{1+2K_0}{3})q^{'} = (\frac{1+2*0.3297}{3}) * 189.01 = 104.546\ kN/m^2 \quad (4.38)$$

The bearing capacity factor was determined to be 162, using Table 12.8 (Das & Sivakugan, 2019), for which I_{rr} and $\phi^{'}$ values were necessary.

$$Q_p = 0.32\ m^2 * 104.546\ kN/m^2 * 162 = 3646.9\ kN$$

Method 3: Coyle and Costello's method

$$Q_p = A_p * q_p = A_p * q^{'} * N_q^* \quad (4.39)$$

where,

N_q^* - the bearing capacity factor, depending on L/D, equals to 100 (Das & Sivakugan, 2019);

$$Q_p = 0.32\ m^2 * 189.00\ kN/m^2 * 100 = 6080.32\ kN$$

Table 4.5. Point bearing capacity in Sand using different methods

Length of pile, m	Depth, m	Layer	Meyerhof, kN	**Vesic, kN**	Coyle and Costello, kN
6	9.81	D F Silty Sand	7816.48	**5448.44**	6080.32
7	10.81	VD F-M Sandstone	11872.3	**7731.10**	9080.36
8	11.81	VD F-M Sandstone	11872.3	**7644.26**	10452.8
9	12.81	D F-M Silty Sand	4233.01	**5230.97**	8825.02
10	13.81	VD F-M Sandstone	7862.07	**6701.72**	10845.5
11	14.81	VD F-M Sandstone	7862.07	**7368.91**	12267.8
12	15.81	VD F-M Sandstone	10674.2	**8686.13**	13604.2
13	16.81	VD F-M Sandstone	4280.17	**5907.42**	10762.9
14	17.81	VD F-M Sandstone	4280.17	**5984.17**	13034.7
15	18.81	VD F-M Sandstone	4454.03	**6408.13**	13420.4

As shown in the table, the values obtained using Vesic's method were considered the most accurate due to the minimal deviations in the calculated results.

Frictional resistance in Sand

The bearing capacity of the pile is affected by the frictional resistance along its length and in order to find frictional resistance several methods, including Coyle and Costello's method and general formula were used.

Method 1. Coyle and Costello's method

$$Q_s = K\overline{\sigma_0'}tan(\delta')pL \qquad (4.40)$$

where,

K - effective earth pressure coefficient, 10 for $\phi' = 42.09^{\circ}$ (Das & Sivakugan, 2019);

δ' - soil–pile friction angle = $0.8 * \phi'$;

p - perimeter of the pile tip, m;

L - length of the pile, m;

σ_0' - average effective overburden pressure, kN/m^2;

$$\overline{\sigma_0'} = \frac{\frac{4.88*0.304}{2} + \frac{(26.59+4.88)*1.22}{2} + \frac{(58.64+26.59)*1.52}{2} + \frac{(90.32+58.64)*1.53}{2} + \frac{(123.4+90.32)*1.52}{2} + \frac{(162.35+123.4)*1.53}{2} + \frac{(196.44+162.35)*1.52}{2}}{8.81} =$$

$$= 96.75\ kN/m^2$$

$$Q_s = 10 * 96.75 kN/m^2 * tan(0.8 * 42.09^{\circ}) * 2.01m * 6m = 4898.69\ kN$$

Method 2. General Formula

$$Q_s = \sum fp\Delta L = \sum K\sigma_0'tan(\delta')p\Delta L \qquad (4.41)$$

where,

K - effective earth pressure coefficient for precast concrete piles = 1.5;

σ_0' - effective vertical stress at the depth under consideration, kN/m^2;

δ' - soil–pile friction angle = $0.8 * \phi'$;

p - perimeter of the pile tip, m;

ΔL - thickness/difference in depth, m;

The concept of critical length (L'), approximately 15 times the diameter (15D), also needs to be considered. For this pile, the critical depth is 9.6 m. Therefore, for z=0 to L'=9.6, $f = K\sigma_0^{'} tan(\delta')$ will be taken. But, for z=L' to L, which is z=9.6 to 18.81, $f = f_{z=L'}$ will be taken:

$$f_{L=5} = 1.5 * 189.01\, kN/m^2 * tan(0.8 * 42.09^{\circ}) = 188.88\, kN/m^2$$

The table below shows skin resistance in sand and sandstone with f values for each length of pile:

Table 4.6. Skin friction of each layer

Length, m	Depth, m	Layer	f
6	9.81	D F Silty Sand	**188.88**
7	10.81	VD F-M Sandstone	**248.16**
8	11.81	VD F-M Sandstone	**274.24**
9	12.81	D F-M Silty Sand	**261.88**
10	13.81	VD F-M Sandstone	**306.83**
11	14.81	VD F-M Sandstone	**331.98**
12	15.81	VD F-M Sandstone	**372.40**
13	16.81	VD F-M Sandstone	**355.65**

14	17.81	VD F-M Sandstone	**378.51**
15	18.81	VD F-M Sandstone	**405.16**

$$Q_s = fp\Delta L = 188.88 * 2.01m * 1.52 = 577.36\,kN$$

Using the same procedure for z=0 to L'=9.6, which is critical depth, the following result will be obtained:

Table 4.7. Skin resistance before critical poin

Length, m	Depth, m	Layer	**Qs**
6	9.81	D F Silty Sand	**577.36**

For z=L' to L, which is z=10.81 to 18.81:

$$Q_{z=10.81} = 577.36 + 553.321 + (\frac{248.16+274.34}{2}) * 2.011 * (11.89 - 10.81) = 1304.01\,kN$$

Finally, the same procedure was done for other lengths of piles and it is shown in the following Table 4.8 as well as result calculated from Coyle ans Costello's Method:

Table 4.8. Skin friction of each layer

Length, m	Depth, m	Layer	**General formula, kN**	Coyle and Costello's, kN
6	9.81	D F Silty Sand	**577.356**	4898.69
7	10.81	VD F-M Sandstone	**1304.01**	9297.47
8	11.81	VD F-M Sandstone	**1895.64**	9185.63

9	12.81	D F-M Silty Sand	**2421.06**	10056.1
10	13.81	VD F-M Sandstone	**2744.97**	13147.7
11	14.81	VD F-M Sandstone	**3058.78**	12586.8
12	15.81	VD F-M Sandstone	**3695.10**	15202.2
13	16.81	VD F-M Sandstone	**4973.29**	15452.2
14	17.81	VD F-M Sandstone	**5109.36**	15126.1
15	18.81	VD F-M Sandstone	**5864.11**	8834.24

In this case, the results from the general formula were considered the most accurate, as the sudden jumps in values from Coyle's and Costello's method raised doubts about their reliability. Finally, the bearing capacity and skin resistance values are shown in the following Table 4.9:

Table 4.9. Allowable bearing capacity in Sand and Sandstone

Length of pile, m	Depth, m	Layer	Q_p, kN	Q_s, kN	Q_u, kN	Q_{all}, **kN**
6	9.81	D F Silty Sand	5448.44	577.356	6025.80	**2008.59**
7	10.81	VD F-M Sandstone	7731.10	1304.01	9035.11	**3011.70**
8	11.81	VD F-M Sandstone	7644.26	1895.64	9539.9	**3179.97**

9	12.81	D F-M Silty Sand	5230.97	2421.06	7652.03	**2550.68**
10	13.81	VD F-M Sandstone	6701.72	2744.97	9446.69	**3148.90**
11	14.81	VD F-M Sandstone	7368.91	3058.78	10427.69	**3475.90**
12	15.81	VD F-M Sandstone	8686.13	3695.10	13659.42	**4553.14**
13	16.81	VD F-M Sandstone	5907.42	4973.29	10880.71	**3626.90**
14	17.81	VD F-M Sandstone	5984.17	5109.36	11093.53	**3697.84**
15	18.81	VD F-M Sandstone	6408.13	5864.11	12272.24	**4090.75**

However, as the allowable bearing capacity is less than Q_{design} (the column load transferred to the foundation, as shown in the table below), single piles cannot be used for our structure.

Table 4.10. The column load transferred to the foundation

	Q_{design}, kN
Exterior Column	3507.604
Interior Column	6287.446
Corner Colimn	2324.301

4.3.1.2 Group Piles

The initial step in calculating the bearing capacity of a group pile was selecting the appropriate number of piles and determining whether the group should behave as a single pile or as a block pile. This decision is influenced by the efficiency of the group pile, as determined by the group efficiency equation (4.42). In our case, n_1, representing the number of piles along the x-axis of the group, was chosen to be greater than n_2, representing the number of piles along the y-axis. Several factors influenced this decision, including the building's footing layout, which is longer horizontally and narrower vertically, the spacing between columns, the design of the pile cap, and several iterations performed to optimize the diameter. These considerations ensured that the foundation was both safe and cost-effective.

Taking into account that the minimum diameter for group piles is 3.5 m (*Minimum Pile Length - Foundation Engineering*, 2005) and the minimum spacing between piles is 2.5D, several iterations were performed to determine the pipe diameter and the number of piles using the group pile efficiency equation:

$$\eta = \frac{2*(n_1+n_2-2)*d+4D}{p*n_1*n_2} \qquad (4.42)$$

n_1-number of piles horizontally;

n_2-number of piles vertically;

p - perimeter of the pile;

d - minimum spacing between piles;

D - pile diameter;

In cases where the efficiency(η) is greater than 1, the group of piles behaves as a single pile, and the total bearing capacity is calculated as the sum of the individual bearing capacities of the piles. This applies to our case too:

$$n_1 * n_2 * \sum Q_u = n_1 * n_2 * (Q_p + Q_s) \qquad (4.43)$$

Next, the distance between columns was taken as 5 m, while the design of the pile cap, with dimensions L_g, B_g, was calculated using the equation below:

$$L_g = (n_1 - 1) * d + 2(D/2) \quad (4.44)$$

$$B_g = (n_2 - 1) * d + 2(D/2) \quad (4.45)$$

The design of group pile foundation was then prepared, depending on the exterior, interior, corner columns of the building and final bearing capacities were compared to ensure that Q_{design} was lower than the allowable bearing capacity of the foundation Q_{all}. All assumed parameters, following several iterations, are presented in Table 4.11:

Table 4.11. Group pile parameters for exterior,interior, corner columns

	L, m	D, m	d, m	n_1	n_2	L_g, m	B_g, m	P, m	A, m
Exterior Column	6	0.35	1.05	3	2	2.45	1.4	1.10	0.096
Interior Column	6	0.4	1.2	3	2	2.8	1.9	1.26	0.126
Corner Colimn	6	0.35	1.05	2	2	2.45	1.4	1.10	0.096

So, technical representation of group piles under each column with assigned diameters is shown in the following figures:

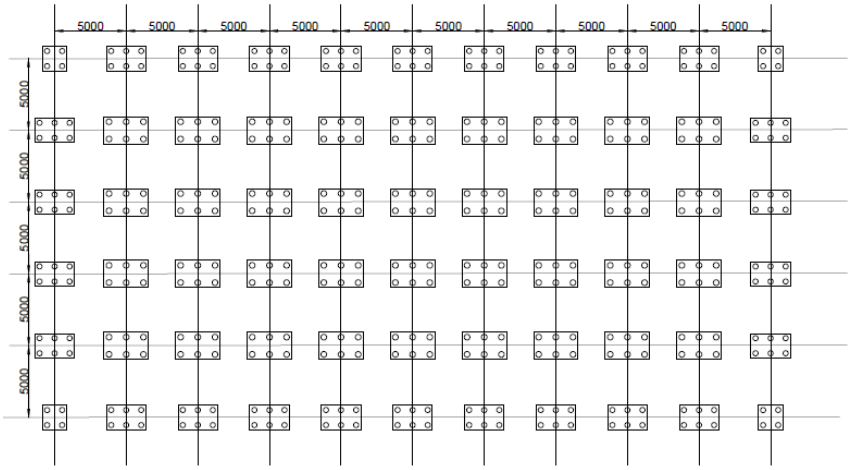

Figure 4.4. Arrangement of Group Piles according to the building's floor plan

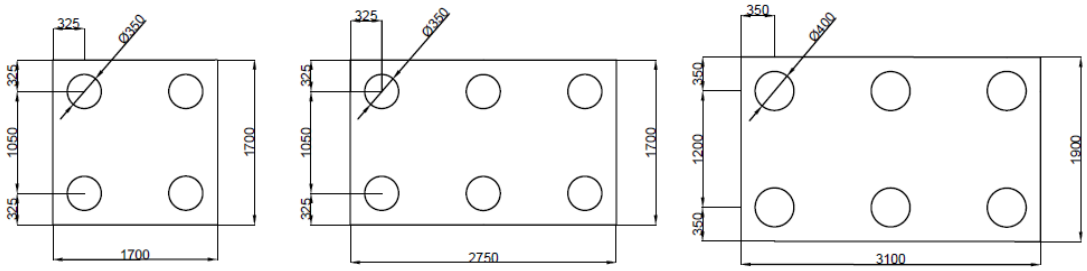

Figure 4.5. Group of Piles under 3 columns: Corner, Exterior, Interior

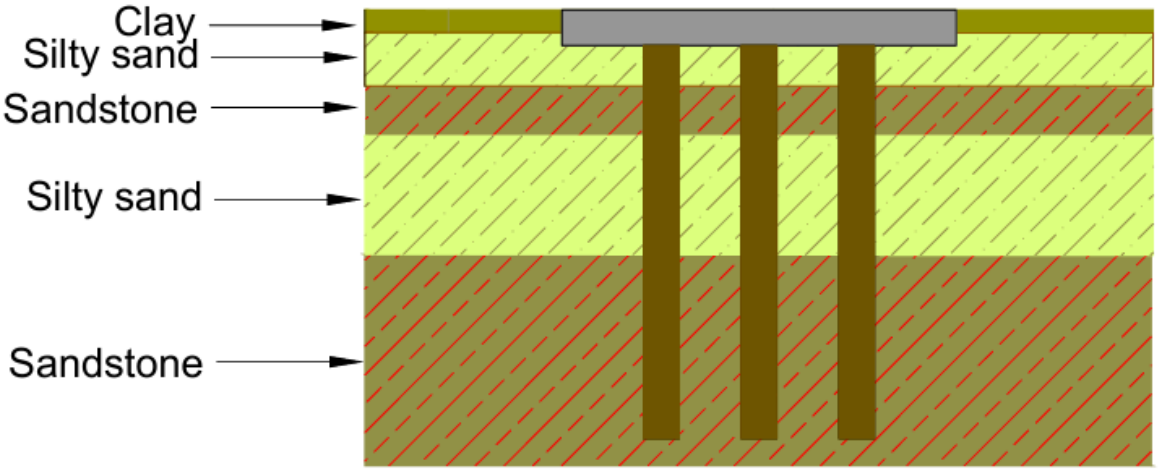

Figure 4.6. Soil layer's cross section

Group efficiency calculation for each column:

$$\eta_{exterior} = \frac{2*(3+2-2)*1.125+4*0.45}{1.414*3*2} = 1.01$$

$$\eta_{interior} = \frac{2*(3+2-2)*1.375+4*0.55}{1.728*3*2} = 1.01$$

$$\eta_{corner} = \frac{2*(2+2-2)*1.125+4*0.45}{1.414*2*2} = 1.11$$

The bearing capacity for each column was calculated using the same equations as those for a single pile foundation. The pile length was chosen to be 6 m, as this corresponds to the soil layer with relatively low parameters. This ensures that if the design works for this layer, it will also be effective for layers with higher parameters.

$$\sum_{u(exterior)} Q = 3 * 2 * (Q_p + Q_s) = 3 * 2 * (1777.38 + 452.775) = 13380.93\,kN$$

$$Q_{all} = \frac{\Sigma Q_u}{FS} = \frac{13380.93}{3} = 4460kN > Q_{design} = 3507kN$$

Same procedure was used for calculation of interior and corner columns and the result is shown on the following Table 4.12:

Table 4.12. Bearing capacity values for group pile foundation

	η	Q_p, kN	Q_s, kN	Q_u, kN	ηQ_u, kN	Q_{all}, kN	Q_{design}, kN
Exterior Column	1.01	1777.38	452.775	2230.16	13380.93	4460.31	3507.604
Interior Column	1.01	2660.49	553.321	3213.81	19282.866	6427.62	6287.446
Corner Colimn	1.11	1777.38	452.775	2230.16	8920.64	2973.55	2324.301

4.3.1.3 Assessment of Bearing Capacity Calculations for Pile Foundation

The soil profile and pile group dimensions were input into the GEO5 software. The bearing capacity calculations performed manually in Capstone 1 were then compared to the results generated by GEO5, demonstrating a high degree of consistency and validating the accuracy of the manual calculations. Results correlation between hand calculation and GEO5 Software is shown in Table 4.13, while sample outcome from Software GEO5 for corner column is shown in Figure 4.7:

Table 4.13. Correlation Between Hand Calculation and GEO5 Software Results.

		FS	η_g	$Q_{u(single)}$, kN	$Q_{u(group)}$, kN	$Q_{all(group)}$, kN	Q_{design}, kN
Corner Column	**Hand calculation**	**3**	**1.11**	**3179.97**	**8920.64**	**2973.55**	**2924.30**
	Software GEO	**3.32**	**0.9**	**2363.73**	**8509.44**	**2563.08**	
Interior Column	**Hand calculation**	**3**	**1.01**	**3179.97**	**19282.87**	**6427.62**	**6287.45**
	Software GEO	**3.08**	**1**	**3182.56**	**20956.21**	**6803.96**	
Exterior Column	**Hand calculation**	**3**	**1.01**	**3179.97**	**13380.93**	**4460.31**	**3507.60**
	Software GEO	**3.02**	**0.9**	**2442.20**	**13187.86**	**4366.84**	

Analysis of bearing capacity of pile group in cohesionless soils

Max. vertical force includes self-weight of pile cap.

Pile skin bearing capacity	R_s	= 1299,36	kN
Pile base bearing capacity	R_b	= 1064,37	kN
Vertical bearing capacity of single pile	R_c	= 2363,73	kN
Efficiency of pile group	η_g	= 0,90	
Vertical bearing capacity of pile group	R_g	= 8509,44	kN
Maximum vertical force	V_d	= 2563,82	kN

Safety factor = 3,32 > 3,00

Vertical bearing capacity of pile group is SATISFACTORY

Figure 4.7. Analysis of bearing capacity of pile group for corner column

4.4 Group Piles' Settlement

Settlement is one of the most important factors in evaluating the performance and long-term functionality of a foundation. Excessive or uneven settlement can lead to structural damage, misalignment of elements, and serviceability issues. That is why, the accurate prediction and assessment of settlement is essential during the design phase. In this section the hand and software calculations of the settlement are reported.

4.4.1 Hand Calculations of the settlement

The settlement was calculated using two ways: the Meyerhof (1976) and Vesic (1969) methods were used and their average value was taken for more accurate results. First, the Meyerhof method was used:

$$S_{g(e)} = \frac{0.96*q*\sqrt{B_g}*I}{N_{60}} \quad (4.46)$$

Where,

I - influence factor; $I = 1\text{-}L/8B_g \geq 0.5$

$q = Q_g/(B_g L_g)$

The settlement was calculated separately for different column, resulted values are given in Table 4.14. As it can bee seen, the settlement is between 17.68 and 20.6 mm. According to IS-1906 (1966), the allowable settlement in sandy soil is around 40 mm.

Table 4.14. Settlement per column according to Meyerhof's method

Pile Group	$I_{calculated}$	I_{taken}	N_{60}	q, kN/m^2	Sqe, mm
Exterior	0.2	0.5	50	1712	20.6
Interior	0.35			1437	19.1
Corner	0.21			1467	17.68

Vesic's method will be calculated based on elastic settlement of the single pile taken from the sum of the three separate settlement types.

$$S_e = S_{e1} + S_{e2} + S_{e3} \quad (4.47)$$

To begin with, the elastic compression of the pile itself is considered. It depends on the axial load on the pile, pile dimensions such as length and the cross area, and the modulus of elasticity of the material. The formula's () (Sunarno et al., 2018) given below were used for the settlement calculations:

$$S_{e1} = \frac{\left(Q_{wp} + \xi Q_{ws}\right)L}{A_p E_p} \quad (4.48)$$

Where,

Q_{wp} - load at the pile point at working condition

Q_{ws} - load by the skin resistance at working condition

ξ - between 0.5 and 0.67

Second component is the elastic deformation of the soil at the pile's tip, which is mainly influenced by the end bearing load. It was calculated using the semi-empirical method by Vesic:

$$S_{e2} = \frac{Q_{wp} C_p}{D q_p} \quad (4.49)$$

Where,

q_p - ultimate pile resistance

C_p - coefficient taken as 0.135 as for bored pile at medium density sand, (Sunarno et al., 2018)

Third component is the settlement due to the shaft friction. It happens when the soil displacement occurs along with the shift where the friction mobilizes. The Vesic's empirical method was used:

$$S_{e3} = \frac{Q_{ws} C_s}{L q_p} \quad (4.50)$$

Where,

$$C_s = (0.93 + 0.1 * \sqrt{\frac{L}{D}}) * C_p \quad (4.51)$$

Then, the the group settlement was calculated based on the individual settlements:

$$S_{g(e)} = \sqrt{\frac{B_g}{D}} S_e \quad (4.52)$$

Table 4.15. Settlement per column according to Vesic's method

Pile Group	Diameter, m	S_e, m	$S_{e(g)}$, m
Exterior	0.35	0.017	0.0414
Interior	0.45	0.0122	0.0299
Corner	0.35	0.0116	0.02852

4.4.2 GEO5 & Plaxis 3D Calculations of the settlement

To confirm the hand calculations of the settlement, the GEO5 software was used for the group piles' calculations. The linear settlement theory (Poulos) was used as the specification procedure. The values of the vertical force, bending moment, and the horizontal force from the structural part were inserted to define the service loads. Analysis was set to

“Effective stress” for the drained conditions. The following Figures 4.8-4.10 show the settlement results for three type of pile groups from the GEO5 software.

Analysis of settlement of pile group in cohesionless soils

Max. vertical force includes self-weight of pile cap.

Group settlement factor	g_f	=	2.83	
Load at the onset of mobilization of skin friction	R_{yu}	=	3881.96	kN
The settlement for the force Ryu	s_y	=	32.9	mm
Total resistance	R_c	=	4099.78	kN
Maximum settlement	s_{lim}	=	40.0	mm

Figure 4.8. The GEO5 results for the Interior Column

Analysis of settlement of pile group in cohesionless soils

Max. vertical force includes self-weight of pile cap.

Group settlement factor	g_f	=	2.83	
Load at the onset of mobilization of skin friction	R_{yu}	=	5781.67	kN
The settlement for the force Ryu	s_y	=	25.7	mm
Total resistance	R_c	=	5984.73	kN
Maximum settlement	s_{lim}	=	40.0	mm

Figure 4.9. The GEO5 results for the Exterior Column

Analysis of settlement of pile group in cohesionless soils

Max. vertical force includes self-weight of pile cap.

Group settlement factor	g_f	=	2.83	
Load at the onset of mobilization of skin friction	R_{yu}	=	3309.67	kN
The settlement for the force Ryu	s_y	=	27.2	mm
Total resistance	R_c	=	3534.29	kN
Maximum settlement	s_{lim}	=	40.0	mm

Figure 4.10. The GEO5 results for the Exterior Column

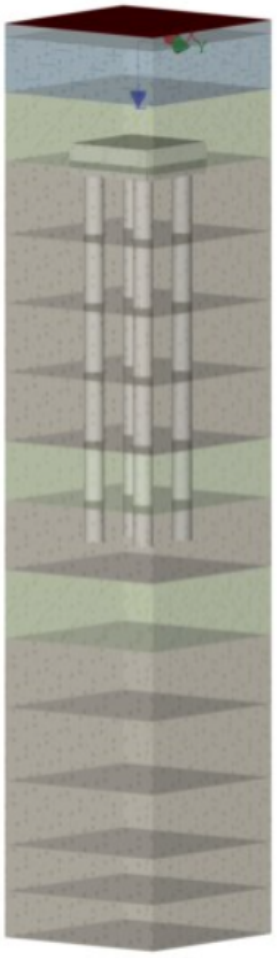

Figure 4.11. 3D Model of Pile in Corner Column Generated in GEO5 Software

To compare settlement results with those obtained from PLAXIS 3D, the piles were modeled as embedded beams within the software, while the pile caps were represented as plate elements. Load combinations generating the highest axial loads were applied to the model to simulate realistic structural behavior. The resulting deformation patterns of the pile groups under these conditions are depicted in Figures 4.12, 4.13, 4.14 and their values are added to table 4.16.

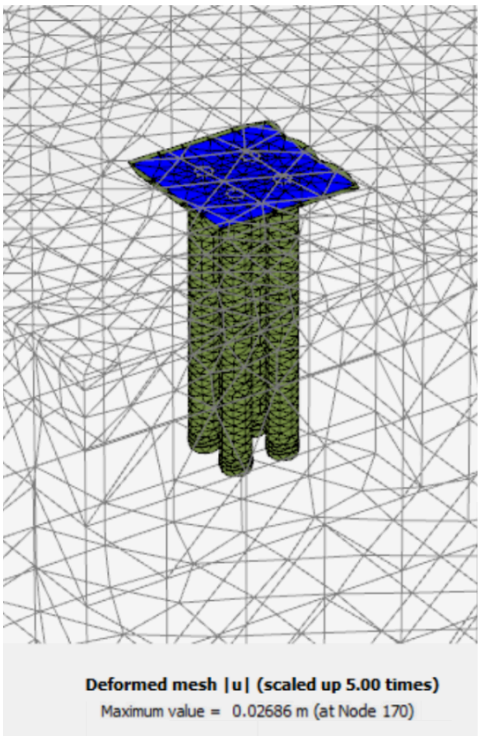

Figure 4.12. Corner Column

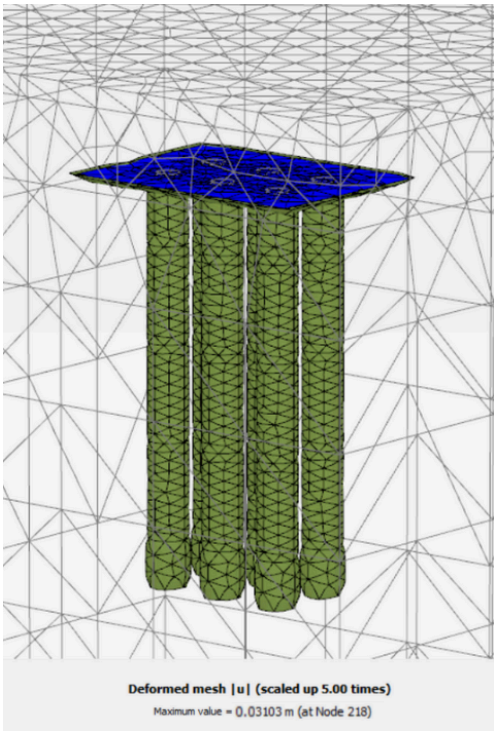

Figure 4.13. Interior Column

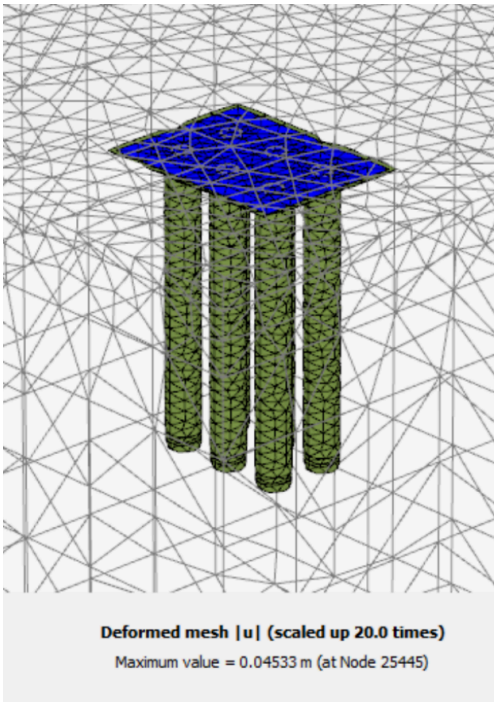

Figure 4.14. Exterior Column

Table 4.16 shows the comparison between the average value of the hand calculations and the settlement values form the Geo5 and Plaxis3D.

Table 4.16. Settlement per column according to Vesic's method

Column	Hand Calculations, m	Geo5, m	Plaxis3D
Interior	0.0310	0.0321	0.03103
Exterior	0.0245	0.0258	0.04533
Corner	0.0231	0.0295	0.02686

4.5 Design under lateral loading

4.5.1 Lateral bearing capacity

Alongside with the axial loads, the foundation design should also be able to resist the lateral loads such as wind and seismic loads. In order to check if the foundation's lateral bearing capacity is enough to handle the design lateral loads, the calculation using the Brom's method were performed.

The worst scenario was applied to calculate the maximum load by the structural analysis. Then, the horizontal and vertical loads were obtained. For the corner and exterior columns the worst case scenario includes one earthquake load at the y direction, the interior column includes half of the lateral load:

$$\varphi P_{max} = 1.2D + 1.6L + 1E_y \tag{4.53}$$

$$\varphi P_{max} = 1.2D + 1.6L + 0.5L_r \tag{4.54}$$

The ultimate bearing resistance was taken according to graph of relation with yield moment as the x axis given in Figure 4.15 below.

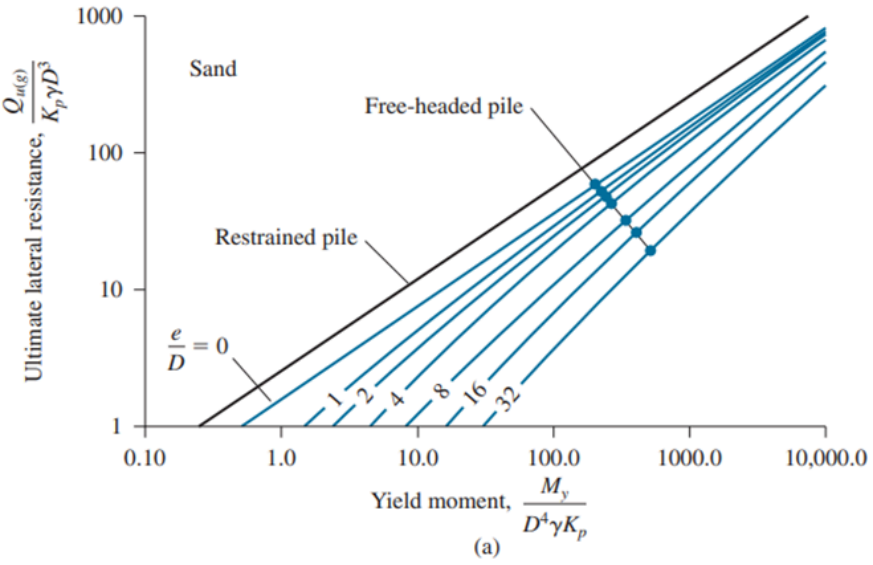

Figure 4.15. Lateral bearing resistance and yield moment relationship

To calculate the yield moment, the moment of the y axis's relation with the diameter and passive earth pressure was calculated:

$$Yield\ moment = \frac{M_y}{D^4 * \gamma * K_p} \tag{4.55}$$

$$M_y = 2F_y I_p / d \tag{4.56}$$

The moment of the inertia of the structural element was calculated as follows:

$$I_p = \frac{\pi D^4}{64} \tag{4.57}$$

The Rankine passive earth pressure was calculated using the equation below:

$$K_p = tan(45 + \varphi'/2) \tag{4.58}$$

Then, the ultimate lateral resistance was obtained using the correlation between the My and e/D ratio graph for short piles in sandy soils. The e/D ratio was taken as 0. The safety factor was taken as 3 in accordance with previous calculations. Table 4.17 shows the data used to calculated the lateral bearing.

Table 4.17. Values for lateral bearing calcultations

Soil type	γ	φ'	K_p	Corner		Interior		Corner	
				M_y	Lateral resist	M_y	Lateral resist	M_y	Lateral resist
Clay	16	24.70	2.75	85.09	65.00	142.3	105	159.6	90.00
MD Clayey Sandstone	17.8	37.89	2.05	112.79	90.00	188.7	1150	211.6	80.00
D Silty Sand	21.0	46.97	5.78	37.13	27.00	62.12	45	69.68	55.00
D F Sandstone	20.7	43.49	4.37	49.38	35.00	82.63	50	92.67	70.00
D F-M Sandstone	21.7	43.89	5.82	34.94	25.00	58.47	47	65.57	35.00
VD F Sandstone	25.5	50.01	6.63	31.00	23.00	51.87	40	58.17	30.00
D F-M Sandstone	22.3	42.09	3.60	62.73	55.00	104.9	80	117.7	80.00
D F Silty Sand	22.7	41.75	4.85	37.25	25.00	62.33	45	69.90	40.00

Then, using the values in the table above, the ultimate and allowable lateral bearing capacities were calculated and given in the Table 4.18. The lateral bering capacity is lower than the allowable which shows the satisfactory results.

$$Q_{all} = \frac{Q_u}{FS} \tag{4.59}$$

Table 4.18. Lateral bearing capacity

Column	Piles in group	Q all, kN	Q lateral, kN

Corner	4	232.36	142.34
Inner	6	172.1	91.31
Edge	6	174.2	88.24

4.5.2 Lateral deflection

To calculate the deflections, the restrained pile's graph in the dimensionless lateral deflection versus dimensionless length plot (Figure 4.16) was considered. Here, to find the η value next equation was used (Mandal et al., 2012):

$$\eta = \left(\frac{\eta_h}{E_p{}^*1000^*I_p}\right)^{1/5} \tag{4.60}$$

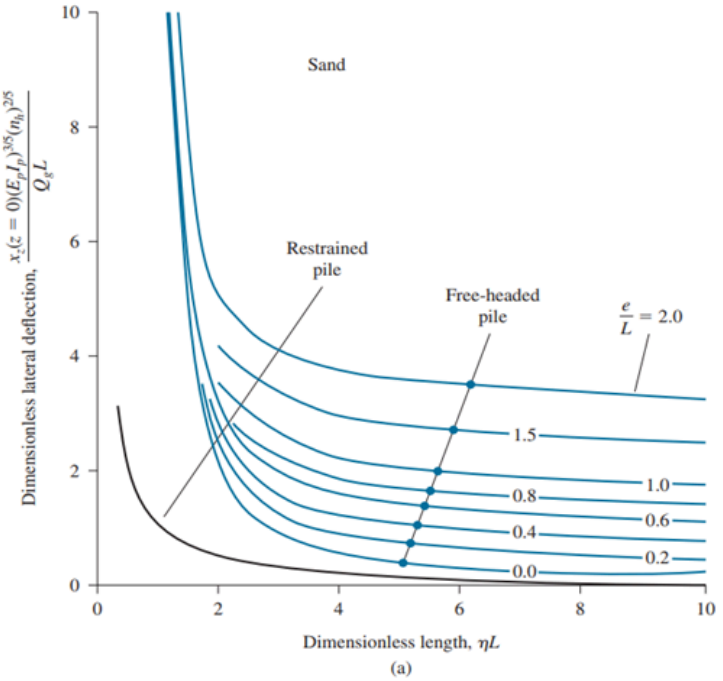

Figure 4.16. Lateral deflection for restrained pile

Using the Excel file, the deflections of each pile group type at the different soil length was calculated. The results are shown in the Table 4.19 an Figure 4.17 below.

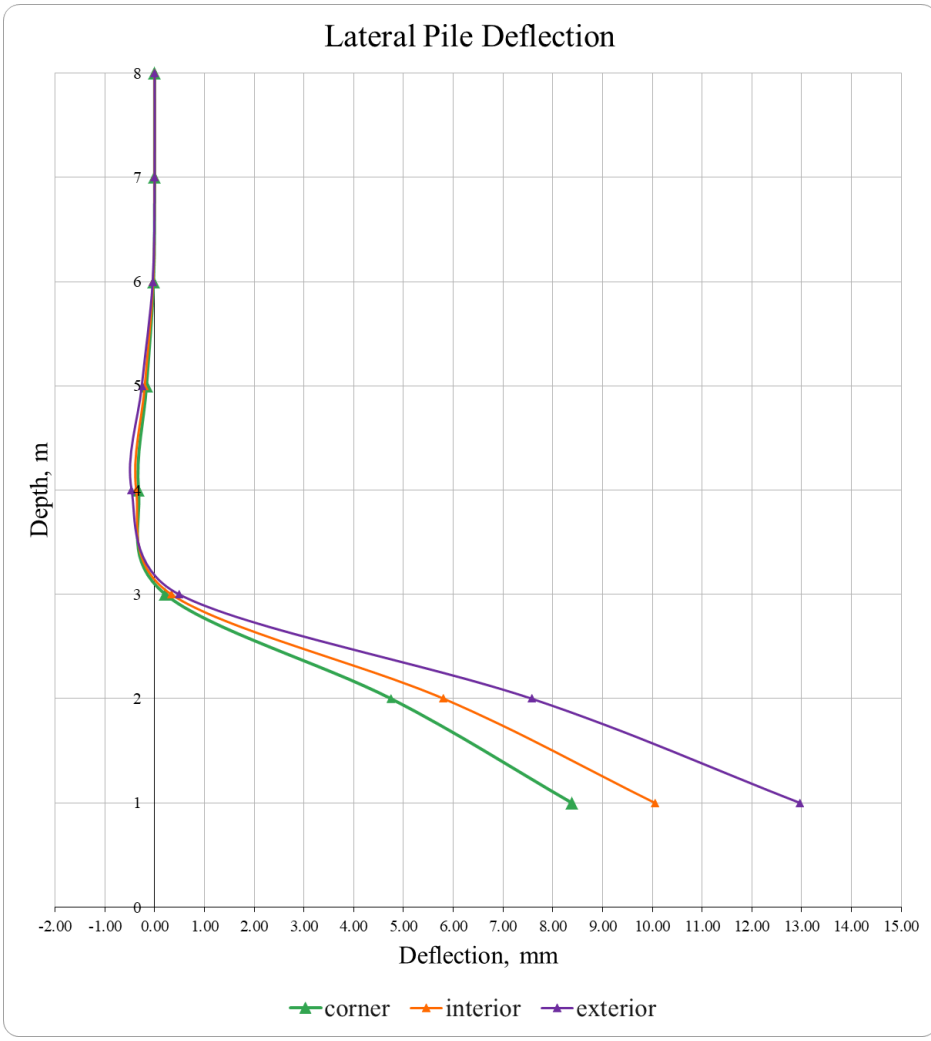

Figure 4.17. Lateral deflection of the piles

Table 4.19. Deflection for each soil depth

Corner, mm	Interior, mm	Exterior, mm
8.39	10.05	12.97
4.75	5.80	7.57
0.22	0.34	0.49
-0.32	-0.37	-0.46
-0.16	-0.20	-0.26
-0.02	-0.03	-0.04

4.6 Reinforcement

4.6.1 Pile Cap reinforcement

According to Patel K. (2023), the pile cap should be fixed if more than 3 piles are present in the group of piles, since the designed pile groups consist of 4 and 6 piles, all piles caps were decided to be fixed. The pile cap's cover was taken as 150 mm and the height is 1.5 times the diameter of the pile. The pile spacing was taken as 3 times the diameter. Embedment of the pile to the pile cap was taken as 75 mm to provide enough bond. All above mentioned estimations are based on specifications mentioned by Patel K. (2023).

Next, the reinforcement of the pile cap was calculated. Here are the values used for the reinforcement calculation of the corner pile group:

$$Pile\ diameter = 350\ mm$$

$$Pile\ spacing c/c = 1050\ mm$$

$$Column\ size = 800 * 800\ mm$$

$$N,\ Column\ load = 3146.107\ kN$$

$$f_y = 460\ N/mm^2$$

$$f_{cu} = 30\ N/mm^2$$

$$Pile\ cap\ height = 350 * 1.5 = 525\ mm$$

$$L_{cap} = B_{cap} = 1700\ mm$$

$$d = 525 - 75 - 28/2 = 436\ mm < 1050/2 = 525$$

Then, the tension force was calculated according to the standard beam theory expression:

$$T = \frac{M}{4d} \tag{4.61}$$

Where,

T - tension force

M - bending moment

d -effective depth of the section

The area of the reinforcement was taken as follows:

$$A_s = \frac{T}{0.95 * f_y} \tag{4.62}$$

Where,

A_s - total required area of steel (mm²)

f_y - yield strength of reinforcement steel (MPa)

0.95 - safety factor (as per design standards)

The number of required bars and the spacing between them was calculated using next equations:

$$Number\ of\ bars = \frac{A_s}{A_{bar}} \tag{4.63}$$

$$Spacing = \frac{L}{number\ of\ bars} \tag{4.64}$$

As it was followed from the calculations, the required pile cap reinforcement is summed up in Table 4.20 below, Figure 4.18 shows the cross section of the corner pile cap reinforcement.

Table 4.20. The pile cap reinforcement

Group Piles	h, mm	Design in x	Design in y
Exterior	525	40 #28mm @ 65mm	24 #22mm @ 70mm
Interior	600	46 #28mm @ 65mm	23 #22mm @ 80mm
Corner	525	23 #28mm @ 70mm	16 #22mm @ 100mm

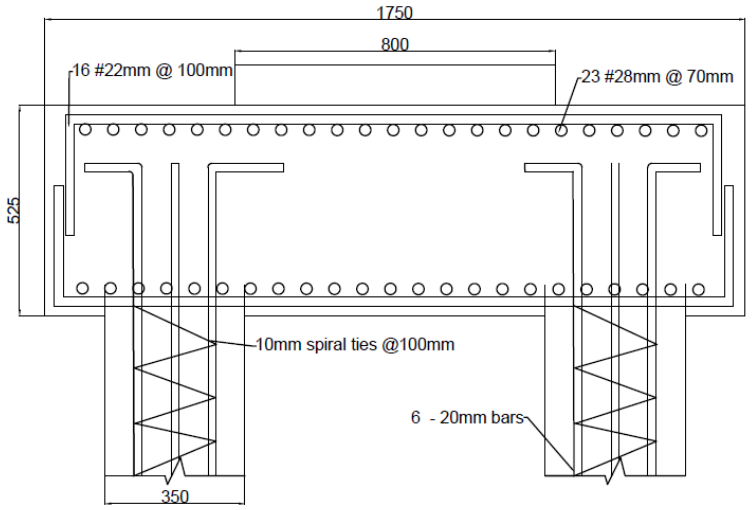

Figure 4.18. Cross section of the corner pile cap reinforcement

4.6.2 Pile reinforcement

According to Patel K. (2023) at least 1.25 percent of reinforcement is required for the pile where the length of the pile is less than 30 times diameter. The h/hs was taken as 0.9, e = 0 m. From the Figure 4.19, the dimensionless load factor is equal to 50, dimensionless yield factor was taken as 110 from the chart. Then using the M/h^3 vs N/h^2 chart in Figure 4.20, the needed reinforcement ratio was taken and related to the bar's area.

$$\frac{Q_u}{c_u * b^2} = 50 \tag{4.65}$$

$$H_{all} = Q_u/2 \tag{4.66}$$

$$\frac{M_\gamma}{c_u * b^3} = 110 \tag{4.67}$$

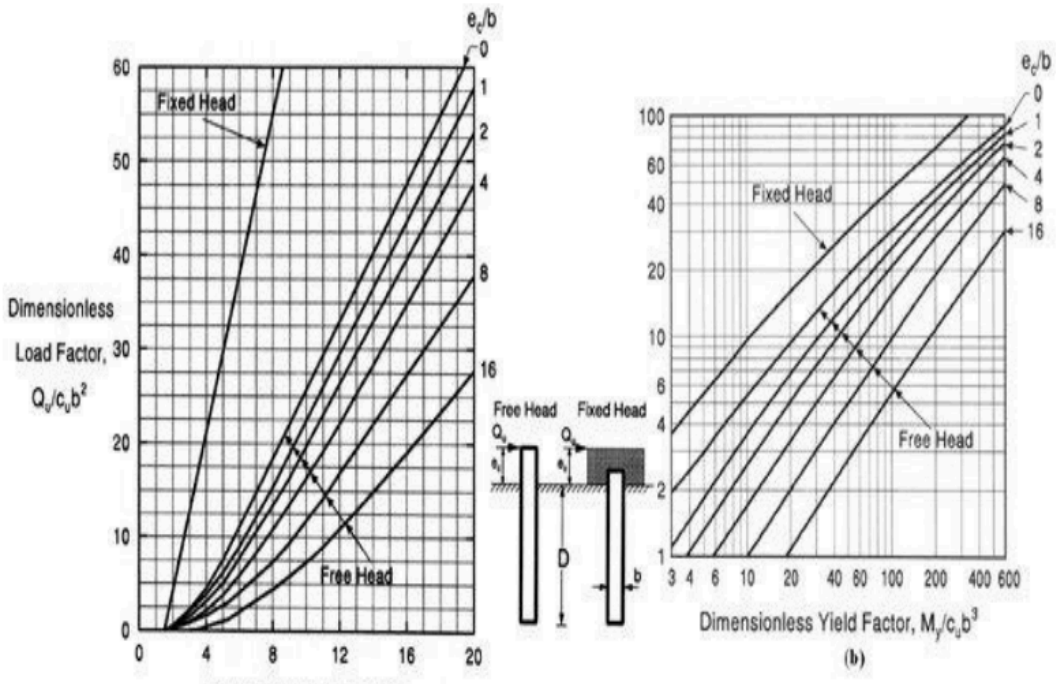

Figure 4.19. Graphs for reinforcement calculation

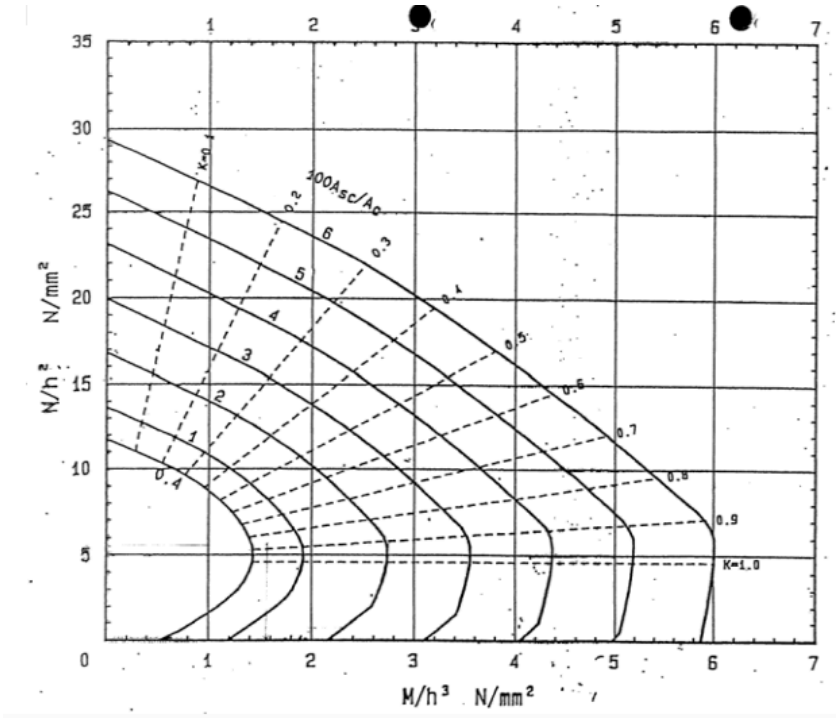

Figure 4.20. M/h^3 vs N/h^2 for reinforcement calculation

The calculated pile reinforcement was then checked using the Geo5 software, shear, bending, compression and reinforcement showed the satisfactory results. The results are given the the Figures 4.21, 4.22, 4.23 below.

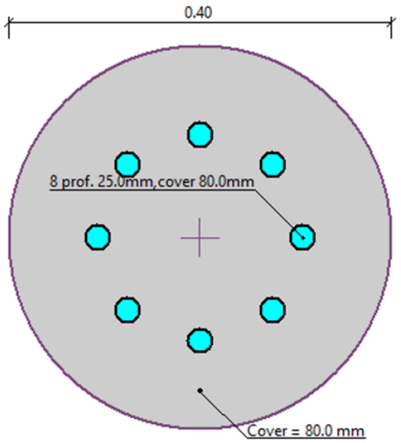

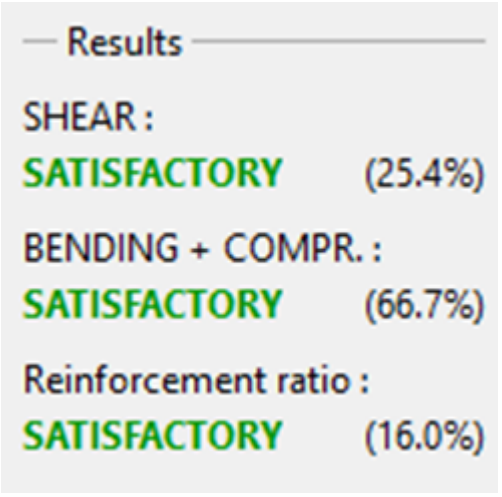

Figure 4.21. Interior piles reinforcement

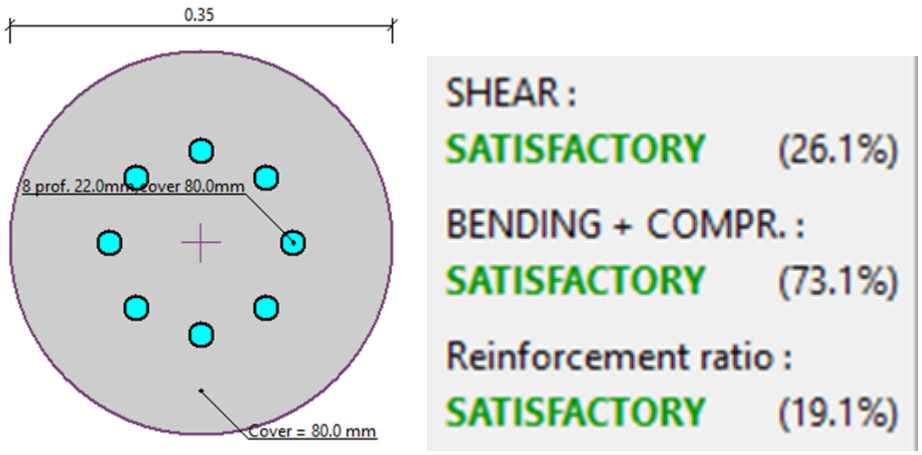

Figure 4.22. Exterior piles reinforcement

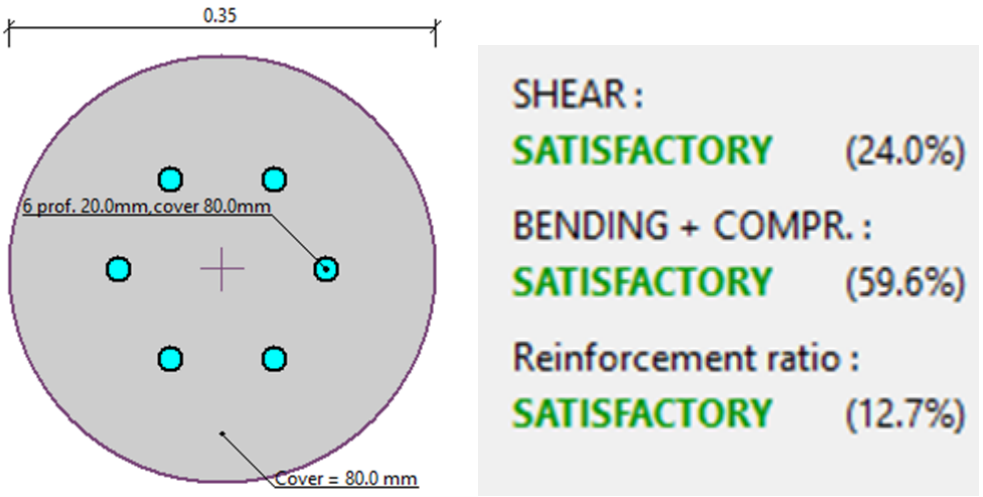

Figure 4.23. Corner piles reinforcement

4.7. Pile Foundation Analysis in PLAXIS 3D

For the 3D numerical simulation in PLAXIS 3D, a complete 3D model of the building was prepared, incorporating every one of the individual columns and their corresponding critical load combinations. Piles caps and sheet piles were incorporated in the design as well. In the model, piles were modeled as embedded beam elements, while the pile caps were modeled as plate elements supported on the basement floor slab. The structural layout includes corner columns, exterior(edge) columns, internal columns, and a 6 × 11 pattern of columns in total, as illustrated in Figure 4.24.

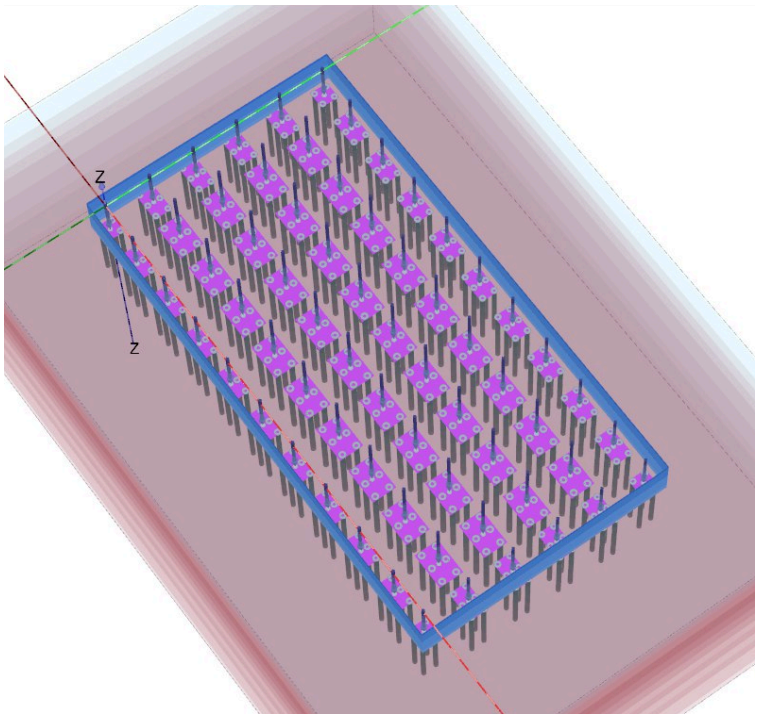

Figure 4.24. Pile Layout in Plaxis 3D

After establishing the pile layout, the meshing process was completed successfully and then certain nodes were selected for further simulation. The sequence of construction of piles was broken into five major phases: the initial phase, excavation, wall and beam construction, installation of pile and pile cap, application of structural load, and finally, the dynamic analysis phase. Numerical analysis in PLAXIS 3D showed that the maximum deformation of the entire building was 20.96 mm. This distribution is illustrated in Figure 4.25.

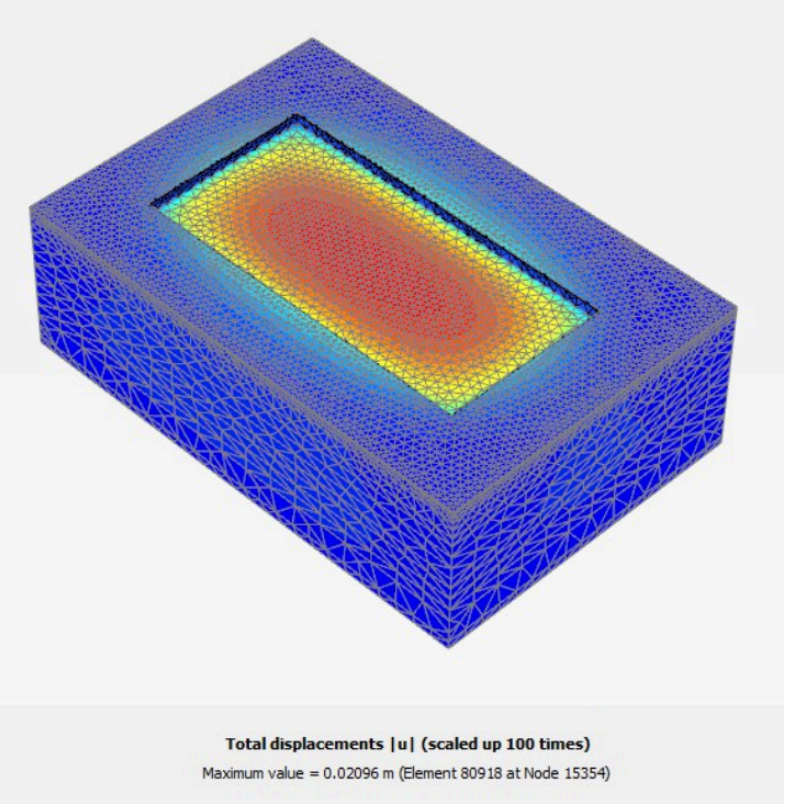

Figure 4.25. Total Displacement in Plaxis 3D

The pile foundation was analyzed using PLAXIS 3D, where load conditions were applied to a corner column. The software computed axial forces, shear forces, and bending moments within the pile group. The results, shown in Figure 4.26, illustrate the distribution of these forces, highlighting the maximum and minimum values for each.

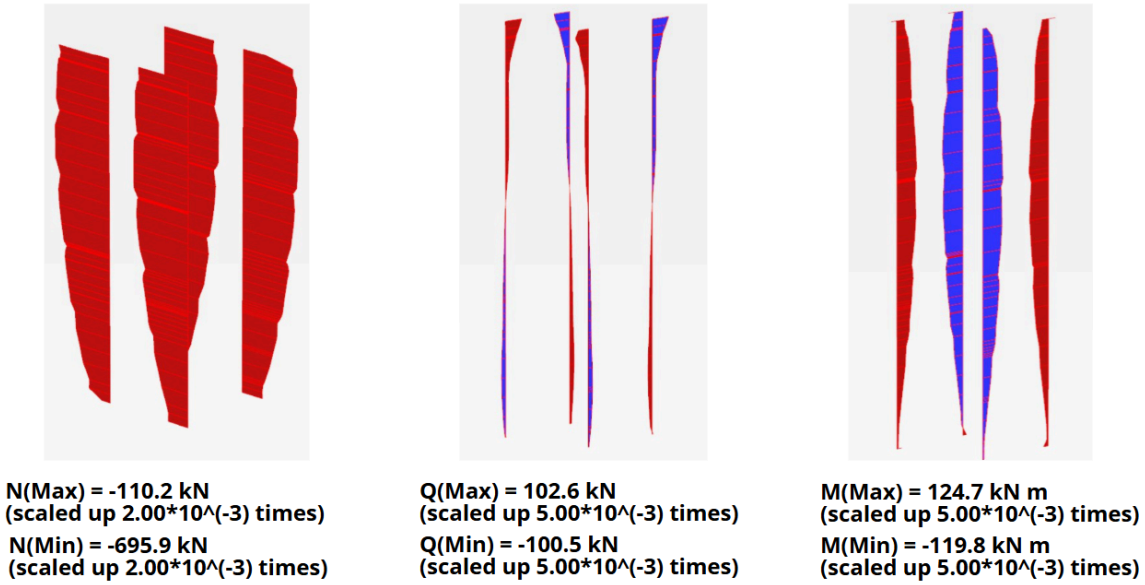

Figure 4.26. 3D Model of Axial, Shear forcer and Bending Moment in Pile Volume for Corner Column

4.8 Sheet Pile design

The comparison between sheet piles and diaphragm walls were performed to choose the one. The comparison taken from Hindustan RMC (2024) is given in Table 4.21.

Table 4.21. Retaining walls comparison

Feature	Sheet Piles	Diaphragm Wall
Depth Capacity	25-30 m	30+ m
Speed	Fast	Slow
Cost	Low	High
Water control	Good	Excellent
Reusability	High	None

So, sheet piles are ideal for temporary works, confined urban spaces, and where quick installation with good water retention is required. However, the installation of the sheet piles can cause vibration. While diaphragm walls offer excellent water control and are used in deep basements and high-load applications but require specialized construction and high cost. It was decided to use the sheet piles due to cost and reusability preferences.

4.8.1 Sheet pile hand calculations

To identify the length of the retaining wall, three lengths should be considered: length of the basement, 3.81m, length where the net pressure equals to zero, and penetration length.

First, equations (4.68), (4.69) were used for the active earth pressure calculations:

$$K_a = tan^2(45 - \varphi'/2) \tag{4.68}$$

Then, the active pressure at the end of the basement, 3.81m was calculated using formula below:

$$\sigma'_1 = L\ K_a\gamma = 20.51\ kN/m^2 \tag{4.69}$$

Next equations were used for passive earth pressure calculations:

$$K_p = tan^2(45 + \varphi'/2) \tag{4.70}$$

$$\sigma'_p = \gamma' K_p(z - L) \tag{4.71}$$

To find the length of the zero net pressure, below the dredge line, and effective stress, next equation was used:

$$L_3 = \frac{\sigma'_1}{\gamma(K_p - K_a)} = 0.75\ m \tag{4.72}$$

$$\sigma'_3 = \gamma\ L_4(K_p - K_a)$$

$$\sigma'_5 = \gamma\ L\ K_p + \gamma L_3 * (K_p - K_a) = 135.21\ kN/m^2 \tag{4.73}$$

$$D = L_3 + L_4 \tag{4.74}$$

Then, to find the length of the L_4, the area and the centroid of the pressure diagram were calculated as follows:

$$P = 0.5\ \sigma'_2 L + 0.5\sigma'_2 L_3 = 36.94\ kN/m \tag{4.75}$$

$$z = \frac{L(2K_a - K_p)}{3(K_p - K_a)} = 2.01\,m \tag{4.76}$$

Then, to proceed with the L_4 calculations, the fourth degree equations should be calculated:

$$L_4^4 + A_1 L_4^3 - A_2 L_4^2 - A_3 L_4 - A_4 = 0 \tag{4.77}$$

Here,

$$A_1 = \frac{\sigma'_5}{\gamma(K_p - K_a)} = 4.821 \tag{4.78}$$

$$A_2 = \frac{8P}{\gamma(K_p - K_a)} = 8.01 \tag{4.79}$$

$$A_3 = \frac{6P(2z\gamma(K_p - K_a) + \sigma'_5)}{\gamma^2(K_p - K_a)^2} = 45.11 \tag{4.80}$$

$$A_4 = \frac{P(6z\sigma'_5 + 4P)}{\gamma^2(K_p - K_a)^2} = 47.61 \tag{4.81}$$

Computing the L_4 value from the equation above, 3.05 m was obtained, so the D is equal to 3.8 meters. The total length of the sheet pile is 3.81+3.8 = 7.61 meters.

To calculate the maximum bending moment, the new axis should be introduced:

$$z' = \sqrt{\frac{2P}{\gamma\,(K_p - K_a)}} = 1.05\,m \tag{4.82}$$

$$M_{max} = P(z - z') - (0.5\gamma\, z'(K_p - K_a)\frac{1}{3}z' = 81\,kNm \tag{4.83}$$

The section modulus of the sheet pile that is needed per the unit length of the structure is calculated by following equation:

$$S = \frac{M_{max}}{\sigma_{all}} = 0.00045\,m^3\ per\ unit\ length \tag{4.84}$$

Figure 4.27 illustrates the final hand calculation results and sheet pile design profile built on Autodesk:

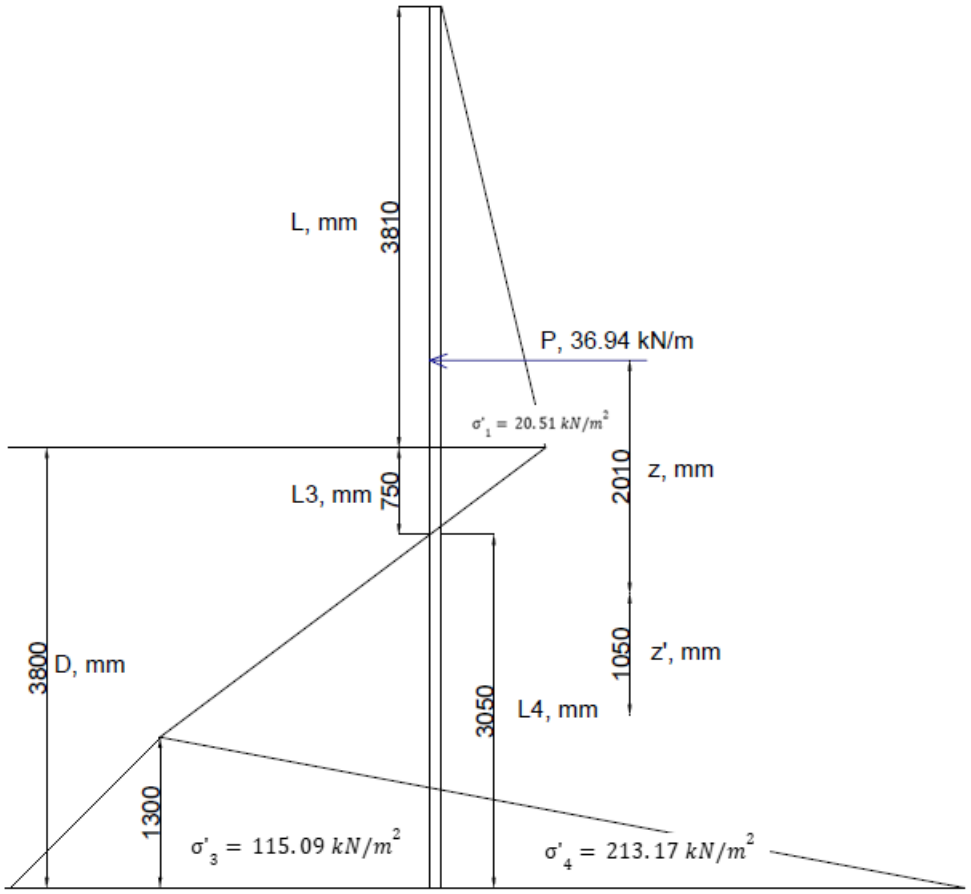

Figure 4.27. Sheet Pile design cross-section

4.8.2 Sheet pile software calculations

The sheet pile design was performed on Geo5 software using the Sheeting Design and Sheeting Check tabs. First, the soil characteristics were uploaded and assigned to each soil depth. The PZ-27 section (Figure 4.28) was used since its effectiveness, excellent statical properties and reusability ("Shunli Steel Group", 2015). It is also has a suitable section modulus derived from the hand calculations. The height of the section is 344 mm, the thickness is 8.5 mm, and the width 770 mm.

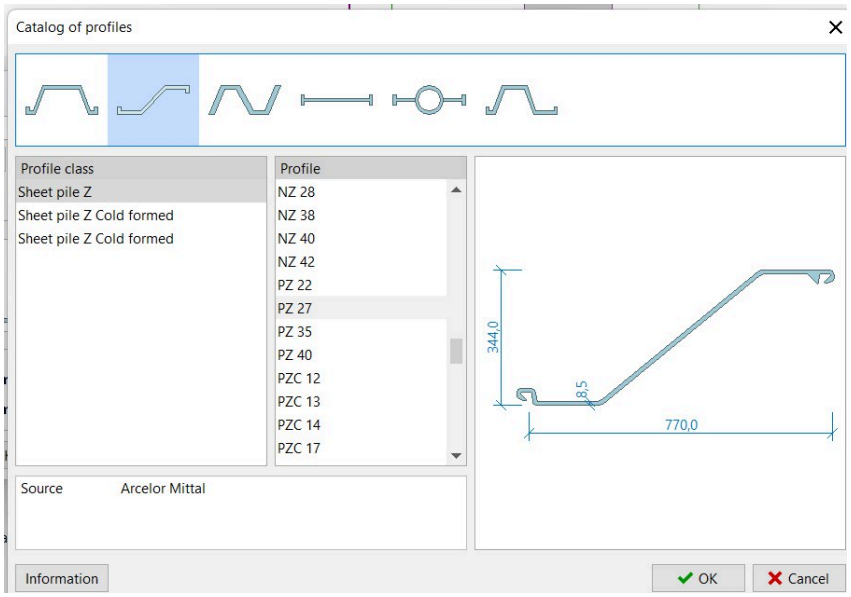

Figure 4.28. PZ-27 Sheet Pile

Then, the analysis of the sheet pile was performed. Total length calculated by GEO5 is 6.97 m and the maximum bending moment is 87.4 kN-m. This values are approximately similar to the hand calculations. The difference can be explained by the fact that GEO5 considered the sheet pile material. The cross section, bending moment and shear force's graphs are givein in Figure 4.29.

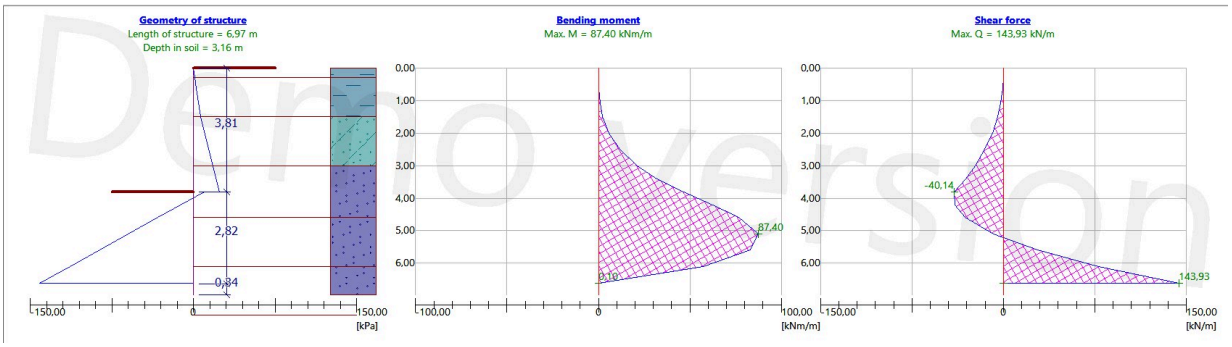

Figure 4.29. Geo5 geometry, bending moment and the shear force for the sheet pile

As it can be seen from the Figure 4.30, the bending, shear and slope stabilities are acceptable and satisfactory. In Figure 4.31, it is given that the displacement is between 5.9 at the top and 1.6 at the bottom, which is within the satisfactory range (Das & Sivakugan, 2019).

Slope stability verification (Bishop)

Sum of active forces : F_a = 266,80 kN/m

Sum of passive forces : F_p = 669,40 kN/m

Sliding moment : M_a = 2342,54 kNm/m

Resisting moment : M_p = 5877,34 kNm/m

Utilization : 39,9 %

Slope stability ACCEPTABLE

Results

BENDING : SATISFACTORY (14,1%)

SHEAR : SATISFACTORY (13,4%)

Figure 4.30. Sheet-pile design's satisfaction check

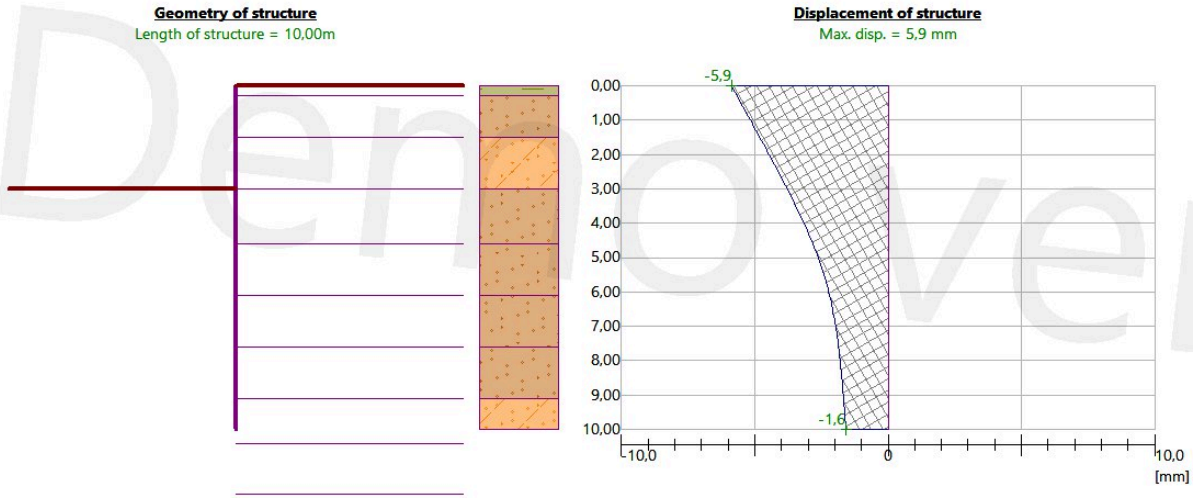

Figure 4.31. Sheet pile displacement Geo5

4.9. Site response analysis

Site response analysis is the process of checking how the ground shakes during an earthquake, depending on the type of soil or rock under the surface. Different soils react differently to earthquake waves — some make the shaking stronger, some make it weaker. So, site response analysis helps us understand how much the ground will shake at a certain place during an earthquake. Since site corresponds to Site Class D and Risk Category III, which shows that it is in high seismic zone, completing site response analysis is necessary.

For these analysis, Plaxis 2D Software was used. At the beginning of the process all the soil parameters were inserted into the Software and it can be shown in the Figure 4.32 below:

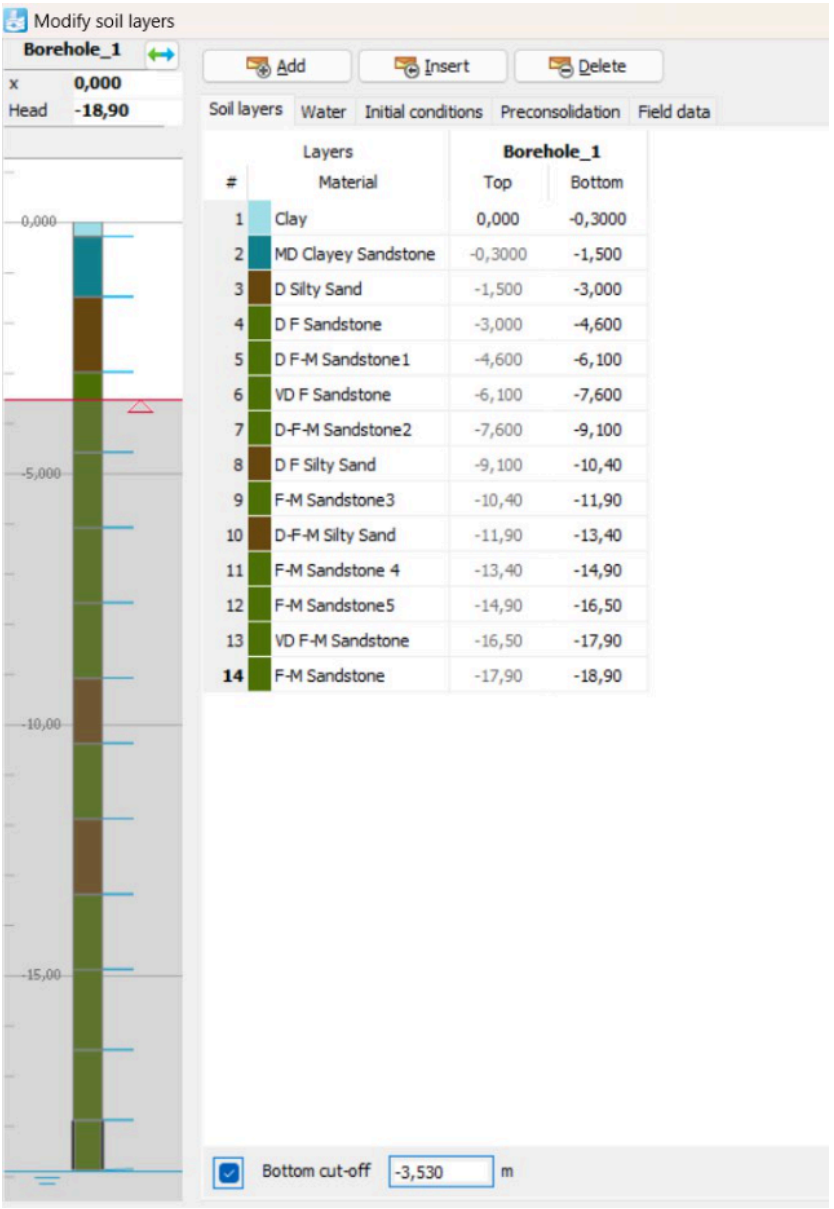

Figure 4.32. Soil parameters needed for site response analysis

After inserting soil parameters, strong motion data taken from Center For Engineering Strong Motion Data was added into the software, after which seismic input signal (often called a ground motion time history) was obtained (Figure 4.33):

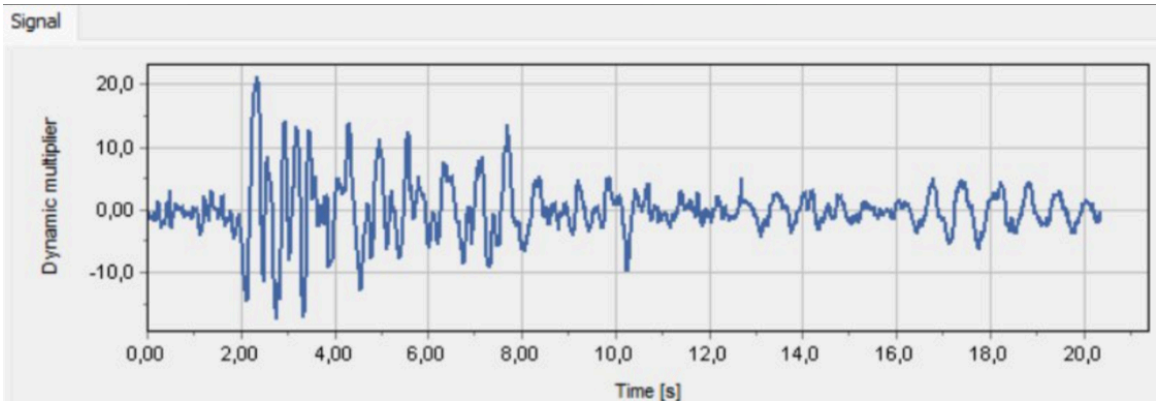

Figure 4.33. Seismic input signal

Then, dynamic multiplier taken from Center For Engineering Strong Motion Data was chosen as Multiplier(x) since Displacement(x) was selected as Prescribed.

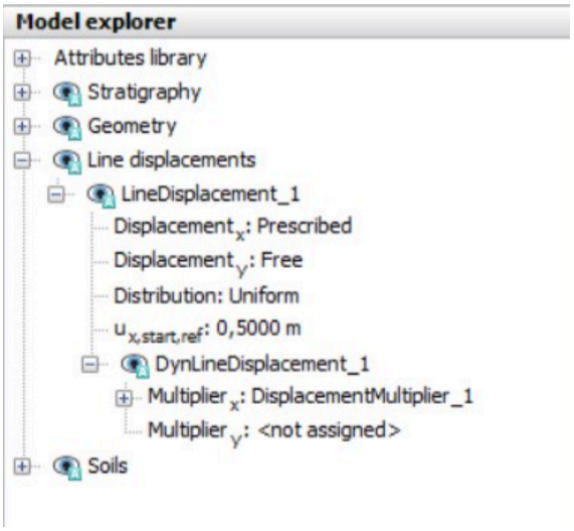

Figure 4.34. Line displacements

For the deformation, several phases were created and different characteristics were set such as dynamic calculation type and staged construction loading type. Time was set to be 20 seconds since it corresponds to the duration of the earthquake signal.

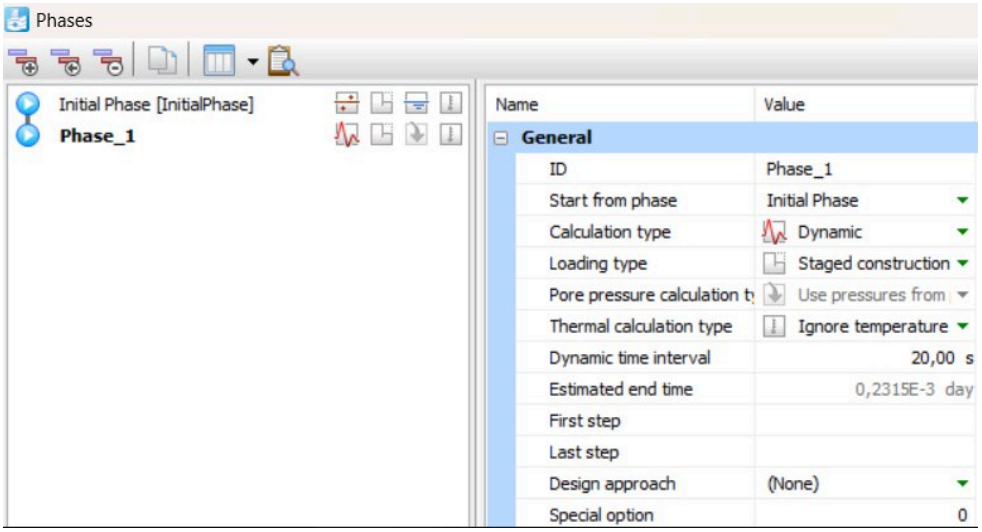

Figure 4.35. Phase_1 characteristics in Plaxis2D

After software did calculation process, and total displacement was obtained in the view section and it is shown in the Figure 4.36 below:

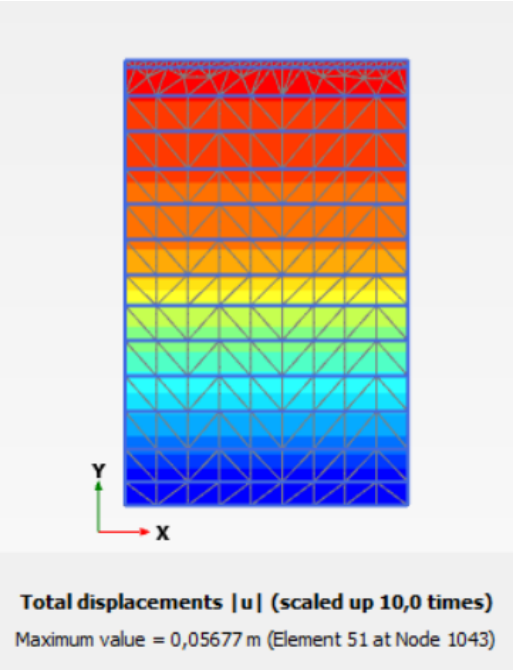

Figure 4.36. Total displacement in Plaxis2D

As can be seen from Figure 18, the soil deformation reaches a maximum value of 56.77 mm.

Figure 4.37 presents the accelerogram of the earthquake, illustrating how ground acceleration varies over time along the x-axis during the seismic event. This time-history

plot captures the dynamic behavior of the ground motion, including both intensity and duration.

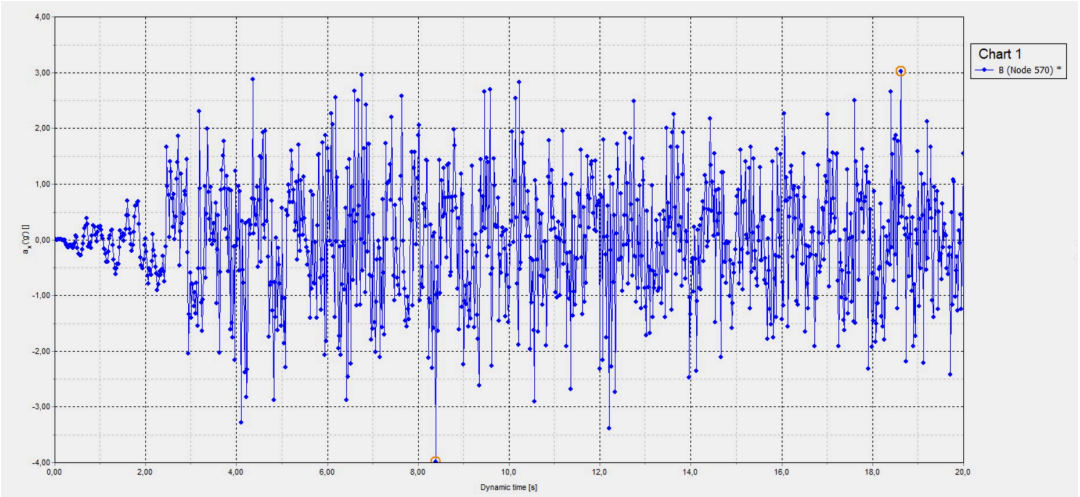

Figure 4.37. A time graph showing acceleration along the x-axis.

To analyze the frequency content of this motion, a Fast Fourier Transform (FFT) was applied to the accelerogram, and the resulting amplitude spectrum is displayed in Figure 4.38. This transformation helps identify dominant frequencies and the energy distribution of the seismic waves.

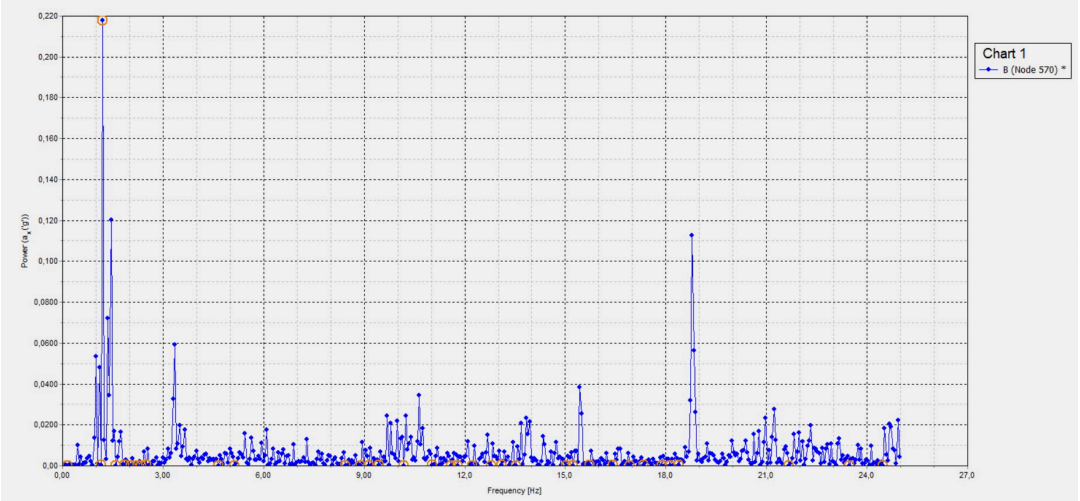

Figure 4.38. Fast Fourier plot performed at the base of the soil.

Figure 4.39 shows the peak spectral acceleration (PSA) derived from the response at a node located at the bottom of the soil layer. This PSA plot provides valuable insight into how different frequencies of ground motion affect structural response, which is critical for seismic design and soil-structure interaction analysis.

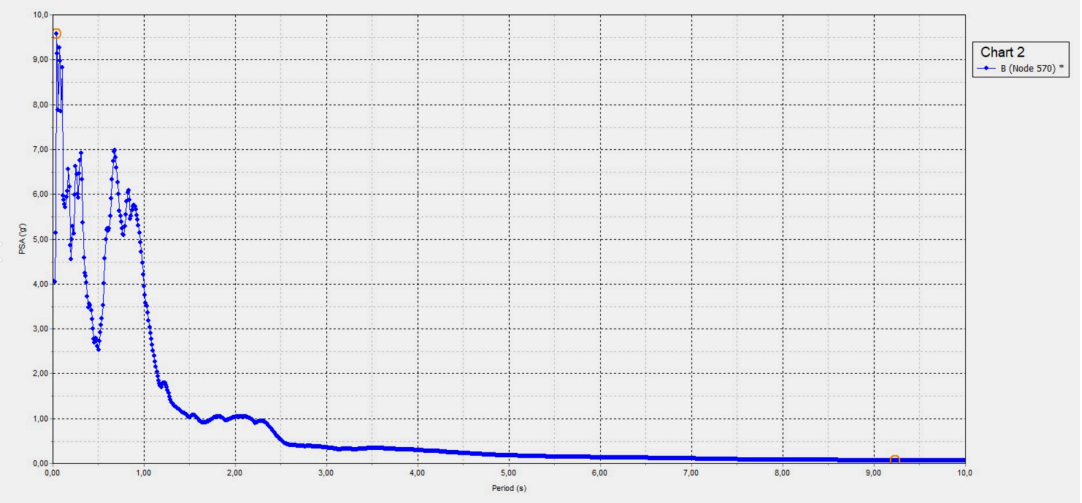

Figure 4.39. Peak spectral acceleration plot

4.10. Detailed construction procedure

Site Preparation

Vegetation, tree roots, shrubs and other organic or compressible material must first be cleared from the construction zone to clear any material that can affect the bearing capacity or lead to differential settlement. Next, surface grading should be done to provide a level and accessible work at area and drainage to prevent water logging during construction. Wherever it is needed, building of working platforms is required, which are generally made of compacted gravel or crushed stone to support the weight and movement of the CFA rig and the equipments associated with it, to ensure safety and efficiency in operations.

Mobilization and Setup

Mobilize and set up required equipments, including a suitable torque and depth piling rig. For a tremie style concrete placement, the concrete pump would connect to the auger. Reinforcement cages should be pre fabricated according to structural design. To maintain concrete quality, agitators or ready-mix trucks will be used.

CFA Pile Construction

CFA rig can be placed exactly at the pre-surveyed pile location. Rotate, apply vertical pressure and advance the continuous flight auger into the ground until the estimated depth of

6 meters is reached. Applying no casing or bentonite slurry results in a reduction of spoil and water management, which enhances the costs.

Concrete Placement

As the stem of the auger is slowly withdrawn the concrete is pumped, under pressure, through the hollow stem. It does not move the soil but rather displaces it laterally to reduce the risk of settlement and impact on the environment. Continuous concrete flow in the pile is maintained to avoid voids or necking within the pile.

Reinforcement Insertion

The reinforcement cage is inserted as soon as concrete is in place into fresh concrete using vibratory or manual assistance immediately following the withdrawal of the auger to its full withdrawal. The reinforcement must be inserted rapidly for workability of concrete and proper embedment.

Pile Cap Construction

Excavate the soil around the pile group to the bottom elevation of the pile cap after pile curing, usually 48–72 hours. Head pile required to be trimmed as required to have a level surface and full contact on the cap. Correct anchorage and cover of reinforcement to place formwork and reinforcement as per structural drawings is required. Permit the concrete for the pile cap in one continuous action. Vibrators can be used to compact and eliminate air voids at pile head and reinforcement intersections. The concrete comes to a required strength and durability via cure based on the specifications.

The CFA method of boring the piles was chosen after the literature review and comparison of several bored piles methods. The CFA advantages given by Brown A. (2006) were satisfactory to choose the CFA. Project-Specific Justification for CFA choice:

- ➔ The medium to dense sandstone and sandy clay layers of the soil profile suited well the CFA technology contents.
- ➔ The performance of the CFA equipment is ideal to install the 6m pile length as this prevents the risk of collapse or refusal when installing.
- ➔ CFA piles provide the best cost and low impact to the environment.

5. Environmental Engineering

5.1 Stormwater Management Design

5.1.1 Topographic Analysis

A topographic map of the selected site was obtained using the online tool at Contour Map Creator. The analysis reveals that the site slopes gently toward the northeast, with an elevation change of approximately ±1 m. This topographic feature provides a natural advantage for stormwater drainage. The house is planned to be located at the highest point (138 m), while the park and parking lot will occupy the lower areas, allowing for a gravity-driven flow of stormwater toward the catch basins.

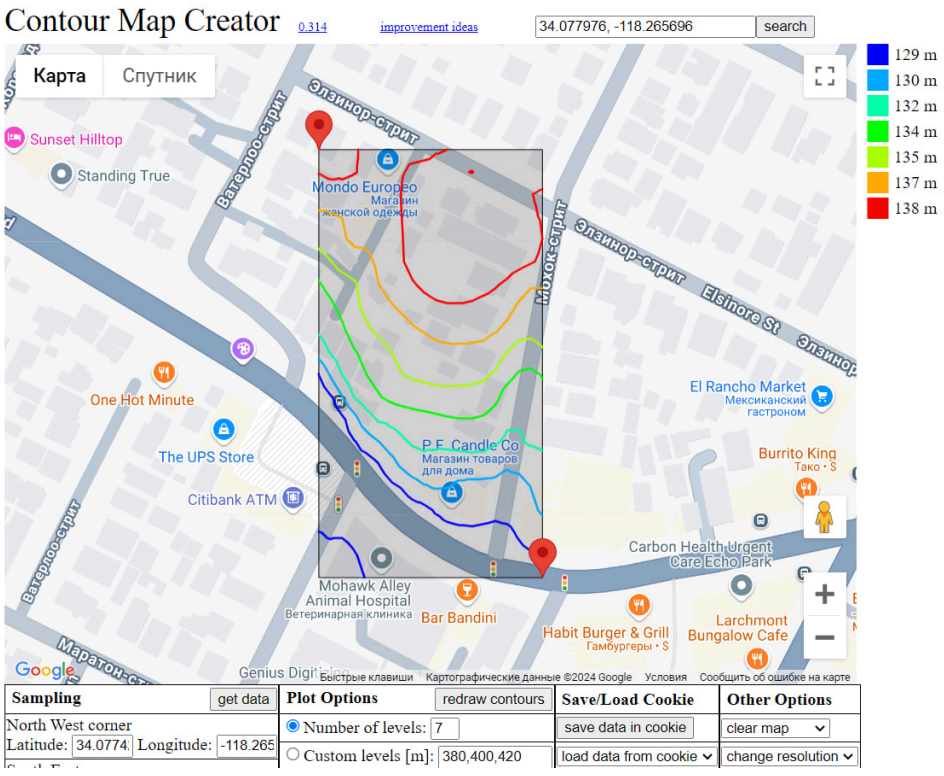

Figure 5.1. Topographic Map: Site slope and elevation.

5.1.2 Stormwater Management System

The stormwater management system is designed to include gutters along the building's perimeter, which collect runoff from the roof. This collected stormwater is then channelled through underground pipes connected to strategically positioned catch basins [Insert View from Above with Site Layout]. The site layout features blue lines for gutters, purple lines for stormwater pipes, and purple circles for catch basins. The parking lot and park areas are at a lower elevation, promoting natural water flow and preventing potential flooding around the structure.

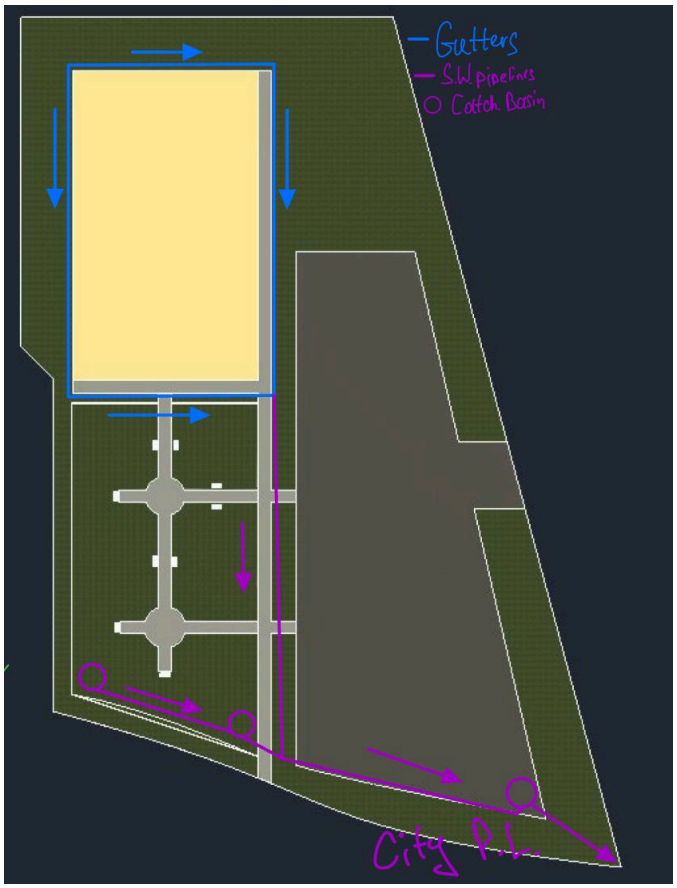

Figure 5.2. Site Layout

The collected stormwater is directed to connect with the main city stormwater pipeline running across Sunset Boulevard. This connection has been manually annotated on the city pipeline map to highlight the planned drainage pathway.

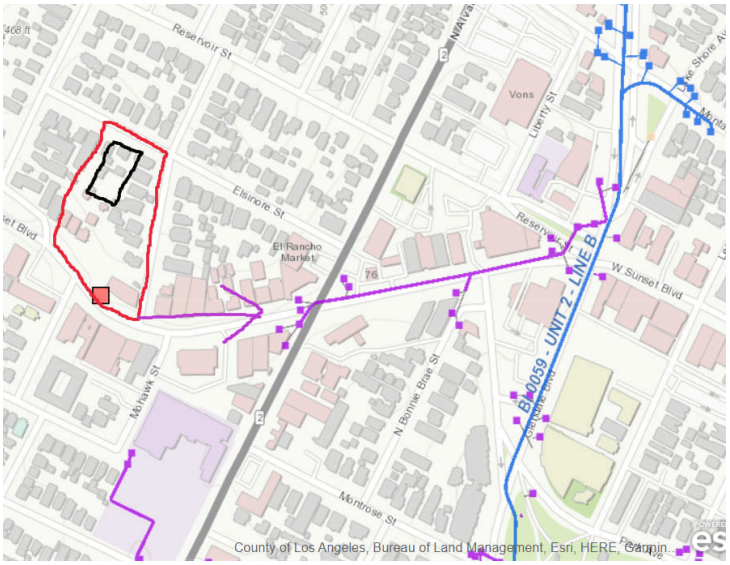

Figure 5.3. City Pipeline Map

5.2 Site Layout Advantages

A significant environmental advantage of the proposed site layout is its natural inclination toward stormwater drainage. By placing the building on an elevated surface while situating the parking and park areas on lower ground, gravity can effectively direct water runoff away from the building. This design minimises flooding risks and reduces the need for mechanical pumping systems, contributing to both cost savings and environmental sustainability.

5.3 Sustainable Water Management

In addition to the stormwater management system, several green infrastructure elements are proposed to enhance water management further:

- Permeable Pavements: Implementing permeable materials in parking areas and sidewalks will reduce surface runoff.
- Rainwater Harvesting: Installing rainwater collection systems will allow for the reuse of water in irrigation and other non-potable applications.
- Green Infrastructure: Incorporating rain gardens and bioswales into the landscaping design will naturally absorb and filter stormwater, mitigating flash flood risks and improving groundwater recharge.

This environmentally conscious approach aligns with the project's sustainability goals and meets the local stormwater regulations and city infrastructure requirements.

5.4 Grading and Drainage Plan

The grading and drainage plan is a critical component of the Verdigris View high-rise project. It ensures the site’s functionality and aesthetic integration while providing effective stormwater management to comply with regulatory requirements and secure construction permits from the municipality. Below, the key elements of the grading and drainage plan are detailed.

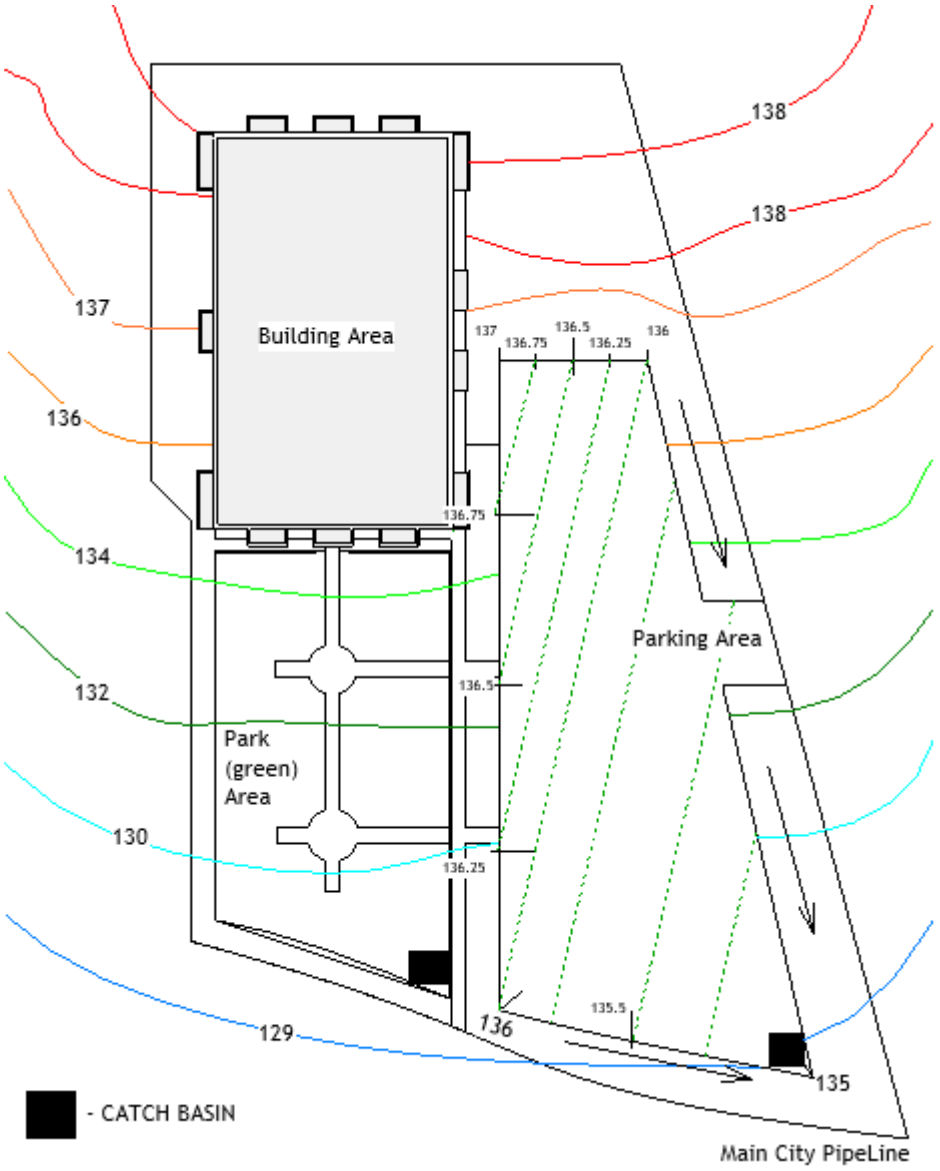

Figure 5.4. Grading and Drainage Plan

5.4.1 Existing and Proposed Grades

The grading plan was designed to show both existing and proposed grades across the construction property. The site slopes gently from its highest point at approximately 138 meters above sea level (near the building's planned footprint) to the lowest point at 133 meters (near the parking lot and landscaped areas). This natural slope was utilized to enhance stormwater runoff towards designated drainage elements.

- Existing Grades: The current topography of the site features a gentle slope towards the northeast. This topography supports gravity-driven stormwater flow and reduces the likelihood of water pooling near the structure.
- Proposed Grades: The building area, located on a slope from 138 meters to 135 meters, will be filled to create a flat surface at 138 meters for construction. This adjustment ensures a stable foundation and optimal drainage around the structure. The park area will retain its natural slope, while the parking lot is designed with a gradient to prevent water pooling, as shown in the provided figure.

5.4.2 Drainage Elements

To ensure effective water management and comply with environmental regulations, the drainage plan incorporates several key elements:

- Gutters and Catch Basins: The provided figure illustrates the placement of gutters around the building perimeter, directing water to catch basins located strategically throughout the site. The catch basins are marked with purple circles in the drainage plan and are connected by underground stormwater pipes (purple lines).
- Drainage Swales: Grass-lined swales have been incorporated into the landscaping plan to provide natural infiltration areas. These swales guide surface runoff toward catch basins while filtering out debris.
- Easements: The plan identifies necessary easements for stormwater pipes crossing the property boundary to connect with the city's stormwater infrastructure along Sunset Boulevard.

5.4.3 Site Elements

The grading and drainage plan considers the functional and aesthetic design of various site components:

- Parking Lot: The parking lot, located at the lower elevations of the site, has been graded to prevent water pooling. Permeable pavement materials will be used to allow natural infiltration of rainwater into the ground.
- Landscaped Areas: The park and greenery areas are designed to promote natural drainage. The natural slope of the park remains unchanged, and rain gardens will be installed to absorb and manage stormwater runoff while enhancing the visual appeal of the site.
- Onsite Roads: Roads within the site are graded with a slight crown to direct water into adjacent gutters, ensuring efficient drainage and safety during rainy conditions.

5.4.4 Earthwork and Site Preparation

- Cut and Fill: The building area's slope will be leveled by filling to 138 meters, while the park retains its natural slope. Soil cut from other areas will be reused for filling, maintaining cost-effectiveness and sustainability.
- Slope Stabilization: Retaining structures and stabilized slopes will be implemented where necessary to prevent erosion and ensure safety during construction and long-term use.

5.4.5 Notes and Instructions

The following details and instructions are included to guide contractors during construction:

- Grading contours to highlight the slope changes across the lot.
- A legend is provided to distinguish between existing and proposed grades, as well as drainage elements.
- All grading and drainage designs comply with local regulations and permitting requirements.

5.5 Stormwater Runoff Analysis and Drainage Design

The Environmental Engineering component of Capstone II presents the complete design of the stormwater runoff system for the project site. This builds upon the preliminary drainage

layout introduced in Capstone I, and now includes detailed runoff calculations, trench drain sizing, material selection, and slope layout - all based on city standards and California stormwater legislation.

5.6 Runoff Estimation Methodology

5.6.1 Objective

To calculate stormwater runoff rates for each section of the project site under a 10-year storm event, using the **Rational Method**, and to size a trench drain system capable of safely conveying this flow toward the municipal drainage network.

5.6.2 Rational Method Formula

$$Q = \frac{C_d * I * A}{4047}$$

- Q: Peak discharge in cubic feet per second (cfs)
- Cd: Runoff coefficient (dimensionless)
- I: Rainfall intensity = **2.56 in/hr**
- A: Area in square meters
- 4047: Conversion from m² to acres

5.7 Time of Concentration (Tc) Calculations

To estimate how long water takes to reach the drains during rainfall, we used a combination of overland flow and shallow channel flow formulas.

5.7.1 Formulas Used

$$T_{t1} = \left(\frac{0.933}{I^{0.4}}\right) * \left(\frac{0.15 * L_1}{304.8 * \sqrt{S_1}}\right)^{0.6}$$

$$T_{t2} = \frac{L_2}{304.8} * \frac{3.28*0.457*n}{\sqrt{S_2}*60}$$

$$T_c = T_{t1} + T_{t2}$$

- L1, L2: Width and Length of flow path (in meters)
- S1, S2: Slopes in decimal (e.g., 1% = 0.01)
- n: Manning's surface roughness coefficient
- Tc: Time of concentration (minutes)

5.8 Stormwater Runoff Results

The Rational Method was applied to all major surface zones in the project: green areas (G1–G7), asphalt parking (A1), and the building rooftop.

Table 5.1. Stormwater Runoff Characteristics – Cd, Tc, Q (cfs)

Section Name	Area m^2	longest Width(m)	longest Length(m)	Slope Width %	Slope Length %	n	Tt1	Tt2	Tc	Q(cfs)
G1	2325,6	38,59	64	1	0	0,15	14,92	6,42	21,34	0,2207
G2	470,5	8	58,14	1	0	0,15	5,80	5,84	11,64	0,0446
G3	276,4	32	8,65	0	1	0,15	13,33	0,87	14,20	0,0262
G4	929,1	29,62	37,66	0	1	0,15	12,73	3,78	16,51	0,0882
G5	331,3	56,92	6	0	1	0,15	18,84	0,60	19,44	0,0314
G6	766,9	8,27	93,75	1	0	0,15	5,92	9,41	15,33	0,0728
G7	86	3,96	21,7	0	1	0,15	3,81	2,18	5,98	0,0082
Roof	1500	30	50	1,5	1,5	0,011	2,67	5,02	7,69	0,7591
A1	2531,5	41	94	1,5	1,5	0,011	3,23	9,44	12,66	1,4412

5.9 Surface Types and Cd Values

Table 5.2. Runoff coefficients for corresponding surface zones

Surface Zone	Description	Runoff Coefficient (Cd)
G1–G7	Grass / Vegetated areas	0.15
A1	Asphalt (Parking)	0.85
Roof	Concrete Roof	0.90

All Cd values follow the **LA County Hydrology Manual (2022)** and local design codes.

5.10 Drain Design – Manning Equation

5.10.1 Manning Formula for Open Channel Flow

$$Q = \frac{1}{n} * A * R^{2/3} * S^{1/2}$$

- Q: Flow rate (m^3/s)
- A: Cross-sectional area (m^2)
- R: Hydraulic radius = A/P
- S: Slope = **2% (0.02)**
- n: Manning coefficient = **0.013**
- Assumed velocity V=1.5 m/s

Table 5.3. Drain Sizing Summary – Q (m³/s), Velocity, Area, Depth, Width

Drains	Areas	Q(cfs)	Q(m3/s)	Velocity	Est. Area (m^2)	Depth(m)	Width (m)
L1	G2	0,0446	0,001264 16143	1,5	0,000843	0,031	0,061
L2	G3	0,0262	0,000742 644462	1,5	0,000495	0,025	0,050
L3	G4	0,0882	0,002496 349384	1,5	0,001664	0,040	0,079
L4	G7+G1	0,2288	0,006479 599799	1,5	0,004320	0,057	0,113
L5	G6	0,0728	0,002060 542829	1,5	0,001374	0,037	0,074
L6	A1+G5	1,4726	0,041700 66875	1,5	0,027800	0,114	0,228
S=	0,02				**Min. Regulations**	**0.15**	**0.3**
n=	0,013						

5.11 Visual Design and Infrastructure Layout

Drainage design was visualized with the following technical illustrations:

Figure 5.5. Territory Drainage Layout

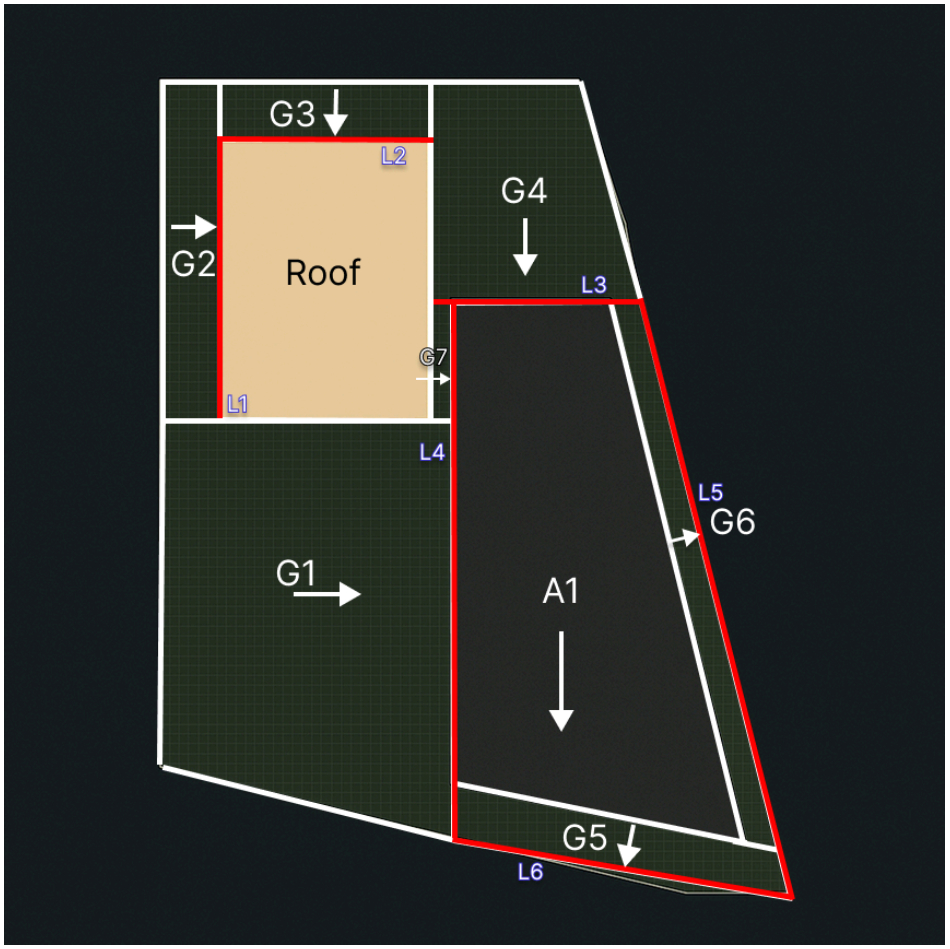

Territory Drainage Layout showing subareas G1–G7, A1, and Roof with their respective stormwater flow paths (L1–L6). The map illustrates how surface runoff is directed from different zones into designated trench drain sections.

Figure 5.6. Cross-Section of Typical Trench Drain

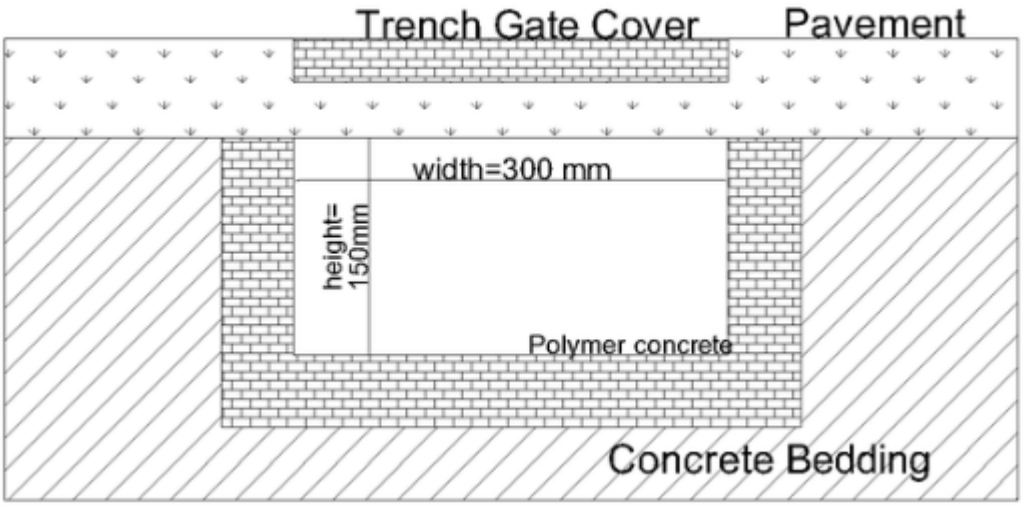

Cross-sectional view of the designed trench drain with a width of 0.30 m and depth of 0.15 m. The section shows the drain grate, polymer concrete body, and concrete bedding in compliance with Los Angeles drainage standards.

Figure 5.7. Longitudinal Profile of L4

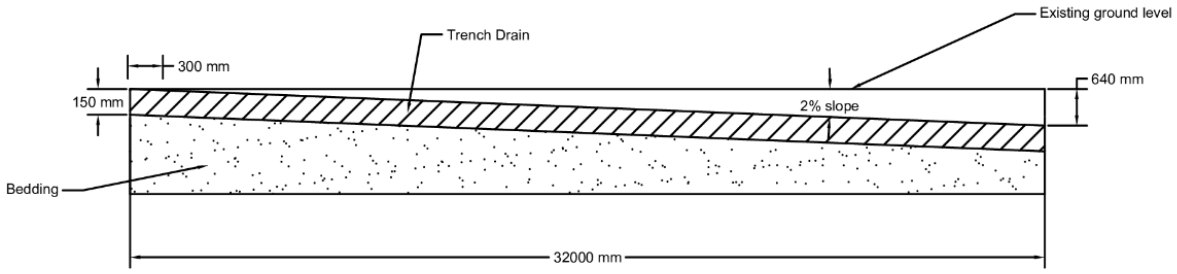

Longitudinal profile of trench drain L4 over an 87-meter length, demonstrating a uniform slope of 2%. The diagram represents the gradual elevation drop required for effective surface runoff conveyance. These drawings were developed in AutoCAD and Revit based on site survey data and slope assumptions. Minimum slope of 2% was maintained across all trench runs.

5.12 Materials and Construction Standards

Component	Specification
Drain Body	Polymer Concrete
Cover	Galvanized Steel Grate
Bedding	Poured Concrete
Trench Width	Minimum 0.30 m
Trench Depth	Minimum 0.15 m
Slope	2% Uniform Longitudinal

The drain design follows **LA City Standard Plans – S-600 series**, **Caltrans Section 68**, and **ASCE 63-18** guidelines.

5.13 Compliance and References

All values, methods, and calculations comply with the following standards:

- **Los Angeles County Hydrology Manual (2022)**
- **California State Stormwater Management Codes**
- **Hydraulic Engineering Circular No. 22 (HEC-22)**
- **Uniform Plumbing Code (UPC)**

- **ASCE Standard 63-18: Stormwater Conveyance Design**

- **Caltrans Section 68: Drainage Facilities**

5.14 Conclusion

This final design meets all required stormwater performance criteria. Using accurate surface runoff estimation, standard-compliant trench sizing, and effective slope integration, the environmental design ensures robust and maintainable water conveyance for the project site. It accounts for current rainfall patterns and urban drainage requirements, with flexibility for future system connection or extension.

6. Construction Management

6.1. Project Charter

General Information	
Project title	*Design of a 12 story "Verdigris View" high-rise building in Los Angeles, California, USA*
Project description	12 story residential high-rise building with outside parking, green garden, commercial first floor, and

	basement. The location for the project was selected at 2217 W Sunset Blvd Los Angeles, CA 90026, United States. The area is located in Echo Park. Area has multiple locality amenities such as Office Complex, Shopping Mall, Restaurants & Entertainment.		
Project start date	August 2024	**Project end date**	August 2030
Project manager	Sanzhar Revshanov	**Project Sponsor**	Nazarbayev University
Purpose	Project Goal: To build a 12-story residential high-rise in a low-density area, providing a more affordable housing option in a neighbourhood with high property prices. This would also support local businesses and increase commercial activity. Benefits: Provides a cost-effective alternative to expensive homes in the area. Features a green garden for residents to enjoy a peaceful outdoor space. Includes a commercial ground floor to support local shops and services.		
Project scope	• Build a 12-story residential high-rise with commercial spaces, basement, and outdoor parking. • Develop a green garden for residents. • Provide affordable housing in a high-cost area. • Ensure compliance with local regulations and sustainability standards.		
Project deliverables	1. A 12-story residential building with commercial units on the ground floor.		

	2. Basement and outdoor parking facilities. 3. A landscaped green garden for resident use. 4. Cost-effective construction focused on affordability in a high-cost area.		
Risk and issues	1. Cost escalation 2. environmental regulations 3. community opposition 4. traffic and access issues 5. permitting delays		
Assumptions/ dependencies	1. The building will be structurally safe and accommodate 570 residents. 2. The green garden will provide a peaceful communal space. 3. The apartments will be in high demand and fully occupied. 4. Traffic and parking will be managed effectively for residents and businesses.		
Estimated budget			
Milestones	**Stage**	**Deadline**	**Status**
	Planning	25.04.2025	In progress
	Site work	21.09.2026	Not started

	Construction	12.10.2029	Not started
	Finishing	24.07.2030	Not started
	Project closure	29.08.2030	Not started

6.2. Feasibility study

A feasibility assessment for a high-rise residential building in Echo Park, Los Angeles at 2217 W Sunset Blvd has been conducted. It includes site suitability, design, environmental impact, legal aspects of the project and the economic benefits of such a project site as well as a calendar with dates on when every stage has to be finished. The site is within a mixed-use residential and commercial area just a short distance from parks, restaurants, transit hubs. Area is large enough to build on and will be providing parking for 264 vehicles along with a landscaped garden, once built. Provides good traffic flow with separate lanes for cars and footpaths.
Visualization was created by developing its building design on Revit. It merges a green garden to allow residents to enjoy a peaceful experience. The project design meets California and LA Building Codes whilst addressing functionality and reducing redundancy of space. This will ensure there are no major compliance issues which is going to make it key in the approval process. It would also comply with California Environmental Quality Act regulations, which dictate mitigation where necessary due to the seismicity of the site. Waste management [during and post-construction] will be recycling, with residents' facilities providing dedicated service.

The project is following all regulations provided by local authorities. They will hold contractors and vendors accountable through binding contracts. Maintaining worker safety: strictly adhering to labor laws with legal professionals on hand at every step of the project ensuring safety; It's hoped the development will have a beneficial effect on the economy in creating jobs for engineers, architects, construction workers and service providers. The apartment complex will contain a total of 176 residential units and 10 commercial ones. Average Market Rate for Apartment Rent is $2,404/Month Approximately. Fast return on investment, to kick-start the growth of Echo Park, is something that we are excited about.

The timeline for the project covers design, construction and final inspections from August 2024 through August 2030. The project will be led by means of a Work Breakdown Structure (WBS) and Gantt chart for effective task management and resource allocation. The schedule incorporates a buffer period to accommodate possible delays, with the target of on-time delivery by August 2030.

6.3. Cost/benefit analysis - RS Means

One of the many ways to reduce the possibility of suffering some monetary loss is by carrying out accurate cost estimation which is undoubtedly one of the most important parts of any construction project. The use of different approaches, methods, tools and types of software to create detailed and accurate cost estimates has become part of the state-of-the-art in modern construction. RSMeans (RSM) were used to model and cost out construction through the high-rise residential building project,

RSMeans, available from the Gordian Group for construction cost estimating and productivity standards (Nicolas, Monjurul, & Ming, 2018). This software relays the current cost data so that engineers, architects and contractors can estimate and control the project budget in one overall number. Furthermore, RSMeans can be used for assessing productivity rate and overhead and profit margins based on the time and location of the construction project (Nicolas et al., 2018).

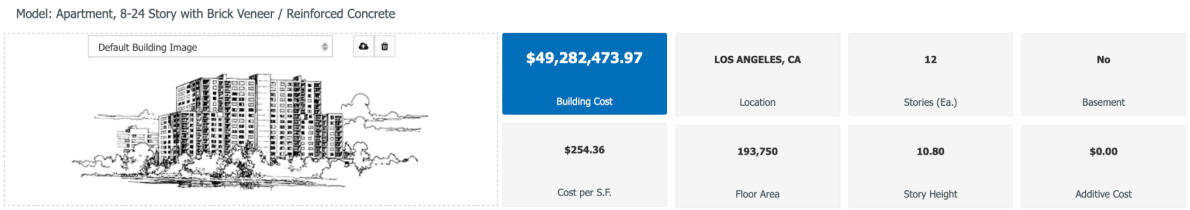

Figure 6.1. Estimated Values from RSMeans

The cost estimation provided by RSMeans is presented in the figure above. With 12 storeys, verdigris View fits average cost per square feet in Los Angeles, CA. The breakdown of the cost estimation is provided in the table below.

A	**Substructure**		**10.13%**	**$18.74**	**$3,631,113.08**
A1010	Standard Foundations			$1.36	$264,039.09
	Foundation wall, CIP, 4' wall height, direct chute, .148 CY/LF, 7.2 PLF, 12" thick	525		$0.28	$54,747.00

	Pile caps, 12 piles, 11' - 6" x 8' - 6" x 49", 40 ton capacity, 19" column size, 900 K column	24.05		$0.57	$109,660.23
	Pile caps, 14 piles, 11' - 6" x 10' - 9" x 55", 80 ton capacity, 29"column size, 2155 K column	16.03		$0.51	$99,631.86
A1020	Special Foundations			$16.80	$3,255,545.35
	Steel H piles, 100' long, 800K load, end bearing, 12 pile cluster	40.08		$16.19	$3,136,008.10
	Grade beam, 30' span, 52" deep, 14" wide, 12 KLF load	525		$0.62	$119,537.25
A1030	Slab on Grade			$0.54	$105,051.90
	Slab on grade, 4" thick, non industrial, reinforced	16145.83		$0.54	$105,051.90
A2010	Basement Excavation			$0.03	$6,476.74
	Excavate and fill, 100,000 SF, 4' deep, sand, gravel, or common earth, on site storage	16145.83		$0.03	$6,476.74
B	**Shell**		**24.56%**	**$45.42**	**$8,801,067.68**
B1010	Floor Construction			$22.26	$4,312,319.81
	Cast-in-place concrete column, 12", square, tied, minimum reinforcing, 150K load, 10'-14' story height, 135 lbs/LF, 4000PSI	1664.25		$0.71	$137,431.10
	Cast-in-place concrete column, 16", square, tied, minimum reinforcing, 300K load, 10'-14' story height, 240 lbs/LF, 4000PSI	1664.25		$0.97	$187,278.05
	Cast-in-place concrete column, 20", square, tied, minimum reinforcing, 500K load, 10'-14' story height, 375 lbs/LF, 4000PSI	1664.25		$1.38	$266,883.29
	Cast-in-place concrete beam and slab, 7.5" slab, two way, 12" column, 25'x25' bay, 40 PSF superimposed load, 149 PSF total load	1776044.16		$19.20	$3,720,727.37
B1020	Roof Construction			$1.58	$305,184.51
	Roof, concrete, beam and slab, 25'x25' bay, 40 PSF superimposed load, 20" deep beam, 9" slab, 152 PSF total load	16145.83		$1.58	$305,184.51
B2010	Exterior Walls			$14.97	$2,900,665.15
	Brick wall, composite double wythe, standard face/CMU back-up, 8" thick, perlite core fill, 3" XPS	55440		$14.97	$2,900,665.15
B2020	Exterior Windows			$2.82	$545,511.12
	Windows, aluminum, sliding, standard glass, 5' x 3'	924		$2.82	$545,511.12
B2030	Exterior Doors			$3.14	$607,889.50

	Door, aluminum & glass, without transom, wide stile, hardware, 3'-0" x 7'-0" opening	5.34		$0.12	$23,396.72
	Door, aluminum & glass, without transom, non-standard, double door, hardware, 6'-0" x 7'-0" opening	2.67		$0.12	$24,154.35
	Door, aluminum & glass, sliding patio, tempered glass, premium, 6'-0" x 7'-0" opening	164.35		$2.89	$560,338.43
B3010	Roof Coverings			$0.67	$129,497.59
	Roofing, single ply membrane, EPDM, 60 mils, loosely laid, stone ballast	16145.83		$0.16	$30,256.48
	Insulation, rigid, roof deck, extruded polystyrene, 40 PSI compressive strength, 4" thick, R20	16145.83		$0.37	$71,302.42
	Roof edges, aluminum, duranodic, .050" thick, 6" face	525		$0.09	$16,902.24
	Flashing, aluminum, no backing sides, .019"	525		$0.02	$3,696.16
	Gravel stop, aluminum, extruded, 4", mill finish, .050" thick	525		$0.04	$7,340.29
C	**Interiors**		**25.10%**	**$46.44**	**$8,997,883.93**
C1010	Partitions			$13.45	$2,605,524.06
	Concrete block (CMU) partition, light weight, hollow, 6" thick, no finish	51666.66		$3.44	$665,549.33
	Metal partition, 5/8"fire rated gypsum board face, 1/4" sound deadening gypsum board, 2-1/2" @ 24", same opposite face, no insulation	120555.55		$5.23	$1,012,929.48
	Furring 1 side only, steel channels, 3/4", 16" OC	103333.33		$1.77	$342,971.60
	Gypsum board, 1 face only, exterior sheathing, fire resistant, 1/2"	103333.33		$0.67	$129,354.73
	Add for the following: taping and finishing	103333.33		$0.47	$90,592.33
	1/2" fire rated gypsum board, taped & finished, painted on metal furring	55440		$1.88	$364,126.59
C1020	Interior Doors			$9.39	$1,819,651.22
	Door, single leaf, kd steel frame, hollow metal, commercial quality, flush, 3'-0" x 7'-0" x 1-3/8"	1354.89		$9.39	$1,819,651.22
C1030	Fittings			$5.10	$987,887.31
	Cabinets, residential, base, hardwood, 1 top drawer & 1 door below x 24" W	986.12		$2.79	$540,320.18
	Cabinets, residential, wall, two doors x 48" wide	493.06		$1.88	$365,042.16

	Cabinets, residential, counter top-laminated plastic, stock, economy	1753.5		$0.43	$82,524.97
C2010	Stair Construction			$4.05	$784,148.74
	Stairs, steel, pan tread for conc in-fill, picket rail,12 risers w/ landing	57.45		$4.05	$784,148.74
C3010	Wall Finishes			$2.78	$538,358.05
	Painting, interior on plaster and drywall, walls & ceilings, roller work, primer & 2 coats	327222.22		$1.89	$366,600.14
	Ceramic tile, thin set, 4-1/4" x 4-1/4"	17222.22		$0.89	$171,757.91
C3020	Floor Finishes			$5.87	$1,136,495.30
	Carpet tile, nylon, fusion bonded, 18" x 18" or 24" x 24", 24 oz	102687.5		$2.62	$508,553.68
	Carpet tile, nylon, fusion bonded, 18" x 18" or 24" x 24", 35 oz	48437.5		$1.41	$273,699.97
	Vinyl, composition tile, maximum	23250		$0.42	$81,565.65
	Tile, ceramic natural clay	19375		$1.41	$272,676.00
C3030	Ceiling Finishes			$5.81	$1,125,819.25
	Gypsum board ceilings, 1/2" fire rated gypsum board, painted and textured finish, 7/8"resilient channel furring, 24" OC support	193750		$5.81	$1,125,819.25
D	**Services**		**39.24%**	**$72.60**	**$14,065,935.89**
D1010	Elevators and Lifts			$14.71	$2,850,781.38
	Traction, geared passenger, 3500 lb,15 floors, 10' story height, 2 car group, 350 FPM	5.34		$14.71	$2,850,781.38
D2010	Plumbing Fixtures			$7.62	$1,475,623.46
	Kitchen sink w/trim, countertop, PE on CI, 24" x 21", single bowl	164.35		$1.51	$292,282.06
	Laundry sink w/trim, PE on CI, black iron frame, 24" x 20", single compt	16.03		$0.17	$33,148.97
	Service sink w/trim, PE on CI, corner floor, 28" x 28", w/rim guard	20.04		$0.37	$72,428.26
	Bathroom, three fixture, 2 wall plumbing, lavatory, water closet & bathtub, stand alone	164.35		$5.56	$1,077,764.17
D2020	Domestic Water Distribution			$8.75	$1,695,519.48
	Electric water heater, commercial, 100< F rise, 50 gallon tank, 9 KW 37 GPH	164.35		$8.75	$1,695,519.48
D2040	Rain Water Drainage			$0.31	$59,432.38
	Roof drain, DWV PVC, 4" diam, diam, 10' high	6.68		$0.06	$11,701.73
	Roof drain, DWV PVC, 4" diam, for each additional foot add	1002.15		$0.25	$47,730.65
D3010	Energy Supply			$9.67	$1,874,097.25

	Apartment building heating system, fin tube radiation, forced hot water, 30,000 SF area,300,000 CF vol	193750		$9.67	$1,874,097.25
D3030	Cooling Generating Systems			$10.72	$2,077,211.19
	Packaged chiller, air cooled, with fan coil unit, medical centers, 40,000 SF, 93.33 ton	193750		$10.72	$2,077,211.19
D4010	Sprinklers			$3.62	$701,064.35
	Wet pipe sprinkler systems, steel, light hazard, 1 floor, 10,000 SF	12787.5		$0.29	$56,547.60
	Wet pipe sprinkler systems, steel, light hazard, each additional floor, 10,000 SF	180768.75		$3.14	$608,814.69
	Standard High Rise Accessory Package 16 story	1.28		$0.18	$35,702.06
D4020	Standpipes			$1.58	$306,515.38
	Wet standpipe risers, class III, steel, black, sch 40, 6" diam pipe, 1 floor	15		$1.39	$269,984.63
	Fire pump, electric, with controller, 5" pump, 100 HP, 1000 GPM	1		$0.17	$32,535.10
	Fire pump, electric, for jockey pump system, add	1		$0.02	$3,995.65
D5010	Electrical Service/Distribution			$1.66	$321,380.10
	Underground service installation, includes excavation, backfill, and compaction, 100' length, 4' depth, 3 phase, 4 wire, 277/480 volts, 2000 A	2		$0.60	$116,733.00
	Feeder installation 600 V, including RGS conduit and XHHW wire, 2000 A	200		$0.59	$113,350.20
	Switchgear installation, incl switchboard, panels & circuit breaker, 120/208 V, 3 phase, 2000 A	2		$0.47	$91,296.90
D5020	Lighting and Branch Wiring			$10.07	$1,950,339.49
	Receptacles incl plate, box, conduit, wire, 10 per 1000 SF, 1.2 W per SF, with transformer	193750		$4.68	$906,953.44
	Wall switches, 2.5 per 1000 SF	193750		$0.74	$143,764.44
	Miscellaneous power, 2 watts	193750		$0.70	$134,944.94
	Central air conditioning power, 3 watts	193750		$0.76	$147,670.44
	Motor installation, three phase, 460 V, 15 HP motor size	4		$0.06	$12,425.22

	Motor feeder systems, three phase, feed to 200 V 5 HP, 230 V 7.5 HP, 460 V 15 HP, 575 V 20 HP	400		$0.03	$5,645.51
	Incandescent fixtures recess mounted, type A, 1 watt per SF, 8 FC, 6 fixtures per 1000 SF	193750		$3.09	$598,935.50
D5030	Communications and Security			$3.89	$753,971.43
	Communication and alarm systems, fire detection, addressable, 100 detectors, includes outlets, boxes, conduit and wire	2.40		$1.14	$220,724.84
	Fire alarm command center, addressable with voice, excl. wire & conduit	1		$0.07	$12,898.55
	Communication and alarm systems, includes outlets, boxes, conduit and wire, intercom systems, 100 stations	1.80		$1.49	$289,164.56
	Communication and alarm systems, includes outlets, boxes, conduit and wire, master TV antenna systems, 30 outlets	1.84		$0.47	$90,618.92
	Internet wiring, 2 data/voice outlets per 1000 S.F.	174.37		$0.73	$140,564.56
E	**Equipment & Furnishings**		**0.96%**	**$1.78**	**$345,798.67**
E1090	Other Equipment			$1.78	$345,798.67
	Architectural equipment, appliances, range, 30" free standing, 1 oven, gas, average	164.35		$1.09	$211,857.18
	Architectural equipment, appliances, dish washer, built-in, 2 cycles, economy	164.35		$0.69	$133,941.49
F	**Special Construction**		**0%**		
G	**Building Sitework**		**0%**		
	SubTotal		**100%**	**$184.99**	**$35,841,799.25**
	Contractor Fees (GC,Overhead,Profit)		**25.0%**	**$46.25**	**$8,960,449.81**
	Architectural Fees		**10.0%**	**$23.12**	**$4,480,224.91**
	User Fees		**0.0%**	**$0.00**	**$0.00**
	Total Building Cost			**$254.36**	**$49,282,473.97**

Table 6.1. Cost Estimation from RSMeans

According to information from RSMeans, the total building cost is $49,282,473.97. In order to finalize and get the final construction cost we need to add labor costs, land acquisition, permits and city fees, utility connections and equipment rental.

The building has a footprint of 1,500 m² and a total height of 39.5 meters with the estimated gross volume of 59,250 cubic meters. According to the Terner Center for Housing Innovation at UC Berkeley (2020), the average hard construction cost for multifamily housing in Los Angeles was about $222 per square feet in 2018 or around $2,390 per square meters. The average floor height is 3.3 meters, which makes the cost of labor to $724 per cubic meter. Since the labor typically makes up about 45% of those hard construction costs, the labor component alone is estimated at $326 per cubic meter. This makes full labor cost for the whole project to approximately $19.3 million.

The cost of the land acquisition can be estimated according to current market rates in the Echo Park area in Los Angeles. As for 2025, the average land price in Echo Park, according to Realtor.com, is approximately $859 per square foot. If we assume a standard lot size of 10,000 square feet, the total land cost is $8,590,000. However, the land acquisition estimate does not include potential closing costs or rezoning expenses, which may vary depending on the transaction specifics.

Permit and regulatory fee estimates were taken from the recent data on multifamily residential developments in Los Angeles. Local government agencies usually require a range of permits, for example those for building, grading, electrical, plumbing, fire safety, and environmental compliance.

In addition, plan check fees, inspection costs, and development impact fees add up to the permits costs. Based on a 2024 report by the Financial Times, the average permitting costs for large residential projects in Los Angeles usually are between $75,000 and $150,000 depending on the difficulty of the project and its location. An average value of $100,000 was selected as expenses for permits for a high-rise residential building in Echo Park.

Utility connection costs were estimated based on standard service fees and infrastructure requirements for new residential construction in Los Angeles. They usually include connection of utilities and costs for water, sewer, electricity, and telecommunications systems installation. For high-density developments, usually, costs increase due to upgrades in existing infrastructure, trenching, permitting, and inspection requirements. According to published rates from the Los Angeles Department of Water and Power (LADWP) and supplemental city planning data the total utility connection costs for mid-rise to high-rise projects go from $150,000 to over $300,000 depending on building size and required

upgrades of capacity. For the purposes of this estimate, a middle value of $225,000 was selected.

Construction equipment rental costs were projected based on typical monthly lease rates for machinery required in high-rise residential construction, including cranes, excavators, concrete pumps, scaffolding systems, and temporary on-site facilities. According to current listings from equipment rental platforms such as DOZR, average monthly rental expenses for a medium-to-large scale construction site in Los Angeles are estimated at approximately $18,000. Given the project's expected duration of six years (72 months), the cumulative cost of equipment rental was calculated at $1,296,000. This figure assumes continuous site activity and covers both primary construction machinery and ancillary equipment necessary to maintain safety and workflow efficiency.

After analyzing the main costs for the project, we assume the initial investments to be around $78,802,974.

Building cost	**Labor Cost**	**Land Acquisition**	**Permits and City Fees**	**Utility Connections**	**Equipment Rental**	**Initial Investment**
$49,282,473.97	$19,309,500	$8,590,000.00	$100,000.00	$225,000.00	$1,296,000.00	**$78,802,974.97**

Table 6.2. Initial investments.

6.4. Work Breakdown Structure

The project scope refers to the work that needs to be done for the desired outcome and deliverables. As changes will happen, and because we want to keep the project within the time and cost restraints, scope management has processes to deal with these changes during the project. Scope is defined with a Work Breakdown Structure (WBS) and can only be altered via formal processes. WBS is an essential building block of the structure of a construction project and therefore one of the most important tools to plan and execute successfully. Structured lifecycle divides up the work so that changes have less downstream impact as you cannot be in two phases at once. Furthermore, WBS serves as the basis for

vital activities such as scheduling, cost analysis, and supervision that will increase the probability of achieving project objectives.

The WBS for this residential building project was developed based on the principles in the PMBOK Guide. The five key milestones of the project were broken down into sub-tasks, with the WBS Diagram created in Lucidchart software.

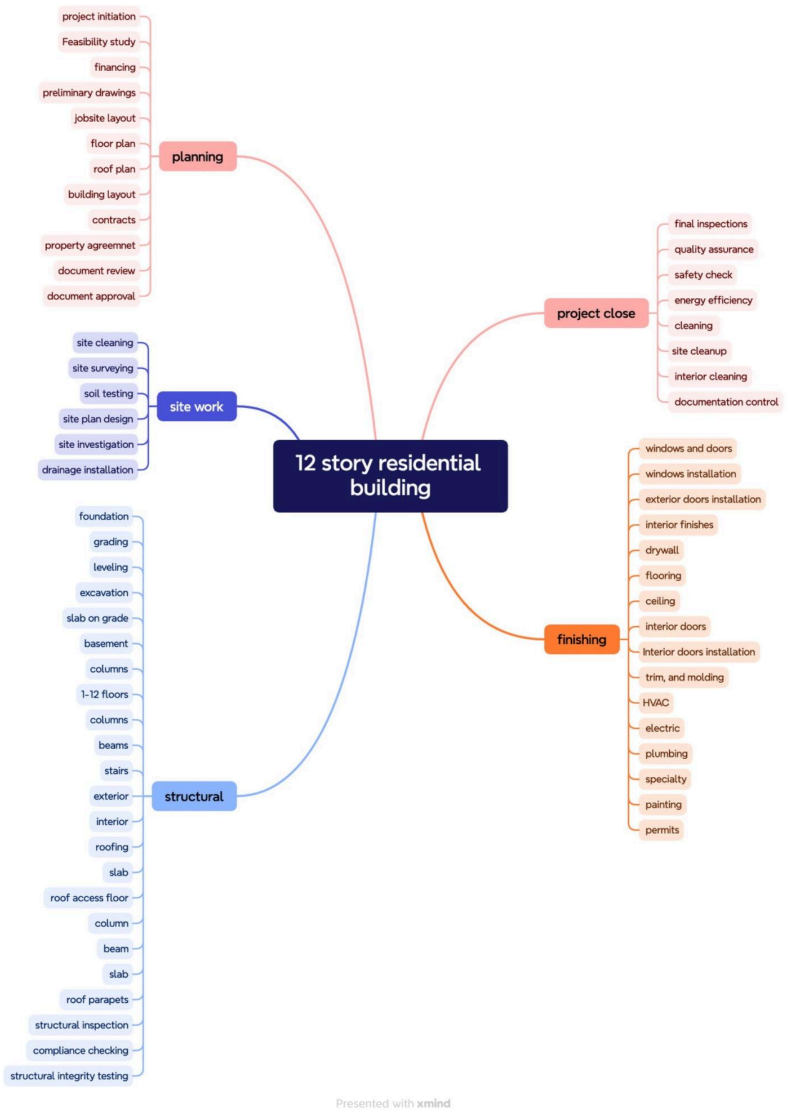

Figure 6.2. Work Breakdown Structure for Verdigris View

WBS Code	WBS Element	Description	Deliverables	Responsible Party
1.1	Planning	Covers project initiation, feasibility, design, and contracts	Signed project charter, preliminary drawings, contracts	Project Manager
1.2	Site Work	Includes site preparation activities like cleaning, surveying, and drainage	Prepared and leveled site, soil reports, drainage systems	Site Engineer
2.1	Structural Works	Covers foundation, columns, slabs, and structural inspections	Completed structural frame, certified inspections	Structural Engineer
3.1	Finishing Works	All finishing activities including HVAC, painting, and interiors	Installed interiors, functioning utilities, final finishes	Finishing Supervisor
4.1	Project Close-out	Final checks, cleanup, documentation and energy efficiency verification	Signed inspection reports, handover documents	Quality Manager

Table 6.3. WBS Dictionary.

6.5. Scheduling

Our project schedule was calculated with the assistance of experts in construction management and compiled using the MindView software in Gantt chart form.

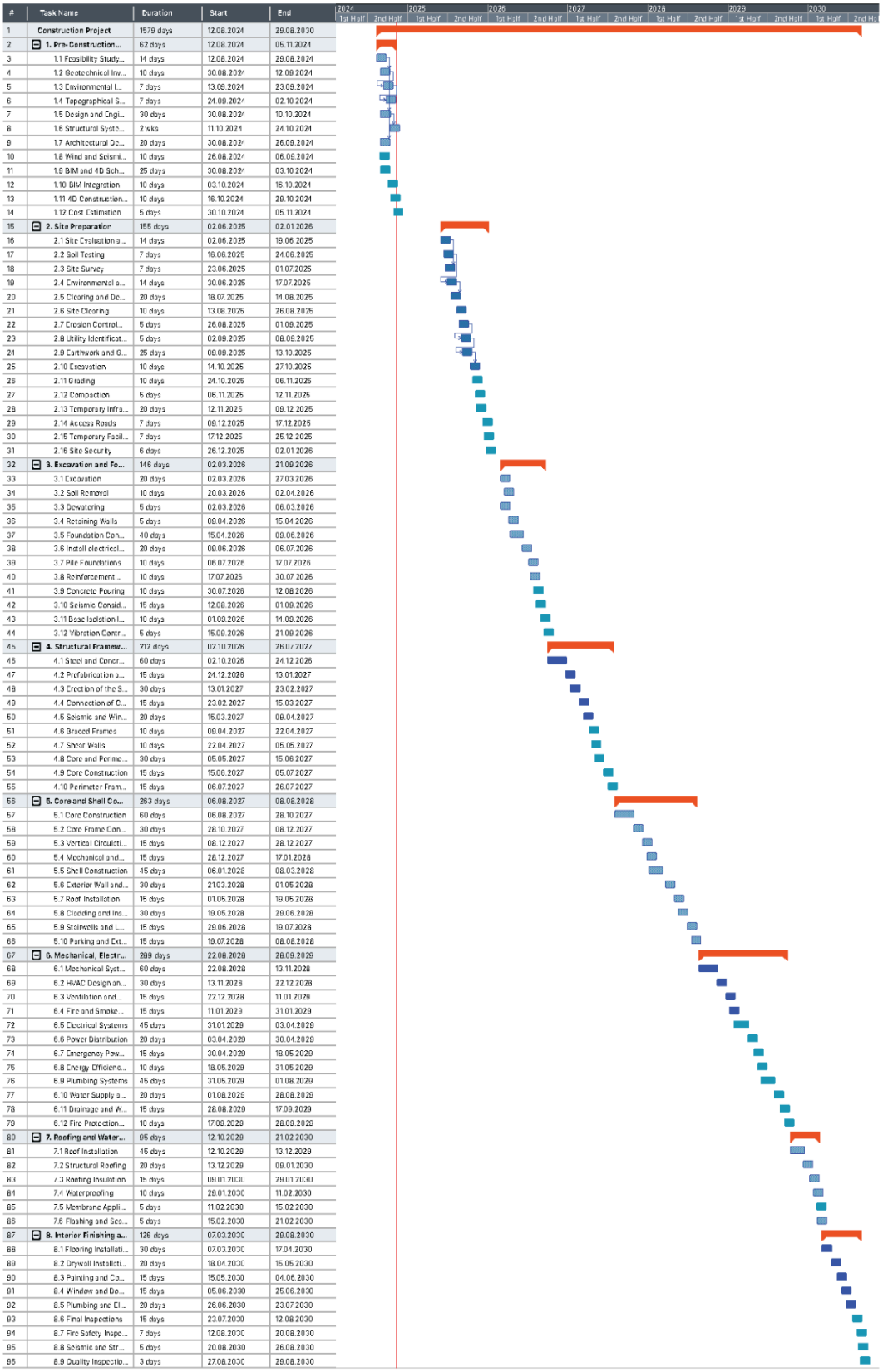

#	Task Name	Duration	Start	End
1	Construction Project	1579 days	12.08.2024	29.08.2030
2	1. Pre-Construction...	62 days	12.08.2024	05.11.2024
3	1.1 Feasibility Study...	14 days	12.08.2024	29.08.2024
4	1.2 Geotechnical Inv...	10 days	30.08.2024	12.09.2024
5	1.3 Environmental I...	7 days	13.09.2024	23.09.2024
6	1.4 Topographical S...	7 days	24.09.2024	02.10.2024
7	1.5 Design and Engi...	30 days	30.08.2024	10.10.2024
8	1.6 Structural Syste...	2 wks	11.10.2024	24.10.2024
9	1.7 Architectural De...	20 days	30.08.2024	26.09.2024
10	1.8 Wind and Seismi...	10 days	26.08.2024	06.09.2024
11	1.9 BIM and 4D Sch...	25 days	30.08.2024	03.10.2024
12	1.10 BIM Integration	10 days	03.10.2024	16.10.2024
13	1.11 4D Construction...	10 days	16.10.2024	29.10.2024
14	1.12 Cost Estimation	5 days	30.10.2024	05.11.2024
15	2. Site Preparation	155 days	02.06.2025	02.01.2026
16	2.1 Site Evaluation a...	14 days	02.06.2025	19.06.2025
17	2.2 Soil Testing	7 days	16.06.2025	24.06.2025
18	2.3 Site Survey	7 days	23.06.2025	01.07.2025
19	2.4 Environmental a...	14 days	30.06.2025	17.07.2025
20	2.5 Clearing and De...	20 days	18.07.2025	14.08.2025
21	2.6 Site Clearing	10 days	13.08.2025	26.08.2025
22	2.7 Erosion Control...	5 days	26.08.2025	01.09.2025
23	2.8 Utility Identificat...	5 days	02.09.2025	08.09.2025
24	2.9 Earthwork and G...	25 days	08.09.2025	13.10.2025
25	2.10 Excavation	10 days	14.10.2025	27.10.2025
26	2.11 Grading	10 days	24.10.2025	06.11.2025
27	2.12 Compaction	5 days	06.11.2025	12.11.2025
28	2.13 Temporary Infra...	20 days	12.11.2025	09.12.2025
29	2.14 Access Roads	7 days	09.12.2025	17.12.2025
30	2.15 Temporary Facil...	7 days	17.12.2025	25.12.2025
31	2.16 Site Security	6 days	26.12.2025	02.01.2026
32	3. Excavation and Fo...	146 days	02.03.2026	21.09.2026
33	3.1 Excavation	20 days	02.03.2026	27.03.2026
34	3.2 Soil Removal	10 days	20.03.2026	02.04.2026
35	3.3 Dewatering	5 days	02.03.2026	06.03.2026
36	3.4 Retaining Walls	5 days	09.04.2026	15.04.2026
37	3.5 Foundation Con...	40 days	15.04.2026	09.06.2026
38	3.6 Install electrical...	20 days	09.06.2026	06.07.2026
39	3.7 Pile Foundations	10 days	06.07.2026	17.07.2026
40	3.8 Reinforcement...	10 days	17.07.2026	30.07.2026
41	3.9 Concrete Pouring	10 days	30.07.2026	12.08.2026
42	3.10 Seismic Consid...	15 days	12.08.2026	01.09.2026
43	3.11 Base Isolation I...	10 days	01.09.2026	14.09.2026
44	3.12 Vibration Contr...	5 days	15.09.2026	21.09.2026
45	4. Structural Framew...	212 days	02.10.2026	26.07.2027
46	4.1 Steel and Concr...	60 days	02.10.2026	24.12.2026
47	4.2 Prefabrication a...	15 days	24.12.2026	13.01.2027
48	4.3 Erection of the S...	30 days	13.01.2027	23.02.2027
49	4.4 Connection of C...	15 days	23.02.2027	15.03.2027
50	4.5 Seismic and Win...	20 days	15.03.2027	09.04.2027
51	4.6 Braced Frames	10 days	09.04.2027	22.04.2027
52	4.7 Shear Walls	10 days	22.04.2027	05.05.2027
53	4.8 Core and Perime...	30 days	05.05.2027	15.06.2027
54	4.9 Core Construction	15 days	15.06.2027	05.07.2027
55	4.10 Perimeter Fram...	15 days	06.07.2027	26.07.2027
56	5. Core and Shell Co...	263 days	06.08.2027	08.08.2028
57	5.1 Core Construction	60 days	06.08.2027	28.10.2027
58	5.2 Core Frame Con...	30 days	28.10.2027	08.12.2027
59	5.3 Vertical Circulati...	15 days	08.12.2027	28.12.2027
60	5.4 Mechanical and...	15 days	28.12.2027	17.01.2028
61	5.5 Shell Construction	45 days	06.01.2028	08.03.2028
62	5.6 Exterior Wall and...	30 days	21.03.2028	01.05.2028
63	5.7 Roof Installation	15 days	01.05.2028	19.05.2028
64	5.8 Cladding and Ins...	30 days	19.05.2028	29.06.2028
65	5.9 Stairwells and L...	15 days	29.06.2028	19.07.2028
66	5.10 Parking and Ext...	15 days	19.07.2028	08.08.2028
67	6. Mechanical, Electr...	289 days	22.08.2028	28.09.2029
68	6.1 Mechanical Syst...	60 days	22.08.2028	13.11.2028
69	6.2 HVAC Design an...	30 days	13.11.2028	22.12.2028
70	6.3 Ventilation and...	15 days	22.12.2028	11.01.2029
71	6.4 Fire and Smoke ...	15 days	11.01.2029	31.01.2029
72	6.5 Electrical Systems	45 days	31.01.2029	03.04.2029
73	6.6 Power Distribution	20 days	03.04.2029	30.04.2029
74	6.7 Emergency Pow...	15 days	30.04.2029	18.05.2029
75	6.8 Energy Efficienc...	10 days	18.05.2029	31.05.2029
76	6.9 Plumbing Systems	45 days	31.05.2029	01.08.2029
77	6.10 Water Supply a...	20 days	01.08.2029	28.08.2029
78	6.11 Drainage and W...	15 days	28.08.2029	17.09.2029
79	6.12 Fire Protection...	10 days	17.09.2029	28.09.2029
80	7. Roofing and Water...	95 days	12.10.2029	21.02.2030
81	7.1 Roof Installation	45 days	12.10.2029	13.12.2029
82	7.2 Structural Roofing	20 days	13.12.2029	09.01.2030
83	7.3 Roofing Insulation	15 days	09.01.2030	29.01.2030
84	7.4 Waterproofing	10 days	29.01.2030	11.02.2030
85	7.5 Membrane Appli...	5 days	11.02.2030	15.02.2030
86	7.6 Flashing and Sea...	5 days	15.02.2030	21.02.2030
87	8. Interior Finishing a...	126 days	07.03.2030	29.08.2030
88	8.1 Flooring Installati...	30 days	07.03.2030	17.04.2030
89	8.2 Drywall Installati...	20 days	18.04.2030	15.05.2030
90	8.3 Painting and Co...	15 days	15.05.2030	04.06.2030
91	8.4 Window and Do...	15 days	05.06.2030	25.06.2030
92	8.5 Plumbing and El...	20 days	26.06.2030	23.07.2030
93	8.6 Final Inspections	15 days	23.07.2030	12.08.2030
94	8.7 Fire Safety Inspe...	7 days	12.08.2030	20.08.2030
95	8.8 Seismic and Str...	5 days	20.08.2030	26.08.2030
96	8.9 Quality Inspectio...	3 days	27.08.2030	29.08.2030

Figure 6.3. Gantt chart of project schedule

The total construction time is estimated to be 6 years due to extensive site work, including significant demolition and excavation. We need to prepare the site properly before the structural framework. By consulting with the experts in construction management we aimed to align our time estimation to real world timelines including all possible delays and ensuring realistic project schedule.

6.6. Risk management

Risk is managed by monitoring the VERDIGRIS VIEW project to meet financial, regulatory and schedule goals. The main financial risk is underestimation of costs, which can cause funding gaps and delays. With an escalating inflation and market fluctuation in material cost, there is need for effective budget monitoring and contingency funding to mitigate against unforeseen financial burdens as well as prevent shortfalls in fund cash flows. Construction projects have long struggled with cost overrun, which oftentimes are caused by inaccuracies in the initial budgeting, or when there is a lack of proper estimating and design changes or even due to ineffective management of contracts. Research shows that a thorough analysis of the financial risk and monitoring the budget through audits will help keep the project within a financial framework.

The main risk in construction is unforeseen problems with the foundations, which could arise from the soil composition being different than what was anticipated, so soil analysis and engineering adjustments should be made early on. Geotechnical investigations form an important part in avoiding failure in the foundation and saving unforeseen costs which may occur due to constructional issues. Insufficient investigation of subsoil causes fatal failure of previous construction works, therefore, detailed preliminary investigation is essential. Moreover, the use of advanced technologies such as ground-penetrating radar and soil-stabilization techniques can help to reduce risks and for the structurally safety and long-term durability.

Non-adherence to regulation represents a significant risk, as a head in the sand approach could result in projects being stopped or heavily modified. Notably, the non-compliance with changing construction laws often leads to lengthy legal fights, penalties, and delays. In order to not be faced with these surprises, a timely permit procurement and an ongoing legal monitoring in all project phases is inevitable. In addition, staying connected to local government ensures easier permit approvals and compliance.

Environmental: Environmental risks, including Los Angeles' frequent seismic activity, require structural strengthening and compliance with seismic codes to protect against possible project delays and damage. Newer reinforcement strategies for retrofits of buildings also help improve structural resiliency, protecting people as well as critical infrastructure investments. With climate-related hazards of increasing import, incorporation of adaptive design elements suited to seismic challenges are essential to meet state and national safety requirements that apply to all new schools.

Social risks, such as community resistance and labor availability, may affect project approval and labor productivity, necessitating early engagement with stakeholders and workforce planning. The construction industry continues to experience long-running skills shortages: Infrastructure Australia (2024) observes that a skills shortage in the construction industry has resulted in higher labour cost and longer lead times for projects. Mitigating workforce risks Preparing for talent shortages As the labor pool becomes tighter, it is important to establish a steady supply of qualified workers through training programs and partnerships with trade schools. Clear communication with local populations about the benefits from the project, environmental impact and economic contributions will also help to ease opposition and legal disputes.

To minimize the risks associated with the above, a structured monitoring mechanism will be established including budget tracking, quality monitoring, legal compliance verification and workforce management techniques. Good leadership and co-ordinated management between contactors is near lawless and is implementing preventative of mismanagement, delay and extra payment. Bardakci (2023) argues that a good enlightened leadership is an obvious factor when it comes to improved construction efficiency when using digital project tracking tools, and accountability at all levels of construction management. The use of AI-based predictive analytics will also help fine-tune risk assessment models, for an early warning and risk mitigation, thereby enhancing project's resilience, long-term viability.

Risk Type		**Risk Description**	**Probability**	**Severity**	**Mitigation**
Design Risks	**D1**	Incorrect architectural or engineering designs	Medium	High	Conduct detailed design reviews before construction.

		leading to structural issues.			
	D2	Non-compliance with local building codes or seismic standards.	Medium	Medium	Allow flexible design approvals for minor adjustments.
	D3	Ineffective layout of residential and commercial spaces, reducing functionality.	Low	Medium	Ensure compliance checks with building codes in the design phase.
	D4	Delays in design approvals, impacting the overall project timeline.	Medium	Medium	Engage with regulators early to speed up approvals.
Financial Risks	**F1**	Budget overruns due to rising material and labor costs.	High	High	Set a contingency budget and monitor costs closely.
	F2	Inaccurate cost estimation, leading to insufficient project funding.	Medium	Medium	Use fixed-price contracts for key materials.
	F3	Delayed cash flow from investors or lenders.	Low	Medium	Diversify funding sources to avoid delays.
	F4	Unforeseen expenses related to design changes or regulatory compliance.	Medium	Medium	Reserve funds for unexpected design-related costs.
Environmental Risks	**E1**	Strict environmental regulations leading to costly adjustments.	Medium	Medium	Consult environmental experts to ensure compliance.

	E2	Delays due to adverse weather conditions affecting construction.	Medium	Medium	Develop a weather delay contingency plan.
	E3	Soil contamination or other environmental hazards discovered on-site.	Low	Medium	Perform site assessments for early contamination detection.
	E4	Negative impact on local ecosystems or neighborhood, causing opposition from the community.	Medium	Medium	Minimize environmental impact and build community support.

Table 6.4. Risk Assessment Table

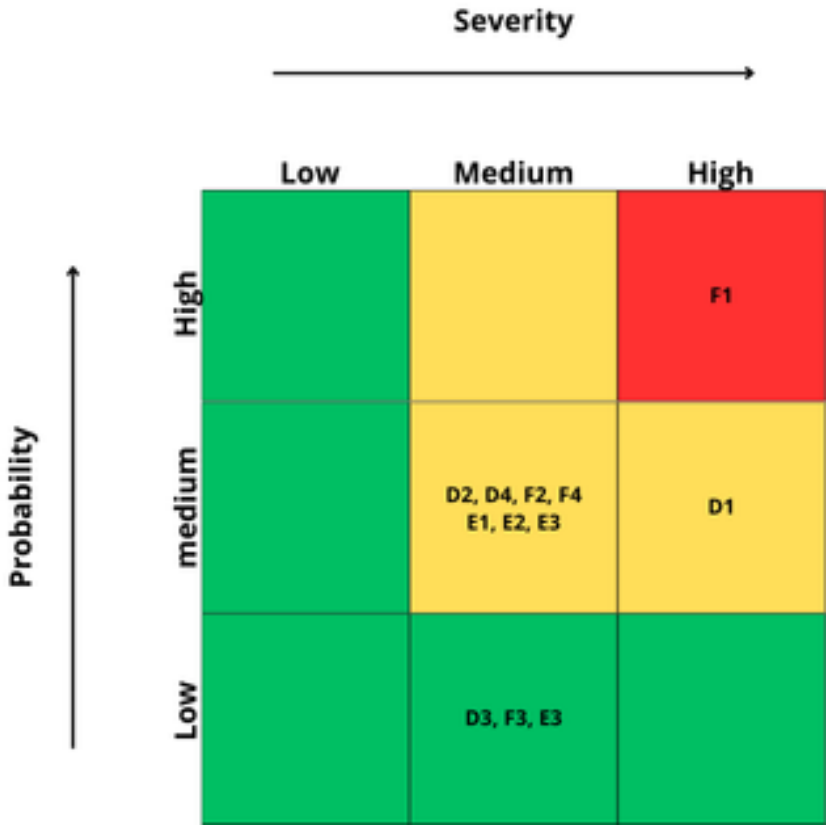

Figure 6.4. Risk Management Matrix

6.7. Quality Management

Effective management of quality is also important to maintaining construction outcomes and processes at standards as defined by given standards, requirements from stakeholders, and long-term performance targets. For the development at Verdigris View, there is quality assurance through a systematic process with pre-agreed controls, systematic checklists, and measures by stage.

One fundamental element in ensuring that there is high-quality construction is having in place measures for ensuring quality catering to material integrity and compliance with regulations at all stages of construction. Such measures include having a defined quality assurance plan, checking on material quality at early stages, conformity with construction codes on-site, and conformity with occupational and environmental protection standards. There are also other control measures such as standardized test procedures and detailed registers used to check conformity as well as ensure traceability at all stages in the entire lifespan of a project.

Figure 6.5. Quality control measures

The use of quality control checklists operationalizes these controls as effective measures. The checklists create a standardized means by which to ensure building operations and major milestones are in compliance with design standards, safety, and regulatory standards. Some checks listed in the pre-construction checklist include site clearance, grading checks, soil stability tests, position placement of the rebar, conformity in concrete

mixes, and provision for safety signs and drainage systems. The tools assist in ensuring constant watchfulness among teams and early detection of deviation.

Building Construction Quality Checklist

Project Information:
Project Name: "Verdigris View" high-rise residential building
Project Manager: Sanzhar Revshanov

Inspection Team Members:
- Temirova Tynyshtyk
- Bazarbek Meiirbek
- Ibrayeva Darina
- Aigerim Zhubandykova
- Baimagambetov Ayan
- Revshanov Sanzhar

Date of Inspection: 15.04.2025

Location: 2217 W Sunset Blvd, Los Angeles, CA 90026, United States

Phase 1: Pre-Construction Checklist

1. Site Preparation and Clearing:
☐ *Ensure complete clearing of vegetation and construction waste from the site*
☐ *Confirm that surface grading and leveling align with approved design documents*
☐ *Verify safe identification and removal of any hazardous substances on site*
☐ *Evaluate erosion control measures for adequacy and compliance*
☐ *Review environmental protection protocols in accordance with local regulations*
☐ *Confirm that the site meets LEED v4.1 criteria for Sensitive Land Protection*
☐ *Inspect the positioning and accessibility of utility connection points*
☐ *Confirm that all required safety and hazard signage is correctly installed*

2. Foundation Inspection:
☐ *Verify excavation depth and footprint match approved structural plans*
☐ *Check that soil compaction meets geotechnical recommendations*
☐ *Ensure reinforcing bars are installed correctly with proper spacing and anchorage*
☐ *Examine the condition and stability of formwork and temporary supports*
☐ *Review concrete mix design and material delivery records for conformity*
☐ *Monitor curing procedures to ensure strength development is not compromised*
☐ *Confirm foundation includes adequate drainage and waterproofing systems*
☐ *Assess compliance with Life-365 concrete service life standards*

Figure 6.6. quality control checklist

These procedural elements are supported by clearly defined measures of quality that span across the entire duration of construction. These measures are grouped by phase and comprise:

- Stage 1: Accuracy of architectural and engineering design, with ramrod compliance with building codes that apply.
- Stage 2: Contractor qualification evaluation and proven project proficiency.
- Stage 3: Ongoing assessment of workplace safety and continuous monitoring of expenditure within budgets.

- Stage 4: Assessment for performance against client input as also on conducting a proper Life Cycle Assessment (LCA) for environmental sustainability.
- Stage 5: Project efficiency analysis of earned value metrics to compare planned and actual.

Figure 6.7. Quality metrics

By combining these three components—control measures, checklists, and measures—the quality management system implemented at the Verdigris View has a strong foundation for standards-building, risk-aversion, and long-term operational resilience.

6.8. Procurement planning

Bid packets will consist of extensive project specs, bid forms, bonding requirements, licensing paperwork, and anti-collusion affidavits. These will ensure that all bidders are pre-qualified, compliant with legislation, and technically qualified. Documents will also be posted on official sites such as LABAVN and the Public Works LA County portal, as where bid notices and vendor lists are posted.

Prequalified vendor lists will be used by the project with the City of Los Angeles for ensuring qualified bid participation and will screen for contractor qualifications on websites such as California DIR registry. This will exclude ineligible or disbarred bidders and enhance local and disadvantaged business participation.

The criteria for source choice will primarily emphasize lowest price bidding that meets financial, legal, and technical requirements. Supplementary review will also take into consideration past performance on projects with comparable parameters, bonding potential, DBE utilization strategies, and compliance with local contracting ordinances. The balanced framework enhances transparency, minimizes costs, and improves procurement public accountability.

6.9. Green building certification

The Verdigris View development also incorporates sustainability objectives based on the LEED v4.1 BD+C: New Construction building rating system with the aim to achieve the status of Gold certification through its location, design effectiveness, and green strategies. Additional examination of the Echo Park property reaffirms the project's eligibility for almost all Location & Transportation credits, with mass transit accessibility, walk scores, and the incorporation of affordable housing units securing an estimated 15 of the possible 16 points in the Location & Transportation category (USGBC, 2023).

Both environmental conditions and LEED target goals informed the design considerations. The compact footprint of the building reduces site disturbance, and the incorporation of vegetated exterior space and permeable surfaces fosters stormwater infiltration and urban heat island mitigation. The Revit-based building model includes rational window placement and high-efficiency glazing to permit daylighting in over 75% of the regularly used areas and enhance the thermal performance. A flat roof provides also potential for photovoltaics systems or a green roof in the future. Low-flow fixtures relieve Indoor Water Use Reduction, while natural ventilation and passive solar positioning minimize the need for mechanical systems. Such elements achieve major credits in Sustainable Sites, Water Efficiency, and Indoor Environmental Quality.

Rating based on final design and building systems indicates the project could achieve about 60–70 points, reaching the LEED Gold level. This comprises verified points from LT, along with additions from SS (7–9 pts), WE (4–5 pts), EA (10–15 pts), MR (2–4 pts), and EQ (10–11 pts), depending on final commissioning and material choice. Such strategies corroborate studies that show high-rise residential buildings in urban infill areas may successfully obtain LEED certification when backed by early-phase green design incorporation and performance modeling (Berardi, 2012).

6.10. Safety Management

Semi-quantitative **likelihood × severity** evaluation was applied to guide safety planning at Verdigris View. This allowed the utilization of a standardized approach to construction hazard examination. The process allowed the team to rank and identify high-risk activities including working at height, exposure to electricity, machinery entrapment, and seismic structural collapse. The results of the evaluation are reflected in the Construction Safety Assessment Table, in which each hazard has been ranked by level of risk and mitigation controls to be implemented.

Based on the analysis above, a project-specific risk register was established and updated regularly throughout the construction project. The register includes all the risks that were identified, the calculated severity of the risks, the responsible people, and accompanying control measures. It serves as a live register in the management of safety and is inspected at regular site inspections and in regular toolbox talks (Balfe et al., 2014).

Besides enhancing the safety program, the project team incorporates programmed audits, training for particular hazards, and new digital technologies like wearable sensors, geofencing, and VR-based modules of safety inductions. Such layer controls follow international standards and best practices from the most current scholarly research in the prevention of accidents as well as reacting in real time to dangers (Newaz et al., 2022; Almaskati et al., 2024).

Risk Identification	Likelihood (1-5)	Severity (1-5)	Risk Rating
Working at height	4	5	20
Electrical Hazards	4	4	16
Caught-In Hazards	4	4	16
Seismic Structural Failure	3	5	15
Toxic Material Stocks	3	4	12
Fire and Explosion Risks	3	4	12
Gas Leak and Explosion Risk	3	4	12
Elevator Malfunction During Emergency	2	5	10
Glass and Facade Hazards	3	3	9
Falls, trips, slips	3	3	9
Structural Collapse	2	4	8
Moving Objectives	4	2	8
Foundation Settlement	2	4	8
Hand-Arm Vibration Syndrome	2	3	6
Inadequate PPE	3	2	6
Heat/Cold Stress	2	3	6
Noise	2	3	6

Figure 6.8. Construction Safety Assessment

6.11. Construction site planning

Verdigris View has a site plan that's designed for an efficient process, clear access, and safety during construction. With an over-sized door from Sunset Blvd the space makes it simple for heavy equipment or material to be delivered. Safe passage is provided with clearly defined construction vehicle routes. The structure also predominates the northern boundary of the site, maximising the excavation and foundation potential of the site. Stockpiles are situated on the eastern side to ensure convenient crane operation and to minimise hauling. The site office is located at the front end of the site near the gate which gives instant visibility on site activities, deliveries and workforce access. Storage and staging areas and equipment placement zones are located on the west side for ease of

operations. All in all, this neat setup maintains an intelligible workflow and also benefits site security and efficiency.

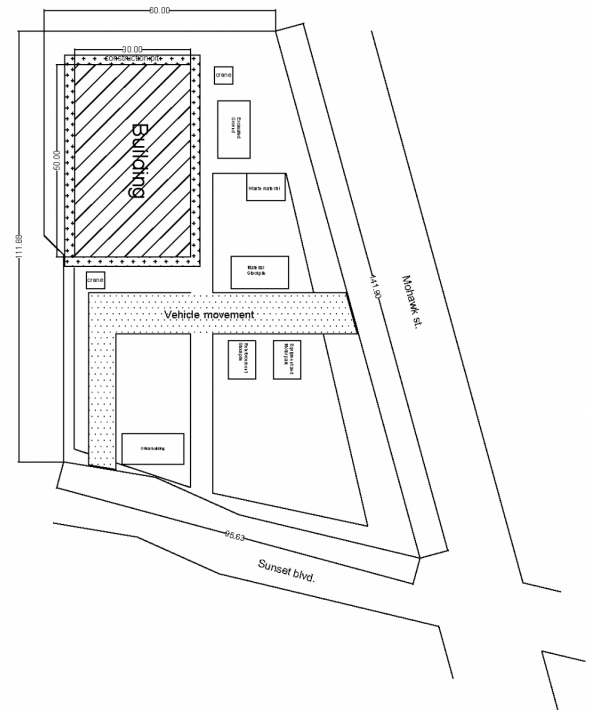

Figure 6.9. Construction Site Layout

Appendix A

Case 2 Wind load calculations:

Story	Short side				Long side			
	Frame	$F_{torsion}$	F_{direct}	F_{total}	Frame	$F_{torsion}$	F_{direct}	F_{total}
1	1	-2.380	13.212	10.831	1	-0.711	15.649	14.938
	2	-1.428		11.784	2	-0.553		15.096
	3	-0.476		12.736	3	-0.395		15.254
	4	0.476		13.688	4	-0.237		15.412
	5	1.428		14.640	5	-0.079		15.570
	6	2.380		15.592	6	0.079		15.728
					7	0.237		15.886
					8	0.395		16.044
					9	0.553		16.202
					10	0.711		16.360
2	1	-2.063	11.631	9.568	1	-0.560	13.858	13.299
	2	-1.238		10.393	2	-0.435		13.423
	3	-0.413		11.218	3	-0.311		13.547
	4	0.413		12.044	4	-0.187		13.672
	5	1.238		12.869	5	-0.062		13.796
	6	2.063		13.694	6	0.062		13.921
					7	0.187		14.045
					8	0.311		14.169
					9	0.435		14.294
					10	0.560		14.418
3	1	-2.198	12.289	10.092	1	-0.624	14.543	13.919
	2	-1.319		10.971	2	-0.485		14.057
	3	-0.440		11.850	3	-0.347		14.196

	4	0.440		12.729	4	-0.208		14.335
	5	1.319		13.608	5	-0.069		14.473
	6	2.198		14.487	6	0.069		14.612
					7	0.208		14.751
					8	0.347		14.889
					9	0.485		15.028
					10	0.624		15.166
4	1	-2.305		10.521	1	-0.675		14.425
	2	-1.383		11.443	2	-0.525		14.575
	3	-0.461		12.365	3	-0.375		14.725
	4	0.461		13.287	4	-0.225		14.875
	5	15.000	12.826	27.826	5	-0.075	15.100	15.025
	6	2.305		15.130	6	0.075		15.175
					7	0.225		15.325
					8	0.375		15.475
					9	0.525		15.625
					10	0.675		15.775
5	1	-2.394		10.889	1	-0.718		14.858
	2	-1.437		11.847	2	-0.558		15.018
	3	-0.479		12.805	3	-0.399		15.177
	4	0.479		13.762	4	-0.239		15.336
	5	1.437		14.720	5	-0.080		15.496
	6	2.394	13.284	15.678	6	0.080	15.576	15.655
					7	0.239		15.815
					8	0.399		15.974
					9	0.558		16.134
					10	0.718		16.293

6	1	-2.472	13.686	11.214	1	-0.755	15.994	15.239
	2	-1.483		12.203	2	-0.587		15.407
	3	-0.494		13.192	3	-0.419		15.575
	4	0.494		14.181	4	-0.252		15.742
	5	1.483		15.170	5	-0.084		15.910
	6	2.472		16.158	6	0.084		16.078
					7	0.252		16.246
					8	0.419		16.413
					9	0.587		16.581
					10	0.755		16.749
7	1	-2.542	14.047	11.505	1	-0.788	16.369	15.581
	2	-1.525		12.522	2	-0.613		15.757
	3	-0.508		13.539	3	-0.438		15.932
	4	0.508		14.556	4	-0.263		16.107
	5	1.525		15.572	5	-0.088		16.282
	6	2.542		16.589	6	0.088		16.457
					7	0.263		16.632
					8	0.438		16.807
					9	0.613		16.982
					10	0.788		17.157
8	1	-2.605	14.376	11.771	1	-0.818	16.711	15.893
	2	-1.563		12.813	2	-0.636		16.075
	3	-0.521		13.855	3	-0.454		16.256
	4	0.521		14.897	4	-0.273		16.438
	5	1.563		15.939	5	-0.091		16.620
	6	2.605		16.981	6	0.091		16.802
					7	0.273		16.983

					8	0.454		17.165
					9	0.636		17.347
					10	0.818		17.529
9	1	-2.662		12.016	1	-0.845		16.180
	2	-1.597		13.081	2	-0.657		16.368
	3	-0.532		14.146	3	-0.470		16.556
	4	0.532		15.211	4	-0.282		16.743
	5	1.597		16.276	5	-0.094		16.931
	6	2.662	14.678	17.341	6	0.094	17.025	17.119
					7	0.282		17.307
					8	0.470		17.495
					9	0.657		17.682
					10	0.845		17.870
10	1	-2.715		12.244	1	-0.871		16.446
	2	-1.629		13.330	2	-0.677		16.640
	3	-0.543		14.416	3	-0.484		16.833
	4	0.543		15.502	4	-0.290		17.027
	5	1.629		16.588	5	-0.097		17.220
	6	2.715	14.959	17.675	6	0.097	17.317	17.414
					7	0.290		17.607
					8	0.484		17.800
					9	0.677		17.994
					10	0.871		18.187
11	1	-2.765		12.457	1	-0.894		16.695
	2	-1.659		13.563	2	-0.696		16.894
	3	-0.553	15.222	14.669	3	-0.497	17.590	17.093
	4	0.553		15.775	4	-0.298		17.291

	5	1.659		16.881	5	-0.099		17.490
	6	2.765		17.987	6	0.099		17.689
					7	0.298		17.888
					8	0.497		18.086
					9	0.696		18.285
					10	0.894		18.484
12	1	-2.812		12.657	1	-0.916		16.930
	2	-1.687		13.781	2	-0.713		17.133
	3	-0.562		14.906	3	-0.509		17.337
	4	0.562		16.031	4	-0.305		17.541
	5	1.687		17.155	5	-0.102		17.744
	6	2.812	15.468	18.280	6	0.102	17.846	17.948
					7	0.305		18.151
					8	0.509		18.355
					9	0.713		18.559
					10	0.916		18.762
13	1	-8.996		14.386	1	-1.865		43.061
	2	8.996	23.382	32.378	2	1.865	44.926	46.791

Appendix B

Case 4 Wind load calculations:

Story	Short side				Long side			
	Frame	$F_{torsion}$	F_{direct}	F_{total}	Frame	$F_{torsion}$	F_{direct}	F_{total}
1	1	-1.622		10.125	1	-2.919		6.998
	2	-0.973		10.774	2	-2.271		7.647
	3	-0.324	11.747	11.423	3	-1.622	9.918	8.296
	4	0.324		12.071	4	-0.973		8.945

	5	0.973		12.720	5	-0.324		9.593
	6	1.622		13.369	6	0.324		10.242
					7	0.973		10.891
					8	1.622		11.539
					9	2.271		12.188
					10	2.919		12.837
2	1	-1.419		8.984	1	-2.555		6.176
	2	-0.852		9.551	2	-1.987		6.744
	3	-0.284		10.119	3	-1.419		7.311
	4	0.284		10.687	4	-0.852		7.879
	5	0.852		11.255	5	-0.284		8.447
	6	1.419	10.403	11.823	6	0.284	8.731	9.015
					7	0.852		9.583
					8	1.419		10.150
					9	1.987		10.718
					10	2.555		11.286
3	1	-1.505		9.411	1	-2.710		6.516
	2	-0.903		10.013	2	-2.107		7.118
	3	-0.301		10.616	3	-1.505		7.720
	4	0.301		11.218	4	-0.903		8.322
	5	0.903		11.820	5	-0.301		8.924
	6	1.505	10.917	12.422	6	0.301	9.225	9.526
					7	0.903		10.128
					8	1.505		10.731
					9	2.107		11.333
					10	2.710		11.935
4	1	-1.574	11.335	9.761	1	-2.832	9.628	6.795

	2	-0.944		10.391	2	-2.203		7.425
	3	-0.315		11.020	3	-1.574		8.054
	4	0.315		11.650	4	-0.944		8.684
	5	0.944		12.279	5	-0.315		9.313
	6	1.574		12.908	6	0.315		9.942
					7	0.944		10.572
					8	1.574		11.201
					9	2.203		11.831
					10	2.832		12.460
5	1	-1.631		10.061	1	-2.935		7.036
	2	-0.978		10.714	2	-2.283		7.688
	3	-0.326		11.366	3	-1.631		8.341
	4	0.326		12.018	4	-0.978		8.993
	5	0.978		12.671	5	-0.326		9.645
	6	1.631	11.692	13.323	6	0.326	9.972	10.298
					7	0.978		10.950
					8	1.631		11.602
					9	2.283		12.255
					10	2.935		12.907
6	1	-1.681		10.326	1	-3.025		7.249
	2	-1.008		10.998	2	-2.353		7.921
	3	-0.336		11.670	3	-1.681		8.593
	4	0.336		12.342	4	-1.008		9.265
	5	1.008	12.006	13.015	5	-0.336	10.274	9.938
	6	1.681		13.687	6	0.336		10.610
					7	1.008		11.282
					8	1.681		11.954

					9	2.353		12.627
					10	3.025		13.299
7	1	-1.725		10.563	1	-3.105		7.440
	2	-1.035		11.253	2	-2.415		8.130
	3	-0.345		11.943	3	-1.725		8.820
	4	0.345		12.633	4	-1.035		9.510
	5	1.035		13.323	5	-0.345		10.200
	6	1.725	12.288	14.013	6	0.345	10.545	10.890
					7	1.035		11.580
					8	1.725		12.270
					9	2.415		12.960
					10	3.105		13.650
8	1	-1.765		10.779	1	-3.177		7.614
	2	-1.059		11.485	2	-2.471		8.320
	3	-0.353		12.191	3	-1.765		9.026
	4	0.353		12.897	4	-1.059		9.732
	5	1.059		13.603	5	-0.353		10.439
	6	1.765	12.544	14.309	6	0.353	10.792	11.145
					7	1.059		11.851
					8	1.765		12.557
					9	2.471		13.263
					10	3.177		13.969
9	1	-1.802		10.978	1	-3.243		7.775
	2	-1.081		11.699	2	-2.523		8.496
	3	-0.360	12.780	12.420	3	-1.802	11.019	9.217
	4	0.360		13.141	4	-1.081		9.937
	5	1.081		13.861	5	-0.360		10.658

	6	1.802		14.582	6	0.360		11.379
					7	1.081		12.100
					8	1.802		12.820
					9	2.523		13.541
					10	3.243		14.262
10	1	-1.836		11.163	1	-3.304		7.925
	2	-1.101		11.898	2	-2.570		8.659
	3	-0.367		12.632	3	-1.836		9.393
	4	0.367		13.366	4	-1.101		10.128
	5	1.101		14.101	5	-0.367		10.862
	6	1.836	12.999	14.835	6	0.367	11.229	11.596
					7	1.101		12.331
					8	1.836		13.065
					9	2.570		13.799
					10	3.304		14.534
11	1	-1.868		11.336	1	-3.362		8.065
	2	-1.121		12.083	2	-2.615		8.812
	3	-0.374		12.830	3	-1.868		9.559
	4	0.374		13.577	4	-1.121		10.306
	5	1.121		14.324	5	-0.374		11.053
	6	1.868	13.204	15.071	6	0.374	11.426	11.800
					7	1.121		12.547
					8	1.868		13.294
					9	2.615		14.041
					10	3.362		14.788
12	1	-1.897		11.499	1	-3.415		8.197
	2	-1.138	13.396	12.258	2	-2.656	11.612	8.955

	3	-0.379		13.017	3	-1.897		9.714
	4	0.379		13.776	4	-1.138		10.473
	5	1.138		14.535	5	-0.379		11.232
	6	1.897		15.294	6	0.379		11.991
					7	1.138		12.750
					8	1.897		13.509
					9	2.656		14.268
					10	3.415		15.027
13	1	-33.353	33.725	0.371	1	-33.353	17.552	-15.801
	2	33.353		67.078	2	33.353		50.906

References

Age of Los Angeles. (n.d.). https://cityhubla.github.io/LA_Building_Age/#17.68/34.07851/-118.26543

Ammar, T., Abdel-Monem, M., & El-Dash, K. (2023). Appropriate budget contingency determination for construction projects: State-of-the-art. *Alexandria Engineering Journal*, *78*, 88–103. https://doi.org/10.1016/j.aej.2023.07.035

Almaskati, D., Kermanshachi, S., Pamidimukkala, A., Loganathan, K., & Yin, Z. (2024). *A review on construction safety: Hazards, mitigation strategies, and impacted sectors*. Buildings, 14(2), 526. https://doi.org/10.3390/buildings14020526

Balfe, N., Leva, M. C., McAleer, B., & Rocke, M. (2014). *Safety risk registers: Challenges and guidance*. Chemical Engineering Transactions, 36, 571–576. https://doi.org/10.3303/CET1436096

Bardakci, T. (2023). Assessment of risk factors in high-rise building projects. *Global Tall Building Review*, 12(4), 213-229. Retrieved from https://global.ctbuh.org/resources/papers/4339-Bardakci_AssessmentOfRiskFactor.pdf

Berardi, U. (2013). Sustainability assessment of urban communities through rating systems. *Environment Development and Sustainability*, *15*(6), 1573–1591. https://doi.org/10.1007/s10668-013-9462-0

California Department of Industrial Relations. (2025). *Public Works Contractor Registration*. Retrieved from https://www.dir.ca.gov/Public-Works/Contractors.html

City of Los Angeles. (2025). *Los Angeles Business Assistance Virtual Network (LABAVN)*. Retrieved from https://www.labavn.org

Coduto, Donald P. *Foundation Design*. Pearson College Division, 2001.

Competitive Enterprise Institute. (2023, July 19). *Global Infrastructure Permitting - Competitive Enterprise Institute*. https://cei.org/studies/global-infrastructure-permitting/

Contour Map Creator: The topographic map for the project site was obtained using the online tool "Contour Map Creator." The tool provides free access to topographic data for different regions, allowing for detailed site analysis. Available at: https://contourmapcreator.urgr8.ch/.

FHWA, et al. *4. Title and Subtitle GEOTECHNICAL ENGINEERING CIRCULAR NO. 5 Evaluation of Soil and Rock Properties 6. Performing Organization Code: 13 Type of Report and Period Covered Unclassified Archived Document*. 2002.

Financial Times. (2024, May). *L.A. development fees: The true cost of permitting multifamily projects*. Retrieved April 22, 2025, from https://www.ft.com/content/ad9a2099-882f-4236-ab61-20fdcb39f023

Geocalc.app, 2024, www.geocalc.app/spt-corr-theory. Accessed 25 Nov. 2024.

Google.com. (2024). Google Earth. [online] Available at: https://earth.google.com/web/@34.07849366,-118.26572449,137.24084424a,365.74536874d,35y,-0h,0t,0r/data=CgRCAggBOgMKATA [Accessed 13 Sep. 2024].

Google Maps (n.d.). Google Maps. [online] Available at: https://www.google.com/maps/place/2223+Sunset+Blvd,+Los+Angeles,+CA+90026,+CIIIA/@34.0781233,-118.265616,20.5z/data=!4m6!3m5!1s0x80c2c7174a53bb2d:0x31546f60e9d803e2!8m2!3d34.078022!4d-118.26565!16s%2Fg%2F11cskyh5yl?entry=ttu&g_ep=EgoyMDI0MDkxMC4wIKXMDSoASAFQAw%3D%3D [Accessed 13 Sep. 2024].

Hussien, M. N., & Karray, M. (2016). Shear wave velocity as a geotechnical parameter: an overview. Canadian Geotechnical Journal, 53(2), 252–272. https://doi.org/10.1139/cgj-2014-0524

Infrastructure Australia. (2024). *Infrastructure Market Capacity Report 2024*. Retrieved from https://www.infrastructureaustralia.gov.au/

Ke L., Guanzhe F. (2023). The structural design and earthquake resistance assessment of composite steel–concrete frame structures with welded dissipative fuses. *Structures,* volume 53, 742-748. https://doi.org/10.1016/j.istruc.2023.04.079

Langan Engineering & Environmental Services. (2019). PRELIMINARY GEOTECHNICAL INVESTIGATION REPORT. In *www.langan.com*. Retrieved September 27, 2024, from https://clkrep.lacity.org/onlinedocs/2021/21-0358_misc_8_04-05-21.pdf

Los Angeles County Department of Public Works. (2025). *Business Opportunities*. Retrieved from https://dpw.lacounty.gov/general/contracts/opportunities/

Los Angeles County Public Works. *Storm Drain System.* The stormwater pipeline system map for the city was sourced from official Los Angeles County Public Works records, providing insights into the existing stormwater infrastructure around Sunset Boulevard. Available at: https://pw.lacounty.gov/fcd/StormDrain/index.cfm.

Los Angeles County Department of Public Works - Stormwater Management Available at: https://pw.lacounty.gov/wmd/stormwater/

Minimum Pile Length - Foundation engineering. (2005, March 15). Eng-Tips. https://www.eng-tips.com/threads/minimum-pile-length.118377/

Newaz, M. T., Ershadi, M., Carothers, L., Jefferies, M., & Davis, P. (2022). *A review and assessment of technologies for addressing the risk of falling from height on construction sites*. Safety Science, 147, 105618. https://doi.org/10.1016/j.ssci.2021.105618

Nicolas, D., Monjurul, H., & Ming, L. (2018) "RSMeans-Guided Approach to Detailed Cost Estimating: A Residential Project Case." Available at: https://www.researchgate.net/publication/326016874_RSMeans-Guided_Approach_to_Detailed_Cost_Estimating_A_Residential_Project_Case

NOAA Atlas 14 Volume 6: Precipitation-Frequency Atlas of the United States, California Available at: https://www.weather.gov/owp/hdsc/Atlas14_Volume6

Pile foundation. (2021). In MUCLecture. https://uomus.edu.iq/img/lectures21/MUCLecture_2022_8536598.pdf

Prebanić, K. R., & Vukomanović, M. (2023). Exploring stakeholder engagement process as the success factor for infrastructure projects. *Buildings*, *13*(7), 1785. https://doi.org/10.3390/buildings13071785

Rahman, MD Mansur. *Foundation Design Using Standard Penetration Test (SPT) N-Value*. 2020, https://doi.org/10.13140/RG.2.2.23159.73123.

Realtor.com. (2025). *Echo Park, Los Angeles, CA Real Estate Market Overview*. Retrieved April 22, 2025, from https://www.realtor.com/realestateandhomes-search/Echo-Park_Los-Angeles_CA/overview

Sangave, P., Madur, N., Waghmare, S., Shete, R., Mankondi, V., & Gundla, V. (2015). Comparative study of analysis and design of R.C. and steel structures. *International Journal of Scientific & Engineering Research*, *6*(2), 256–267. https://www.ijser.org/researchpaper/Comparative-Study-of-Analysis-and-Design-of-R-C-and-Steel-Structures.pdf

Saraogi, A., Dongre, A., Gupta, D., Lachhwani, S., Potdar, S., Rathore, T., & Garg, T. (2018). A comparison between RCC and steel structure. *International Journal of Research in Engineering, Science and Management (IJRESM)*, *1*(4), 106–108. https://www.ijresm.com/vol1%2Ciss4%2CApril18/IJRESM14_32.pdf

Simulated historical climate & weather data for Los Angeles. (n.d.). Meteoblue. https://www.meteoblue.com/en/weather/historyclimate/climatemodelled/los-angeles_united-states_5368361

Stormwater Management in Los Angeles - LADWP. Available at: https://www.ladwp.com

Terner Center for Housing Innovation. (2020). *The Hard Costs of Construction: Recent Trends in Labor and Materials Costs for Multifamily Housing in California*. University of California, Berkeley. Retrieved from https://ternercenter.berkeley.edu/wp-content/uploads/pdfs/Hard_Construction_Costs_March_2020.pdf

"Vesic Bearing Capacity Spreadsheet." *CivilWeb Spreadsheets*, civilweb-spreadsheets.com/foundation-design-spreadsheet/soil-bearing-capacity-calculation-excel/vesic-bearing-capacity/. Accessed 23 Sept. 2021.

U.S. Green Building Council. (2023). *LEED v4.1 Building Design and Construction Guide*. Retrieved from https://www.usgbc.org/resources

U.S. Green Building Council. (2023). *LEED v4.1. Building Design and construction*. https://build.usgbc.org/bdc41